Molecular definition of group 1 innate lymphoid cells in the uterus

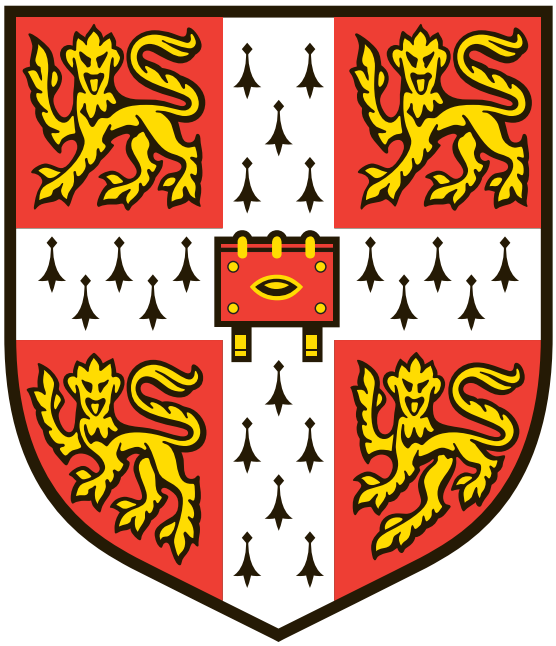

Iva Filipovic

King's College

Submitted in December 2018

This dissertation is submitted for the degree of Doctor of Philosophy at the University of Cambridge.

Declaration of originality

This dissertation is the result of my own work and includes nothing which is the outcome of work done in collaboration except as declared in the Preface and specified in the text.

It is not substantially the same as any that I have submitted, or, is being concurrently submitted for a degree or diploma or other qualification at the University of Cambridge or any other University or similar institution except as declared in the Preface and specified in the text. I further state that no substantial part of my dissertation has already been submitted, or, is being concurrently submitted for any such degree, diploma or other qualification at the University of Cambridge or any other University of similar institution except as declared in the Preface and specified in the text.

This thesis does not exceed the recommended word limit of 60,000 words set by the Degree Committee of Biology.

Molecular definition of group 1 innate lymphoid cells in the uterus

Iva Filipovic

Summary

Uterine NK cells (uNKs) are group 1 (g1) innate lymphoid cells (ILCs) that have been shown to regulate remodelling of uterine blood vessels, an event necessary to support fetal growth. Recently, other ILCs were identified in the mucosa and wall of the uterus of mice and women, pregnant or not. They may regulate important functions as they produce factors known to impact on uterine physiology and pathology. Unique to the mouse uterus is a population of $CD49a^{+}Eomes^{+}$ g1 ILCs (trNK), resembling human uNK cells. However, how they relate to uterine $Eomes^{+}CD49a^{-}$ conventional NK cells (cNK) and $CD49a^{+}Eomes^{-}$ ILC1 has been unknown. Determining the function of uterine lymphocytes is challenging because of the rapidly changing nature of the organ in response to sex hormones and, during pregnancy, to the invading fetal trophoblast cells. In my work, I provide the first genome-wide transcriptome atlas of mouse uterine g1 ILCs at mid-gestation. I show that the composition of g1 ILCs fluctuates throughout reproductive life, with $CD49a^{+}Eomes^{-}$ ILC1s dominating before puberty and specifically expanding in second pregnancies, when the expression of CXCR6, a marker of memory NK cells, is upregulated. Tissue-resident $CD49a^{+}Eomes^{+}$ NK cells (trNK) are most abundant during early pregnancy, and showcase gene signatures of responsiveness to TGF-β. On the transcriptome level, they are also equipped with the machinery that may allow them to interact with majority of other cells at the maternal-fetal interface, as well as with the extracellular matrix. Conventional NK cells expand late in gestation and may interact with trNK cells through the production of IL-18 and IFN-γ. These results identify trNK cells as the cellular hub of uterine g1 ILCs at mid-gestation and mark $CXCR6^{+}$ ILC1s as potential memory cells of pregnancy. I have also identified in the uterus an early developmental stage along the g1 ILC lineage. The identification of this stage of lymphoid development should facilitate the delineation of g1 ILC differentiation in the uterus. This study represents the first report of the uterine g1 ILC transcriptome and it will be an essential resource for designing future studies in the field of reproductive immunology. Determining the molecular identity and function of mouse uterine g1 ILCs as demonstrated here will be instrumental to guide further work with human uNKs.

Foreword

Despite my general lack of appreciation for motivational quotes, I came across several over the course of last three years that I found captivating. The reason why they have remained so ingrained in my mind is because they summarised some of the main lessons I learnt during my PhD. Nevertheless, not all of these quotes came from scientists, which, for me, was another important lesson during the time that it took to get here: skills one needs in order to be a competent scientist are not unique. They are skills essential for anyone in position where leadership, resourcefulness and creativity are required to bring change. I will cite them here, each one with my own reflections and advice for scientists who may find themselves reading this dissertation.

'*Do what you can, with what you have, where you are*' – Squire Bill Widener, from chapter IX of *Theodore Roosevelt: An Autobiography* (1913).

There is a common misconception that this quote originated from Theodore Roosevelt himself, the 26th President of the United States, but looking back at the original autobiography, a reader can discover that Roosevelt himself attributed the quote to the person above. Similarly, scientific reviews can often leave a reader convinced in a piece of evidence that may have been unintentionally misinterpreted and cited by the review authors. *Whenever possible, look at the original research paper.* And in relation to the quote, it is important to remember that science is a critical thinking process. As scientists, we often depend on a limited supply of tissue samples and, occasionally, we may find ourselves constrained by the resources or infrastructure available. *Critical thinking and asking simple, yet insightful questions can overcome such limitations. Resourcefulness is the key.*

'*Discovery is seeing what everybody else has seen, and thinking what nobody else has thought*' – Albert Szent-Györgyi von Nagyrápolt, a Hungarian biochemist and a winner of the Nobel Prize in Physiology or Medicine (1937) for the isolation of vitamin C and his work which laid the foundations for the discovery of the citric acid (Krebs) cycle.

I find this quote highly relatable to the work in the field of reproductive immunology. As explained in the Introduction to this dissertation (sections 1.2.2.2 and 1.2.2.9 and represented in **Fig. 1.7**), although uterine Natural Killer cells were not truly known as Natural Killer cells, they have been observed by researchers of various backgrounds since the end of the 19th century, long before conventional Natural Killer cells were discovered almost a full century later. *As we move forward in science, it will become increasingly important to address long-standing questions using novel technologies and interdisciplinary approaches. This will offer new insights that will allow for a deeper understanding of potentially misunderstood and/or underappreciated knowledge that we had available for centuries.*

'*The only way to get ahead is to find errors in conventional wisdom*' – Larry Ellison, the founder of the Oracle (a database used by The Central Intelligence Agency).

This quote is somewhat related to the previous one. There are numerous landmark studies without which it would be impossible to get to where we are today in science. Historical papers are among the most valuable resources available to young scientists today and there is nothing wrong with the 'conventional wisdom'. However, by using technologies mentioned above, new discoveries make it a challenge to update the textbooks with new data generated almost daily. *In 2018, we are overwhelmed with the data originating from the technological advances and we must be thorough in further exploration of the findings that will lead to understanding, and possibly revisiting, the basic physiological mechanisms. Ultimately, this will benefit the medical advances and human health.*

‘***But I am very poorly today and very stupid and hate everybody and everything***’ – Charles Darwin

Even the most famous scientists had rough weeks. This, however, never made me doubt my academic goals. As long as I am able to navigate my way through academia, I will remain a scientist, because I could never imagine myself doing anything else. *Every project is a puzzle where I have to both (1) come up with the pieces and (2) put them together. For me, to be able to do this every day for the rest of my life, is a great privilege.*

Table of contents

List of figures

List of tables

List of abbreviations

AGM	Aorta-gonad-mesonephros
APC	Antigen-presenting cell
BM	Bone marrow
bp	base pairs
CL	Corpus luteum
CLP	Common lymphoid progenitor
DBA	*Dolichus biflorus* agglutinin
DC	Dendritic cell
DEG	Differentially expressed genes
DMEM	Dulbecco's Modified Eagle's Medium
EDTA	Ethylenediaminetetraacetic acid
EPC	Ectoplacental cone
EVT	Extravillous trophoblast
HLA	Human leukocyte antigen
HPG	Hypothalamus-pituitary-gonadal
HSC	Haematopoietic stem cell
ECM	Extracellular matrix
FACS	Flow Cytometry Activated Sorting
FCS	Fetal calf serum
FGR	Fetal growth restriction
FRT	Female reproductive tract
FSH	Follicle-stimulating hormone
FW	FACS wash
gd	gestational day
GOS	Great Obstetrical Syndromes
GnRH	Gonadotropin-releasing hormone
ICM	Inner cell mass
ILC	Innate lymphoid cell
IVF	In vitro fertilisation
LH	Luteinising hormone
LN	Lymph node
KIR	Killer cell immunoglobulin-like receptors

KO	Knockout
MEM	Minimum essential media
MHC	Major histocompatibility complex
MLAp	Myometrial lymphoid aggregate of pregnancy
NK	Natural Killer cell
NKP	NK progenitor
NKR	Natural Killer Receptor
PC	Principal component
PCA	Principal component analysis
P/S	Penicillin and streptomycin
pbNK	Peripheral blood NK cell
PCR	Polymerase chain reaction
PBS	Phosphate buffered saline
pp	post-partum
QC	Quality control
RIF	Repeated implantation failure
RM	Recurrent miscarriage
RNA-seq	RNA-sequencing
rpm	rotations per minute
RPMI	Roswell Park Memorial Institute medium
RT	Room temperature
SA	Spiral arteries
sc	single cell
SGA	Small for gestational age
SLT	Secondary lymphoid tissue
TE	Trophectoderm
TF	Transcription factor
TGC	Trophoblast giant cells
Treg	Regulatory T cell
trNK	Tissue-resident NK cell
uNK	Uterine NK cell
w	week
WT	Wild-type

Acknowledgements

I would like to thank my PhD supervisor, Francesco Colucci, for giving me a chance to undertake this study in his group and for encouraging me to apply for a PhD position when I first contacted him with a list of 27 questions about uterine NK cells, fascinated by the immunology of reproduction. His supervision helped me develop into a scientist I am today. If not for our discussions and his insightful questions, my critical thinking and analytical skills would not be of such a high standard as they are today as I am finishing my PhD. I am also extremely grateful to Francesco for appointing Martin Ivarsson as my co-supervisor. Martin's guidance was instrumental for my work, especially when I first started in Cambridge. I am thankful to Martin for endless Skype conversations even when he left Cambridge – he made sure that he was always available to discuss science with me, troubleshoot experiments and develop ideas. I remember thinking to myself, during the first year of my PhD, how I wanted to be like Martin when I academically 'grow up'.

To my PhD colleagues, Norman Shreeve and Oisín Huhn: I hope the King's Holy Trinity of Reproductive Immunology and Jacket Potatoes will never cease to exist. You two made last three years unforgettable and I consider myself lucky to have shared my PhD journey with yours. It is so rare and precious to have such bright, funny and most importantly, genuinely kind people in your life.

I would also like to acknowledge all past and current members of Colucci and Moffett groups. They were here for me, whenever I needed them. From the Colucci group, I would like to particularly thank Delia Hawkes, as her help with animal work was crucial for my project, and from the Moffett group I would like to thank Andrew Sharkey for sharing his molecular biology tips and tricks with me and for remaining so involved in my work over the years.

I am grateful to Russell Hamilton for the bioinformatic analyses he has done for this study. Not only has he been involved in every step of our published paper in *Nature Communications*, but he has also been a great R teacher to me. I hope to further these computational skills as I move forward in science.

None of the work I have done in this thesis would have been possible without the financial support from the Centre for Trophoblast Research (CTR), which provided me with a PhD studentship. This studentship was a great success, as one of the Centre's aims is to train the next generation of placental researchers and I most certainly do not intend to leave this wonderful field in the foreseeable future. I hope that my ties with CTR will remain strong in the years to come. The Centre provides an excellent platform for knowledge exchange and I thank each and every member of the CTR, including its Scientific Advisory Board (with special thanks to Hilary Critchley) which reviewed my project in the first year and offered excellent feedback.

Within the CTR management, I will be eternally grateful to Ashley Moffett and Graham Burton, who have been there for me every step of the way. I am humbled and honoured to have had a chance to interact with them.

Finally, I would like to thank my fiancé Ryan, for putting up with me over the last three years, for listening to me practise almost every talk I ever gave (and I have given many) and for continuous encouragement when the PhD life would get rough. Same goes for the two dearest people in my life, my parents, Sonja and Dragan, with an addition: none of this would be possible without them and the values they instilled in me. They have always insisted how it is my hard work that got me here, but such hard work was only possible through their sacrifices and investment in my personal and professional development.

There are not enough pages to mention all the helpful staff from various facilities at the University of Cambridge who were involved in this study in one way or another, so I will just thank you all. It has been a pleasure to spend the time working closely with you.

Publications arisen from this study

Filipovic I, Chiossone L, Vacca P, Hamilton R, Ingegnere T, Doisne JM, Hawkes DA, Mingari MC, Sharkey AM, Moretta L, Colucci F. Molecular definition of group 1 innate lymphoid cells in the mouse uterus. *bioRxiv* (2018)

Filipovic I, Chiossone L, Vacca P, Hamilton R, Ingegnere T, Doisne JM, Hawkes DA, Mingari MC, Sharkey AM, Moretta L, Colucci F. Molecular definition of group 1 innate lymphoid cells in the mouse uterus. *Nat Commun,* **9**, 4492 (2018)
This publication can be found attached at the end of this dissertation.

Statement of collaborative work

Chapters 3 and 4

Group 1 ILCs which were RNA-sequenced and analysed were sorted by Dr Laura Chiossone from the Giannina Gaslini Institute in Genoa, Italy and Dr Paola Vacca from the Department of Experimental Medicine (DIMES) at the University of Genoa, Italy. Bioinformatic analyses of RNA-sequencing files (up to and including generating normalised genes and differentially expressed gene lists) were performed by Dr Russell Hamilton at the Centre for Trophoblast Research.

Chapter 5

Preliminary data generated using the $Ncr1^{iCre}Tbx21^{fl/fl}$ and $Ncr1^{WT}Tbx21^{fl/fl}$ mouse models was obtained using the animals generously shared by Dr Victoria Male and Antonia Cuff at the University College London.

1. Introduction

1.1 Reproduction

1.1.1 A brief guide to the tree of life: focus on modes of reproduction

Recent technological advances in the field of genomics have allowed sequencing of the genomes of many novel organisms, particularly of the ones living in the extreme habitats. Genetic information obtained from the sequencing of over 1,000 new genomes has led to a reconstruction of the molecular tree of life. However, the new data reveals diversification principally in the domain Bacteria, while Eukarya exhibits much less phylogenetic diversity due to a more recent evolution (Hug et al., 2016). One of the most important traits that differentiates multicellular eukaryotic animals (biological kingdom Animalia in the scientific classification) from the rest of the living organisms is the ability to reproduce sexually, via fusion of the two gametes created by meiosis. Despite the lower level of diversity in Eukarya and consequently in its kingdom Animalia, there is still a very poor understanding of the events post-fertilisation at the molecular level. Of particular importance in the evolutionary history of life is the phylum Chordata of the animal kingdom, also known as chordates. These are deuterostomes that go through a notochord stage during their development. Looking further into the classification, chordates consist of three subphyla: Cephalochordata, Tunicata and Vertebrata (Craniata). It is a superclass Tetrapoda, or tetrapods (four-limbed vertebrates) that represent an exceptional model of evolutionary success, as documented by their ecological diversity today. The main reason behind this is that the evolution of tetrapods took place around the time that the colonisation of dry land started, which was about 360 million years ago (Sander, 2012). The first tetrapods were aquatic animals but with a move from the sea, through swamps, onto the land habitat about 50 million years later, they had to adapt in order to survive. The evolutionary changes in reproduction were essential to drive this

survival. Tetrapods include two groups of animals: anamniotes and amniotes. The first tetrapods were mainly anamniotes and predominantly aquatic, represented by fishes and amphibians. This is a more primitive group that lays eggs in water. Anatomically, the anamniotic egg is characterised by the lack of amnion, an innermost membrane of an amniotic egg, filled with amniotic fluid during the embryonic development. Physiologically, the lack of amnion means that the anamniote embryo is able to develop in an aquatic environment through a direct exchange of oxygen, CO_2 and waste with the water in which the egg is laid.

However, most tetrapods are amniotes (represented by reptiles, birds and mammals) which lay eggs on the land or are carried by the mother who gives birth to the live young. This was made possible by the adaptations brought by the development of the amniotic egg and driven by the tetrapods' conquest of the dry land. Amniotes have developed a more complex egg, characterised by four extraembryonic membrane structures: yolk sac, amnion, chorion and allantois. The amnion is the innermost membrane, enclosing the embryo in amniotic fluid which serves a protective purpose, but this environment is also a water replacement because now it provides an interface between the embryo and its environment allowing for respiratory, excretory and nutritional functions. This evolutionary innovation has permitted amniotes to inhabit terrestrial environments much more successfully than anamniotes (Reisz, 1997).

Various reproductive solutions as described above have led to the following classification of a birth process:

(1) Oviparity – undeveloped eggs are released. This is a process in which the undeveloped fertilised eggs are released and they finish their development externally. All birds, some fishes and most reptiles are oviparous. As introduced earlier, mammals are tetrapod amniotes and there are three classes of mammals – Prototheria (monotremes), Metatheria (marsupials)

and Eutheria. Within mammals, monotremes are oviparous animals, and one example is the duckbill platypus as an egg laying mammal.

(2) Viviparity – a solution in which the mother bears live young and the offspring is born without the requirement to finish their development outside the parental body. Viviparity is represented by the development of placenta which will allow the nutrient supply from the mother. The amniote egg has allowed the move from oviparity to viviparity because it increased the capacity of respiration, excretion and nourishment from the mother, without the need for surrounding water. Eutherian mammals are viviparous and they have the most complex placental development (Moffett & Loke, 2006), especially compared to a much simpler marsupial placenta. Viviparity has independently evolved many times within the subphylum Vertebrata (Romer, 1967; Blackburn, 1998). Another example of viviparous animals are the blue sharks with a yolk sac placenta (Hamlett & Wourms, 1984; Hamlett et al., 1985).

(3) Ovoviviparity – an intermediate solution between oviparity and viviparity, where embryos develop inside the mother getting all their nutrients from a yolk sac, until the mother either gives birth to live young or lays eggs to hatch. An example is the tiger shark.

Although viviparity comes with reproductive advantages, it is an immunological conundrum that a zygote, created by the fusion of gametes from two genetically distinct individuals, now can exist inside of a maternal body for any period of time, remaining unharmed until the end of gestation. This defies one the main immunological concepts, allorecognition, which is the process of immune cells recognising antigens derived from a genetically distinct individual organism of the same species, or in simpler terms, a capability to differentiate between ‘self’ and ‘non-self’. Pregnancy, therefore, represents the only phenomenon in mammals in which allorecognition occurs physiologically (Moffett-King, 2002). The concept of the developing embryo as an allograft was originally introduced by Peter Medawar (Medawar, 1953). This

concept led to a dogma in the field of reproductive immunology that maternal tolerance is essential for successful pregnancy, because it enables the mother to not reject an implanted embryo. However, Moffett and Loke point out that the focus should not be on the interactions between the mother and the fetus, because they are not in a direct contact. Rather, the direct tissue contact occurs between maternal cells in the uterus and the cells derived from the fetal membranes and this is the key to understanding the immunology of placentation (Moffett & Loke, 2006). It is this maternal-fetal contact zone that represents the placenta. The placenta is essential for the exchange of gases, nutrients and waste products between the mother and the growing fetus.

1.1.2 Placental types

Placental mammals can be further classified into distinct groups according to the type of placenta they establish for nourishment of the growing embryo. There are several systems of classification, but one feature is common to all types of placentas: a complete separation of fetal and maternal circulatory systems. The differences in placental shape, maternal-fetal interdigitation and histological organisation will determine the type of the placenta in a particular species (Benirschke et al., 2012). In order to understand how placental anatomy is tied to functions they perform in each system of classification, it is important to describe the formation of individual extraembryonic membranes. A common misconception is that the placenta is formed by the mother, but it is fully formed by a developing embryo and an implanting embryo is responsible for all downstream tissue remodelling changes that will happen in the mother to allow for a successful pregnancy outcome. Therefore, a basic understanding of the embryonic development is necessary to understand how and when the placenta is established. Human embryonic development will be used as an example here, but it is important to note that various stages will occur at different timepoints in different species

and the timing of these stages as well as differences will be described in other sections (sections 1.1.3 and 1.1.4).

When the oocyte fuses with the sperm it is called a zygote and this initial event involves the fusion of the pronuclei from the two germ cells. The zygote then goes through distinct stages during gestation to develop into a healthy baby. Initially, this happens via transition into the embryonic stage and in humans this happens over approximately the first three days post-fertilisation. Not only is this transition a period of general transcriptional silence, but more importantly, it is a period of cleavage cell divisions where each cell (now called a blastomere) undergoes a series of divisions. During this process, the embryo size remains the same but the number of cells increases from 2- via 4- to 8-cell stage and a major burst of transcription happens between the 4- and 8- cell stage, known as the embryonic genome activation (EGA) (Niakan et al., 2012). Throughout all cleavage divisions up to this point, individual blastomeres are reducing in size, acquiring a ratio of cytoplasm to nucleus that resembles more the one of adult cells. The first major morphological change in a growing embryo is at the stage of morula (approximately 16 blastomeres), when compaction of cells takes place via maximising intercellular contacts and a breaking of the radial symmetry. This leads to a formation of the blastocyst, which is a highly polarised stage. Inside the blastocyst lies a fluid-filled cavity, blastocoel, and inside it the inner cell mass (ICM) can be found lying to one side. ICM is surrounded by an outer layer of cells called trophectoderm (TE). TE is essential in formation of the placenta because it is this layer that contains extra-embryonic cells giving rise to all cells of the trophoblast lineage. Trophoblast cells are in direct contact with the maternal cells of the uterine wall and will be the main constituents of what is called a maternal-fetal interface. ICM, on the other hand, will differentiate into the epiblast and hypoblast (**Fig. 1.1**).

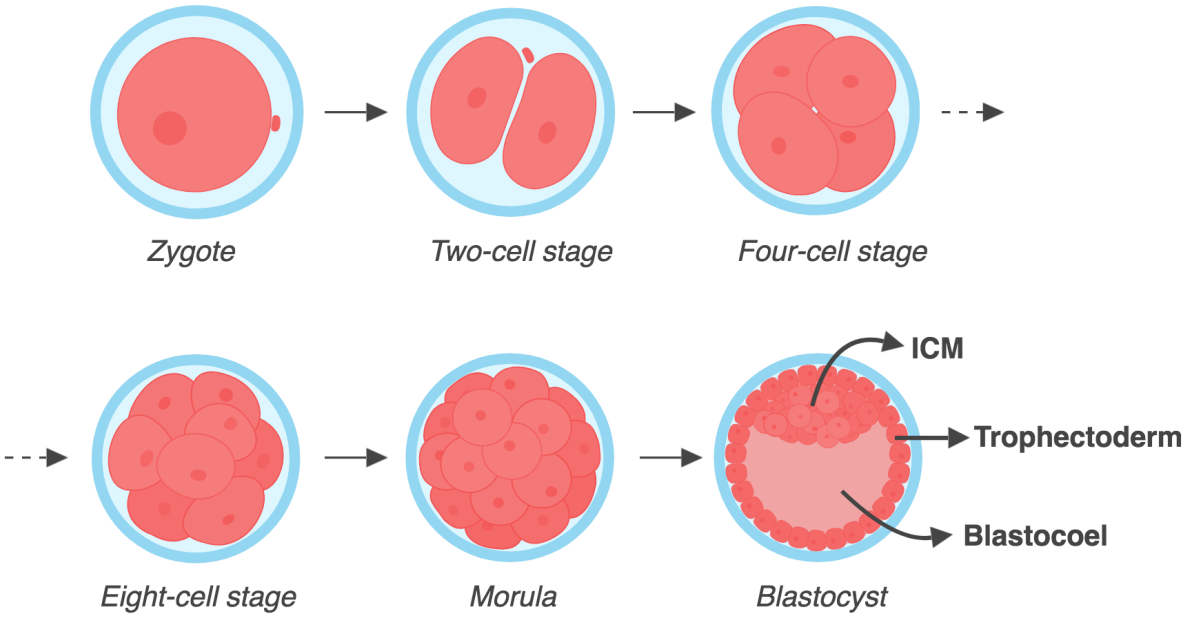

Figure 1.1. First stages during the embryonic development. First several stages during the embryonic development are illustrated and explained in text (section 1.1.2). ICM: inner cell mass.

Although ICM exclusively gives rise to all cells of the future embryo, certain components of it contain additional extra-embryonic cells (similarly to TE) which will contribute to the formation of one of the extraembryonic membranes: the yolk sac, in a manner summarised in the following paragraph.

The epiblast is also called primary ectoderm and the hypoblast is known as primary endoderm. Between the two, a third layer, the mesoderm, forms after which cavities will start developing: the extraembryonic coelom within mesoderm and the proamniotic cavity within epiblast. Hypoblast spreads out underneath the trophoblast and its edges meet to form a yolk sac cavity. These three cavities, extraembryonic coelom, proamniotic cavity and a yolk sac cavity now grow in size and eventually lead to a formation of a definitive embryo because three layers will be organised in a following way:

(1) Epiblast: amniotic ectoderm and embryonic ectoderm.

(2) Hypoblast: yolk sac cavity and embryonic endoderm.

(3) Mesoderm: extraembryonic mesoderm and embryonic mesoderm.

Embryonic components of each one of the layers above will fuse, form the embryonic disk, which will form the definitive embryo and later a fetus (**Fig. 1.2**). Everything else forms the extraembryonic membranes through the fusion of distinct layers:

(1) Amnion: amniotic/extraembryonic ectoderm with extraembryonic mesoderm.

(2) Yolk sac: extraembryonic hypoblast/endoderm (yolk sac cavity) with extraembryonic mesoderm.

(3) Chorion: blastocyst wall derivative, trophoblast, with extraembryonic mesoderm.

(4) Allantois: in a developing embryo, allantois forms by fusing of a diverticulum of the endoderm (allantoic endoderm) on a posterior part of the embryo with the surrounding mesoderm (allantoic mesoderm).

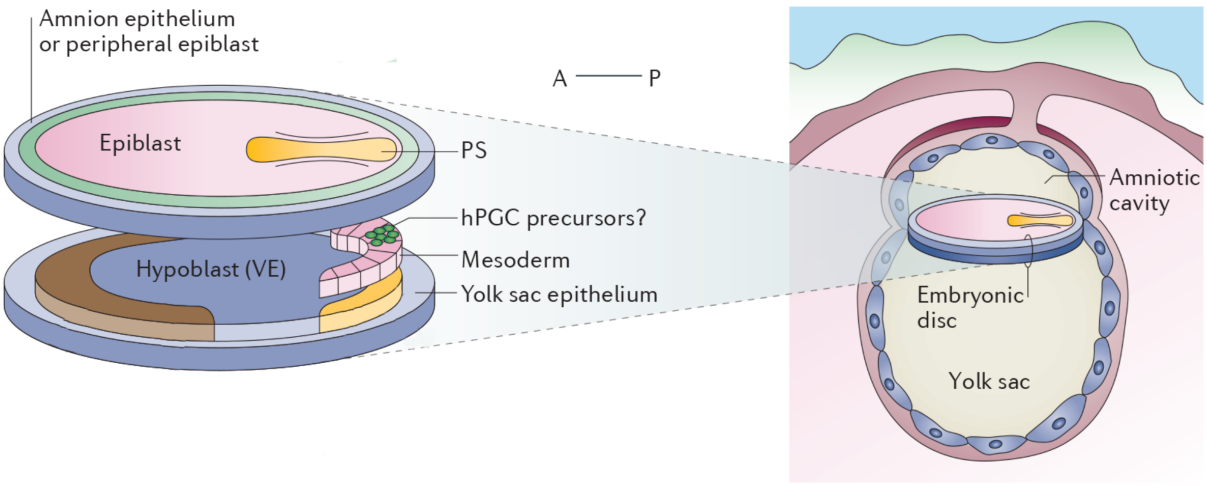

Figure 1.2. Overview of human post-implantation development. Relevant details are explained in text (section 1.1.2). Adapted from Tang *et al*., 2016.

The chorion is a very important layer because in most mammals, being formed by the fusion of trophoblast and extraembryonic mesoderm, it represents the main exchange membrane. The chorion itself is not vascularized and depending on how this developmental issue is

resolved, there are two different types of placentas. Both extraembryonic and embryonic mesoderm develop their blood vessels and if the chorionic mesoderm fuses with now prominently vascularised mesoderm of the yolk sac, a choriovitelline placenta will form. Also called the yolk sac placenta, this is a solution for the eggs of reptiles, birds and the duckbill platypus within mammals and it is phylogenetically older. However, in most mammals, this yolk sac placenta is never functional because chorioallantoic placenta forms instead, by fusion of the chorionic mesoderm with the allantoic mesoderm. Since both of these are very well vascularised, this will become the only exchange site. Chorioallantoic placenta is a characteristic of higher primates, including humans.

Another commonly used systems of placental classification is based on the number of tissue layers separating fetal blood vessel lumen from the maternal circulation. This histological organisation also defines how deeply the blastocyst will invade into the maternal tissue. Epitheliochorial placenta contains six layers. It is also termed the 'attached' placenta because there is no invasion of the blastocyst into the endometrium. This type is seen in pigs, whales and horses. On the maternal side, there are three layers: uterine (endometrial) epithelium, connective tissue and endothelium of the maternal blood vessels (moving from the site of the implanting blastocyst towards the lumen of the uterus). On the fetal side, in same order, there are another three layers: trophoblast, connective tissue and fetal endothelium.

Cats, dogs and bats establish the endotheliochorial placenta in which the uterine epithelium and connective tissue are removed through the tightly regulated level of invasion of the blastocyst. There is no contact of maternal blood with trophoblast cells, however. Instead, the trophoblast is in direct contact with the maternal endothelium.

Finally, haemochorial placenta is marked by the deepest invasion of trophoblast cells into the endometrium to establish the contact with maternal blood, through the erosion of the maternal endothelium. It is called haemochorial because the trophoblast cells are bathing in

maternal blood directly. Rodents and higher primates, including humans, are examples of organisms with a haemochorial placenta. Menarche, menstruation and menopause are some of the phenomena taking place only in species with the haemochorial placenta. There are, however, examples of other species that menstruate, in addition to human females and old world primates, and these are the elephant shrew (van der Horst, 1954) and several species of bats (Rasweiler, 1991; Zhang et al., 2007).

Based on the shape of the placenta and the surface area of contact between fetal and maternal tissue, there are four different types of placentas (**Fig. 1.3**).

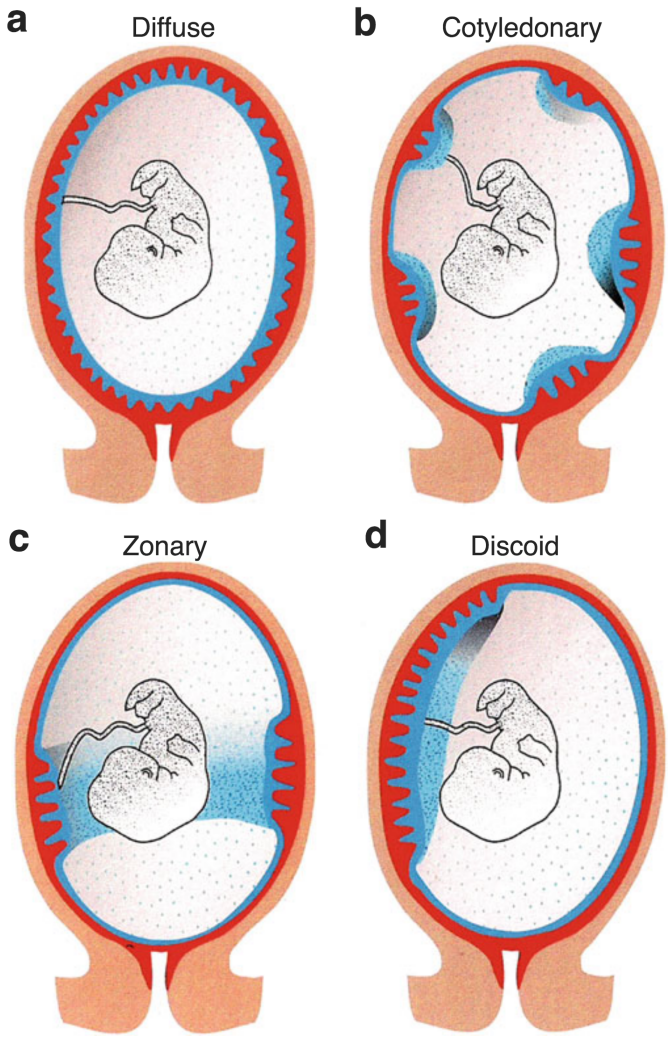

Figure 1.3. Overview of placental types. Illustration of four types of placenta defined by the shape of the placenta and the surface area of contact between fetal and maternal tissues. Relevant details are explained in text (section 1.1.2). Adapted from Benirschke *et al*., 2012.

Cotyledonary placenta is seen in ruminants, where multiple areas of attachment (cotyledons) to the endometrium are observed, usually elliptical in shape. Zonary placenta surrounds the fetus completely and can be seen in dogs and cats. Horses and pigs are examples of animals with a diffuse placenta where maternal-fetal interdigitations can be observed over the entire chorion. Finally, a discoid placenta is discoid in shape and can be observed in primates and rodents. Here, the interactions between the mother and the fetus are only limited to one or more poles of a spherical chorion (Benirschke et al., 2012).

1.1.3 Mouse reproduction

Mus musculus (commonly known as the house mouse), a small mammal of the order Rodentia (rodents), has been an invaluable model organism for the studies of biological processes. Although used much earlier in the history of scientific research, major progress was made in 1902 when French geneticist Lucien Cuénot had showed that the Mendelian inheritance applies to animals by following the coat colours in mouse crosses (Hedrich & Bullock, 2004). At a similar time, the work conducted by Clarence Little in William Castle's laboratory at the Harvard University, in collaboration with Abbie Lathrop, a renowned mouse breeder at the time, marked the beginning steps towards making mouse a mammalian model organism of choice in today's biomedical research (MSG Consortium, 2002). Strains of laboratory mice are inbred and therefore genetically identical, which enables researchers to perform accurate and reproducible experiments among the institutes. More importantly, the fully sequenced mouse genome can be manipulated through creation of transgenic animals by a pronuclear injection of any gene(s), for example. This allows for the investigation of specific genes' contributions to homeostasis and disease. The most commonly used approach of genome manipulation includes deleting genes of interest and generating 'knockout' (KO) animals by modifying embryonic stem cells and re-injecting them into a blastocyst. These

genes can either by systemically deleted or specifically, in a tissue or cell of interest through the use of a Cre/loxP approach (conditional KO). Other examples include generation of 'reporter' animals with fluorescent proteins translated together with a gene of interest, allowing tracking of cells that express genes of interest through measurements of the fluorescence, or 'knock-in' animals where one sequence of interest is replaced with a transgene (by one-for-one substitution). Additionally, a whole plethora of genes responsible for generation of various immune cells can be deleted to create various immunodeficient strains. Finally, it is possible to replace mouse genes with human genes in order to generate 'humanised' mouse models that allow adoptive transfer of human cells and a subsequent assessment of human immune cell behaviour in vivo. The latter have recently become increasingly appreciated as essential preclinical models. Mouse husbandry allows for processes of genome manipulation to run smoothly and under strictly controlled conditions. Due to their size (adult mice weighing around 20 g), mice do not require as much housing space as some other mammalian model organisms, but most importantly, they have a very high fecundity. This is not only important for quick generation of novel, genetically manipulated, mouse models, but also makes them desirable models in a study of the reproductive system.

The tubular components of the mouse female reproductive tract (FRT) (vagina, cervix, uterine body and two horns and the oviducts) are covered in mucosa, similarly to other barrier tissues such as the respiratory and intestinal tissues (Zhou et al., 2018). Having a tubular anatomy, there are several anatomical axes used to describe the organisation of the uterus: longitudinal, vertical and transverse. Out of these, the vertical axis is the most relevant when describing the events occurring during gestation and embryonic development. This axis is determined by the orientation of the tissue structures to the mesometrium – the mesentery-like tissue which connects the uterus to the abdominal cavity wall (Tam, 2004) and functions

as a uterine suspensory ligament. A structure in the uterus can either lie on the mesometrial pole (proximal pole, on the mesometrial side of the uterus) or the anti-mesometrial pole (distal pole, on the anti-mesometrial side).

The female mouse is a polyestrous animal which means that it undergoes the estrous cycle and can reproduce multiple times a year. The word estrous is derived from the ancient Greek οἶστρος (madness, frenzy) and refers to a phase during the cycle (estrus) when the animal displays a sexually receptive behaviour to signal that it is ready for mating. In all mammals, the hypothalamus-pituitary-gonadal (HPG) axis drives the progression through the estrous cycle. The cycle in mice spans over approximately four (4.3) days through four stages: proestrus (approximately lasting for 32.4 h), estrus (20.7 h), metestrus (21.8 h) and diestrus (29.3 h) (van Ebbenhorst Tengbergen, 1955). One of the most commonly used methods of determining the phase of the estrous cycle is the vaginal cytology method (Byers et al., 2012). This method assesses the morphology of vaginal epithelial cells as well as their numbers in relation to the immune cells obtained from the vaginal smears. During proestrus, only small and round, nucleated epithelial cells can be observed with almost no immune cells present. In estrus, now squamous epithelial cells appear cornified, without observable nuclei and gradually towards the end of this stage, an influx of leukocytes appears in the vaginal smears. A female mouse in metestrus is characterised by dominant leukocytes and a very few clusters of both nucleated and cornified epithelial cells in the smears, while it is safe to assume that a female is in diestrus if the smears show mainly leukocytes and a lack of their association with rare epithelial cells (Byers et al., 2012).

Hormonal fluctuations induced by the HPG axis tightly regulate uterine changes occurring at each of these four stages, while also regulating the development of the preovulatory follicles in the ovaries and ovulation (not discussed here). Gonadotropin-releasing hormone (GnRH) secreted from the GnRH neurons in the hypothalamus stimulates the secretion of the two

gonadotropins, follicle-stimulating hormone (FSH) and luteinising hormone (LH) by the gonadotropic cells of the anterior pituitary gland (**Fig. 1.4**).

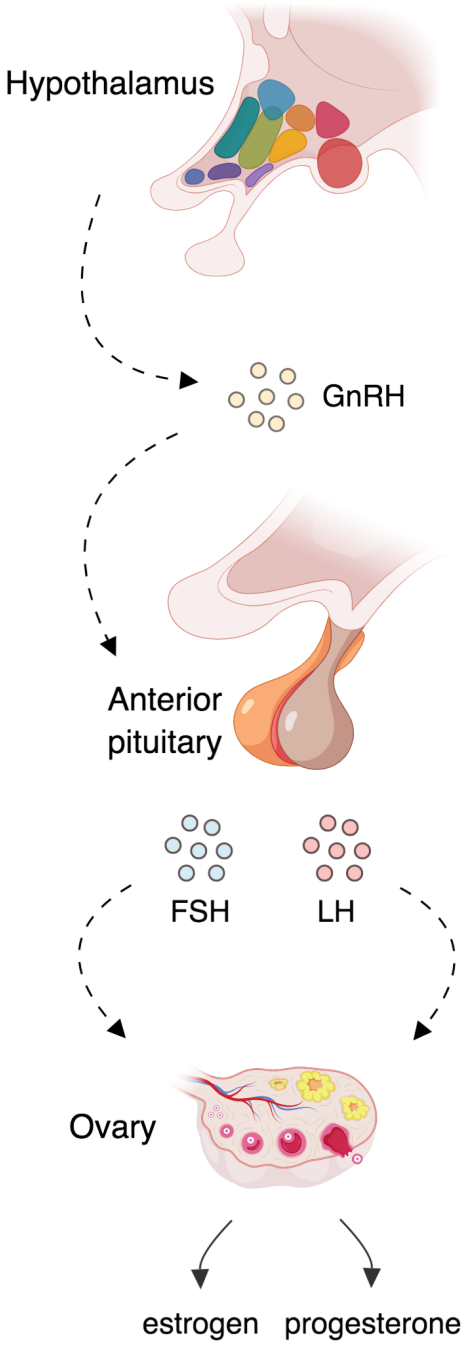

Figure 1.4. Hormonal fluctuations are induced by the hypothalamus-pituitary-gonadal axis. Illustration of the hypothalamus-pituitary-gonadal (HPG) axis as explained in text (section 1.1.3). GnRH: gonadotropin-releasing hormone, FSH: follicle-stimulating hormone, LH: luteinising hormone.

Concentrations of FSH and LH increase during the proestrus, which leads to a production of estrogens (mainly 17β-estradiol, also known as E2) through the mechanisms occurring in the ovaries. E2 induces an LH surge through a positive-feedback mechanism throughout proestrus and into estrus, which leads to ovulation at the onset of estrus. During metestrus and diestrus, progesterone is the dominant gonadal hormone which also inhibits the secretion of LH. However, throughout metestrus and closer to the end of the diestrus, progesterone is replaced with a weaker 20α-OH-progesterone which is not as effective in the LH inhibition. This allows for the cycle to continue by entering into the proestrus again (**Fig. 1.5**).

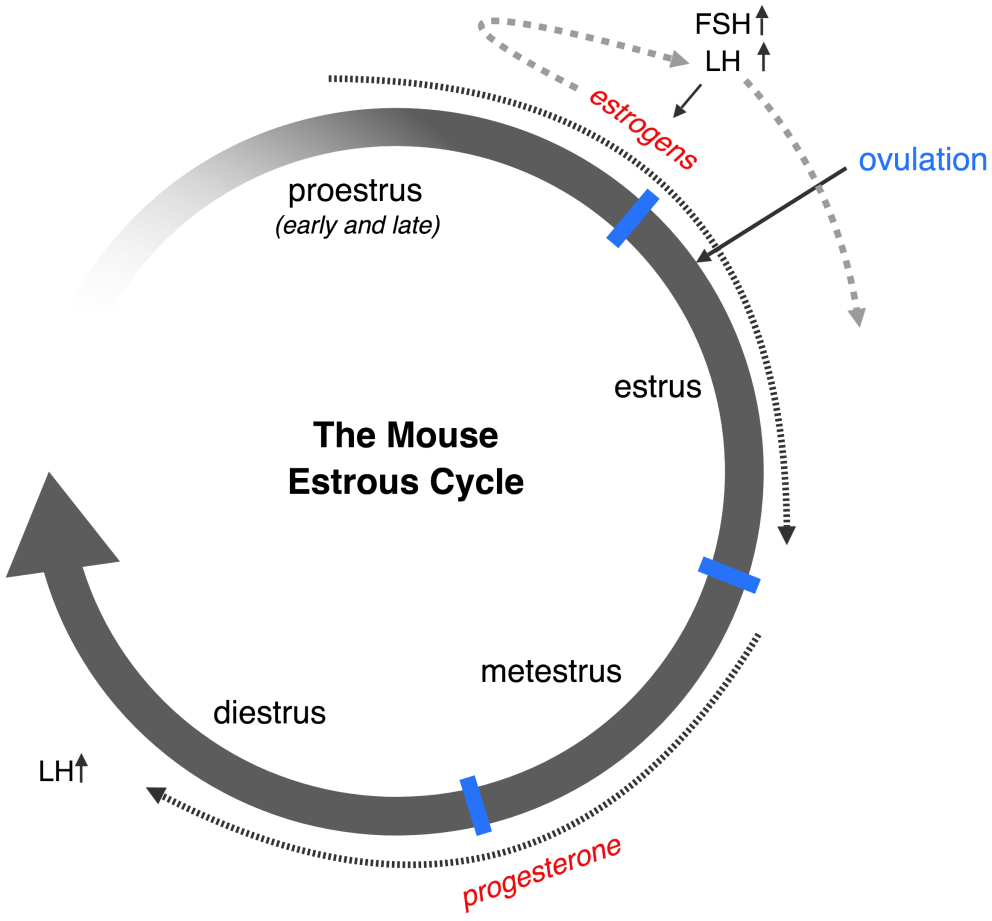

Figure 1.5. The mouse estrous cycle. Illustration of the mouse estrous cycle as explained in text (section 1.1.3). Dotted grey arrow indicates positive feedback event. Ovulation is indicated by an arrow. FSH: follicle-stimulating hormone, LH: luteinising hormone.

It is important to note that the post-estrus changes in progesterone synthesis will only occur as a consequence of the corpus luteum (CL) regression in the absence of mating during estrus. If the mating occurs, the CL will not regress and progesterone will not be converted into 20α-OH-progesterone through a mechanism involving prolactin secreted from the pituitary (Croy et al., 2014).

On the morphological level, the uterus appears enlarged and thick during proestrus and estrus, correlating with E2 levels. During this time, there is an increase in the level of proliferation of stromal cells but a decreased level of the proliferation of the uterine glands' epithelium, although they are less apoptotic at this stage. The thickness of the uterus at this stage is due to stromal cell proliferation but also the hypertrophy of the uterine glands later in proestrus and early in estrus when they are the most active. The uterus is also most vascularized during estrus. Progressing into the metestrus and diestrus with an increase in progesterone, the uterus becomes elongated and thin. The uterine epithelium undergoes vacuolar degeneration, thins out and at the same time, the glands display minimal activity. This is when leukocytes can be observed in the stroma, with their numbers peaking during the diestrus.

Mouse gestation spans over 19-21 days (**Fig. 1.6**). During the embryonic development, the TE and ICM are already formed by embryonic day (E) 3.5, and the blastocyst is ready to implant around E4.5. This initially happens on the anti-mesometrial side of the uterus (Tam, 2004). In mice, implantation of the blastocyst is necessary to induce the decidualisation of the endometrium and therefore, the decidua will not form in every estrous cycle, but just in the one that ends in a successful pregnancy post-estrus. This is an important difference compared to higher primates and a reason why none of the commonly used lab mouse strains menstruate, as the endometrium is reabsorbed in lack of fertilisation. Interaction of the

blastocyst and uterine epithelium during implantation is essential to transduce the signals to the endometrial stroma (fibroblasts) around the embryo.

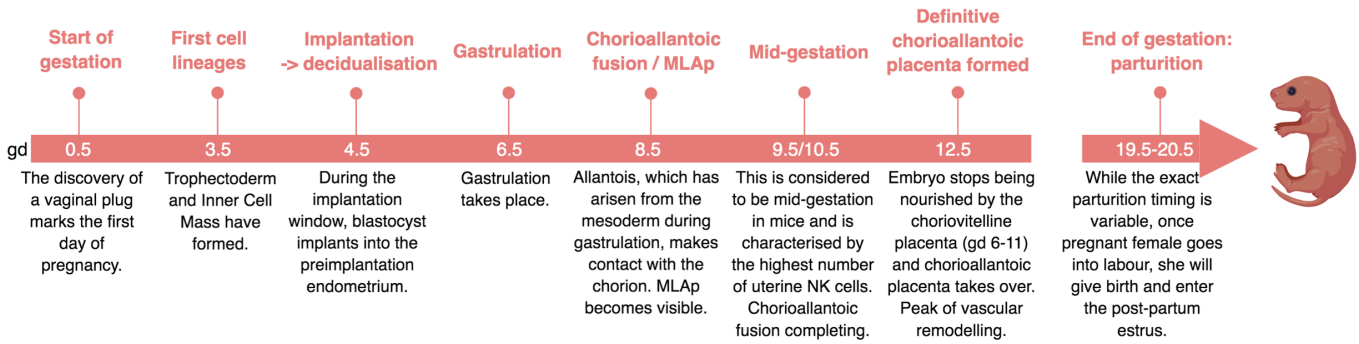

Figure 1.6. Summary of the main events during mouse gestation. Mouse gestation has been summarised and illustrated in this figure based on the explanation in the text (section 1.1.3). MLAp: myometrial lymphoid aggregate of pregnancy, gd: gestational day, NK: natural killer cell.

This is why decidualisation only occurs at the implantation sites, while the endometrium remains intact between distinct implantation sites, without any extracellular matrix (ECM) remodelling taking place. The main event characterising the decidualisation induced by implantation at gd 4.5 is the transformation of the endometrial stromal cells into the decidual stromal cells along with ECM remodelling. This is accompanied by the endometrial blood vessel remodelling as well as a marked influx of immune cells (mainly uterine Natural Killer cells) which have been shown to regulate these processes (Croy et al., 2006). There is some evidence that the ECM remodelling occurs earlier, in the absence of the implantation, during the preimplantation period, on gd 2 (Bijovsky et al., 1992). It is changes in the hormone fluctuations during the estrous cycle (**Fig. 1.5**) that are responsible for the preparation of the endometrium for the decidualisation: during the first two days of pregnancy high estrogen levels induce epithelial proliferation, but progesterone inhibits this process and induces proliferation of the endometrial stroma instead on gd 3 and gd 4 of gestation (Tan et al., 1999). The initial epithelial proliferation is important because, as mentioned previously,

epithelial cells transduce signals necessary for fibroblasts' transformation and a lack of epithelial cells results in a decidualisation defect (Lejeune et al., 1981). From E4.5 onwards, trophectoderm differentiates into distinct subsets of the trophoblast lineage, including the extra-embryonic ectoderm and ectoplacental cone (EPC). Trophoblast cells on the opposite end of the ICM undergo DNA endoreduplication and become trophoblast giant cells (TGCs), surrounding the EPC (**Fig. 1.7**). Formation of mesoderm, ectoderm and endoderm through gastrulation take place around day E6.5 (Rossant & Cross, 2001).

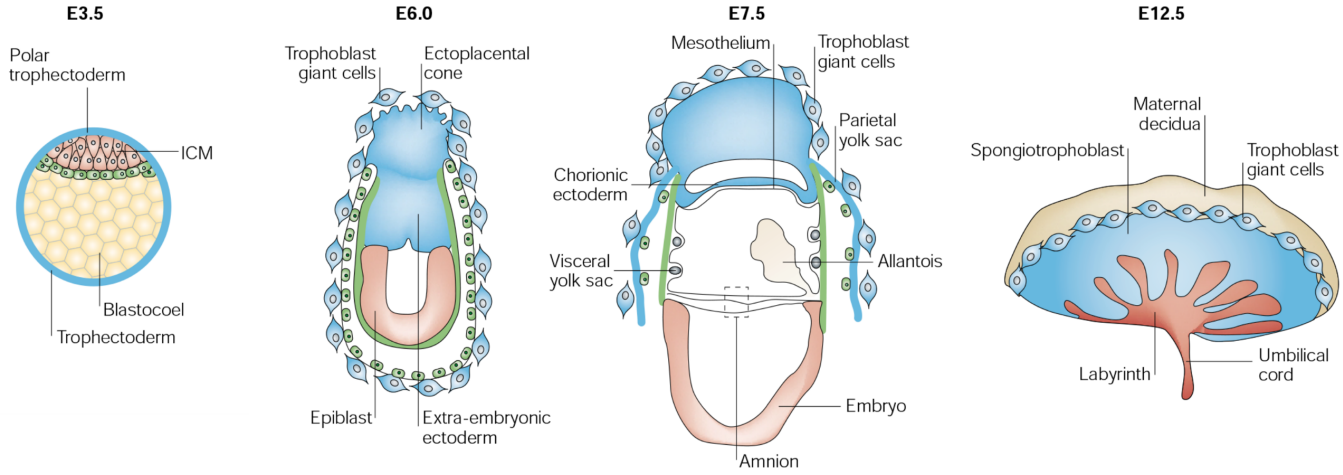

Figure 1.7. Early development of the mouse placenta. Relevant details are explained in text (section 1.1.3). Adapted from Rossant and Cross, 2001.

The allantois, arisen from this mesoderm, starts fusing with chorion arisen from the extraembryonic ectoderm at day E8.5 and this is when the labyrinth (a derivative of extraembryonic ectoderm) starts forming, as the area of a direct exchange between the fetal and maternal blood. At this point, the structural changes will also start occurring on the maternal side, in myometrium, a muscular layer surrounding the endometrium. A structure called the myometrial lymphoid aggregate of pregnancy (MLAp) develops at each implantation site on the mesometrial side within the myometrium. It is hard and white in appearance and harbours a large number of immune cells (**Fig. 1.6** and **Fig. 1.8**).

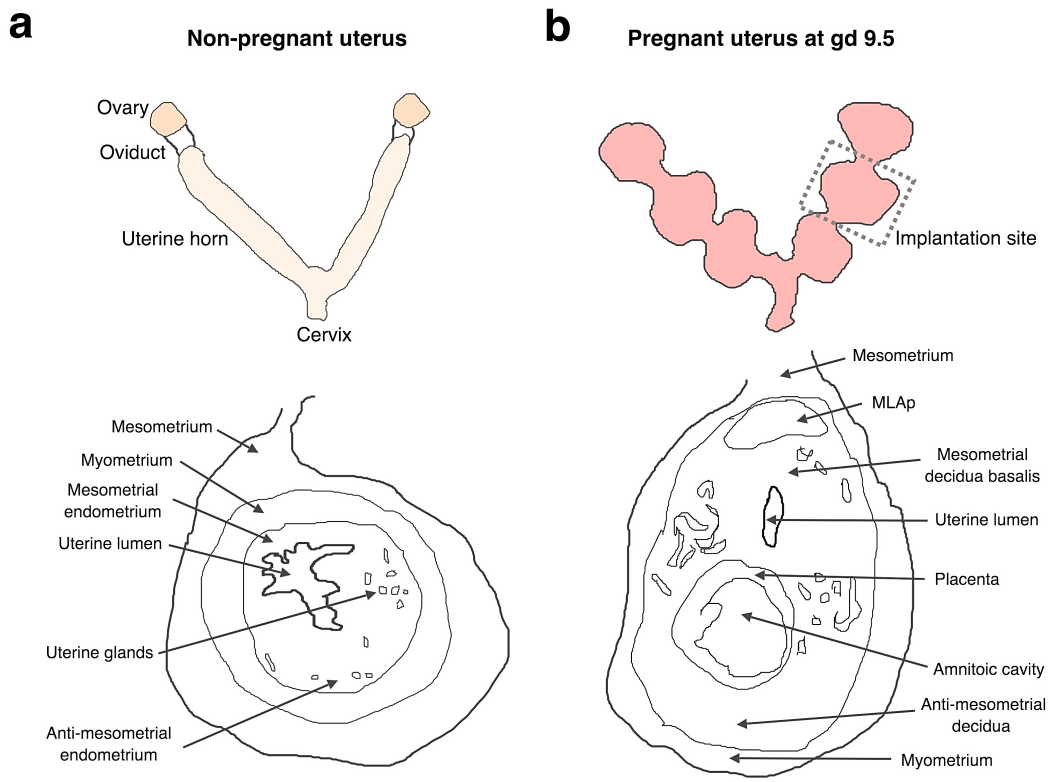

Figure 1.8. Comparison of the uterine structures in the non-pregnant and pregnant mouse uterus. Illustration of the main differences in the structure of the uterus of (**a**) a non-pregnant sexually mature mouse and (**b**) a pregnant mouse at mid-gestation (gd 9.5), described in the text (section 1.1.3). MLAp: myometrial lymphoid aggregate of pregnancy, gd: gestational day.

Subsequent days will lead to a formation of the definitive chorioallantoic placenta, which in mice is also described as a labyrinthine placenta and is mature by around E10.5 and completely functional by E12.5. This type of placenta is the one in which all different trophoblast cell types are perfused by a network of channels through which the maternal blood circulates (Benirschke et al., 2012). At E12.5 (**Fig. 1.7**), this placenta consists of maternal decidua and two trophoblast zones: labyrinthine trophoblast/labyrinth (made up of two layers of syncytiotrophoblast) and the junctional zone (originating mainly from the EPC and consisting of the spongiotrophoblast, the TGCs and glycogen cells). This is different compared to the early, choriovitelline placenta (from E6-11) which consists mainly of the trophoblast giant cells and the yolk sac. The maternal component of the placenta, decidua,

initially starts developing anti-mesometrially with the implanting blastocyst but then shifts mesometrially to become the decidua basalis. Decidua is the dominant tissue at the implantation site between gd 4.5 and 8.5 but the anti-mesometrial decidua begins its regression at gd 8.5 (this thin layer is also termed a decidua parietalis), while the decidua basalis remains.

TGCs are very important in the process of placentation, because out of all the trophoblast cells in mouse, these are the most invasive ones which penetrate into the endometrial stroma and lead to the remodelling of the maternal blood vessels, a process essential for the proper functioning of the definitive placenta (Charalambous et al., 2012). This happens through a breakdown of the smooth muscle cells and displacement of the endothelial cells of the maternal spiral arteries (SA) (Woods et al., 2018). A peak of vascular remodelling can be observed at gd 12.5. Over the next several days, the placenta and the fetus develop further and grow in size, until between gd 19.5 and 20.5, a pregnant female (dam) gives birth to the litter. Recently, the first rodent to undergo cyclic endometrial shedding, *Acomys cahirinus* (spiny mouse), was described (Bellofiore et al., 2016). Further work has shown that these rodents have a cycle of variable length (8-9 days) with an average 3-day menses (a ratio similar to human cycle). Although there are several differences compared to the human menstrual cycle, this small, non-primate species remains an attractive model for reproductive biology studies and must be explored in future studies (Bellofiore et al., 2018).

1.1.4 Comparison of human and mouse reproduction

In humans, similarly to what was described for the mouse in previous section, the HPG axis is responsible for hormonal changes regulating the menstrual cycle, which can be described by both ovarian (changes in the follicles in the ovaries) and uterine (changes in the endometrium) cycle. Within the ovarian cycle, there is a follicular and a luteal phase, while

the menstrual cycle consists of menstruation, proliferative and secretory phase. It is therefore incorrect to refer to the term 'estrous cycle' when describing the reproductive physiology of higher primates, although they technically still exhibit a less noticeable estrus at the time of ovulation, which occurs between the follicular and luteal phase of the ovarian cycle. Each uterine cycle begins with the menstruation phase, day 1 represented by the start of the menstrual flow and with a length of 4.5-8 days and the entire cycle 24-38 days. This variation in the cycle length usually comes from a variability in the follicular phase length between women (Reavey et al., 2018). Prior to menstruation, FSH levels increase, and this trend continues throughout the follicular phase, to stimulate the maturation of the ovarian follicles (**Fig. 1.9**). Closer to the end of the follicular phase, these levels of FSH induce the proliferative phase of the uterine cycle, characterised by the proliferation of endometrial cells in response to estradiol produced by the aromatase from follicle cells.

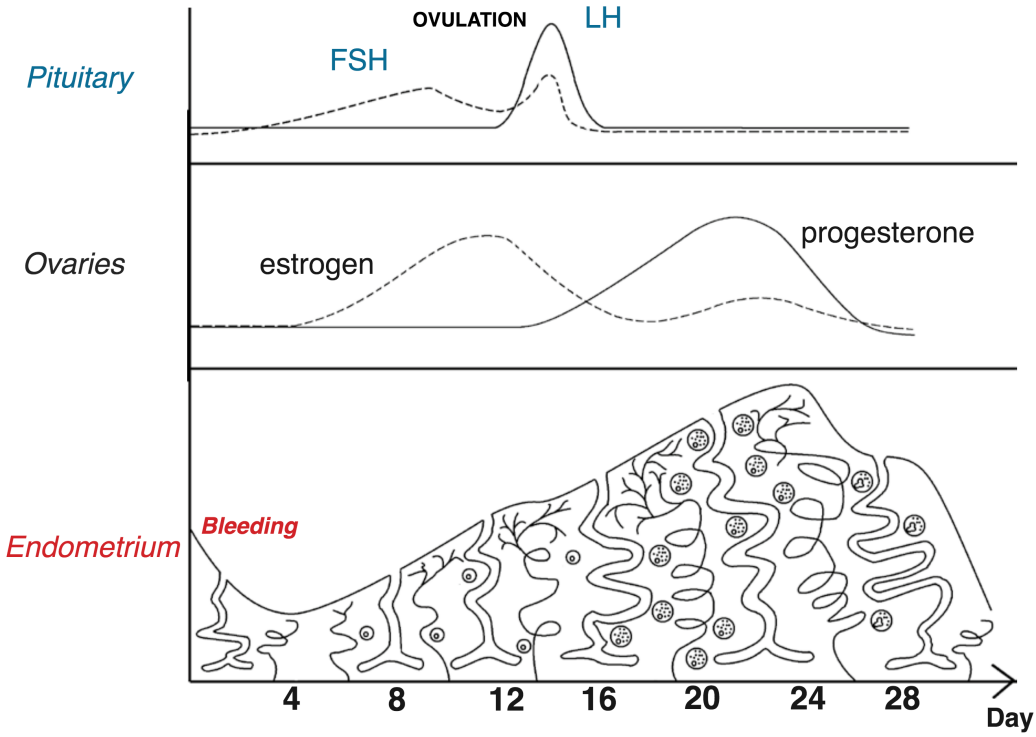

Figure 1.9. Overview of the normal menstrual cycle. Relevant details are explained in text (section 1.1.4). Adapted from Moffett and Male, 2009. FSH: follicle-stimulating hormone, LH: luteinising hormone.

In a similar manner, LH starts increasing during the follicular phase, surges right in between the proliferative and secretory stage of the cycle through a positive feedback mechanism similar to the one seen in a rodent estrous cycle and leads to the ovulation. Again, similarly to mice, the secretory phase is dominated by progesterone secreted by the CL, which inhibits FSH and LH secretion and this eventually leads to the demise of the CL. This reduction in local progesterone concentration will lead to the shedding of the endometrium and also release the inhibition of FSH and LH allowing the entrance to another cycle. If fertilisation occurs, the CL will not regress and menstruation will not take place as the high progesterone levels will remain, allowing for the gestation to begin. The main difference between rodents and higher primates, including humans, is that in humans there is no need for an implanting blastocyst to trigger the decidualisation reaction (Rossant & Tam, 2017). The endometrium undergoes transformation spontaneously into a decidua during each cycle in preparation for a potential implantation. Human decidua consists of two regions, a decidua basalis which is in direct contact with the invasive trophoblast and decidua parietalis which is interacting with the chorionic fetal trophoblasts (Tilburgs et al., 2006).

If fertilisation occurs, the blastocyst will implant into already receptive transformed maternal decidual tissue and this happens about 6 days post-conception. In humans, the placenta is of a villous type. Whether a placenta is labyrinthine, like previously discussed for rodents, or villous, is tightly connected to the placental shapes described in section 1.1.2. A reduced surface area of the chorionic sac where the maternal-fetal interdigitations take place in formation of the maternal-fetal interface means that these interdigitations have to be organised in a way that maximises the output of the surface area available. Villous placenta, found in higher primates and ruminants, forms a tree-like branching extensions and folds of the chorion (‘villi’), which are directly surrounded by the maternal blood. Therefore, the placental villi are analogous to the mouse labyrinth (Woods et al., 2018). Invasion of human

trophoblast cells occurs during the first trimester of pregnancy in humans, unlike for mice where it takes place during the entire first half of gestation. In both human and mouse, trophoblast cells that are in direct contact with the maternal blood are syncytial, but unlike mice, humans have only one layer of syncytiotrophoblast (Woods et al., 2018). The cells of trophoblast lineage which are analogues of TGCs in mouse are called extravillous trophoblast cells (EVTs) and they will erode through the decidual stroma and along the arteries against the flow of blood. One important difference between mice and humans is the level of trophoblast invasion: trophoblast invades much deeper into the human uterus, reaching into the myometrium, while the invasion in a mouse uterus stops in the decidua basalis formed from the endometrium (Georgiades et al., 2002; Ratsep et al., 2014).

In both human and mouse, the remodelling of the maternal blood vessels is as an essential event during placentation because this is what ultimately allows the 'hemotrophic' nutrition through the exchange between the maternal and fetal circulation, which is one of the main functions of the placenta. Prior to that, 'histiotrophic' nutrition via the uterine glands is essential for the human fetal development and represents the main resource for the first 12 weeks of human gestation (Burton et al., 2002). The differences between mouse and human placentation and cycling can be found summarised in **Table 1.1**.

Feature	***Mouse***	***Human***
Placentation	Haemochorial	Haemochorial
Placenta shape	Discoid	Discoid
Maternal-fetal interdigitations	Labyrinthine	Villous
Gestation length	19.5 – 20.5 days	280 days (approximately 40 weeks)
Cycle type	Estrous (around 4 days)	Menstrual (24-38 days)
Decidualisation trigger	Implanting blastocyst, post-implantation	Every cycle (depending on the progesterone levels), pre-implantation
Placenta functional	From gd 10.5	From 10 weeks post-conception

Table 1.1. Comparison of the placentation and cycling between humans and mice.

1.2 Immunology of the maternal-fetal interface

Various populations of immune cells have been identified in the FRT. Haematopoiesis is the process of formation of the blood cells and all blood lineage cells originate from a haematopoietic stem cell (HSC), but the microenvironment in which the HSC will develop (its haematopoietic niche) changes during the development. For example, in the adult mice, the primary site of the haematopoiesis is a bone marrow (BM), which becomes an additional haematopoietic niche only at E17.5 when the first functional HSCs are found in the long bones, and it is thought that these HSCs generate all haematopoietic lineages in adults. However, this is not the first site where HSCs originate during the embryonic development – four other compartments are involved in differentiation of the HSCs during the embryonic development and these are the yolk sac, aorta-gonad-mesonephros region (AGM), placenta and fetal liver (Mikkola, 2006). In the fetal liver, HSCs can be detected at E11.5 and reach their highest number around E15.5. Although not considered to be the major site of haematopoiesis in the embryo, AGM is the first site of the definitive HSCs at E10.5. A relatively low number of HSCs can be found in the AGM region at this point (Cumano et al., 1996), which could not explain rapid expansion of the HSCs in the fetal liver a few days later (Gekas et al., 2005). This led to a discovery that, compared to the AGM, the placenta also exhibits HSC activity and to a much larger extent (Ottersbach & Dzierzak, 2005). HSCs are suspected to be recruited to the fetal liver from placenta via umbilical veins at a similar time when they can first be detected in the fetal liver (E11.5), because HSCs found in placenta have a similar surface phenotype to those in the fetal liver, although the first phase of seeding of the fetal liver with HSCs is observed around E9.5. At this stage seeding presumably occurs from the yolk sac where haematopoiesis originally starts in mouse around E7.0. Since the yolk sac cannot support the proliferation and differentiation of the definitive progenitors,

these progenitors are carried out via the vitelline veins to the fetal liver (Gekas et al., 2005) (**Fig. 1.10**).

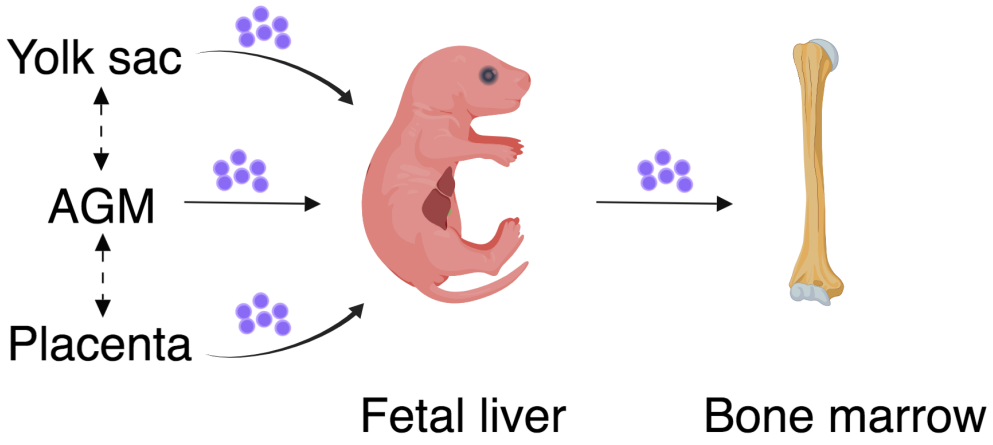

Figure 1.10. Sites of haematopoiesis during the embryonic and adult life. Illustration of the main sites of haematopoiesis at the fetal stage before the bone marrow takes over and as explained in text (section 1.2). Purple cells represent an illustration of the haematopoietic stem cells. AGM: aorta-gonad-mesonephros.

When considering the yolk sac haematopoiesis, it is important to note that despite a high level of functional conservation between mice and humans (Cindrova-Davies et al., 2017), human secondary yolk sac starts regressing closer to the end of the first trimester, while the one in mouse is active throughout the entire pregnancy (Palis & Yoder, 2001). Recent evidence, however, has demonstrated that some immune cell lineages, such as certain tissue-resident mast cells and macrophages, are generated from the yolk sac progenitors and gradually replaced by the definitive BM-derived mast cells (Gentek et al,. 2018), challenging the current dogma and suggesting a dual developmental origin of distinct tissue-resident immune cells (Guilliams & Scott, 2017).

Regardless of where the differentiation pathway occurs, the multipotent HSC has two possible fates: to commit to either a myeloid or a lymphoid lineage, via differentiation through either a common myeloid progenitor (CMP) or a common lymphoid progenitor

(CLP), respectively. Immune cells of both lineages can be identified in both human and mouse maternal-fetal interfaces and contribute to their homeostasis in unique ways.
While systematic mapping of all the immune cells present at the maternal-fetal interface in mouse is lacking at the moment, a vast amount of data has been generated on the immune cells at the maternal-fetal interface in the first trimester of human pregnancy. These are predominantly natural killer (NK) cells (around 70% of all immune cells), followed by macrophages (representing 20%) as well as about 10% T cells. B cells, dendritic cells (DCs) and granulocytes were identified in previous studies, but found to be rare (Erlebacher, 2013; Trundley & Moffett, 2004; Bulmer et al., 2010).

1.2.1 Myeloid cells at the maternal-fetal interface

1.2.1.1 Dendritic cells

Dendritic cells (DCs) belong to a group of myeloid cells also known as the professional antigen-presenting cells (APCs). This means that they can engulf antigens through a process of phagocytosis, traffic to a relevant lymph node (LN) where they undergo necessary maturation steps, and once mature, present an antigenic peptide within major histocompatibility complex (MHC) molecules to T cell-receptor (TCR) on a surface of the T cell. This is also known as the 'first signal', but mature DCs also provide a second, costimulatory signal that is required for the T cell to acquire its effector function (McGovern et al., 2015; Schuijs et al., 2018; Eisenbarth, 2018). DCs have always intrigued reproductive immunologists because of the assumption that fetally-derived trophoblast alloantigens would trigger a T cell-response. Moreover, one would expect DCs to be processing these alloantigens, similarly to their function in respiratory or intestinal tissues. The first study of human decidual DCs showed that although some cells were present in the first trimester decidua (just under 2 % of all immune cells), they displayed an immature phenotype, as

lineage negative, $CD11c^{+}HLA\text{-}DR^{+}DC\text{-}SIGN^{-}DEC\text{-}205^{+}CD40^{+}$ cells (Gardner & Moffett, 2003). Later work performed in mouse offered an explanation for why the decidual DCs were immature: decidualisation trapped DCs within the uterus and they were not able to reach the draining LNs (Collins et al., 2009). Therefore, a prohibition of DC migration in pregnant uterus and a subsequent lack of antigen presentation has been established as a model of how pathological T cell activation during pregnancy induced by alloantigens is avoided. Alternative roles, such as trophic functions during artery remodelling via crosstalk with NK cells, were proposed for DCs despite evidence that alymphoid mice can still have a normal decidualisation reaction (Tagliani et al., 2011). Nevertheless, DCs remain a hot topic in light of the phenotype exhibited by an inducible DC knockout mouse (CD11c-diphteria toxin receptor DTR), characterised by a severe impairment in implantation and embryo resorption (Plaks et al., 2008). Recently, one research group used multicolour flow cytometry and computational methods to follow the dynamics of various subsets of DCs throughout mouse gestation, and while confirming that plasmacytoid DCs are absent from the decidua and almost no CD4+ T cells present, they observed a very significant increase in myeloid DCs numbers early in pregnancy (Li et al., 2018).

1.2.1.2 Macrophages

Macrophages are another subset of APCs and represent a typical example of tissue-resident cells. They can be influenced by the environment to become functionally 'polarised' towards distinct functions, and therefore they are commonly described as either M1 or M2 macrophages (a parallel with Th1/Th2 responses from distinct effector T cells). M1 macrophages are induced by pro-inflammatory cytokines and develop further the pro-inflammatory state through the secretion of pro-inflammatory cytokines such as tumour necrosis factor (TNF) and other typically Th1 cytokines. On the other hand, M2 polarisation

is induced by Th2-type cytokines, such as IL-13, IL-4 and IL-5 and leads to an anti-inflammatory, suppressive macrophage phenotype (Nagamatsu & Schust, 2010). M2 macrophages are usually associated with tissue-remodelling properties and high production of IL-10 as well as scavengers of apoptotic cells. In the decidua they constitute up to 20 % of all $CD45^+$ immune cells. In vitro macrophage differentiation models demonstrated that macrophage colony-stimulating factor (M-CSF) and IL-10 may be instrumental in polarisation of the decidual macrophages towards M2 (anti-inflammatory) type, as they expressed surface markers such as CD206, CD209 and CD163 (Svensson et al., 2011) and there is some evidence that DNA methylation patterns are responsible for this, because genes responsible for M1 phenotype were hypermethylated and genes encoding the alternative activation (M2) hypomethylated (Kim et al., 2012). Another study has clarified that this decidual subset is also characterised by a low expression of CD11c and that it is predominantly involved in interactions with extracellular matrix (ECM), but also demonstrated that there is an additional subset of CD11c-high decidual macrophages which had a pro-inflammatory transcriptome and a higher capacity of processing antigens compared to CD11c-low. This study highlighted that decidual macrophages cannot conform to traditional M1/M2 designations because it showed that both CD11c-low and CD11c-high could produce both pro- and anti-inflammatory cytokines (Houser et al., 2011). One of the proposed roles of macrophages at the maternal-fetal interface is that, through secretion of proteases, angiogenic growth factors and a range of cytokines, they mediate the SA remodelling together with the EVT and uterine NK cells, but this study looked at all macrophages by staining for $CD14^+$ only and did not differentiate between CD11c-low and high subsets (Lash et al., 2016). In mouse, decidual macrophages were shown to localise in the vicinity of the trophoblast but also that during the estrous cycle, their numbers and

localisation change was dependant on the hormonal status (De & Wood, 1989; Helige et al., 2013).

1.2.1.3 Granulocytes

Similarly to majority of other seminal studies in the field of reproductive immunology, granulocytes were originally assessed by measurements in the peripheral blood, or in some cases, by examining the lower reproductive tract where it was demonstrated that exposure to sperm dramatically increases the numbers of neutrophils in the human cervical mucosa, representing the major leukocyte subset in this setting (Thompson et al., 1992), something that was later shown to be a consequence of a postcoital inflammatory response and exposure to the seminal fluid (Sharkey et al., 2012). Only more recent studies have started focusing on granulocytes at the maternal-fetal interface and there is recent evidence that CXCL9-producing neutrophils can be recruited to the mouse decidua during a prenatal infection with *Listeria monocytogenes*, contributing to the fetal demise through recruitment of CXCR3-expressing $CD8^+$ T cells. Blocking this CXCL9 receptor by using the CXCR3-neutralising antibody protected against fetal resorption (Chaturvedi et al., 2015). Second-trimester decidual neutrophils were shown to express a higher levels of factors related to blood vessel remodelling compared to peripheral blood neutrophils, potentially induced by CXCL8 (Amsalem et al., 2014) and suggesting a role in the uterine SA remodelling. Another group suggested a similar, but indirect role for human neutrophils, as they demonstrated that progesterone- and estriol-stimulated neutrophils induced proangiogenic $CD4^+$ T cells, and a non-redundant role of these interactions through the use of neutrophil-specific KO mouse (Nadkarni et al., 2016). Finally, decidual neutrophils may also be involved in crosstalk with another decidual subset in the first trimester, innate lymphoid cells (ILC3s). They localise closely together and CXCL8 and granulocyte-macrophage CSF (GM-CSF), produced by

ILC3s, induced migration, survival and production of factors by decidual neutrophils necessary for neoangiogenesis and blastocyst implantation (Croxatto et al., 2016).

There is no evidence on the role of other granulocytes, such as eosinophils and basophils, and their involvement in the Th2-like immune response at the maternal-fetal interface. However, mast cells (MCs) have been characterised in the decidua in recent years, especially in mouse models. Combined MC- and NK cell-deficiency was associated with almost complete absence of the SA remodelling and severe fetal growth restriction. On the other hand, individual knockouts (just MC or NK cells) had only minor impairment of the SA remodelling and a higher number of the other cell that has not been knocked out, suggesting compensatory mechanisms between the two cell types (Meyer et al. 2017a; Meyer et al., 2017b). Only one study so far has looked for mast cells in the human uterus and proposed the existence of three subsets of MCs in the endometrium, all expressing steroid receptors and suggesting dynamic regulation by the microenvironment (De Leo et al., 2017). Most recent data coming from a single-cell RNA sequencing of the human maternal-fetal interface in first trimester pregnancy samples did not demonstrate presence of any mast cells in the first trimester decidua (Vento-Tormo et al., 2018).

1.2.2 Lymphoid cells at the maternal-fetal interface

1.2.2.1 Adaptive immunity

There is conflicting evidence on the involvement of B cells in the uterus. This is because the majority of the literature on the B cells during pregnancy describes findings based on the assessment of human B cells in the peripheral blood (Lima et al., 2016). The studies that analysed B cells in the human endometrium or decidua found only a few or no B cells in these tissues (Trundley & Moffett, 2004; Moffett & Shreeve, 2015). In contrast to this recently it was shown that human decidua contains between 1-2.5 % of B cells in late

gestation and that in pre-term labour, these B cells were functionally perturbed, acquiring more B-1-like phenotype (Huang et al., 2016). This was in support of earlier work that detected B cells of similar phenotype in preeclamptic placentas, while acknowledging that there were no B cells in the healthy placentas (Jensen et al., 2012). In addition, cytokine IL-33 was shown to induce a production of PIBF1 by the decidual B cells, a factor shown to be essential in ensuring term labour by the use of B cell-deficient mice, especially in an inflammatory setting (Huang et al., 2016).

However, more work has to be done to understand fully whether B cells are indeed important for the physiology of the uterus, particularly in mouse, as there is currently no substantial evidence on involvement of B cells in mouse pregnancy, although there are reports suggesting pregnancy-related changes, for example in the BM, LN, and spleen B cell numbers and maturity (Muzzio et al., 2014). *EBF1*, encoding early B-cell factor 1, is involved in the B cell development and there is evidence that variants in *EBF1* are significantly associated genome-wide with preterm birth (Zhang et al., 2017). In the aforementioned single-cell RNA sequencing study of the entire human maternal-fetal interface in first trimester of pregnancy the presence of B cells in the human decidua was not investigated since $CD19^+$ cells were excluded at the sorting stage based on the previous literature (Vento-Tormo et al., 2018) and therefore no conclusions could be drawn.
On the other hand, uterine T cells have intrigued immunologists ever since Peter Medawar had first proposed the immunological paradox of pregnancy as explained in section 1.1.1 (Medawar, 1953). This led immunologists to often compare the immunology of reproduction to the transplantation immunology and to hypothesise that the suppression of the maternal T cells (maternal tolerance) is the main reason why a mother does not ‘reject the fetus’ and that the T cells are essential regulators of the trophoblast invasion. Because of the anatomy of the

maternal-fetal interface this is unlikely to be an important interaction regulating complex events leading up to a successful pregnancy. Two types of interactions occur here: (1) maternal blood contacts directly the syncytiotrophoblast, which does not express any MHC molecules and therefore cannot deliver a conventional T cell stimulus and (2) decidua interacts with the EVTs which only express human leukocyte antigens (HLA) HLA-G, HLA-E and polymorphic HLA-C (all belonging to MHC class I molecules) (Trundley & Moffett, 2004).

Out of T cells at the maternal-fetal interface (10-20 % of all $CD45^+$ cells in human), less than half are $CD4^+$ T cells, while 45-75% are $CD8^+$ T cells (Erlebacher, 2013). $CD8^+$ T cells are also called cytotoxic T cells (CTLs) and as granular cytolytic cells they resemble NK cells morphologically and functionally. In addition to the NK cells, they are the only other cells in the decidua that can potentially recognise fetally derived MHC class I on the EVTs as foreign, leading to them fulfilling their effector functions. This is, however unlikely to be the case, because it was shown that (1) direct allorecognition does not occur and (2) indirect allorecognition occurs, but $CD8^+$ T cells that can indirectly recognise fetal antigens undergo clonal deletion (Erlebacher et al., 2007) because they cannot be primed due to entrapment of DCs within the uterus (described in more detail in the section 1.2.1.1, (Collins et al., 2009)). Impaired accumulation of $CD8^+$ T cells was in part also explained by the epigenetic silencing of T cell chemoattractants produced by the decidual stromal cells (Nancy et al., 2012).

Within the $CD4^+$ T cells in mouse uterus, the majority of cells belongs to the $CD4^+CD25^+$ regulatory T cells (Tregs) (Guerin et al., 2011). A pool of these cells was shown to expand during gestation in an alloantigen-independent manner, since they increased in percentages in both syngeneic and allogeneic pregnancies. Additionally, neutralising $CD25^+$ Tregs led to fetal demise (Aluvihare et al., 2004). In human pregnancy, an association was made between HLA-C and the Treg pool. HLA-C mismatched pregnancies had a higher percentage of

$CD25^{dim}$ activated T cells as well functional $CD25^{bright}$ Tregs, suggesting that HLA-C specifically activates decidual T cells and increases Treg proportion (Tilburgs et al., 2009). Mouse studies have demonstrated that fetal-specific Tregs were maintained even after delivery, preserving tolerance to a fetal antigen they previously encountered and proliferating in a subsequent gestation (Rowe et al., 2012). This provides evidence that there might be a regulatory memory of the fetal antigen imprinted during pregnancy on the $CD4^+$ Tregs. FOXP3 is a transcription factor (TF) essential for the differentiation of Tregs and only in allogeneic matings it was shown that the percentage of these $FOXP3^+$ Tregs was significantly increased. This suggested that trophoblast-specific Tregs may home to the uterus (Samstein et al., 2012).

Most recent single-cell RNA sequencing study of the maternal-fetal interface of the first trimester maternal-fetal interface has shown the expansion of $CD8^+$ T cells in the decidua and suggested indirect regulation of trophoblast invasion through interactions of these T cells with myeloid, NK and stromal cells, rather than a direct and exclusive interaction with the trophoblast (Vento-Tormo et al., 2018).

1.2.2.2 Innate lymphoid cells

One of the major advances in the field of innate immunity was made in mid-1970s, when the NK cells were first described as large granular lymphocytes through observation of high background lysis of YAC-1 tumour cells incubated with mouse splenocytes. Today it is well established that NK cells are members of a much larger family of innate cells, collectively known as innate lymphoid cells (ILCs). ILCs represent innate counterparts of T cells, however with several notable differences. None of the ILCs express antigen-specific receptors (such as TCRs and BCRs) and therefore do not rely on somatic gene rearrangement for their receptor repertoire. ILCs also do not rely on clonal expansion of cells with a specific

antigen receptor. Based on the TFs and cytokines essential for their development as well as their effector cytokines, ILCs are further classified into subsets (**Fig. 1.11**). Until recently, three major groups of ILCs were recognised.

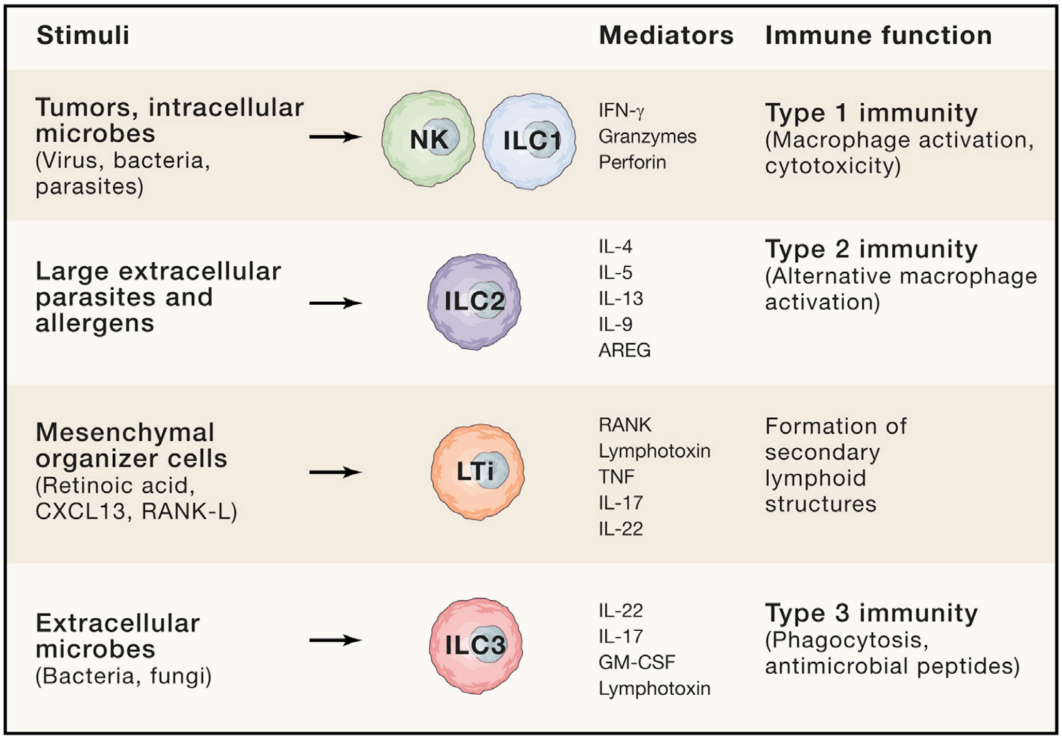

Figure 1.11. Innate lymphoid cell subsets. Illustration of the main subsets of ILCs as explained in text (section 1.2.2.2). Adapted from Vivier *et al.*, 2018.

These include ILC1s, which require T-bet for their development and produce IFN-γ as their effector cytokine. According to this nomenclature, NK cells belong to the ILC1 group as the cytotoxic ILC1s, while all the other ILC1s are designated as helper ILC1s. In mice, these subsets have in common expression of natural cytotoxicity receptors (NCRs) NK1.1 and NKp46 and the TF T-bet. NK cells and helper ILC1s can be distinguished based on expression of TF Eomesodermin (Eomes) and specific surface markers. NK cells express and rely on Eomes for their development. Helper ILC1s do not. The second major group, ILC2s, require GATA-3 TF and these cells are major producers of IL-4, IL-5 and IL-13. The third group, ILC3s, express TFs RORγt and aryl hydrocarbon receptor (AHR) and secrete type 3

cytokines, such as IL-17, IL-22 and IL-23. They consist of three subsets, NCR^- ILC3s, NCR^+ILC3s and lymphoid-tissue inducer (LTi) cells. However, with the accumulation of data obtained through transcriptome studies and fate-mapping over the last decade, new nomenclature which describes 5 ILC subsets was proposed (Vivier et al., 2018) and approved by the International Union of Immunological Societies (IUIS). According to this new nomenclature, NK cells and LTi cells are sufficiently distant during their development from ILC1s and ILC3s, respectively, to be considered distinct lineages, in addition to ILC1, ILC2 and ILC3s. While ILCs are also described as circulating cells in blood, they constitute a small fraction of total blood leukocytes. On the contrary, ILCs are usually described as tissue-resident immune cells, found in lymphoid and non-lymphoid organs, where they mainly populate mucosal surfaces. They are found in both primary lymphoid tissues including bone marrow and thymus, as well as in the secondary lymphoid tissues (SLTs); tonsil, spleen, LNs and Peyer's Patches of the intestine. Moreover they have been characterised in the following non-lymphoid tissues: skin, liver, intestine, gingival tissue, salivary glands, uterus (Bernink et al., 2013; Sojka et al., 2014; Cortez et al., 2016; Kindstedt et al., 2018; Brown et al., 2018). Interestingly, they are observed in fluids other than blood, such as in the breast milk, with potential implications on neonatal immunity (Baban et al., 2018), as well as in the synovial fluid of patients with juvenile idiopathic arthritis (Velasco-Herrera et al., 2018). A timeline of main discoveries in the ILC biology, as well as whether they were first identified in humans or mice is summarised in **Fig. 1.12**. Uterine NK cells are also displayed in this figure and the reason behind this will be explained in section 1.2.2.9.

ILCs are involved in a range of functions such as regulating tissue homeostasis, providing innate protection against intracellular parasites or involved in responses to chronic inflammatory diseases (Tait Wojno & Artis, 2016).

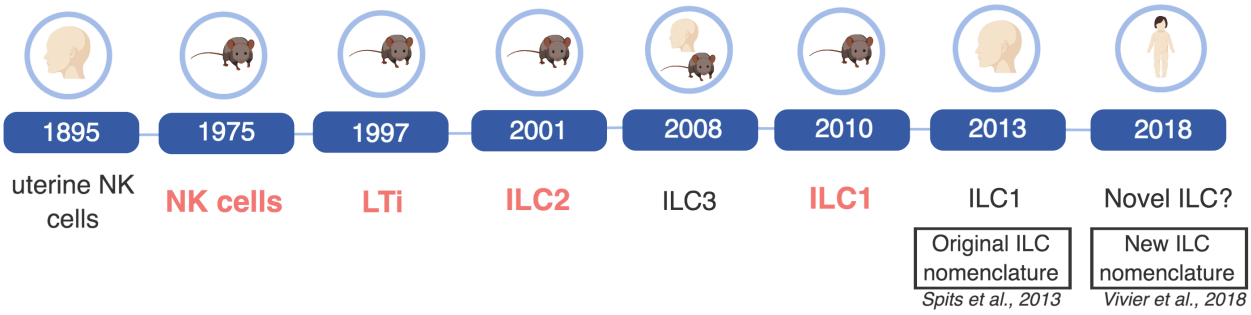

Figure 1.12. Timeline of the main discoveries in the ILC biology. Summary of the main events that led to the discovery of the various subsets of the innate lymphoid cells, as described in the text (sections 1.2.2.2-1.2.2.7). Uterine NK cells are represented in this figure because that was the year they were first observed and to illustrate that they were first ILCs to have been identified, although at that time they were not termed NK cells (explained in section 1.2.2.9). LTi: lymphoid-tissue inducer, NK: natural killer, ILC: innate lymphoid cell.

1.2.2.3 Innate lymphoid cell-centric view of the evolution: from Proteozoic to discovery

Precambrian era was marked by the appearance of primitive single cell organisms, and even though multicellular organisation did not take place for another 500 hundred million years, it was these single cell organisms that eventually led to the evolution of innate immunity. Domains Bacteria, Archea and Eukarya evolved so successfully during the Proteozoic that they changed the environment, fostering the metazoan development and marking the beginning of Paleozoic era through Cambrian Explosion about 550 million years ago. Explosion of new metazoan species provided a range of new hosts for pathogenic single cell organisms which subsequently led to evolution of the earliest form of defence, innate immune mechanisms, which relied on germline-encoded pattern recognition receptors. With the evolution of phylum Chordata, two different adaptive immune systems have evolved. Around 500 million years ago, with the appearance of subphylum Vertebrata, clonally expanded lymphocytes with somatic gene rearrangement appeared, allowing response to a specific antigen. Although this is a hallmark feature of jawed vertebrates of the infraphylum Gnathostomata, understanding of the immune system evolution was blurred by

the discovery of an alternative adaptive immune system that evolved in jawless vertebrates of the infraphylum Cyclostomata within vertebrates (hagfish and lamprey). Instead of V(D)J gene segment recombination used for assembling of T cell (TCR) and B cell receptors (BCR) in Gnathostomata, jawless vertebrates utilise variable leucine-rich repeats (LRR) to assemble variable lymphocyte receptors (VLRs) bound by an invariant stalk region to the lymphocyte surface (Pancer et al., 2004; Guo et al., 2009; Hirano et al., 2013). These two adaptive immune systems are presumed to have evolved separately in two infraphylums, because TCR, BCR and Major Histocompatibility Complex (MHC) genes were not identified in Cyclostomata and none of the VLR genes were identified in Gnathostomata (Mayer et al., 2002). Despite the breadth of knowledge on the evolution of the earliest innate immune mechanisms, followed by cellular and humoral arms of the immunity, it is still an enigma when the earliest Natural Killer cells have entered the evolutionary scene. There is, however, much more phylogenetic evidence available for NK cells than any other subset of innate lymphoid cells (ILCs). This is complicated further by the fact that NK cells, just like all other ILCs, are marked by features of both innate and adaptive immunity. Urochordates are the closest subphylum to vertebrates that undergo the transplantation reaction naturally. In a study analyzing the gene expression of a commonly used urochordate model (*Botryllus schlosseri*) during an allorecognition experiment, a subset of *Botryllus* blood cells expressed a human CD94/NKR-P1-related receptor, BsCD94-1 (Khalturin et al., 2003). NKR here and throughout the rest of the text stands for the Natural Killer cell Receptor. This suggested the existence of an ancestral population of NK cells in a non-vertebrate immune system, even though other studies have argued that while BsCD94-1 was without a doubt a group V C-type lectin, it was not an orthologue of the human CD94 protein (Sato et al., 2003). Within the non-mammalian vertebrates, receptors that are structurally related to mammalian killer cell immunoglobulin-like receptors (KIRs) and leukocyte immunoglobulin-like receptor (LILR)

receptors were identified in Osteyichties (bony fishes), but NK cell-like cytotoxic cells were also shown to exist in vertebrate groups: amphibians, reptiles and birds (Yoder & Litman, 2010). This suggests that there may have been an ancestral population of NK cells in a common ancestor of Cyclostomata and Gnathostomata but potentially also in a common ancestor in chordate subphylums Tunicata and Vertebrata. However, as illustrated by the example of the BsCD94-1 gene, it is still not completely clear when the NK cells appeared in the evolutionary history due to a lack of clear orthologue of NK-associated genes and more work will have to be done in the future studies to address this. These cells might have even evolved before placentation, which would prove important for understanding the immunology of reproduction. Identifying other cells of ILC family in other non-mammalian vertebrates and possibly urochordates will aid in reconstructing how these cells evolved (Vivier et al., 2016).

1.2.2.4 ILC2

A range of terms was used to describe the innate immune cells that produce type 2 cytokines over the years and that we now know under the term ILC2s: nuocytes (Neill et al., 2010), natural helper cells (Moro et al., 2010), innate type 2 helper cells (Price et al., 2010). They were an unexpected discovery of a study describing a novel cytokine produced by Th2 cells, IL-25. In wild-type mice, IL-25 treatment induced IL-4, IL-5 and IL-13 cytokines, which then augmented Th2-associated diseases. This was documented by striking histological changes in both lungs and GI tract, eosinophilia and splenomegaly. However, even $Rag^{-/-}$ mice (which are depleted of all T and B cells) exhibited the same pathological changes when treated with IL-25, demonstrating that there were cells other than T cells inducing the disease. At this early stage, they were characterised only as $lineage^{-}MHC\text{-}II^{+}CD11c^{-}$ (Fort et al., 2001). It was later shown that these IL-25-responding cells indeed are important

mediators of airway hyperreactivity and allergic disease via aforementioned induced cytokines, but principally, the mechanism of action involves IL-5 and IL-13 (Hurst et al., 2002). The cells were also named non-B/non-T (NBNT) cells, and shown to assist in worm expulsion during helminth infection (Fallon et al., 2006). Later work has phenotypically characterised ILC2s in more detail and it was shown that they respond to another type-2-inducing cytokine, IL-33, which causes rapid proliferation at various sites, including spleen, liver, intestines, mesenteric LNs and fat-associated lymphoid clusters –FALCs. These studies have described ILC2s as cells highly expressing IL-7 receptor (CD127), c-Kit, Thy1, ST2 (also known as IL1RL1) – a subunit of IL-33 receptor and Sca-1 (Ly6a) (Moro et al., 2010). A study published at the same time showed expression of IL17RB (IL-17 receptor B which is also a receptor for IL-25), thus revealing that ILC2s are poised to respond to both IL-33 and IL-25 directly. IL-13 was confirmed to be essential for clearance of helminth infection, because the adoptive transfer of IL-13-deficient ILC2s was not sufficient to facilitate the worm expulsion compared to wild-type ILC2s (Neill et al., 2010). It is important to note that all work on ILC2s described so far has been performed using mouse models. It was not until 2011 that the first report of human ILC2s was published. Mjösberg and colleagues described cells in the fetal and adult gut and lung, as well as in adult blood, and defined them as $CD127^{+}CD161^{+}$ cells that also express CRTH2, a chemoattractant receptor commonly expressed on Th2 cells, basophils and mast cells (Mjösberg et al., 2011). This work also showed that nasal polyps in chronic rhinosinusitis, a disease marked by type 2 inflammatory response, were enriched for ILC2s. ILC2s exist in the murine uterus (uILC2), which is not surprising considering that original research on ILC2s showed the highest levels of IL-25 mRNA in the uterus, in addition to the GI tract (Fort et al., 2001). In mouse, they can be found deep in the wall of the non-pregnant uterus and in the myometrium of the pregnant uterus at mid-gestation, with notable absence in the decidua. They can be identified within

CD11b$^-$NK1.1$^-$NKp46$^-$CD90.2$^+$ lineage negative uterine leukocytes as ST2 and GATA-3 positive cells (Doisne et al., 2015). Small populations of ILC2s are found within CD127$^{low/-}$ endometrial and decidual ILCs in humans (Balmas et al., 2018), although, as previously stated, they were not identified within the CD127^{high} ILCs in both mouse and human uterus (Doisne et al., 2015; Vacca et al., 2015).

1.2.2.5 ILC3

The first ILC3s to be described were LTi cells, first identified in 1997 as the CD4$^+$CD3$^-$ cells expressing lymphotoxin-β (LTβ). Interestingly, they were scattered throughout the LNs until 2 days post-birth when they would exhibit a specific spatial organisation in the cortical area of the LNs (Mebius et al., 1997), leading to the hypothesis that they might be involved in the initiation of lymphoid structures during ontogeny because they were observed in neonatal LNs. Additional studies have shown that these cells might also be important for inducing the organisation of Peyer's patches (Yoshida et al., 1999).

As mentioned earlier, RORγt has an essential role in the development of ILC3s and while this will be discussed in greater detail later, it is worth noting here that *Rorc* gene mouse mutants were instrumental in describing ILC3 subsets. Through analysis of *Rorc*(γt)-EGFP knock-in mouse, it became clear that in the fetus only LTi cells express RORγt and that when RORγt is deleted, LTi cells do not develop and LNs as well as Peyer's patches subsequently do not form (Eberl & Littman, 2004).

One of the first studies to define non-LTi ILC3s was performed in humans, unlike the majority of other ILC discoveries that were initially made in mouse models. Originally observed in human tonsils and Peyer's patches, they were named NK-22 cells because they co-expressed CD56 with the natural cytotoxicity receptor NKp44 and produced IL-22. They were also observed within NKp46$^+$NK1.1$^+$ fraction in mouse mucosal-associated lymphoid

tissues and lamina propria of the small intestine when bacterial infection was induced. Both mouse and human NK-22s were capable of response to IL-23 and expressed the surface chemokine receptor CCR6 (Cella et al., 2008). Even though this resembled Th17 responses, NK-22 cells were not able to secrete IL-17, were faster to respond to IL-23 and were not derived from blood NK cells when incubated with Th17-polarising cytokines, thus demonstrating that this was indeed a distinct lineage of cells (Cella et al., 2008).However, this and other work has shown that these cells are not capable of producing IFN-γ or expressing perforin, which are common features of NK cells (Satoh-Takayama et al., 2008; Sanos et al., 2008). Within the group 3 ILC, in addition to LTis, there are two clearly distinct subsets in mice, based on CCR6 expression: $CCR6^+$ ILC3s and $CCR6^-$ ILC3s. Moreover, $CCR6^-$ ILC3s can be either $NKp46^+$ or negative. In humans, CCR6 is instead expressed on the majority of ILC3s. Human ILC3s are therefore distinguished on the basis of NKp44 and there are $NKp44^+$ and $NKp44^-$ cells (Cupedo et al., 2008). For the vast majority of ILC3s in both human and mouse tissues, RORγt was found to be essential for development (Luci et al., 2008). Over the years, they have been given various names, such as NCR22 (Satoh-Takayama et al., 2010), before a uniform nomenclature was proposed in 2013 when all these cells were collectively named ILC3s (Spits et al., 2013). Just like ILC2s and the third big family, ILC1s (which will be explained in more detail in the next section), they populate the uterus (uILC3). In mouse, uILC3 can be identified within $CD11b^-NK1.1^-$ $CD90.2^+ROR\gamma t^+CD127^+$ lineage negative uterine leukocytes and similarly to ILC2s, in mouse they can only be found in the non-pregnant uterus and in myometrium at mid-gestation. uILC3s in mouse include two subsets, LTi-like and NCR^- uILC3s. NCR^+ ILC3s were not observed in the mouse uterus. In human uterus, however, ILC3s are present in both endometrium and decidua and the majority of cells belong to the NCR^+ILC3 subset, even

though LTi-like as well as very few NCR$^-$ILC3 cells were observed (Doisne et al., 2015; Vacca et al., 2015).

1.2.2.6 ILC1

ILC1s are the most extensively described group of ILCs. This is because Natural Killer cells, until recently included as members of ILC1 family, have been known for over forty years, longer than any other subset of ILCs. In this section, both NK cells and ILC1s will be described – NK cells as the 'cytotoxic' ILC1s and ILC1s as the 'helper/noncytotoxic' ILC1s. Helper ILC1s were originally discovered in a research study set up to determine whether RORγt and NKR expressing NK cells (in this study called NKR-LTi cells) described above (ILC3s) belong to the NK or LTi lineages. This work demonstrated the existence of mouse RORγt$^-$ NKR-LTi cells that were powerful IFNγ producers and inducers of innate colitis (Vonarbourg et al., 2010). Subsequently, the existence of ILC1s, for the first time termed 'ILC1s', was demonstrated in humans (Bernink et al., 2013), as cells distinct from conventional NK cells, that express T-bet, produce IFNγ and can be found in inflamed mucosal tissues. This work also suggested that ILC1s could develop from RORγt$^+$ ILC3s when stimulated with IL-12, adding to a growing body of evidence on plasticity between ILC3 and ILC1 subsets, which will be described in more detail in the section on the ILC development.

1.2.2.7 NK cells: discovery

Natural Killer cells were discovered just over forty-three years ago. First identified in mouse, they were named after an observation that there are naturally occurring cytotoxic, 'killer' cells in cell suspensions prepared from spleen, capable of lysing Moloney leukemia target cells (Kiessling et al., 1975a; Kiessling et al. 1975b). Kiessling and colleagues reported

several observations that laid foundations for future research into the NK cell biology in the following decades and that deserve a mention in this study:

(1) Natural Killer cells could rapidly kill target cells *in vitro* and *in vivo* (on average it took 4 hours to observe the lysis of target cells).
(2) Natural Killer cells exhibited differential cytotoxicity against different tumour cell lines.
(3) Natural Killer cells from mice of various origins and different wild-type strains were equally efficient at lysing target cells.
(4) Cytotoxicity may be mediated by the direct cell-cell contact because supernatants failed to induce cytotoxic activity.
(5) Splenic Natural Killer cells were the most efficient in lysis assays compared to other tissues cell isolates were prepared from.
(6) Animal age affected the cytotoxic potential of Natural Killer cells, with cells isolated from 3-week to 2-month-old mice showing increased lysis of target cells compared to younger (newborn) and older (6-month old) animals.
(7) Natural Killer cell cytotoxicity was responsible for majority of lysis observed and independent of other lymphocytes. Natural Killer cells isolated from spleens originating from nude mice, which lack T cells, as well as splenic cell suspensions depleted of T cells, B cells and phagocytic cells retained their capability of lysis without reduction compared to whole preparations of cells.

Another study from the same year supported the majority of Kiessling et al. findings with several minor exceptions, such as the observation that NK cells isolated from the LNs were more cytotoxic than the splenic NK cells, in contrast to what Kiessling et al. had previously showed (Herberman et al., 1975). However, both studies speculated that while this cytotoxicity was not dependent on antibodies, it may have been dependent on the

sensitisation with an antigen, presumably coming from murine leukemia viruses or endogenous type C-viruses which are ubiquitously distributed (Herberman et al., 1975). They further assumed that these latent infections become active later in the neonatal period, explaining in part significant reduction in target cells' lysis in cells isolated from newborn mice, when NK cells still have not been 'sensitised by viral antigens'.

1.2.2.8 NK cells perform their functions via engagement of surface receptors

NK cells are still known as the potent killer cells described forty years ago, but now it is established that they have a variety of other roles, such as in immunity to bacteria and viruses, responses during transplantation, autoimmunity, hypersensitivity and pregnancy (Croy et al., 2002; Vivier et al., 2008). They exhibit a wide range of functions by either modulating the immune system, e.g. regulating functions of the effector cells of adaptive immunity via secretion of cytokines, or by directly secreting cytotoxic proteins granzymes and perforin from their large cytotoxic granules which represent one of the most striking morphological properties of these killer cells (Krzewski & Strominger, 2008). NK cells do not rely on antigen-specific cell receptors for antigen recognition, similarly to other innate immune cells. At the same time their developmental origins, morphology and effector functions resemble the adaptive immunity, despite the lack of gene rearrangement and clonal distribution. NK cells therefore truly bridge the gap between the innate and adaptive immunity (Vivier et al., 2011). They do not require immunisation and sensitisation, which makes them 'natural' killers. Granularity is essential for NK cells and their function, as it is their degranulation and a subsequent release of granule contents what determines the level of the NK cytotoxicity. However, the other important component regulating NK cell function is the receptors expressed on its surface (NKRs) (Long et al., 2013; Chiossone et al., 2018), which regulate whether or not the degranulation will occur. NK cells in both humans and

mice express a non-polymorphic receptor FcγIII, also termed CD16. The most direct way of killing is by utilising CD16 receptor via antibody-dependent cellular cytotoxicity (ADCC). In ADCC, NK cells can bind the Fc portion of an antibody through CD16 which allows them to detect any cell that is opsonised by the antibodies and they can then kill it. Therefore, although NK cells are able to function independently of the adaptive immune system, B cells can utilise NK cells as killers if they produce the appropriate antibody that will interact with the CD16. Some other receptors that are non-polymorphic include NKp30, NKp44, NKp46 which are termed Natural Cytotoxicity Receptors (NCRs), NKG2D or receptors of the SLAM family such as 2B4 (CD244) (Long et al., 2013). This is far from an exhaustive list of receptors.

However, there is another way of how NK cells can differentiate self vs non-self and this is the regulation via array of germline-encoded inhibitory and activating receptors. Examples of these receptors are very polymorphic KIR receptors in humans and their analogues in mice, Ly49. The fine-tuning of these interactions is made even more complex by the fact that ligands for these receptors on NK cells, human leukocyte antigen (HLA/MHC-I) molecules and MHC-I molecules in mouse are also extensively polymorphic. Killing by NK cells is triggered immediately upon the detection of a pathogen by an APC (DC for example), which then will rapidly produce cytokines such as IL-12, IL-15 and IL-18. These cytokines act on NK cells in the vicinity and lower their threshold for activation (Long et al., 2013). NK cells represent the third major lymphocyte subset in the peripheral blood (PB) in humans, accounting for approximately 15% of the lymphocytes (Purdy & Campbell, 2009). In addition to these circulating, conventional NK (cNK) cells found in PB and spleen, they have been identified in many organs (thymus, liver, skin, salivary glands and uterus) where they regulate the physiology and represent main components of tissue-specific immunity. Tissue resident NKs (trNK) do not have the same phenotype in all of these tissues and they appear to

be dependent on different TFs for their development (Sojka et al., 2014). There are subtle differences between tissue resident NK cells which may point to different developmental pathways, or to distinct lineages of trNKs present in different organs. Although NK cells can recognise a range of antigens, they are utilising mechanisms slightly different compared to lymphocytes of the adaptive immune system. The killing machinery of CTLs and NK cells are very similar. Key difference is the lack of a TCR, since both CTLs and NKs can express KIRs and CD16. However, CTLs need to be engaged via TCR and costimulatory signal, while the NK cell needs the right shift in balance between inhibitory and activating receptors in its array of receptors. One more important difference is that NK receptors are germline encoded, while TCR genes are rearranged. Thus, the capacity to engage different targets comes from the fact that there is a range of inhibitory and activating receptors expressed that can be engaged without rearranging.

1.2.2.9 Uterine NK cells

It is due to the remarkable progress made by histologists that the study of uterine NK cells has begun. Uterine NK cells had been observed long before the scientific community became aware of the existence of conventional NK cells in 1975 (**Fig. 1.7**). Back in the 19th century, granulated cells were observed in the decidua (Marchand, 1895) and not long after, some investigators speculated for the first time that these decidual cells might be of lymphoid origin (Weill, 1921). In later years, observations were made about the existence of similar cells in the non-pregnant endometrium. One of the first names was the endometrial K-cells (short for Körnchenzellen, term originally coined by Hamperl and Hellweg in 1958). Around the similar time, Von Numers termed this peculiar type of cell ‘globular leukocytes’ (Von Numers, 1953). However, granularity was a prominent feature of these cells and continuously triggered the interest of researchers and often led them to compare to a subset of granulocytes, neutrophils. Therefore, it is not surprising that in following years, terms such as

‘endometrial granular cells’ (Kazzaz, 1972) remained in use. Only with the advent of monoclonal antibodies it became possible to look into the phenotype of the uterine granular cells in more detail. Gradually, it became clear that these are immune cells, derived from the bone marrow, with CD45 on the surface (Bulmer and Sunderland, 1984). Later work has led to the conclusion that these $CD45^{+}$ leukocytes are NK cells after positive expression of CD56 (King et al., 1989). This is also when the first reports of uterine NK cells in the rodents appeared, although in the beginning they were termed ‘granulated metrial gland cells’ (Peel, 1989).

Uterine NK (uNK) cells represent a dominant subset of lymphocytes in human and rodent uterus (Moffett & Colucci, 2014; Colucci, 2015; Doisne et al., 2015). The mouse is a good model system for studying uNKs as it relies on invasive haemochorial placentation to support the development of a growing embryo, similarly to higher order primates (Carter, 2012; Mori et al., 2016). uNK cells in murine pregnancy reach their maximal number at mid-gestation (gestational day (gd) 9.5-10.5). Their numbers dramatically reduce towards end of gestation (gd 18.5 and onwards). In humans, the endometrium is shed and regenerated with every menstrual cycle, but if the fertilisation has occured a number of histological changes takes place, influenced by change in progesterone levels. uNK cells are present in both endometrium and decidua, accounting for about 70% of decidual lymphocytes in humans and about 20-30% in mice (Moffett & Colucci, 2014). They remain the dominant immune cells in the first half of pregnancy. Human uNK cells are $CD56^{superbright}$ and $CD16^{-}$, unlike PB cytotoxic cNKs which are $CD56^{dim}CD16^{+}$ or $CD56^{bright}CD16^{-}$ (Koopman et al., 2003; Male et al., 2010). In humans, however, there is another subset of PB CD56-negative NKs. Using novel approaches of studying the proteome, such as LEGENDplex, it has been established that these cells are very similar to $CD56^{dim}$ cytotoxic NK cells, apart from several vesicle trafficking- and lytic granule secretion-related downregulated proteins. These features might

explain the reduced responsiveness of these cells, which are commonly found in HIV-1 and HCV patients (Voigt et al., 2018). As not all NK cells express CD56 in humans, it is very important that there are additional markers established for uNKs, such as CD9 (Moffett & Colucci, 2014). Although this is not the topic of this thesis, KIR receptors on the human uNKs are essential for the recognition of the HLA expressed on the trophoblast. Different combinations of KIR-HLA interactions can correlate with extremes of the obstetric dilemma: low birth weight correlates with preeclampsia and high birth weight with obstructed labor (Hiby et al., 2014; Moffett & Colucci, 2015; Kennedy et al., 2016).

Mouse uterine NK cells have traditionally been defined staining positive for *Dolichus biflorus* agglutinin (DBA) (Paffaro et al., 2003; Yadi et al., 2008). Only later it was discovered that there were two subsets of uNK cells, DBA^+ and DBA^- with different functional capabilities (Chen et al., 2012a). This will be discussed in more detail in Chapter 3. Alymphoid $Rag2^{-/-}Il2rg^{-/-}$ mice which lack all B cells, T cells, ILCs and NK cells as well as $IFN\gamma^{-/-}$ animals were unable to fully perform the modification of the spiral arteries at their implantation sites (Ashkar et al., 2000; Björkström et al., 2013), which pointed to an involvement of uNK cells in this process. Despite this failure in remodelling their spiral arteries, such knockout females were still fertile and had a normal litter size, but low fetal weight in each litter (Ashkar et al., 2000; Barber & Pollard, 2003). NK cells in humans and mice localise around spiral arteries (Moffett & Loke, 2006; Zhang et al., 2012).

Recently, trNK cell population has been defined within all murine uNKs and is distinguished from cNKs based on the expression of CD49a and DX5 (Doisne et al., 2015; Sojka et al., 2014). trNKs are the most abundant subset in the uterus of both virgin and pregnant female mice and they are $CD49a^+$ and $DX5^-$. In addition to this, trNK seem to be dependent on Eomes TF for development, which is a hallmark cNK TF. There are two more subsets identified in uterus: $CD49a^+Eomes^-$ which are designated as uterine ILC1 subset and also

CD49a^{-}Eomes^{+} cNKs. At the moment the lineage relationships between these 3 subsets are unknown. Together, they are termed uterine Group 1 ILCs (g1 ILCs). Uterine trNKs are similar to hepatic and salivary gland trNKs as they express CD49a and are E4bp4-independent, but unlike in liver and salivary glands, they are T-bet independent. However, they do depend on Eomes for their development, similarly to salivary gland NK cells (Sojka et al., 2014). In general, suggested by the currently available data, the main proposed role of the uterine NK cells in both humans and mice is regulation of the vascular remodelling of spiral arteries (Ashkar et al., 2000; Wilkens et al., 2013) as well as regulation of the trophoblast invasion (Hanna et al., 2006; Chakraborty et al., 2011). This is however complicated by the identification of new subsets and requires another assessment of each individual subset and its associated functions (Doisne et al., 2015).

1.2.2.10 Group 1 ILC development and plasticity

All ILCs develop from the CLP resident in BM, which can also give rise to B cells and T cells. Transcription factor TCF-1 will induce differentiation of an early innate lymphoid precursor (EILP) from CLP, and EILPs are able to give rise to both NK cells and ILC1s, through distinct developmental pathways (Yang et al., 2015). ILC1s develop from EILPs through another developmental intermediate, termed common helper-like innate lymphoid precursor (CHILP) in mouse, and characterised by expression of another TF, Id2. Not only can CHILP develop into ILC1s, but also the into ILC2s and ILC3s, and importantly, no NK cells develop from this precursor (Klose et al., 2014). This was confirmed through the use of mouse models that showed the requirement for Id2 in the development of ILCs (Seillet et al., 2016). Requirement for other TFs for the development of ILC1s has been shown through fate-mapping models for example, so although PLZF is not expressed in mature ILC1s, it is important in early stage of the development of ILC1s, ILC2s and ILC3s and PLZF^{+}

progenitors are downstream of Id2^{+} CHILPs (Constantinides et al., 2014; Constantinides et al., 2015) (**Fig. 1.13**). NFIL3 (also known as E4BP4) was initially described as a master regulator of the NK cell development (Gascoyne et al., 2009; Male et al., 2014); discussed below. Later work however showed that NFIL3 is also involved in the development of all the ILC lineages in the lung and gut (Seillet et al., 2014; Geiger et al., 2014), through regulating directly the development of Id2^{+}PLZF^{+} CHILPs (Xu et al. ,2015). Moreover, Nfil3$^{-/-}$ mice lack CHILPs, suggesting that NFIL3 is essential for maintaining the earliest ILC progenitors (Yu et al., 2014; Cortez & Colonna, 2016). ILC1s in mice are CD127^{+} and depend on T-bet for their development, but not on Eomes. They express CD127, which is IL-7 receptor and IL-7 is required for the ILC development. By contrast, intestinal ILC1s are instead dependent on IL-15, thus resembling NK cells (Klose et al., 2014).

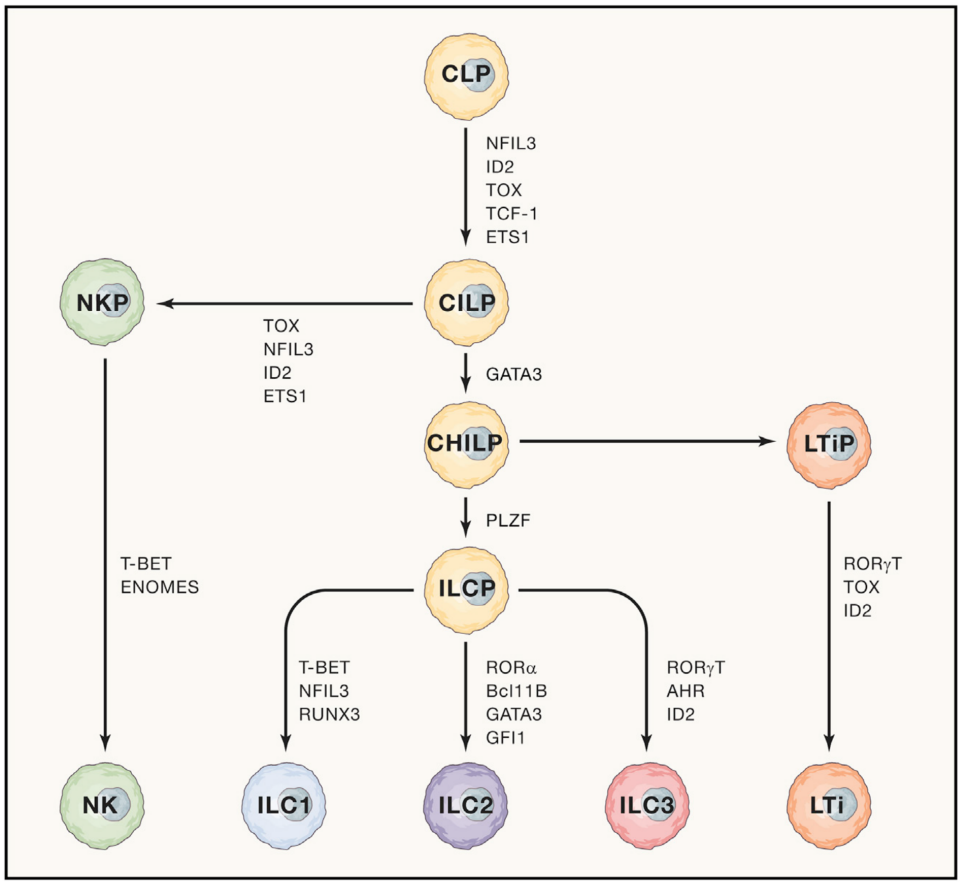

Figure 1.13. Innate lymphoid cell development. Illustration of the main ILC developmental pathways, as explained in text (section 1.2.2.10). Adapted from Vivier *et al.*, 2018.

Due to a distinct developmental pathway, NK cells are now considered a separate lineage from the ILC1s (Vivier et al., 2018). From the CLP and through the EILP, they develop via the NK cell progenitor (NKP). Further differentiation into a particular lineage is a result of a fine balance between activation and repression of essential TFs and cytokines (Male & Brady, 2014).

In the murine NK developmental pathway, CLP develops into two NK-committed progenitors, pre-NKPs, followed by refined NKPs (rNKPs) (Carotta et al., 2011; Fathman et al., 2011). rNKPs acquire NK1.1 which marks transition into immature NK cells (iNK), which further develop into mature NKs (mNK) with the acquisition of additional surface receptors. It is of importance to note that while NFIL3 was found to be essential for the development of NK cells in the BM (Gascoyne et al., 2009; Male et al., 2014), in some tissues this was not the case (Sojka et al., 2014). Additionally, NFIL3 is important for early stages of NK cell development, at the transition from the pre-NKP to rNKP stage, but it was not required for the development of all NK cell subsets. Specifically, $Nfil3^{-/-}$ animals infected with MCMV still had functional $Ly49H^{+}$ NK cells (discussed in more detail in the section 1.2.2.11) (Firth et al., 2013), but certain subsets persist in the uterus of these animals (Boulenouar et al., 2016). More recent work has demonstrated that NFIL3 directly regulated Notch1 gene expression, by rescuing the phenotype of NK deficiency in these animals through a short exposure to Notch peptide ligands (Kostrzewski et al., 2018).

It might be that Notch signalling, or possibly another target gene of NFIL3, is responsible for the NK cell development in the tissues where NK and ILC1 populations persist despite the lack of Nfil3 gene. Notch signalling was shown to regulate intrinsic levels of T-bet and Eomes expression using mouse models, by supressing Eomes in both cNK and ILC1, and to a higher extent in liver ILC1s compared to other analysed tissues (Chaves et al., 2018; Perchet

et al., 2018). This a similar principle to the one in salivary glands, where Eomes is supressed by TGF-β signalling, inducing the differentiation of ILC1s (Cortez et al., 2017).

Human NKPs have been elusive for a long time, but recently have been identified for the first time in a range of tissues, including fetal liver and adult tonsil (Renoux et al., 2015). Another study (Scoville et al., 2016) identified a RORγt^{+} progenitor of all human ILCs in the tonsils, a stage of the development that was previously dismissed due to mouse fate-mapping studies which failed to identify it (Klose et al., 2014).This is in contrast to previous reports showing that RORγt^{+} progenitors are ILC3-committed progenitors (Montaldo et al., 2014). In general, current knowledge on the NK development in humans (with the exception of (Renoux et al., 2015)) comes mainly from the studies on SLTs such as tonsils, where originally a five-stage development model was proposed, based on the differential expression of surface markers such as CD34, CD94, CD117 and CD16 (Freud et al., 2014). More recently, however, expression of a surface receptor NKp80 has allowed increased resolution of the NK development in the SLT because now stage 4 could be divided into distinct stages 4a and 4b: 4a were NKp80^{-} and could give rise to both NKs and ILC3-like cells, while 4b were NKp80^{+} and NK-restricted (giving rise to CD56^{bright} NK cells) (Freud et al., 2016) .This work was built upon by a discovery that there were CD34^{-}CD117^{+}CD56^{+} cells that gave rise to NK cells and ILC3s but not ILC2s, further suggesting a distinct developmental pathway for ILC2s in humans (Chen et al., 2018), unlike in mouse where CHILP was identified that gave rise to all ILCs (Klose et al., 2014). Elegantly executed single-cell culture assays enabled the discoveries summarised in this section. Future studies employing techniques such as single-cell RNA-sequencing (scRNA-seq) should define various progenitors in depth and dissect developmental pathways of distinct lineages.

Finally, there is a considerable plasticity between ILC3 and ILC1 subsets and within all ILC subsets altogether (Spits et al., 2016). It has been shown that under certain conditions, a

population of RORγt- and AHR-expressing ILC3s, NCR$^+$ILC3s (they express NCRs such as NKp44 and NKp46), can downregulate RORγt and upregulate T-bet and also start secreting IFN-γ, thus adopting ILC1 characteristics. These cells are termed 'ex-ILC3-ILC1s'. The existence of such a population suggests that the ILC3 lineage may be a transient step in the development of some NK cells and ILC1s. One of the mechanisms shown to regulate this process is AHR signalling. AHR is a ligand-activated TF which has been shown to regulate differentiation of many immune cells, including NCR$^+$ILC3s (Cella et al., 2010; Vonarbourg et al., 2010). Although not all endogenous ligands are known, it is well established that products of tryptophan metabolism upon exposure to light *in vitro* include agonist of AHR, 6-formylindolo[3,2-b]carbazole (FICZ). The same process takes place in skin cells upon exposure to UV-light. It has been shown that AHR signalling stimulation of NCR$^+$ILC3s in human tonsils ex vivo with FICZ agonist suppressed differentiation into NK cells and maintained ILC3 phenotype. Blocking AHR signalling with an antagonist, on the other hand, led to differentiation of fully mature NK cells (Hughes et al., 2014). However, other conditions, such as exposure to IL-12, were also found to induce production of IFN-γ by ILC3s and it was suggested that exposure to microbial flora is one of the reasons this switch takes place (Bernink et al., 2013). These cells have been implicated in colitis.

Cells largely overlapping with NCR$^+$ILC3s have also been identified in human PB and uterine mucosa and have been found to express *Rorc* and produce IL-22 while also giving rise to mature uNK cells (Male et al., 2010). There is even evidence for an essential role of Notch signalling in an ILC3/cNK progenitor identified in human PB, so only Notch signalling in combination with IL-7 led to NCR$^+$ILC3 differentiation in one type of progenitor, while it suppressed the IL-15 dependent cNK development in the same cell; mouse studies confirmed only the importance of Notch signalling in NCR$^+$ILC3s (Chea et al., 2016; Kyoizumi et al., 2017) . This makes the study of ILC1 and cNK differentiation more

complex but also demonstrates that the microenvironment (available cytokine milieu) might be essential in lineage decision-making. Further studies are necessary to investigate whether NCR^+ILC3s found in human uterus are developmental intermediates of uNK cells or a distinct lineage with a specific function in physiology of the uterus.

1.2.2.11 Adaptive/memory-like NK cells

Immune memory, or recall response, is one of the main features of the adaptive B and T cells. After encountering a specific antigen, these cells are able to mount a more powerful and rapid response upon secondary exposure to the same antigen and this is due to the engagement of their BCRs and TCRs, respectively, which display antigen-specificity. NK cells do not have such antigen-specific receptors and yet 'adaptive' or 'memory-like' NK cells have been described in recent years (O'Sullivan et al., 2015). In 2009, it was suggested for the first time that there may exist a subset of NK cells that exhibit features commonly associated with immune cells capable of developing immunological memory. This was shown in a mouse model of mouse cytomegalovirus infection (MCMV), where $Ly49H^+$ NK cells proliferate specifically in response to MCMV in spleen and liver, where they are long-lived, self-renewing cells (Sun et al., 2009). Some of the surface markers of these memory $Ly49H^+$ cells were KLRG1, CD43 and Ly6C, which were not expressed by other $Ly49H^+$ (naive) NK cells and upon adoptive transfer into naive animals, memory NK cells were protective when these animals were challenged by infection (Sun et al., 2009). IL-12 was shown to be indispensable for the maintenance of memory NK cells in mouse (Sun et al., 2012). Costimulation through other molecules, such as DNAM-1 was also shown to be essential for proliferation of the $Ly49H^+$ cells, as DNAM-1 knockout NK cells failed to differentiate into memory cells (Nabekura et al., 2014). Using five biologically and chemically distinct antigens, another group demonstrated the existence of memory NK cells in the liver. These cells (about 50 %

of NK cells in the liver) were characterised by surface expression of a receptor CXCR6 and this receptor was essential in retaining the memory NK cells in the liver through engagement with its chemokine, CXCL16, in liver sinusoids (Paust et al., 2010). In humans, another NK receptor, NKG2C, marks the adaptive NK cells (Gumá et al., 2006) and unlike the mouse analogues, they are not dependent on IL-12, but rather on IL-18 costimulation during the encounter with target cells in order to produce cytokines. This report also suggests that adaptive NK cells as a target cell sensing hub that can then recruit surrounding cells through augmented production of pro-inflammatory cytokines (Hammer et al., 2018).

It is important to note that epigenetic regulation might be essential for the maintenance of these 'memory' NK cells. A mouse study has demonstrated that MCMV-specific memory NK cells exhibited different chromatin accessibility state to other NK cells, but similar to MCMV $CD8^+$ T cells (Lau et al., 2018; Dulson et al., 2018).

1.3. In the clinic

1.3.1 The Great Obstetric Syndromes

The latest update of the International Statistical Classification of Diseases and Health Problems (ICD-11) published by the World Health Organisation (WHO) defines the perinatal period as a period of time between 22 completed weeks after fertilisation and 7 days post-partum. There are no gold standards for identifying conditions behind perinatal mortality and morbidity. Instead, clinical syndromes are the best indicators of these complications which can also cause maternal mortality. Fetal growth restriction (FGR), premature labor, premature rupture of membranes, pregnancy-induced hypertension and congenital anomalies are among the major causes of perinatal mortality and morbidity (Romero, 2009). FGR occurs when the fetus does not reach its expected size at a given gestational age and one of the best definitions of the condition is 'fetal growth that has failed to reach its genetically determined potential'

(Gaccioli et al., 2018). FGR is a major determinant of perinatal mortality and morbidity and yet the screening methods to detect the FGR have been far from sensitive enough to successfully diagnose small babies. An example of a proxy commonly used for FGR detection is 'small for gestational age' (SGA), referring to babies with birthweights below the 10th percentile for those at the same gestational age. It is important to make a distinction between FGR and SGA, because many SGA babies are born small but healthy (Gaccioli et al., 2017). FGR on the other hand, has been to shown to lead to chronic diseases later in life (Barker & Osmond, 1986; Cooper et al., 1997). Elegant and well executed recent work has suggested that applying well established ultrasound methods in FGR detection, in combination with placental biomarker measurements in mother's blood might improve the maternal and perinatal outcomes (Gaccioli et al., 2018), but placental biomarkers currently have no role in clinical practice.

Instead, in addition to the initial ultrasound screening, which will identify all babies that are SGA, more features are assessed to diagnose FGR. One of them is the middle cerebral artery (MCA) pulsatility index (PI), detected by Doppler sonography to identify brain-sparing as a consequence of the FGR. Brain-sparing is the phenomenon when the fetus adapts its circulation to maximise oxygen and nutrient supply to the brain (Cohen et al., 2015). Together with MCA-PI, ductus venosus and umbilical artery Doppler assessments are advocated under the current UK guidance (Mone et al., 2014).

Similarly to FGR, other diseases in obstetrics are defined by the clinical manifestations of the mother, rather than on the underlying mechanisms of the diseases (Romero et al., 2006). This led to the term Great Obstetric Syndromes (GOS) to be coined in order to better define the obstetrical diseases. Characteristics of the GOS are (1) multiple etiologies, (2) fetal involvement, (3) clinical symptoms which are adaptive in nature, (4) long preclinical stage and (5) potential interactions between the maternal/fetal genes and the environment (Romero

et al., 2006; Di Renzo, 2009). Such heterogeneity in the etiologies between various obstetrics syndromes showcases that more research is required to be able to predict disease outcomes with higher precision, and emphasis has been on identifying additional biomarkers that could be tested for in the clinic.

In conditions such as FGR, coexistence of other clinical syndromes in addition to the SGA, such as maternal preeclampsia, are much better indicators of an unhealthy manifestation of the SGA (Gaccioli et al., 2017) due to placental dysfunction as has been shown for the majority of FGR cases (Mifsud & Sebire, 2014). Defective deep placentation, characterised by the incomplete or non-existent transformation of the decidual and myometrial spiral arteries' segments, has been shown to be present in almost every GOS (Brosens et al., 2011). Better characterisation of spiral artery remodelling during the early stages of placental development therefore might offer an opportunity to identify women who may go on to develop GOS (Pijnenborg et al., 2006). While there is some evidence that immune cells at the maternal-fetal interface are involved in the regulation of SA remodelling, more research is required to identify the exact cellular interactions that support this process. Ultimately, these discoveries should guide future clinical practice.

1.3.2 Uterine NK cells: victims of the nomenclature

Although NK cells were first identified as cytotoxic cells capable of lysing tumour cells, this is not the case for uNK cells, as introduced earlier. When incubated with the same cancer cell lines as conventional peripheral blood NK (pbNK) cells, uNK cells were poor killers (King et al., 1989). Although a large body of evidence in the literature suggests that a certain level of activation of uNK cells is essential for appropriate placentation to take place (Moffett & Colucci, 2014), it is still a practice of many clinicians to treat women with infertility problems and recurrent miscarriage (RM) with therapies aimed at suppressing NK cells.

Unfortunately, this misnomer is responsible for many unsubstantiated hypotheses that uNK cells are 'embryo killers' in cases of reproductive failure, and this has proven to be a powerful advertisement for expensive treatments at the IVF clinics (Moffett et al., 2004; Moffett & Shreeve, 2015). These therapies are not backed by enough evidence and stem from mainly inaccurate interpretations of currently available literature (Moffett et al., 2004). In fact, only pooling of published studies looking at pbNK cell numbers between infertile and fertile women showed a significantly higher number of NK cells in infertile women. Meta-analysis of studies looking at the percentages of pbNK and uNK between these two groups of women did not show any significant differences. Similarly, live birth rates between women with an increase in pbNK cells versus women with a decrease in pbNK cells showed no significant difference. In the same report, a meta-analysis of studies looking at pbNKs in RM showed that both percentages and numbers are higher in women with RM compared to controls, but such significance was not observed for uNK cells in the same setting (Seshadri & Sunkara, 2013). Regardless, there are still clinics all over the world which use 'NK Cell Testing and Activity Investigation' as a reliable indicator of whether NK cells play a causative role in infertility/RM (Sacks, 2015). The problem with this approach is that a sample of peripheral blood is a main source for testing the number and/or activity of the NK cells. Endometrial biopsy to extract uNKs is optional and not always recommended. Test results made on the basis of pbNK measurements are often extrapolated and applied to uterine NK cells, even though it is well established that these are phenotypically and functionally two completely different cell types (Koopman et al., 2003). Most importantly, cell numbers should not be correlated with any fertility outcome, because numbers of pbNKs can vary greatly (2-20% of lymphocytes), just like is the case for the endometrial uNKs, depending on a range of factors (Bisset et al., 2004). However, once high numbers or excessive activity of pbNK cells has been 'diagnosed' in women with infertility or RM, they

are prescribed one of the commonly used therapies and some examples will be discussed here.

Treatment of a woman who had 10 miscarriages with a steroid (prednisolone) led to a successful 11th pregnancy and it was speculated that this was due to the inhibition of Th1 response initiated by NK cells, because prednisolone treatment reduced the number and activity of pbNKs (Ogasawara & Aoki, 2000). This dogma that Th1/Th2 balance has to be maintained (with Th2 cytokines responsible for a successful pregnancy) was then furthered by a study on a larger sample of RM patients where similar treatment led to a significant reduction in CD56^{+} NK cells in the endometrium pre-conception (Quenby et al., 2005). More recently, a stronger glucocorticoid with an even higher anti-inflammatory effect than prednisolone, dexamethasone, was reported to have a beneficial effect on patients with repeated implantantation failure (RIF) because it reduced the number of uNK cells, but with mixed results, including some completed pregnancies but also cases of miscarriage and failure to get pregnant, demonstrating that suppression of uNK cells is not a universal solution (Zhang et al., 2017). This study did, however, mention work shown that dexamethasone use in pregnancy can lead to birth defects and that it is not known how dexamethasone is metabolised in the uterus, which is a big concern for the majority of therapies aimed at uNK/pbNK suppression. None of these therapies target specifically uNK cells and the supposedly beneficial effect can be far outweighed by systemic effects of these drugs, such as through the HPG axis.

Other examples of therapies include intravenous immunoglobulin (Ruiz et al., 1996; Moraru et al., 2012). Intravenously given Intralipid has shown some success, with around 50% of live births post-intralipid treatment in women with RIF history (Lédée et al., 2018). Intralipid, a fat emulsion containing soy bean oil, has originally been proposed as an alternative to glucocorticoids as some patients were found resistant to them (Lédée et al., 2018). The

authors suggested that it had similar anti-inflammatory effect to steroids, presumably through the reduction of $CD56^{+}$ cells and mRNA ratios of IL-18 to tumor necrosis factor-like weak inducer of apoptosis (TWEAK) and of IL-14 to (fibroblast growth factor-inducible 14) FN-14 which they consider biomarkers over-immune activation (Locksley et al., 2001). A range of other therapies were suggested over the years, such as granulocyte colony-stimulating factor (G-CSF) (Scarpellini & Sbracia, 2009), but also anti-TNF-α (Raghupathy et al., 2000), despite the evidence that an immunosuppressive treatment with TNF-α inhibitor, prednisolone and Intralipid may lead to severe systemic candidiasis (Akhanoba et al., 2014). In summary, it is clear that there is a need for a detailed understanding of the interactions occurring between uNK cells and other cells at the maternal-fetal interface. Such interactions might be direct cell-to-cell communication or indirect through the maternal-fetal secretome or synthetic compounds. Defining why uNK cells are different from their pbNK counterparts will lead to precision medicine advances and development of effective and safe medications for women with pregnancy complications and infertility problems.

1.4. Objectives of this study

Determining the function of uterine cell types, including ILCs, is challenging due to a very dynamic nature of the organ and limited access to human samples. Currently, there is a lack of knowledge on gene expression profiles of distinct subsets of mouse uterine g1 ILCs. Knowledge of the proteins expressed on the surface of these subsets is not sufficient to explain how each one of them contributes to regulating the uterine homeostasis. Proteins can have different functions depending on their localisation and phenotype can be highly influenced by the microenvironment. Therefore, understanding a molecular profile of g1 ILCs would aid in constructing a map of their potential interactions with other immune and non-immune cells in the uterus. Modern immunology relies on systems biology to dissect cell heterogeneity and ascribe functions to discrete subsets in an attempt to define the cellular and molecular pathways of tissue physiology and pathology orchestrated by ILCs. The aim of this study was to:

1) Resolve the heterogeneity of mouse uterine group 1 innate lymphoid cells and provide the first transcriptome atlas of these cells at mid-gestation (Chapter 3).

2) Explore and validate the findings of the RNA-sequencing experiment and demonstrate the value of the resource provided in Chapter 3 (Chapter 4).

3) Understand the origin, plasticity and memory-like properties of the group 1 innate lymphoid cells in both mouse and human uterus (Chapter 5).

2. Materials and Methods

2.1 Mice

All mice were maintained in house, unless specified in text. C57BL/6 (B6) wild-type (WT) mice were purchased from Charles River UK. *Rag2*$^{-/-}$*Il2rg*$^{-/-}$ mice were generated by Francesco Colucci. Eomes-GFP reporter mice were a gift of Thierry Walzer (International Centre for Infectiology Research, Lyon, France), *Rorc(γt)-Cre*^{TG} mice from Gérard Eberl (Institut Pasteur, Paris, France) and *Rosa26R-EYFP* (R26R-EYFP) from Ionel Sandovici (Department of Obstetrics and Gynaecology, University of Cambridge, UK) and Dr Helle Jorgensen (Department of Haematology, University of Cambridge, UK). *Tbx21*$^{fl/fl}$ crossed with *Ncr1*-iCre were originally used in collaboration with Victoria Male (University College London, UK) and *Tbx21*$^{fl/fl}$ were later purchased from the Jackson Laboratory (strain ID: 022741) and further bred in-house. *Ncr1*-iCre strain was obtained from Eric Vivier (Centre d'Immunologie de Marseille-Luminy, France) via The European Mutant Mouse Archive (EMMA) at the Sanger Institute. All strains were on a C57BL/6 background. Animals were used at 8-12 weeks of age and were age-matched for every experiment and all time-matings. The morning of the copulation plug discovery was counted as the gestation day (gd) 0.5 for timed-matings. Fine details regarding the husbandry during experiments involving second gestation are described in the corresponding section of Results. Mice were bred, maintained and mated under specified pathogen-free conditions at the University of Cambridge Central Biomedical Service in accordance with the University of Cambridge Animal Welfare and Ethical Review Body and United Kingdom Home Office Regulations. For the experiments performed in collaboration, mice were bred, maintained and mated at the Animal Facility of the IRCCS-AOU San Martino-IST (Italy) in accordance with the Italian and European Community guidelines. All experiments were carried out in accordance with Home Office

Project Licences PPL 70/8222 and 70/7798. Mouse strains used in this study can be found summarised in **Table 2.1**.

Mouse Strain	***Source***
C57BL/6	Purchased from Charles River UK
Rag2$^{-/-}$*Il2rg*$^{-/-}$	Dr Francesco Colucci (Institut Pasteur, now at the University of Cambridge)
Rorc(γt)-Cre^{TG}	Courtesy of Dr Gérard Eberl (Institut Pasteur)
Rosa26R-EYFP	Dr Ionel Sandovici, Dr Helle Jorgensen (University of Cambridge)
Eomes-GFP	Courtesy of Dr Thierry Walzer (University of Lyon)
Tbx21$^{-/-}$	Courtesy of Dr Victoria Male (University College London)
Tbx21$^{fl/fl}$ (also B6.129-*Tbx21*^{tm2Srnr}/J)	Courtesy of Dr Victoria Male, then Jackson Laboratory (strain ID 022741)
Ncr1-iCre (also B6.Cg-*Ncr1*$^{tm1.1(icre)Viv}$)	Courtesy of Dr Eric Vivier (via Sanger Institute, strain ID EM:05625)

Table 2.1. Mouse strains used in this study.

2.2 Genotyping

2.2.1 DNA isolation

Ear biopsies (2 mm) from genotyped mice were collected and kept at -20 °C until DNA isolation. Biopsies were lysed and DNA isolated by placing them into 20 µL of Dilution Buffer (Thermo Fisher Scientific) containing 0.5 µL of DNARelease Additive (Thermo Fisher Scientific). The samples were incubated for 55 minutes at 55 °C, followed by 3 minutes at 98 °C. Samples were then centrifuged briefly to pellet debris. Supernatant containing DNA was diluted 1 in 5 in nuclease-free water (New England Biolabs) for the downstream use.

2.2.2 Polymerase Chain Reaction (PCR)

Three different sets of DNA polymerases and associated buffers were used for conventional PCR genotyping of various mouse strains described in this study using the DNA obtained as described above: (1) Phire Hot Start II DNA Polymerase with 2x Phire Animal Tissue PCR Buffer (Thermo Fisher Scientific) for *Tbx21*$^{fl/fl}$, *Ncr1*-iCre and

PCR programme	**Eomes-GFP**		***Rosa26R-EYFP***		***Ncr1*-iCre, *Tbx21*$^{fl/fl}$**		***Rorc(γt)-Cre*^{TG}**	
Step	*Length*	*Temp (℃)*	*Length*	*Temp (℃)*	*Length*	*Temp (℃)*	*Length*	*Temp (℃)*
Initial Denaturation	*5 min*	94	*2 min*	94	*5 min*	98	*2 min*	94
Denaturation	*30 sec*	94	*30 sec*	94	*5 sec*	98	*1 min*	94
Annealing	*30 sec*	63	*1 min 30 sec*	65 and 55*	*5 sec*	63.1	*1 min*	55
Elongation	*2 min*	72	*1 min 30 sec*	72	*20 sec*	72	*1 min*	72
Cycles	35		*20 at 65 followed by 20 at 55 °C		40		35	
Final Elongation	*5 min*	72	*5 min*	72	*1 min*	72	*5 min*	72
Size	WT– 359 bp, GFP – 374 bp		WT – 239 bp, Mut – 301 bp		*Ncr1*$^{wt/wt}$ – 300 bp , *Ncr1*$^{Cre/wt}$ – 376 bp *Tbx21*$^{wt/wt}$ – 470 bp, *Tbx21*$^{fl/fl}$ – 650 bp		WT – 250 bp TG – 1 kb	

Table 2.2. PCR programmes used in to genotype mouse strains used in this study.

Rorc(γt)-Cre^{TG} strains, (2) REDTaq® DNA Polymerase ReadyMix™ (Sigma-Aldrich) for *Rosa26R-EYFP* strain and (3) 5x FIREPol® Master Mix Ready to Load (Solis BioDyne) for Eomes-GFP mouse strain. These were used in the combination with primers (as described in **Table 2.3**), DNA template and nuclease-free water (New England Biolabs), according to an appropriate programme (as described in **Table 2.2**). PCR was performed using either TProfessional (Analytik Jena) or SureCycler 8800 (Agilent Technologies) thermal cycler instruments. Primers used for genotyping the mouse strains can be found in **Table 2.3**. Representative bands required to interpret the genotyping results can be found in **Figure 2.1**.

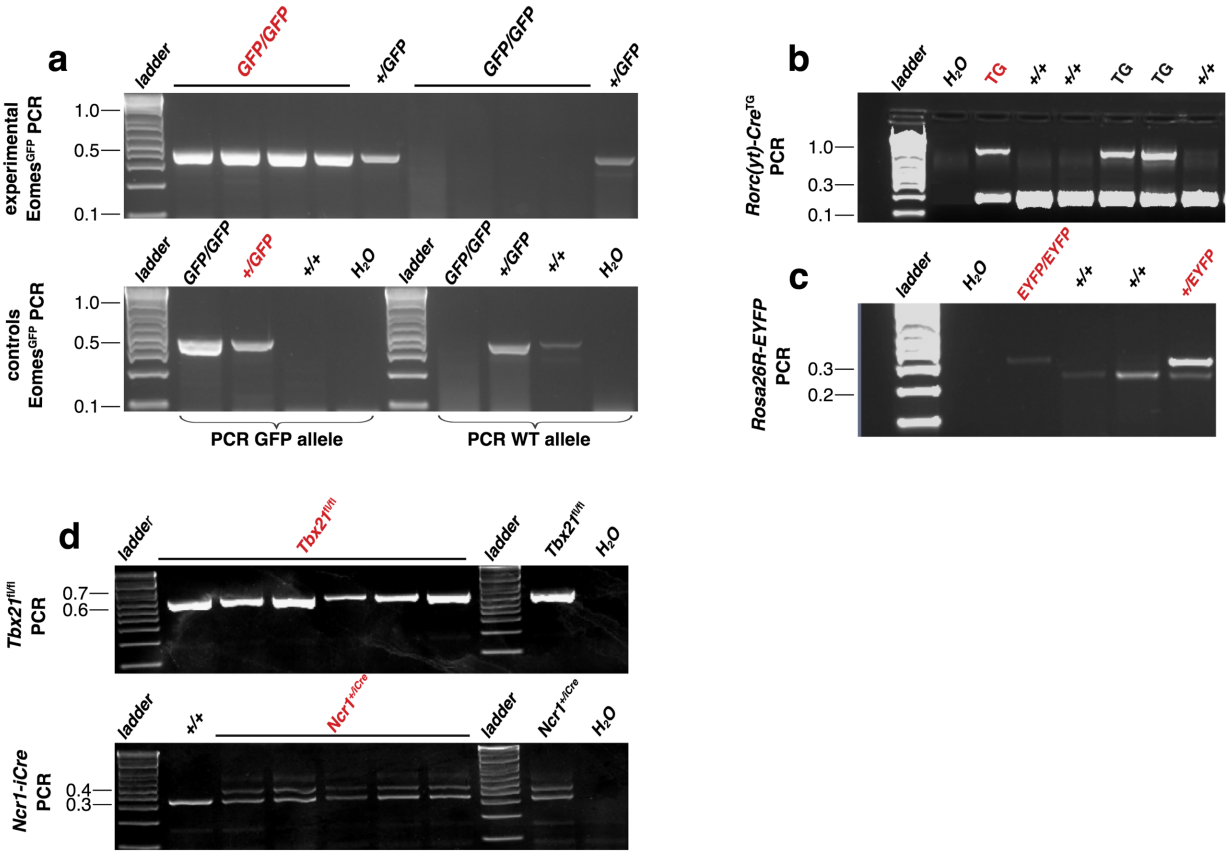

Figure 2.1. Representative PCR results for genotyping various strains of mice used and described in this study. Genotypes of interest for the experiments in this study are highlighted in red.

Rosa26-YFP and Ncr1-iCre were the only strains where three primers were used. PCRs for these utilised the same forward primer but two different reverse primers: one for the wild-type locus and the other one for the YFP or Cre locus. For all other PCRs, two primers were used to amplify the transgene of interest. Reactions were performed in 96-well plates (Thermo Fisher Scientific).

ID	Name	Sequence (5' – 3')	Use
3	Rorgt Forw	CCCCCTGCCCAGAAACACT	Rorgt-Cre genotyping (conventional PCR)
4B	Rorgt Rev	GGATGCCCCCATTCACTTACTTCT	
R26 F	R26 Forw	TGTTATCAGTAAGGGAGCT	Rosa26 YFP genotyping (conventional PCR)
R26 RM	R26 Rev mut	AAGACCGCGAAGAGTTTGT	
R26 RW	R26 Rev WT	CACACCAGGTTAGCCTTTA	
T F	Tbx21 FW	AGTCCCCCTGGAAGAACACT	Tbx21 fl/fl genotyping (conventional PCR)
T R	Tbx21 RV	TGAAGGACAGGAATGGGAAC	
N F	Ncr1 FW	GGAACTGAAGGCAACTCCTG	Ncr1-iCre genotyping (conventional PCR)
N R W	Ncr1 RV wt	TTCCCGGCAACATAAAATAAA	
N R M	Ncr1 RV knockin	GTCCATCCCTGAAATCATGC	
EG F	eGFP-F	AAGCTGACCCTGAAGTTCATCTGC	Eomes GFP genotyping (conventional PCR)
EG R	eGFP-R	AAGTTCACCTTGATGCCGTTCTTCT	
EW F	Eomes-Ex6-5p1	ACTACCATGGACATCCAGAATGAGC	Eomes WT genotyping (conventional PCR)
EW R	Eomes-Ex6-3p2	CAAAGAACACAACAAAACACCACCA	
1F	SPP1-F	TTCACTCCAATCGTCCCTAC	Spp1 RT-qPCR
1R	SPP1-R	TTAGACTCACCGCTCTTCAT	
2F	OGN-F	TGCTTTGTGGTCACATGGAT	Ogn RT-qPCR
2R	OGN-R	GAAGCTGCACACAGCACAAT	
3F	PTN-F	TGGAGAATGGCAGTGGAGTGT	Ptn RT-qPCR
3R	PTN-R	GGCGGTATTGAGGTCACATTC	
4F	CXCL16-F	CCAGATACCGCAGGGTACTT	Cxcl16 RT-qPCR

4R	CXCL16-R	CCAGTTCCACACTCTTTGCG	
5F	TGFb-F	CTCCCGTGGCTTCTAGTGC	Tgfb1 RT-qPCR
5R	TGFb-R	GCCTTAGTTTGGACAGGATCTG	
CF	GAP-F	TGCACCACCAACTGCTTAG	Gapdh RT-qPCR
CR	GAP-R	GGATGCAGGGATGATGTTC	

Table 2.3 Primers used for PCRs and RT-qPCRs used in this study.

2.2.3 Gel electrophoresis

PCR product was analysed using agarose gel electrophoresis. 1.5% agarose gel was prepared by dissolving agarose (Sigma-Aldrich) in 1x Bionic™ buffer (Sigma-Aldrich). For post-electrophoresis agarose gel staining, 1x GelRed® (Biotium) was mixed into the gel pre-casting. Quick-Load® 1kb DNA ladder (100-1,517 bp) (New England Biolabs) was run on the gel with the PCR products for approximately 45 minutes at 135 V in 1x Bionic™ buffer. Stained gel was visualised and analysed via ChemiDoc™ XRS+ imaging system (Bio-Rad).

2.3 Fetal/placental weight

Uterine horns of pregnant mouse females at gd 18.5 were dissected and placed on a cold plate. Fetuses were dissected out of the uterine horns and placentas were separated. Fetuses and placentas were cleared of all adjacent tissues. They were then weighed using a balance (Mettler Toledo).

2.4. In vivo experiments

2.4.1 Adoptive transfer

Femur and tibia were dissected out of each limb of a C57BL/6 wild-type (WT) mouse. The bone marrow was flushed out using 2.5 ml syringe with a 25 g x 16 mm needle (Terumo). Cell suspension obtained in this way was filtered through a 100 µm cell strainer (Miltenyi)

and then counted using the Cedex® XS automatic cell counter (Roche). The appropriate number of cells, according to the antibody manufacturer's instructions (Miltenyi), was then incubated with Fc-block for 10 minutes at RT, followed by incubation with biotinylated lineage antibodies (Miltenyi), antibodies can be found in section 2.9) for 10 minutes at 4 °C. Suspension was then washed twice with MACS buffer (1x phosphate-buffered saline (PBS), 2 mM Ethylenediaminetetraacetic acid (EDTA) and 0.5 % Bovine Serum Albumin). Washing steps during this protocol were performed by centrifuging at 300 x g for 10 minutes, unless stated differently. After this, cells were resuspended in 90 µl of MACS buffer and 10 µl of Streptavidin MicroBeads (Miltenyi) were added and incubated with cells for 15 minutes at 4 °C. Cells were washed again, and then passed through the LS Column (Miltenyi) on the MidiMACS™ Separator magnet (Miltenyi) with a 30 µm strainer (Miltenyi) placed on top of the column. LS Column was prepared by passing through 3 ml of the MACS buffer and then the cell suspension was passed through to isolate the lineage negative cells from the bone marrow sample. Column was washed 3 times with 3 ml of MACS buffer each time. Cells were then counted manually using the Neubauer chamber haemocytometer (Celeromics) and stained for the analysis as described in 2.9.1 and 2.9.2 or stained for cell sorting as described in 2.9.3. Post-cell sorting cell populations of interest were diluted in sterile 1x PBS and injected intravenously into animals via the tail vein. The volume injected did not exceed 200 µl as per Home Office Project Licence. Control animals were injected with 1x PBS only.

2.4.2 Progesterone injections

For the experiments involving progesterone injections, 2 mg of ≥ 99 % Progesterone (Sigma-Aldrich) in 100 µl of Sesame seed oil (Sigma-Aldrich) was subcutaneously injected into each of the females daily (100 mg/kg), for 3 consecutive days. Sesame seed oil was warmed to 37 °C prior to resuspending progesterone. Once this emulsion was prepared, it was injected into

females via 1 ml Insulin Syringe with 25 g x 16 mm needle (Terumo). Control group of females was injected with sesame seed oil only and this represented a vehicle control in experiments.

2.5 Human tissue

Decidual tissue was obtained from donors undergoing elective termination between 7 and 12 week of pregnancy. Informed written consent was obtained from all donors and protocols used were approved by the Cambridge Research Ethics Committee (study Q4/Q0108/23).

2.6 Cell isolation

2.6.1 Mouse tissue processing

2.6.1.1 Accutase protocol

Mouse uterus, liver and spleen were processed using a protocol involving both mechanical and enzymatic processing. Two different types of enzymes were used, depending on the downstream use of cell suspensions obtained. For the method involving the use of enzyme Accutase (Invitrogen), an adaptation of the protocol developed by Arenas-Hernandez and colleagues was used for the work presented in this thesis (Arenas-Hernandez et al., 2015). Finely minced tissues were placed into 2-ml tubes with 1 ml of Accutase (5 ml for the liver) for 35 minutes at 37 °C with gentle orbital agitation of 80 rotations per minute (rpm). For virgin mice, no dissection of the uterine tissues was performed, apart from the removal of surrounding adipose tissue. For pregnant females processed this way, the only dissection of the uterus was to remove the fetus together with trophoblast. Therefore, the resulting cell suspensions represented the whole uterine tissue, without the distinction of myometrium and decidua. Following digestion, tissues were passed through the cell

strainer (100 μm for uterus, 70 μm for liver and 40 μm for spleen; Miltenyi) using a syringe plunger to mechanically dissociate the remaining tissues and then washed with 1x PBS (Gibco). Washing steps were performed by centrifugation at 1500 rpm, for 10 minutes at 4 °C, in 1x PBS, unless stated differently. Leukocytes were then separated using 80%/40% Percoll gradient (GE Healthcare Life Sciences) and by centrifuging without brakes for 20 minutes at 850 x g. After another round of washing, red blood cell lysis was performed on the resulting cell pellet using 1x BD Pharm Lyse buffer (BD Biosciences) according to manufacturer's instructions and for 3 minutes. Single cell suspensions washed and obtained in this way were passed through a 30 μm filter (Miltenyi) and counted manually using the Neubauer chamber haemocytometer (Celeromics) for downstream analysis and assays. The Accutase protocol was used to obtain single-cell suspensions for all experiments in which cells were analysed immediately ex vivo, since a high cell yield was not a requirement. It was a protocol of choice whenever possible, because it allowed for a substantial reduction of the number of animals used per experiment in this study.

2.6.1.2 Liberase DH protocol

For virgin mice, no dissection of the uterine tissues was performed, apart from the removal of surrounding adipose tissue. For pregnant mice, after removal of the fetus and associated trophoblast, myometrium/mesometrial lymphoid aggregate of pregnancy (MLAp) and decidua were dissected by cutting away the mesometrial pole. Therefore, the resulting cell suspensions obtained this way allowed for the distinction of myometrium/MLAp and decidua. Dissected tissues were then incubated in a hybridisation oven at 37°C in Hank's Balanced Salt Solution (HBSS) (Gibco) supplemented with 10% fetal calf serum (FCS) (Gibco), 5 mM EDTA (Gibco) and 15 mM HEPES (Gibco) with gentle orbital agitation. Following such pre-digestion, tissue was macerated to 1 mm^3 pieces and digested at 37°C

for 30 minutes in Roswell Park Memorial Institute medium (RPMI-1640, or RPMI for short) supplemented with 2% FCS (Gibco), 1 WU/ml Liberase DH (Sigma) and 30 mg/ml DNase I (Roche). In addition, enzymatically digested uteri were mechanically forced with a syringe plunger through a 100 μM cell strainer to increase the cell yield and release as many cells as possible. Washing steps were performed by centrifugation at 1500 rpm, for 10 minutes at 4 °C unless stated differently. Leukocytes were isolated from these cell suspensions using 80%/40% Percoll gradient (GE Healthcare) and by centrifuging without brakes for 20 minutes at 850 x g. Red blood cells were lysed by adding 1 ml of 1X BD PharmLyse (BD) buffer for 3 minutes at RT. Single cell suspensions washed and obtained in this way were passed through a 30 μm filter (Miltenyi) and counted manually using the Neubauer chamber haemocytometer (Celeromics) for downstream analysis and assays. The same protocol was followed for isolation of cells from liver and spleen, but 70 and 40 μM cell strainers were used during the mechanical processing step described above, respectively. The Liberase DH protocol was used to obtain single-cell suspensions for all experiments in which a high cell yield with a high purity of leukocytes was required, such as Fluorescence Activated Cell Sorting (FACS) and/or in vitro culturing of distinct cell subsets.

2.6.2 Human tissue processing

Decidua originating from consented donors was separated from trophoblast and washed in RPMI-1640 (Gibco) for 20 minutes. Washed tissue was manually minced and then enzymatically digested in RPMI-1640 with 10% FCS (Gibco) and 10 mg/ml collagenase V (Sigma) using GentleMACS (Miltenyi) for 4x 20 seconds, followed by a 45-minute incubation at 37 °C. Suspension obtained in this way was passed through 100 μm and 40 μm cell strainer, after which it was layered onto Lymhoprep (Axis-Shield) to isolate the decidual

leukocytes (by centrifuging for 20 minutes, at 700 rpm at room temperature (RT)). Cells from the interface were washed in PBS and counted using EVOS XL Core Cell Imaging System (Thermo Fisher Scientific) before downstream application.

2.7 Cell culture

The primary tissue-resident NK cells (trNKs) isolated from the mouse spleen and uterus were cultured in a medium as previously described (Gao et al., 2017) and briefly summarised here. trNKs were cultured in the 96-well flat-bottom plates in RPMI-1640 with GlutaMax, supplemented with: 10% FCS (Gibco), 1% non-essential amino acids (Gibco), 1 mM sodium-pyruvate (Gibco), 10 mM HEPES buffer (Gibco), 0.1% 2-mercaptoethanol, 100 IU/ml P/S (Gibco), 25 ng/ml IL-15 and/or 6.25 ng/ml TGF-β1 (Peprotech).

2.8 In vitro stimulation of lymphocytes

For in vitro stimulation, cells were incubated in 96-well U-bottom plates in medium (RPMI-1640 with pen/strep and FCS in concentrations described previously) containing Cell Stimulation Cocktail (phorbol 12-myristate 13-acetate (PMA)/Ionomycin with protein transport inhibitors; Invitrogen) and anti-CD107a antibody (conjugated to FITC or BV421 and used 1 in 100). At the end of a 4-hour assay according to manufacturer's instructions, cells were stained for analysis as described in section 2.9. Protein Transport Inhibitor Cocktail (Invitrogen) was added to the medium instead of the Cell Stimulation Cocktail for control wells. Negative control for the stimulation assay was (1) a well of stimulated cells without added anti-CD107a antibody or (2) a well of non-stimulated cells incubated in the medium only.

2.9 Flow cytometry

2.9.1 Surface staining

After isolation, primary cells were filtered through a 30 µm strainer (Miltenyi). Cells were counted and $2x10^6$ cells/well were distributed into wells of V-bottomed 96-well plates in 200 µl of Fluorescence-Activated Cell Sorting (FACS) Wash (FW) buffer (1x PBS, 0.5 % bovine serum albumin (BSA), 0.1 % sodium azide). Number of cells plated was adjusted if fewer cells were isolated during the tissue processing steps as described in 2.6. Cells were then washed and subsequently incubated with TruStain fcX (anti-mouse CD16/32) for Fc-receptor blocking for 10 minutes at RT. They were then stained with selected antibodies against surface antigens and incubated for 20 minutes at 4 °C in a volume of 25 µl. After this incubation, cells were washed and stained with a Fixable Viability Dye (Invitrogen) to allow for live/dead discrimination and, if necessary, with a fluorescently-labelled streptavidin if the biotin-labelled antibodies were used in the first step of the staining, for a period of 30 minutes at 4 °C. After this, the suspension was resuspended in a volume of approximately 400 µl of FW with EDTA for flow cytometry analysis. All washing steps during surface and intracellular staining were done by centrifuging at 4 °C and 1500 rpm for 3 minutes unless stated differently.

2.9.2 Intracellular staining and analysis

For the intracellular staining, cell pellets in V-bottomed 96-well plates (either surface stained as described in the section 2.9.1 or freshly stained for intracellular purposes only) were resuspended in 25 µl/well of eBiosciences fixation reagent (Invitrogen) and incubated at RT for 45 minutes. Following incubation and washing with eBiosciences Permeabilisation Buffer (PB) (Invitrogen) diluted 1:10 in Milli-Q Water (EMD Millipore), cells were stained with the selected intracellular antibodies diluted in PB for 30 minutes at RT. After two more washes with PB, stained cells were resuspended in 200-400 µl of FW for flow cytometry analysis.

All antibodies were purchased from Biolegend, eBioscience, BD Biosciences, R&D Systems and Miltenyi. For the multicolour flow cytometry analysis, UltraComp eBeads (Invitrogen) compensation beads were used to optimise the fluorescence compensation settings. For all flow cytometric analyses, unstained and fluorescence minus one (FMO) controls were used to ensure proper gating. Raw data were acquired using BD LSRFortessa™ Analyser (BD Biosciences) at the Cambridge National Institute for Health Research Cambridge Biomedical Research Centre Cell Phenotyping Hub and they were further analysed by FlowJo software, version vX (BD Biosciences).

2.9.3 Fluorescence Activated Cell Sorting

For Fluorescence Activated Cell Sorting (FACS) where the sorted cells were subsequently cultured in vitro in the sterile environment, the same steps were undertaken as for the regular flow cytometry staining (described in section 2.9.1), with several notable exceptions: (1) antibodies used, while same clones used in the analysis, came from a sterile stock used only for FACS purposes; (2) instead of FW, buffer used for sorting was sterile 1x PBS with 0.01 % BSA; (3) sterile polypropylene tubes, rather than polystyrene, were used for sorting to minimize the binding of cells to the tubes. Samples were sorted on FACSAria III instrument (BD Biosciences) and sorting files were analysed using FlowJo vX software (BD Biosciences). All the sorting experiments were performed with the help of staff at the Cambridge National Institute for Health Research Cambridge Biomedical Research Centre Cell Phenotyping Hub.

The list of all antibodies used in this study can be found in **Table 2.4**.

Antigen	***Clone***	***Manufacturer***
CD45	30-F11	BD Biosciences
CD3	17A2	BD Biosciences

CD19	1D3	BD Biosciences
CD11b	M1/70	BD Biosciences
NK1.1	PK136	BD Biosciences
NKp46	29A1.4	Biolegend
CD49a	Ha31/8	BD Biosciences
Eomes	Dan11mag	Invitrogen (eBioscience)
CD86	GL1	Invitrogen (eBioscience)
F4/80	BM8	Biolegend
B220	RA3-6B2	Biolegend
MerTK	REA477	Miltenyi
CXCR6	SA051D1	Biolegend
IL-22	1H8PWSR	Biolegend
MHC-II	M5/114.15.2	Invitrogen (eBioscence)
CD16/32	TruStain fcX	Biolegend
Fixable Viability Dye	eFluor 506	Invitrogen
CD107a	1D4B	BD Biosciences
CD115	AFS98	Biolegend
CD45.1	A20	Biolegend
CD45.2	104	Biolegend
CD244	2B4	BD Biosciences
CD27	LG.3A10	Biolegend
CD117	2B8	Biolegend
CD127	A7R34	Biolegend
CD122	Tm-b1	Biolegend
human CD34	AC36	Miltenyi
human CD38	REA671	Miltenyi
human CD123	AC145	Miltenyi
human CD45RA	REA562	Miltenyi
human CD7	CD7-6B7	Miltenyi

human CD10	97C5	Miltenyi
human CD127	MB15-18C9	Miltenyi

Table 2.4. Antibodies used in this study.

2.10 RNA isolation

2.10.1 RNA isolation for RT-qPCR

The whole uterus was isolated at time-points of interest and collected in RNA*later*™ (Invitrogen) to stabilise the RNA. Fresh tissue was cut to ≤ 0.5 cm in any dimension and immersed in 5 volumes of RNA*later*™, according to manufacturer instructions. It was kept in this solution at 4 °C for twenty-four hours, before being transferred into -80 °C where it was kept until the RNA isolation. Tissue was weighed to ensure the same amount was used for all samples, immersed in 900 µl of QIAzol Lysis Reagent (Qiagen) in the Lysing Matrix S homogenisation tubes (MP Biomedicals) and homogenised on a FastPrep-24 5G Homogenizer (MP Biomedicals). Programme used to homogenise tissue on a FastPrep-24™ 5G was: 20 seconds at 6 m/s followed by 5-minute rest of the tubes on ice. The programme was repeated 2-3 times, depending on the size of the tissue, until most of the tissue was finely homogenised. Homogenates were centrifuged at maximum speed for 15 minutes at 4 °C. The supernatants were then treated with gDNA Eliminator Solution (Qiagen) and chloroform (Sigma-Aldrich) according to RNeasy Plus Universal Kit (Qiagen) instructions. Downstream steps were according to the Kit.

2.10.2 RNA isolation for RNA-sequencing

Group 1 ILCs from uterus and liver were sorted from Eomes-GFP reporter mice into the TRI Reagent (Sigma). RNA extraction was carried out by following TRI Reagent manufacturer's instructions, followed by RNeasy Micro kit (Qiagen).

2.11 Real-Time Quantitative Polymerase Chain Reaction (RT-qPCR)

Quality and integrity check as well as quantification of the RNA isolated as described in 2.10.1 was performed using RNA 6000 Nano kit (Agilent) on the 2100 Bioanalyzer instrument (Agilent). cDNA was amplified using SuperScript VILO cDNA Synthesis kit (Invitrogen) and qPCR was performed using PowerUP SYBR Green Master Mix (Applied Biosystems), on the Quant Studio 6 Flex Real-Time PCR System (Thermo Fisher – Applied Biosystems). *Gapdh* was used as a reference gene. Data were analysed using the ΔΔCt method.

2.12 RNA-sequencing (library preparation)

Quality and integrity check as well as quantification of the RNA isolated as described in 2.10.2 was performed using RNA Pico Nano kit (Agilent) on the 2100 Bioanalyzer instrument (Agilent). cDNA was amplified from this RNA using Ovation RNA-seq system V2 (NuGEN) and DNA libraries were produced using Ovation Ultralow System V2 (NuGEN) and following manufacturer's instructions. All mRNA and cDNA quality controls and quantifications were performed using RNA 6000 Pico and High Sensitivity DNA kits (Agilent) on the 2100 Bioanalyzer instrument (Agilent). Single-end 50 base pair (SE50bp) RNA sequencing (RNA-seq) run was performed on Illumina HiSeq4000 instrument at the Cancer Research UK Cambridge Institute Genomics Core.

2.13 RNA-sequencing (computational analyses)

Data were aligned to GRCm38 mouse genome (Ensembl Release 84) with TopHat2 (v2.1.1, using bowtie2 v2.2.9) with a double map strategy. Alignments and QC were processed using custom ClusterFlow (v0.5dev) pipelines and assessed using MultiQC (0.9.dev0). Gene quantification was determined with HTSeq-Counts (v0.6.1p1).

Additional quality control was performed with feature counts (v 1.5.0-p2), qualimap (v2.2) and preseq (v2.0.0). Differential gene expression was performed with DESeq2 package (v1.16.1, R v3.4.2) and with the same package read counts were normalised on the estimated size factors. Proportions of specific immune cell types from bulk RNA-Seq can be estimated using reference data generated from known proportions of the cell types of interest. DeconRNASeq was applied to take these tables of known cell proportions, defined by gene expression profiles, and used to deconvolute bulk dataset generated in this study to estimate cell proportions within each of the sequences samples. Gene Ontology (biological process) analysis was performed using PANTHER (Protein ANalysis THrough Evolutionary Relationships database http://www.pantherdb.org). Lists of differentially expressed genes (adjusted $p<0.05$ and log2 Fold Change greater than 2) were submitted to PANTHER Overrepresentation Test (released 2017-12-05), with Fisher's exact testing utilising a false discovery rate multiple test correction and a *Mus Musculus* reference list. Further details on annotation versions and release dates can be found in the online Tables in the attached publication (Filipovic et al., 2018) at the end of this thesis. Lists of differentially expressed genes are provided in the Appendix to the thesis.

2.14 Statistical analyses

Statistical parameters and tests applied are reported in the figure legends. All statistical analyses were performed in Prism 7 (GraphPad Software) with a confidence level of 0.95. P-values above 0.05 were considered insignificant and are not indicated in the figures. Figures were prepared using BioRender and Illustrator CC 2018 (Adobe).

2.15 Data and code availability

RNA-seq data are deposited in ArrayExpress (EMBL-EBI E-MTAB-6812). An open-source repository (https://github.com/CTR-BFX/2018-Filipovic-Colucci) has been created with access to the code used in this study.

3. Establishing a resource for investigating the functions of uterine group 1 ILCs

3.1 Introduction

Following up on the landmark studies on the uNK cells introduced in the Introduction section 1.2.2.9, a major driver for future studies in the field of tissue-resident immune cells, including uNKs came from Sojka and colleagues. The premise for this work was a distinct absence of studies on NK cells in tissues, due to researchers previously focusing on the cytotoxic, conventional NK (cNK) in the spleen (Sojka et al., 2014). There were attempts before to redefine murine uNK cells, and for a long time, DBA has been used as a standard to define DBA^+, IL-22 and VEGFA producing uNK cells as well as DBA^-, IFN-γ producing uNK cells (Chen et sl., 2012). However, following the work done in other non-lymphoid tissues (Sojka et al., 2014), an even higher level of cell heterogeneity has been discovered in the mouse uterus. Termed tissue-resident NK (trNK) cells, these murine uNKs were distinguished from now termed conventional NK (cNK) cells based on the expression of CD49a and DX5 (Doisne et al., 2015; Sojka et al., 2014). trNKs were shown to be the most abundant subset in the uterus of both virgin and pregnant female mice and they are $CD49a^+$ and $DX5^-$. In addition to this, trNK seem to be dependent on Eomes TF for development, which is also required for cNK development, and they both express high levels of it in the uterus. cNK cells resembled DBA^- uNK cells while trNKs appeared more similar to DBA^+ uNKs phenotypically (Chen et al., 2016). A third subset, designated as uterine ILC1s of $CD49a^+Eomes^-$ cells was also defined as a distinct subset consistently present in the uterus. At the moment the lineage relationships between these three subsets are unknown. Together, they are termed uterine Group 1 (g1) ILCs. A very elegant study recently described g1 ILCs on the transcriptomic level in mouse spleen, liver and small intestine several years ago

(Robinette et al., 2015). These tissues, however, do not undergo such an extensive level of tissue remodelling as the uterus. The uterine g1 ILC subsets have only been described on the basis of the surface phenotype, using techniques such as flow cytometry and immunohistochemistry. The aim of Chapter 3 was to assess whether the composition of g1 ILCs is dependent on the stage of reproductive life and to establish a similar resource to the one in other non-lymphoid tissues (Robinette et al., 2015), with the goal of describing the transcriptome of murine uterine g1 ILCs for the first time.

3.2 Results

3.2.1 Flow cytometry panel for analysis of group 1 ILCs

In this study, unless otherwise specified, mouse g1 ILCs were isolated from the following tissues: spleen, liver and uterus. Full gating strategy used was the same for all the tissues and summarised in **Figure 3.1** for spleen (**Fig 3.1a**), liver (**Fig 3.1b**) and uterus (**Fig 3.1c**). All tissues in the gates shown here originated from pregnant female mice at mid-gestation (gd 9.5) to illustrate the gating process. The percentages of the cells in each gate, however, were variable and dependent on the method of tissue isolation (mechanical vs. enzymatic processing and type of the enzyme used) and the experimental setting. For example, percentage of the dead cells was always higher, and frequency of $CD45^+$ cells was lower, in the uterine samples, regardless of the stage of gestation. A likely reason for this is that the uterus in general , and the maternal-fetal interface in particular, displays a much higher cell heterogeneity compared to spleen and liver. More abundant non-immune ($CD45^-$) cells in the uterus are also more likely to die during the cell preparation, causing the aforementioned increased level of cell death.

The gating strategy for the uterine samples originating from the pregnant animals presented here in **Figure 3.1** at gd 9.5 represents the entire pregnant uterus (both myometrium and

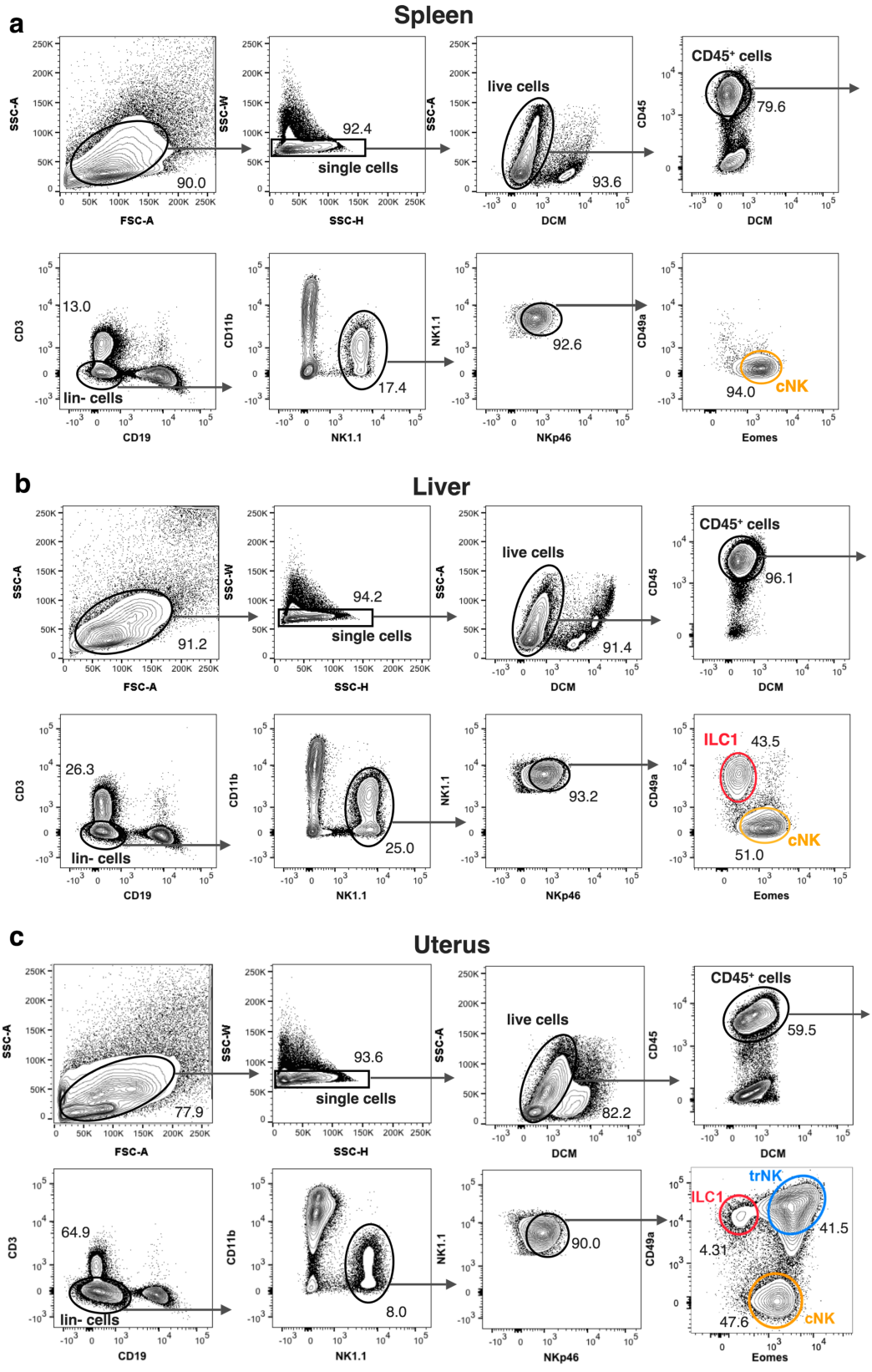

Figure 3.1. Gating strategy of g1 ILCs in different mouse tissues. Gating strategy used for the isolation of g1 ILCs from different tissues is shown at mid-gestation. The same strategy was employed when analysing the cells from the (**a**) spleen, (**b**) liver and (**c**) uterus. In (**a-c**), cNKs were defined as single, live, $CD45^{+}Lin^{-}NK1.1^{+}NKp46^{+}CD49a^{-}Eomes^{+}$ cells, ILC1s as single, live, $CD45^{+}Lin^{-}NK1.1^{+}NKp46^{+}CD49a^{+}Eomes^{-}$ cells and

uterine trNKs as single, live, $CD45^+Lin^-NK1.1^+NKp46^+CD49a^+Eomes^+$ cells. Colour coding employed here will be used in Figure 3.2 and Chapters 4 and 5, but not for the rest of Chapter 3 for reasons explained in text. Some of the gates (single cells, live cells and $CD45^+$ cells) have been indicated in the plots. Percentages displayed are only representative of this sample for the demonstration purposes. All gates were set using appropriate controls, such as FMO and isotype controls. Lineage negative cells were defined as $CD3^-CD19^-$ cells. Colour coding shown here will be used in Figures 3.2 and 3.3 (yellow for cNKs, blue for trNKs and red for ILC1s).

decidua), as described previously in (Montaldo et al., 2016). The reason for this is that some of the following experiments in Chapter 3 were carried out in collaboration with the colleagues who performed the work in (Montaldo et al., 2016), using a mouse model that our laboratory had not yet started breeding at the time.

It is important to note the colour coding (**Figure 3.1c** bottom right: yellow for cNK cells, red for ILC1 cells and blue for trNK cells), which will be used in this chapter in sections 3.2.1 and 3.2.2 as well as throughout the Chapters 4 and 5. However, for the rest of this chapter (sections 3.2.4 - 3.2.7), a different colour coding, explained appropriately, will be used. This is because the generic settings for the processing and performing the quality control of the RNA-sequencing data in R were not changed. These settings were used only temporarily and until the quality control of the data has been fully performed. In conclusion, splenic, liver, and uterine cNKs were defined as single, live, $CD45^+Lin^-NK1.1^+NKp46^+$**$CD49a^-Eomes^+$** cells, liver and uterine ILC1s as single, live, $CD45^+Lin^-NK1.1^+NKp46^+$**$CD49a^+Eomes^-$** cells and uterine trNKs as single, live, $CD45^+Lin^-NK1.1^+NKp46^+$**$CD49a^+Eomes^+$** cells. This was adapted from a previously published report (Doisne et al., 2015).

3.2.2 Distribution of group 1 ILCs during reproductive life

As introduced earlier, the uterine tissue undergoes a remarkable tissue remodelling. This remodelling is orchestrated by sex hormones at all main stages of the reproductive life, such as puberty, implantation, placentation, parturition and lactation. However, less is known

about the composition of uterine g1 ILCs throughout the reproductive life of a female. Since it is ethically unacceptable to sample the endometrium and decidua from healthy human females, the power of mouse models was harnessed in this study to address the question of how g1 ILCs fluctuate throughout the reproductive life of a female mouse. Females were sacrificed at four different time-points: pre-puberty (neonates at 3 weeks (w) of age), sexual maturity (from 4 w of age onwards, when the animals enter puberty and subsequently sexual maturity), gestation (4 time points sampled: gd 5.5, gd 9.5, gd 13.5, gd 17.5) as well as the post-partum period (days 1, 10 and 18 post-partum). Results of this work are summarised in **Figure 3.2**, where the circles represent a percentage of the subset within its parent population (total g1 ILCs: single, live $CD45^+CD3^-CD19^-CD11b^-NK1.1^+NKp46^+$ cells). The most striking trend observed in the uterus in early life was the abundance of distinct $CD49a^+$ subsets at different stages of reproductive life. In females before the onset of puberty (3 w-old neonatal females), $Eomes^-CD49a^+$ ILC1s accounted for around 75% of all g1 ILCs. Percentage of the ILC1s, however, dramatically decreased with the onset of the sexual maturity and this trend was consistent during the later stages of reproductive life (with about 3-15% of ILC1s at all later time-points), while the other two subsets, $Eomes^+CD49a^+$ trNK and $Eomes^+CD49a^-$ cNK were gradually increasing. As indicated in the **Figure 3.2**, sexually mature females were always mated with the males after 8 w of age (and no later than 12 w of age). This was consistent throughout this study, unless specified otherwise. trNKs became the most abundant g1 ILCs in early pregnancy upon mating, at gd 5.5, with percentages similar to what was observed for ILC1s in the neonatal females. At mid-gestation (gd 9.5), trNK and cNK cells were found to be present at similar percentages (around 40-50% each), but the continuous decrease of ILC1s was still apparent. From gd 13.5 onwards, once the placenta has been established, cNK cells were the dominant population among g1 ILCs. This trend continued into the post-partum period, at both 1 and 18 days post-partum (pp). However,

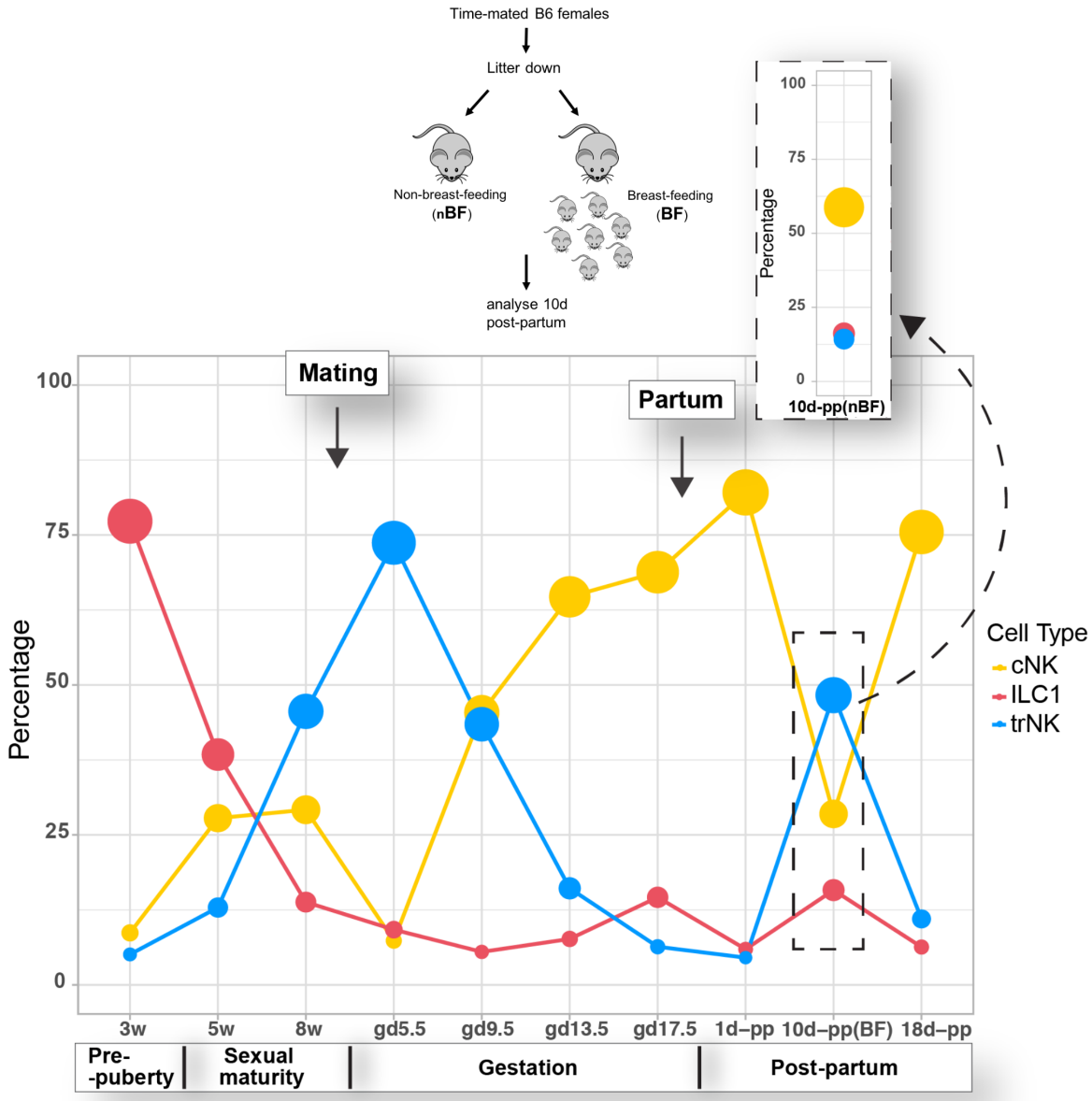

Figure 3.2. Distribution of uterine g1 ILCs during various stages of reproductive life. Landscape of g1 ILCs during reproductive life (including first pregnancy) is presented. The circles on the plots indicate the mean percentages and the size of the circles is increasing with the increasing percentage of the indicated subset within g1 ILC parent population of single, live, $CD45^{+}Lin^{-}NK1.1^{+}NKp46^{+}$ cells from B6 (C57BL/6 mice). Mating (at any point between 8-12 weeks of age) and parturition are indicated in the Figure. Inset shows the same time point as the one below it (10 days post-partum), but in non-breastfeeding females and the experimental set-up for this time-point can be found illustrated to the left of the inset. cNK (yellow, $Eomes^{+}CD49a^{-}$), trNK (blue, $Eomes^{+}CD49a^{+}$), ILC1 ($Eomes^{-}CD49a^{+}$) w: week, gd: gestational day, BF: breastfeeding, nBF: non-breastfeeding, pp: post-partum.

lactation status appeared to affect the distribution of g1 ILCs. While non-breastfeeding females at day 10 pp retained high percentages of cNK cells, in the breastfeeding females there was a significant increase of trNK cells at the same time-point, similarly to what was observed at mid-gestation (experimental set-up and non-breastfeeding data points can be found in the inset and above the plot of **Figure 3.2**).

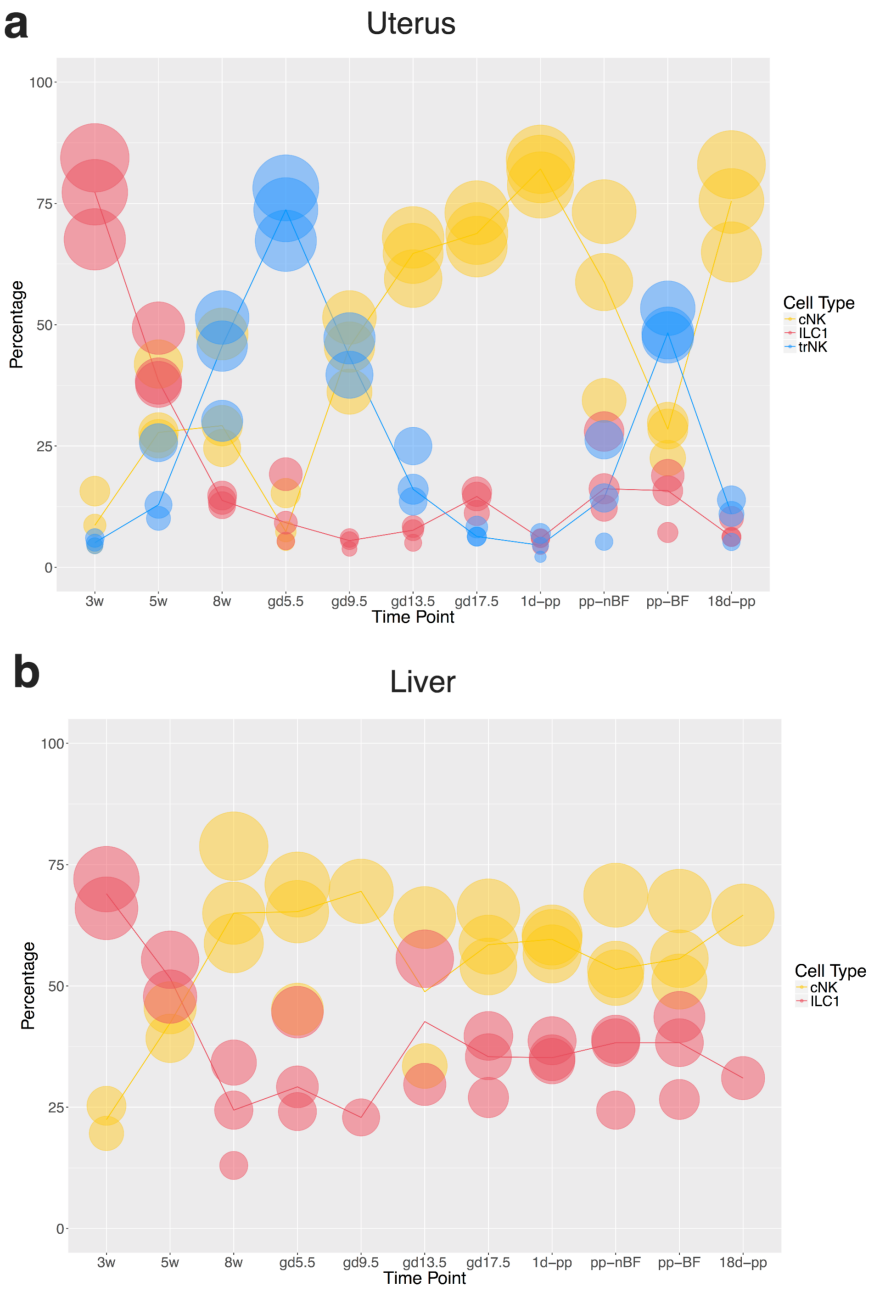

Figure 3.3. Variability of uterine and liver g1 ILCs during various stages of reproductive life. Individual data points were shown for the percentages of g1 ILCs during reproductive life (including first pregnancy) in

uterus and liver within their parent population of single, live, $CD45^+Lin^-NK1.1^+NKp46^+$ cells. (**a**) Individual data points used to generate the summary in Figure 3.2 (**b**) Individual data points showing the percentages of liver g1 ILCs at various stages of the reproductive life. The uterine and liver samples were matched wherever possible. Unlike in Figure 3.2, the non-breastfeeding time-point is indicated in the main plot here. w: week, gd: gestational day, BF: breastfeeding, nBF: non-breastfeeding, pp: post-partum.

In majority of the experiments throughout this study, liver was used as a reference tissue since ILC1s as $Eomes^-CD49a^+$ cells were originally described in the liver (see introduction to this chapter). Therefore, individual data points for both uterine and liver g1 ILCs throughout the reproductive life are shown in **Figure 3.3**. **Figure 3.2** has been derived from data points presented in **Figure 3.3a**, while the data for equivalent time-points was also collected for the liver and is shown in **Figure 3.3b**. A trend that was observed in the liver was that during the adult life of the female, cNK cells were always present in higher percentages within total g1 ILCs, compared to ILC1s.

3.2.3 Eomes-GFP as a mouse model for the study of group 1 ILCs

Once it was established that the percentages of uterine g1 ILCs subsets fluctuate throughout the reproductive life, a possible explanation was that this dynamic distribution of g1 ILCs may reflect subset-specific functions. Eomes as a TF has been shown as essential to make the phenotypical distinction between g1 ILC subsets (Sojka et al., 2014; Doisne et al., 2015). In order to study the functions of these subsets separately, it was necessary to use a mouse model that would allow for FACS-sorting using Eomes without intracellular staining which would permeate and kill the cells. Therefore, an Eomes-GFP knockin reporter mouse model (Daussy et al., 2014; Montaldo et al., 2016) was used in this study. The mouse model was obtained from the original author (Daussy and colleagues) and rederived in the Cambridge Biomedical Services Animal housing facility. The objective was to use the Eomes reporter mouse to FACS-sort g1 ILCs and investigate their transcriptome by using RNA-seq. Since

rederivation took a long time, sorting of the subsets for the RNA-seq experiment was performed by the collaborators at the University of Genoa, Italy (details in the Statement of collaborative work), who had an ongoing colony of this strain. The subsets were sorted using the gating strategy shown in **Figure 3.1(b-c)** and this will be discussed later in this section. As soon as the first litters of the Eomes-GFP reporter mice were weaned in the Cambridge facility, their phenotype and reliability as a mouse model were assessed. As expected, there was no detectable GFP signal in the WT females (**Fig. 3.4a** and **3.4b**).

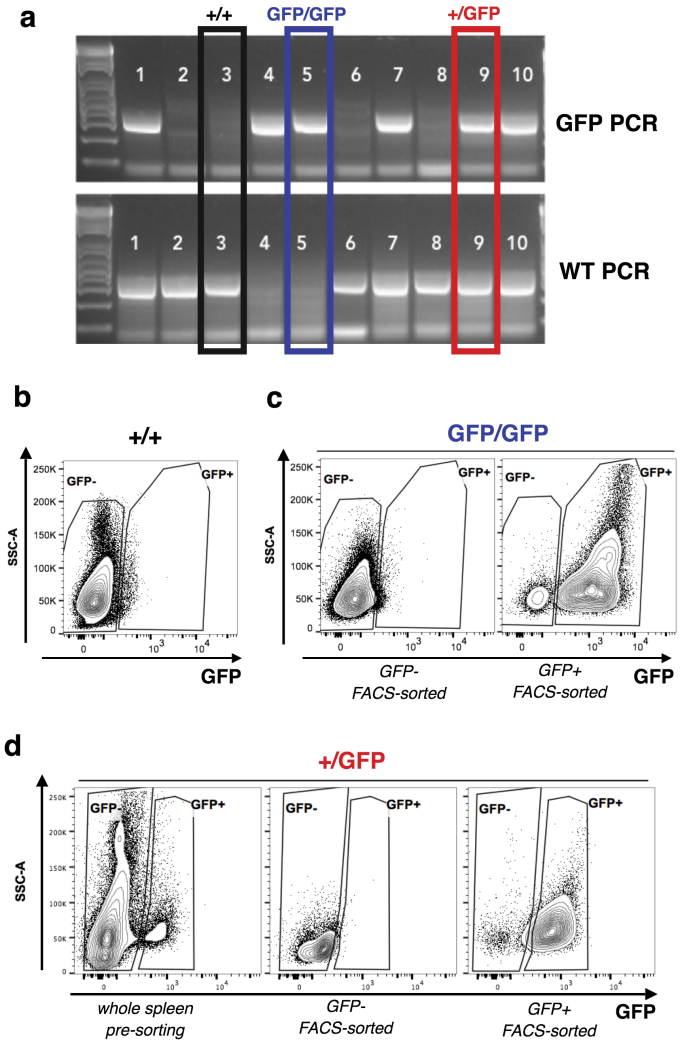

Figure 3.4. Genotyping data of Eomes-GFP mouse model is confirmed by the phenotype. Spleens were used to test the expression of GFP by flow cytometry and to verify the genotype of Eomes-GFP animals rederived in the Cambridge Biomedical Services animal facility. (**a**) Genotyping data for a litter of Eomes-GFP animals. Rectangles indicate animals from which spleens were used to test for the GFP expression by flow cytometry (black, lane 3: wild-type allele only, blue, lane 5: GFP homozygous, red, lane 9: GFP heterozygous

animal). (**b**) Flow cytometry plot showing the level of GFP expression in all cells isolated from the spleen of the animal in lane 3. (**c**) Spleen of the animal from lane 5 was FACS-sorted for GFP^+ and GFP^- cells and the 2 sorted populations were then analysed for GFP expression. (**d**) Spleen of the animal from lane 9 was FACS-sorted for GFP^+ and GFP^- cells and the 2 sorted populations were then analysed for GFP expression to validate the efficiency of sorting. A section of the spleen was analysed pre-sorting as well (first plot on the left). In all settings, cells from a C57BL/6 spleen purchased from Charles River (that were never crossed to Eomes-GFP animals) were used as a non-GFP expressing control sample to set the gates (data not shown).

To address the reliability of the GFP signal for future experiments, both homozygous and heterozygous Eomes-GFP spleens were assessed phenotypically. Briefly, cells were isolated from the whole spleens, and cell suspensions were then FACS-sorted for either GFP^+ or GFP^- cells. In both homozygous ($Eomes^{GFP/GFP}$) and heterozygous ($Eomes^{+/GFP}$) animals, there was a lack of GFP^+ cells in the GFP^- FACS-sorted tubes. In the GFP^+ FACS-sorted fractions, however, there was a high frequency of GFP^+ cells in both $Eomes^{GFP/GFP}$ and $Eomes^{+/GFP}$ animals.

Therefore, the genotyping data was confirmed by the phenotype (**Fig. 3.4a,c** and **d**). It is essential to note that in the future experiment in our laboratory where $Eomes^{GFP/GFP}$ and $Eomes^{+/GFP}$ females were used, intracellular staining using the eBiosciences Fix/Perm kit (used for other strains) was not performed. This was because the GFP signal is susceptible to degradation when using formaldehyde-based buffers (data not shown here). Therefore, where intracellular staining was necessary in work with these animals, pH value of the buffers was adjusted to 8 to preserve the signal (Daussy et al., 2014).

In total, 15 samples were sorted into the TRI Reagent and shipped by the collaborators. These samples originated from uterus (cNK, trNK, ILC1) and liver (ILC1, cNK) at mid-gestation (gd 9.5). This time-point was chosen because it offers the highest absolute cell numbers from the least number of animals. Three biological replicates in total were performed. The information on the sorted samples that was of relevance for the downstream application can be found summarised in **Table 3.1**. For this section, it is important to note a

variable number of cells obtained from different replicates, as well as the previously mentioned different colour coding for the subsets that will be used until the end of Chapter 3.

	Uterus	Number of cells	Total amount (ng)	Total amount/5 µl (ng)	RIN value	Sample
First replicate	cNK	17,500	1.339	0.515	8.8	**1**
	trNK	12,000	2.782	1.070	9.9	**2**
	ILC1	25,000	4.680	1.800	10	**3**
	Liver					
	ILC1	70,000	12.831	4.935	9.4	**4**
	cNK	n/a	6.118	2.185	9.6	**5**
Second replicate	*Uterus*					
	cNK	23,500	2.310	0.825	9.5	**6**
	trNK	14,000	11.368	4.060	9.9	**7**
	ILC1	44,000	11.830	4.225	10	**8**
	Liver					
	ILC1	15,100	2.618	0.935	9.5	**9**
	cNK	47,000	8.946	3.195	9.5	**10**
Third replicate	*Uterus*					
	cNK	10,700	4.046	1.445	9.5	**11**
	trNK	18,300	9.506	3.395	9.9	**12**
	ILC1	38,000	5.992	2.140	10	**13**
	Liver					
	ILC1	n/a	5.005	1.925	10	**14**
	cNK	30,000	8.008	3.080	9.2	**15**

Table 3.1. Summary of the sorted samples from animals at mid-gestation for RNA-sequencing. Three biological replicates were performed and within each, five cell types were FACS-sorted into TRI reagent for the RNA isolation: cNK, trNK and ILC1 from uterus as well as cNK and ILC1 from liver. The table contains a summary of the relevant data for all the steps undertaken in sections 3.2.3-3.2.7. Column 'Number of cells' represent the number of cells obtained from the collaborators, while all the other columns represent the values obtained during the library preparation in Cambridge. Samples have been assigned IDs 1-15, as labelled. Colour coding of the samples shown here will be used until and including the Figure 3.12 in section 3.2.7. n/a: not applicable, ng: nanogram, µl: microliter, RIN: RNA Integrity Number.

3.2.4 RNA isolation: selection of a method

Each sample within the three experimental replicates was obtained by pooling a variable number of pregnant animals at gd 9.5 to ensure that enough cells could be sorted for the downstream application. It was therefore essential to optimise the RNA isolation method to

ensure the optimal RNA yield prior to commencing with the RNA-seq of the 15 samples of variable, and in some cases, low cell numbers (**Table 3.1**).

Firstly, the kit for the RNA isolation was selected. The samples were sorted into TRI Reagent by the collaborators. This allows the extraction of the DNA, RNA and proteins from the cells. Two different kits available on the market allowed isolation of the total RNA from the low number of cells sorted into the TRI-reagent and they were both tested. One kit was Zymo Research Direct-zol RNA kit (in further text Zymo) while the other one was Qiagen RNeasy Micro Kit (in further text Qiagen). Both kits were used according to the manufacturer instructions, with one notable exception. Prior to passing the RNA through the Qiagen column, phase separation using chloroform was performed to isolate the aqueous RNA phase from the sorted and lysed cells.

a

Test	*Cultured Cells*	Number of cells	Total amount (ng)	Total amount/5 µl (ng)	RIN value	Sample
	K562	50,000	255.97	98.45	9.4	1Q
	K562	50,000	169	65	8.1	1Z

b

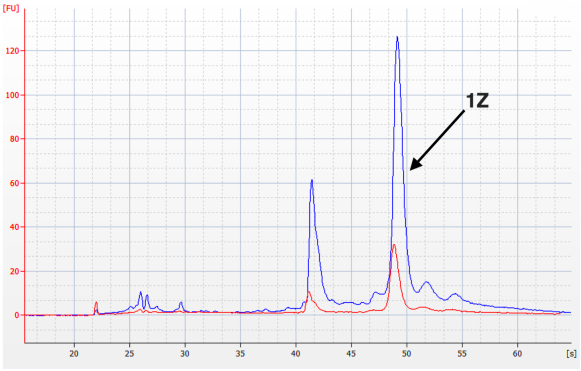

c

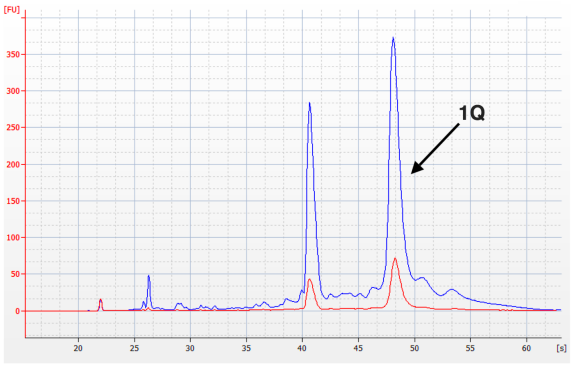

Figure 3.5. Qiagen RNeasy Micro Kit is superior over Zymo kit for the isolation of total RNA. K562 leukemia cell line was used to test the isolation of the RNA with two kits: Zymo Research Direct-zol RNA kit and Qiagen RNeasy Micro kit. Two different numbers of cells were tested with each kit: 10,000 (data not shown) or 50,000 cells. (**a**) Summary of the cell numbers used and the integrity and quality of RNA obtained by two different isolation methods. (**b**) Representative Eukaryote Total RNA Pico assay results for the Zymo kit. (**c**) Representative Eukaryote Total RNA Pico assay results for the Qiagen kit. In (**b-c**), blue histograms represent the RNA profile from 50,000 cells, while the red histograms represent 10,000 cells' RNA profiles. Q: Qiagen, Z: Zymo, RIN: RNA Integrity Number, FU: fluorescence units, s: seconds.

Cells used in the initial test where only the kit was assessed were K562 cells, a commonly used leukemia cell line. For each of the two kits tested, two different cell numbers were used: 50,000 and 10,000 (the data for this test can be found summarised in the **Figure 3.5a**, but only the data for 50,000 K562 cells was shown). Eukaryote Total RNA Pico assay was used on a 2100 Bioanalyzer system (Agilent) to assess the integrity and quantity of the isolated RNA. As shown in **Figure 3.5**, both Zymo (**Fig. 3.5b**) and Qiagen (**Fig 3.5c**) protocols allowed the isolation of the RNA of the acceptable integrity, as measured by the RNA Integrity Number (RIN) value, and quantity, displayed in the 'Total amount' column (**Fig 3.5a**). However, as both the quantity and integrity of the RNA isolated from 50,000 cells (and similarly for 10,000 cells) were slightly better when the Qiagen kit was used, it was decided to continue with this kit as some of the FACS-sorted samples to be sequenced had very low cell numbers. A very important step of the Qiagen protocol was to incorporate the DNAse step to ensure that the obtained total RNA was as clean as possible.

Secondly, another test was carried out to investigate how the yield of the total RNA obtained correlated with number of cells isolated. For this, various numbers of splenic cNKs were sorted, RNA isolated and then analysed using the Eukaryote Total RNA Pico assay again. As shown in **Figure 3.6** and as expected, more RNA was isolated from 40,000 cNK cells compared to 20,000 cells, but less total RNA was extracted from the 25,000 cNK cells than expected, suggesting a certain level of yield variability to be expected in the RNA extraction process.

Finally, total RNA was extracted from all 15 samples in order to amplify cDNA and begin a process of the library preparation for the RNA-seq. Total amount in nanograms obtained from each of the samples can be found in Table 3.1 (section 3.2.3) and one representative

Total RNA Pico assay plot per sample, for each of the 5 subsets (3 from the uterus and 2 from the liver) is shown in **Figure 3.7** (with the same colour coding used in **Table 3.1**).

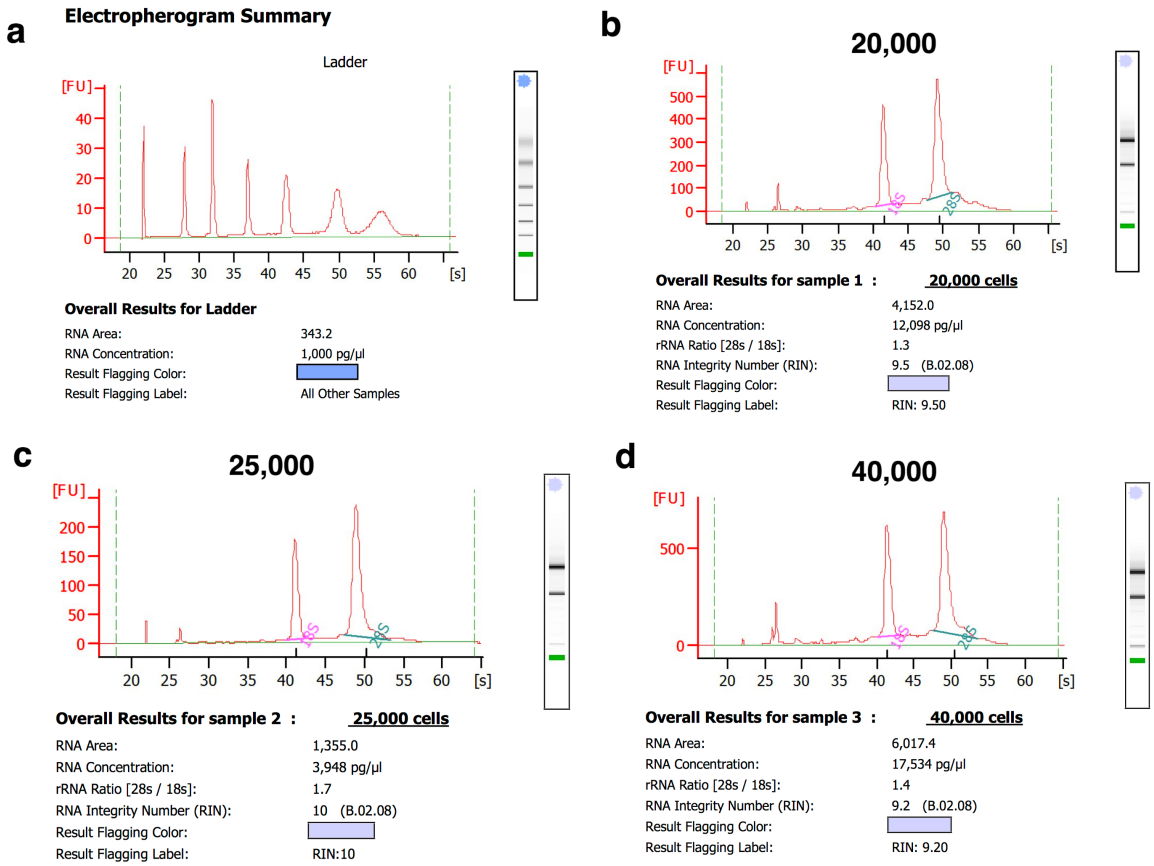

Figure 3.6. Variable yield of total RNA from different numbers of test cells. Splenic cNK cells were sorted and three different total numbers of cells per sample were tested using previously selected Qiagen RNeasy Micro kit. Representative Eukaryote Total RNA Pico profiles are shown. (**a**) RNA Pico profile of the ladder as a quality control of the 2100 Bioanalyzer run. (**b**) RNA Pico profile of the total RNA isolated from 20,000 cells. (**c**) RNA Pico profile of the total RNA isolated from 25,000 cells. (**d**) RNA Pico profile of the total RNA isolated from 40,000 cells. Details of the run for each sample can be found under each summary electropherogram. FU: fluorescence units, s: seconds.

The RIN values (Table 3.1) were variable, but all samples were of a high quality. **Table 3.1** also shows the total amount of RNA in 5 microliters. This was relevant to ensure that there was enough material for the first step of the library preparation. The manufacturer's instructions for the Ovation RNA-Seq System V2 protocol were followed, which came with a recommendation to start with no less than 500 picograms of total RNA in 5 µl. Table 3.1

demonstrates that this was achieved in all of the 15 samples, including the lowest amount of 515 pg in sample 1.

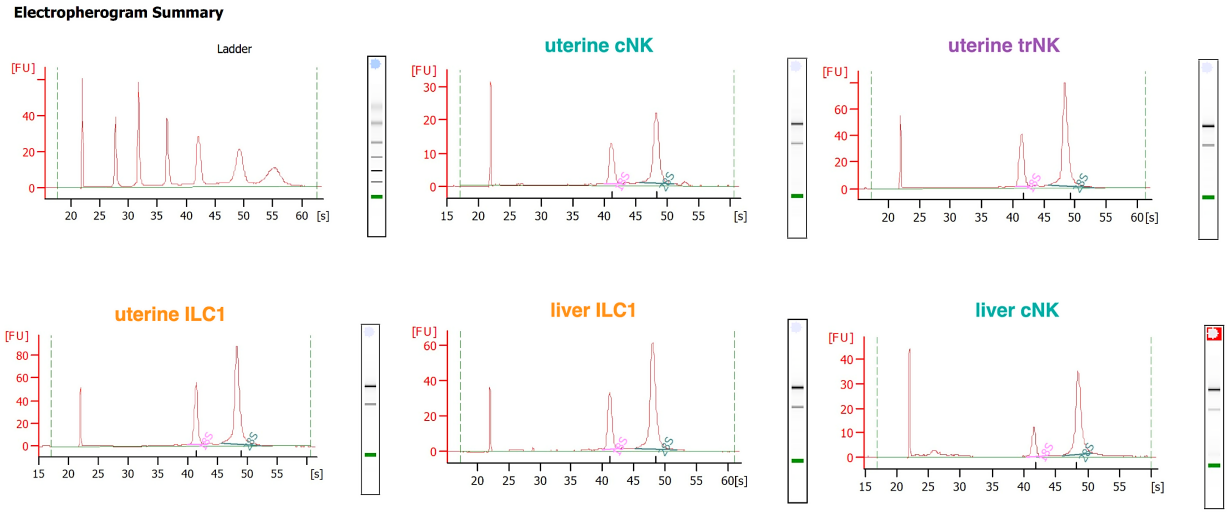

Figure 3.7. Isolated RNA from g1 ILCs was of a high quality. Using Qiagen RNeasy Micro kit, total RNA was isolated from the sorted g1 ILCs summarised in Table 3.1 (titles of each electropherogram are colour-coded as in Table 3.1). Post-extraction, a quality control of the RNA using Eukaryote Total RNA Pico assay was performed and one representative profile per each of the samples (3 from the uterus and 2 from the liver) is shown here, including the ladder. Quantification of these results, including the ones not presented here, can be found in Table 3.1. FU: fluorescence units, s: seconds.

3.2.5 Library preparation

The DNA generated in the previous step was used as a template for the Ovation Ultralow System V2 kit in order to produce the libraries for the RNA-seq. Using the High Sensitivity DNA chips on 2100 Bioanalyzer instrument, it was confirmed that the produced libraries were of a very good integrity, without contaminants and of sufficient quantities. Similarly to the RNA profiles, one plot per sample (same samples as in **Figure 3.7**) is shown for the produced libraries (**Fig. 3.8**).

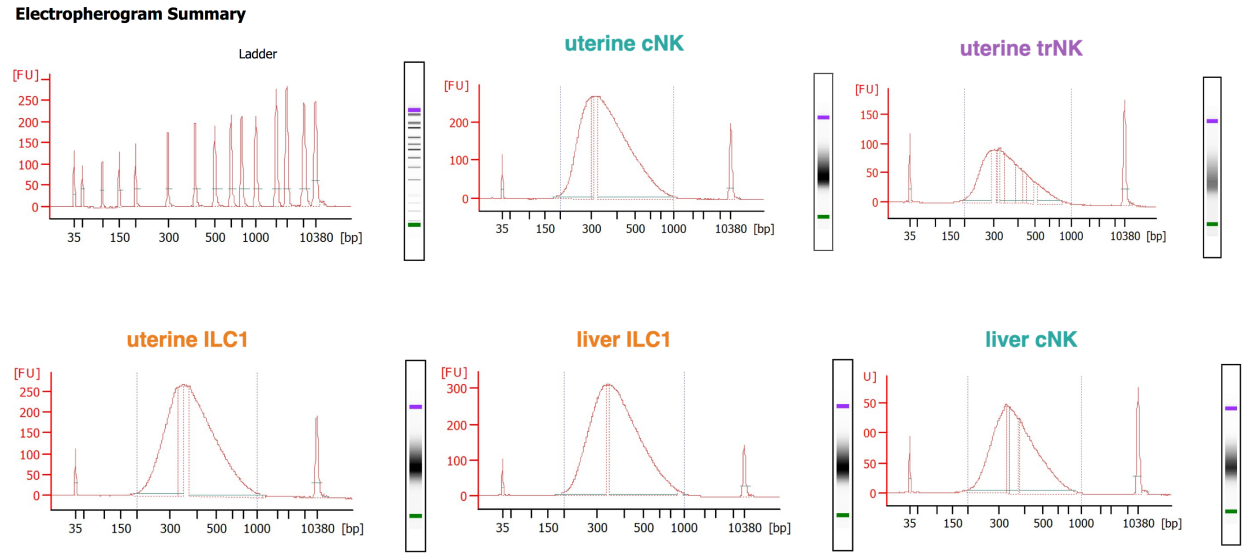

Figure 3.8. Produced libraries for RNA-sequencing were of a high quality. Once the libraries were produced using amplified cDNA from samples shown in Figure 3.7 and Table 3.2, a quality control of the DNA libraries was assessed using High Sensitivity DNA assay. One representative profile per each of the samples (3 from the uterus and 2 from the liver – same samples as in Figure 3.7) is shown here, including the ladder. FU: fluorescence units, bp: base pairs. Titles of each electropherogram are colour-coded as in Table 3.1.

In addition, the pooled library containing all 15 samples, submitted to the Cancer Research UK Cambridge Institute Genomics Core, was also run on the High Sensitivity DNA chip and was of sufficient quality and quantity to be sequenced using Illumina Hiseq 4000 (**Fig. 3.9**). As the aim of this experiment was to analyse genes differentially expressed between samples, in consultation with the CRUK Genomics Core it was decided to proceed with the single-read 50 base pair (bp) sequencing, which yields enough reads per sample.

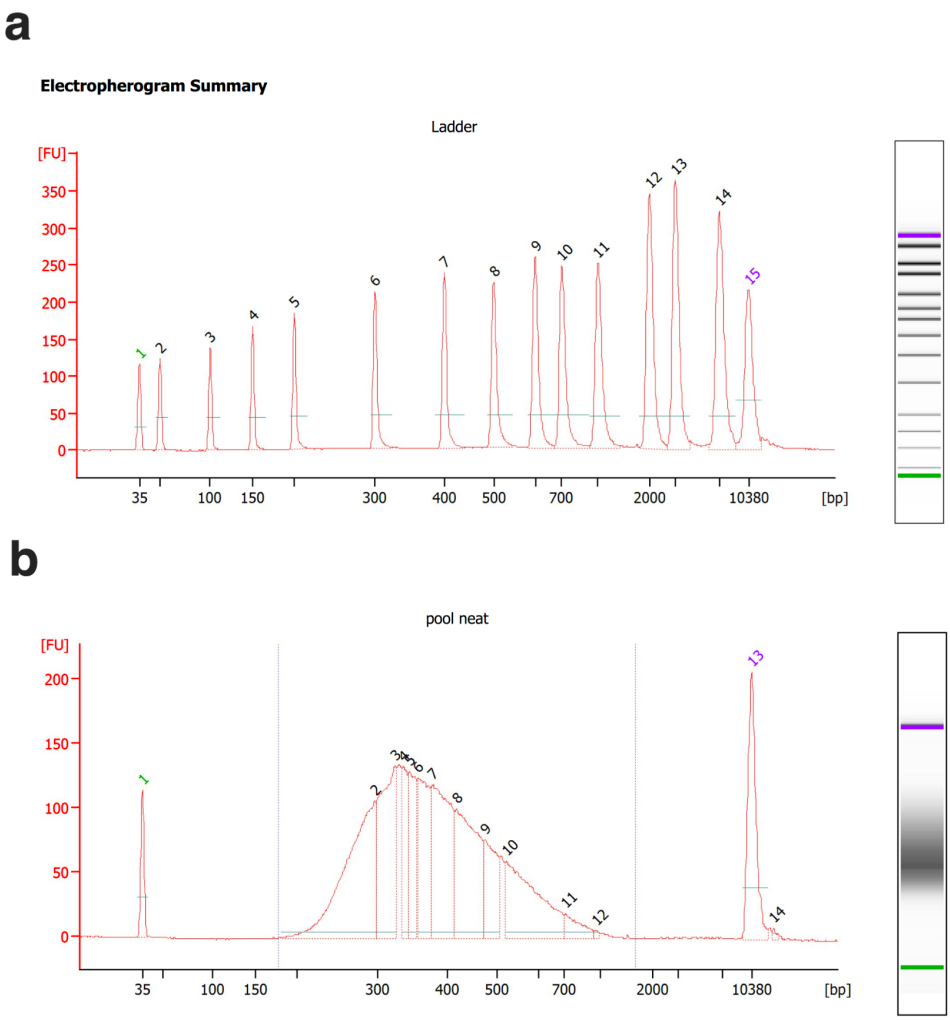

Figure 3.9. Pooled library submitted for RNA-sequencing was of a high quality. 15 produced libraries were pooled and a quality control of this pooled library, which was submitted for RNA-seq to the CRUK Genomics Core, was assessed using High Sensitivity DNA assay. Electropherograms show (**a**) ladder as a quality control of the assay run and (**b**) DNA profile of the pooled library. FU: fluorescence units, bp: base pairs.

3.2.6 Quality control of the RNA-sequencing data

After the sequencing had been completed, it was essential to perform the alignment and quality control of the sequenced samples. Each sequencing sample can fail the quality control in a range of different ways, which could cause major issues in the interpretation of the data and lead a researcher to come to wrong conclusions. Should any anomalies arise, further steps may be required to resolve them before proceeding. Bioinformatic analyses of the

RNA-seq data in this and following chapters, including the quality control presented in this section, were performed with Dr Russell Hamilton at the Centre for Trophoblast Research (details in the Statement of collaborative work).

15 samples that have been submitted for sequencing were assigned the sequencing IDs as explained in the **Table 3.2**. This was summarised for the ease of understanding of the quality control summary figures, although each sequencing ID (starting with L2V...) ended in a number corresponding to the sample number (01-15).

Sample number	***Sample origin***	***Sequencing ID***
1	u-cNK-1	L2V18DRBC01
2	u-trNK-1	L2V18DRBC02
3	u-ILC1-1	L2V18DRBC03
4	l-ILC1-1	L2V18DRBC04
5	l-cNK-1	L2V18DRBC05
6	u-cNK-2	L2V18DRBC06
7	u-trNK-2	L2V18DRBC07
8	u-ILC1-2	L2V18DRBC08
9	l-ILC1-2	L2V18DRBC09
10	l-cNK-2	L2V18DRBC10
11	u-cNK-3	L2V18DRBC11
12	u-trNK-3	L2V18DRBC12
13	u-ILC1-3	L2V18DRBC13
14	l-ILC1-3	L2V18DRBC14
15	l-cNK-3	L2V18DRBC15

Table 3.2. Summary of the sequencing IDs. 15 samples that have been submitted for sequencing were assigned the sequencing IDs by the Cancer Research UK Cambridge Institute Genomics Core. The column on the left indicates which sequencing sample corresponds to which sample from Table 3.1.

Quality control was performed using the MultiQC tool (created by Phil Ewels at the SciLife Lab, Sweden), which puts together a summary report of multiple bioinformatic tools commonly used to align the RNA-seq reads to a genome of interest (in this case to the mouse genome), and subsequently assess their quality. This allows for the timely assessment of the possible batch effects and outlier samples (Ewels et al., 2016), prior to continuing with the analysis. In summary, the MultiQC tool reported that all 15 samples had passed the quality control. This included the post-alignment tools, such as Qualimap (**Fig. 3.10a**) and featureCounts (**Fig. 3.10b**), which were used to evaluate the alignment quality carried out by the alignment tool TopHat (**Fig 3.10c**).

Although one of the most basic steps of this process, FastQ Screen was important as it is this screening that showed whether there was any contamination present in the sequenced samples. This was done through screening 15 fastq library files generated here against the preset reference genome sequences, such as E. Coli, bacteriophage PhiX genome also commonly used as a control library or another organism (Wingett & Andrews, 2018). Results of this analysis are shown in **Figure 3.10d**, where the proportion of the reads which mapped against each individual reference genome is displayed.

Reassuringly, the majority of reads mapped against the mouse genome (light blue colour: one hit/one genome, which means that these reads mapped uniquely to the specified mouse genome and did not map to any other genome or any other location in the genome). There were no bars that showed unique mapping to any of the other genomes. However, a significantly higher proportion of two other types of mapping were observed against the human genome, and this was particularly prominent for sample 3, as pointed out with an arrow in **Figure 3.10d**. One of these was the dark red coloured bar (multiple hits/multiple genomes) that indicated that a proportion of reads mapped not only to mouse genome but also

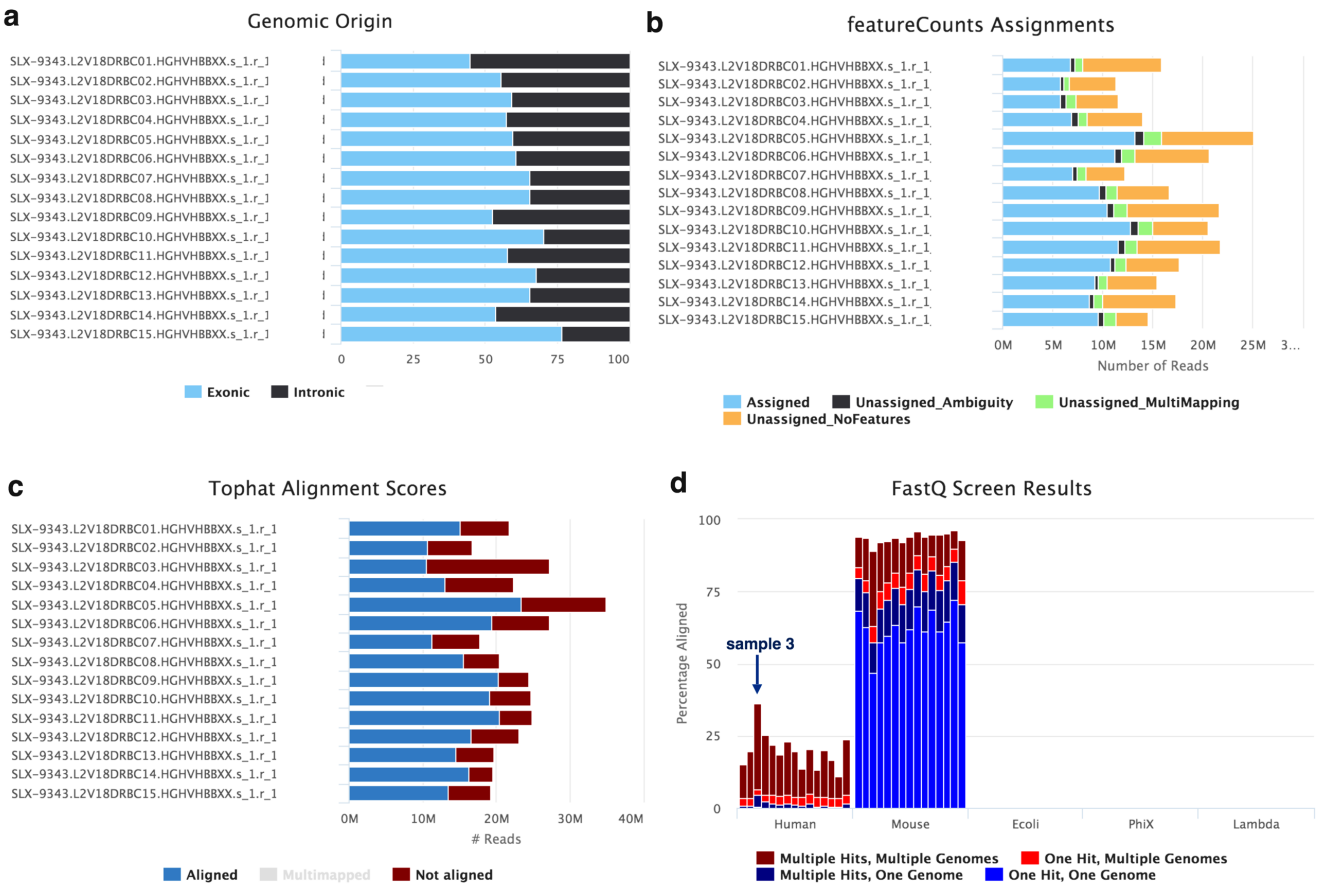

Figure 3.10. MultiQC report summary. After sequencing files in the fastq format had been received, they had to undergo a quality control using a range of bioinformatic tools. MultiQC puts together summary of these results, which include steps pre-alignment, during alignment and post-alignment and they are shown here. Sequencing IDs in each of the panels (**a-d**) are summarised in Table 3.2. (**a**) Genomic origin of the reads. (**b**) Assignment of the reads. (**c**) Alignment scores. (**d**) FastQ Screen results, where an arrow is used to indicate sample 3 discussed in text. Each report summary in (**a-d**) is accompanied by a legend described in the Figure.

to the human and at several locations in both. The other type was a dark blue bar (multiple hits/one genome), which means that these reads mapped to the specified genome (human), but not uniquely, as they mapped to two or more separate locations, suggesting a possibility of the contamination. This issue with sample 3 (uILC1, replicate 1, **Table 3.2**) was taken into account for the future analyses.

Finally, the remaining plots from the FastQC report (created by Simon Andrews from the Babraham Institute, UK) demonstrated that all the libraries were of extremely high quality

and none of the samples were flagged as poor quality (summarised in **Fig. 3.11**). A per base sequence quality plot showed that the base calls were of a very good quality (the higher the y-axis value, the higher the quality score) and similarly, per sequence quality scores plot showed that not even a subset of reads was of poor quality since they all had a quality score of 30+ (**Fig. 3.11a** and **b**).

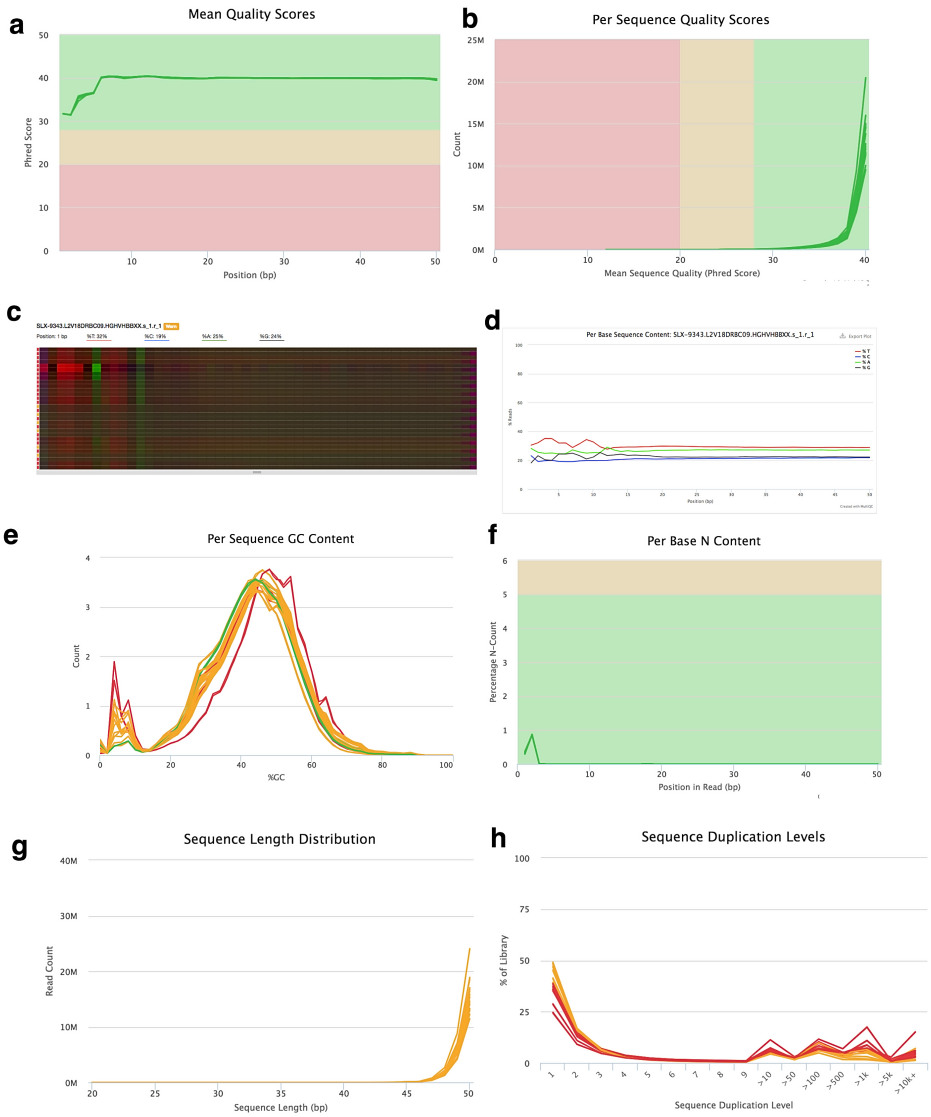

Figure 3.11. FastQC report summary demonstrated that all sequenced libraries were of a very high quality. All plots feature all sequenced samples, unless otherwise specified for a particular panel. (**a**) Per base sequence quality plot. (**b**) Per sequence quality scores' plot. (**c**) Per base sequence heatmap. (**d**) Per base sequence heatmap: individual display for a sample 9 as a representative example from (**c**). Other samples had a similar profile. (**e**) Per sequence GC content. (**f**) Per base N content. (**g**) Sequence length distribution. (**h**) Sequence duplication levels. N: non-identified base call, bp: base pairs.

Figure 3.11c displays per base sequence content, which demonstrated the proportion of each base position where each of the 4 bases (A, T, G, C) was called. Although none of the samples failed this step, a lot of them were issued a warning due to the default setting where warning comes from a difference greater than 10% between A and T or G and C in any position.

However, FastQC report tutorial explains that nearly all RNA-seq libraries fail this module due to a selection bias in the first 12 bp of each run, since there is a biased selection of random primers, but this bias does not extend to any of the sequences and therefore was not a reason for concern. A representative example for this selection bias is shown in **Figure 3.11d** (using sample 9). Per sequence GC content (**Fig. 3.11e**), N content (base calls when the sequencer was unable to confidently make a base call; **Fig. 3.11f**), sequence length distribution (**Fig 3.11g**) and sequence duplication levels (**Fig. 3.11e**) all passed the quality control, similarly to other modules within the FastQC report.

3.2.7 The last step of the quality control: initial Principal Component Analysis

As the final step of the quality control, an initial Principal Component Analysis (PCA) cluster plot, with Principal Components (PC) 1 and PC2, taking into account all genes, was created. Surprisingly, sample 11, representing uterine cNKs (**Table 3.2**), clustered with the uterine trNKs (**Fig. 3.12a**) instead of with the other two biological replicates (samples 1 and 6), and therefore this sample was removed from the subsequent analyses. Another PCA plot was created to demonstrate this initial quality control once these two samples were excluded (**Fig. 3.12b**). Although sample 3, representing uterine ILC1s, caused concern due to a potential human contamination (as pointed out in section 3.2.6 and in **Figure 3.10d**), it clustered as expected (**Fig. 3.12b**). However, in order to ensure that the subsequent analyses were of the highest standard, it was decided to remove this sample.

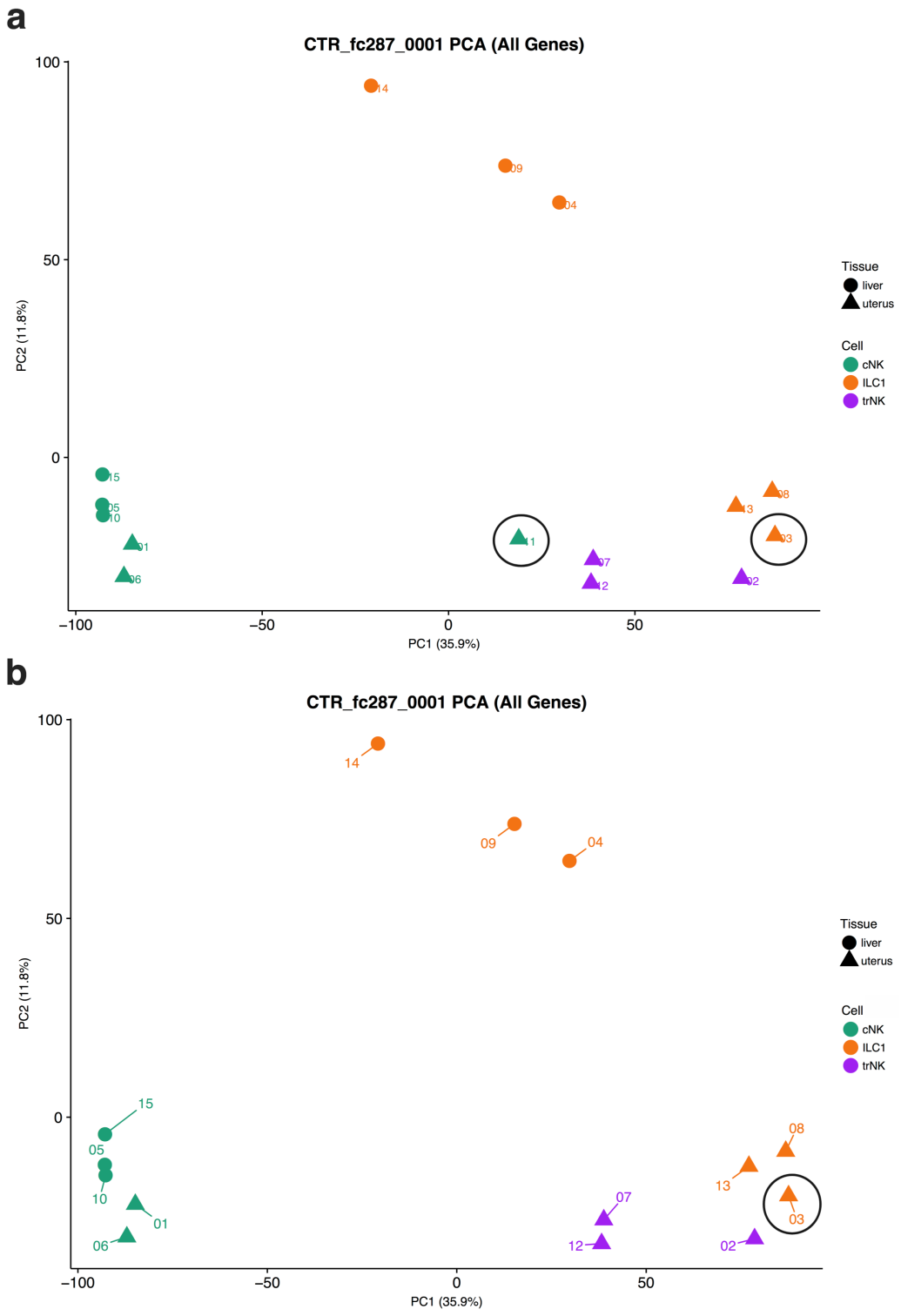

Figure 3.12. Initial Principal Component Analysis. All genes covered by the RNA-sequencing were used to generate the initial PCA cluster plot as final step of the quality control. (**a**) PCA cluster plot with all 15 sequenced samples. Black circles indicate samples which misclustered or did not have the highest scores in all previous quality control samples. (**b**) PCA cluster plot where sample 11 was removed, while sample 3 remained. However, this sample is circled as it was decided to exclude it in addition to sample 11, as explained in the text.

3.3 Summary

In Chapter 3, it was shown that there were dramatic changes in the distribution of g1 ILCs throughout the reproductive life of a female mouse. As shown in the Figure 3.3a, there was a great variability in the non-pregnant (virgin) samples, both before and after gestation. This is a very important point, because such variability was not observed in the samples acquired during gestation. This variability may reflect the dynamic changes that occur over the course of the estrous cycle and its accompanying tissue remodelling. None of the methods which allow the determination of the estrous cycle were on the Home Office licence (PPL) used for this work and therefore it was not possible to take this parameter into account. However, several trends became obvious from the data presented in Figures 3.2 and 3.3:

ILC1s are the most dominant g1 ILCs pre-puberty.

By the 3 w of age, sex hormones have not started circulating yet, and the most abundant immune cells in the uterus at this time may be essential in the protection of the mucosal barrier surfaces or even in the development of the uterus, which is still ongoing in the neonates (Filant et al., 2012).

trNKs are the most abundant g1 ILC population early in gestation (gd 5.5).

One of the essential first steps to establishing the maternal-fetal interface is implantation. In mouse, this process starts around the gd 4 and ends by gd 6, when the embryo is fully attached to the endometrium. Around gd 5, endometrium begins the process of decidualisation. After gd 9, progressive thinning of the decidua is observed until about gd 12. Therefore, the sampled pregnant uterus at gd 5.5 was representative of a time mid-implantation and at the onset of the decidualisation. trNK cells, as the most abundant cells at this time-point may be the main drivers of the extensive tissue-remodelling required to establish the maternal-fetal interface. trNKs may mediate SA remodelling in pregnancy in

cooperation with cNKs, as they cNKs can be found in similar percentages by mid-gestation (gd 9.5). More work is required to investigate this hypothesis further.

cNKs are the most abundant starting from the second half of gestation (gd 13.5). Post-partum period is still marked by the domination of cNKs, unless the females are breastfeeding.

It is an established fact that female mice can ovulate immediately post-partum, within the first 24h. Fertility is less efficient during this first post-partum estrus, but it is still possible for a female to become pregnant. However, once this estrus ends, there will not be any further estruses until the end of the lactation period (Bronson et al., 1966). Looking at the days 1, 10 and 18 post-partum represented attempts to address three events during the post-partum period: first post-partum estrus on day 1, mid-lactation period (with either breastfeeding or non-breastfeeding females) on day 10 and finally the end of lactation on day 18, just a day before the offspring was weaned on the day 19. A finding that requires further investigation is the rise in percentage of trNKs in the breastfeeding females. This was not observed at any other point during gestation or before and after pregnancy. Overall, g1 ILCs appear to be highly sensitive to gonadal hormone fluctuations at every stage of the reproductive life.

Eomes-GFP was shown to be a reliable reporter mouse model and successfully established as a strain for the future studies in Cambridge.

Three subsets of uterine g1 ILCs (cNK, trNK and ILC1) and two liver subsets (cNK and ILC1) were successfully FACS-sorted. Following the optimisation of the RNA isolation method, these sorted cells were RNA-sequenced as explained in sections 3.2.3 to 3.2.7. Quality control of the sequenced samples showed a very good quality for majority of the samples. Two samples, however, were excluded from the future data analyses to ensure high quality data interpretation. Sample 3 was excluded from further analyses. due to a non-identified source of the human contamination. Although sample 11 had passed all the quality

control tests, it clustered with trNKs rather than cNKs. These samples were obtained from the collaborators' laboratory and since it was not possible to determine with a high level of confidence if this misclustering was indeed due to a previously unappreciated cell heterogeneity, sample 11 was dismissed from further analyses, too.

4. Exploration of the RNA-sequencing dataset and identifying the core gene signatures of uterine group 1 ILCs

4.1 Introduction

The main intention of this dissertation was to provide the first transcriptome atlas of uterine group 1 ILCs. As shown in the Chapter 3, the RNA-sequencing dataset of uterine and liver g1 ILCs at mid-gestation was successfully generated. It also passed all the necessary quality controls required during the computational analysis of the RNA-seq data.

The main aims of the work in this chapter were to explore this RNA-seq dataset. This was done through the validation of the dataset in various ways presented in this chapter, together with exploration and identification of the core gene signature of uterine g1 ILCs.

4.2 Results

4.2.1 Distinct gene signatures of CD49a$^+$ and CD49a$^-$ group 1 ILCs

As shown in the previous chapter, the decision was made to remove two samples from further analyses: sample 3 (one of the three replicates of uterine CD49a$^+$Eomes$^-$ ILC1s) and sample 11 (one of the three replicates of uterine CD49a$^-$Eomes$^+$ cNKs). This was displayed in the **Figure 3.12**. However, the PCA clustering performed in **Figure 3.12** included all genes from the obtained RNA-seq dataset, as the aim of such clustering was a quality control of the samples, rather than interpretation of variance between the samples.

In order to explain the variance between all samples, unbiased clustering was performed, similarly to the PCA analysis in the previous chapter. It is a common practice to calculate the variance in expression between the samples and only select the genes that are highly variable.

This is because highly variable genes are more likely to provide information required to cluster samples, especially for the PCA which specifically looks to explain the variance between samples. **Figure 4.1** shows that regardless of how many of these most variable (MV) genes are used to produce the PCA plots, the clustering does not change.

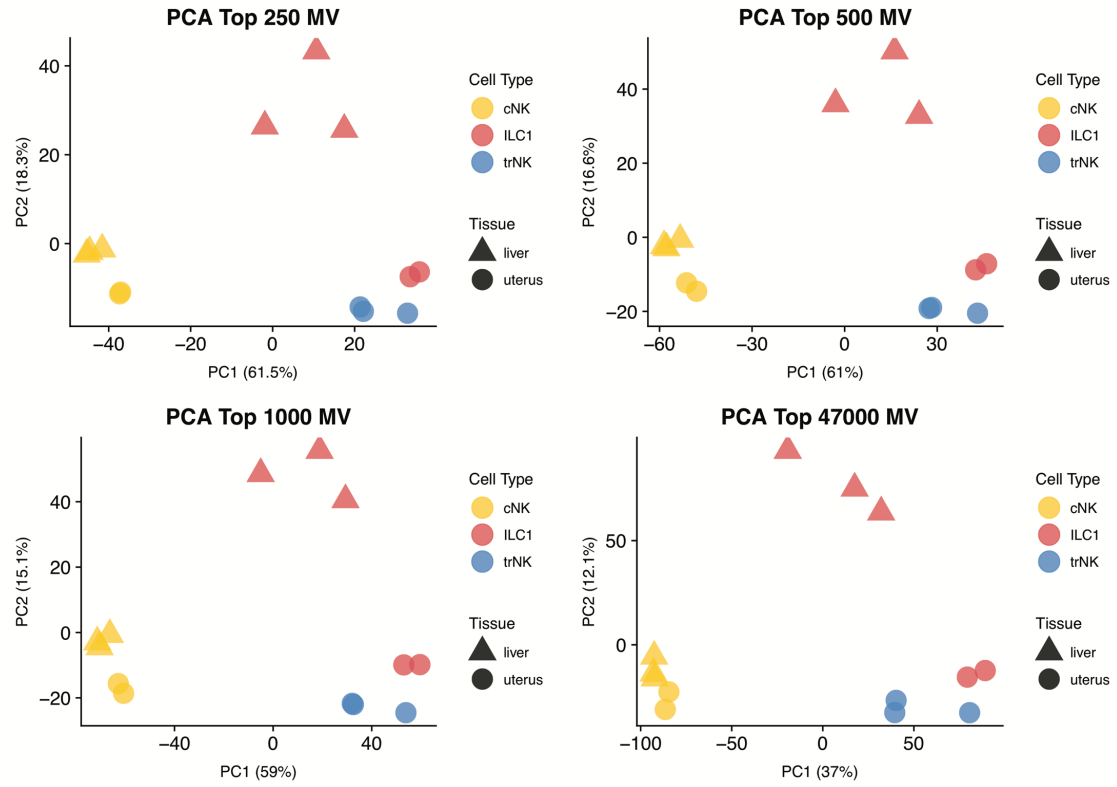

Figure 4.1. Unbiased clustering by selecting various numbers of most variable genes does not affect the clustering. Variance in expression between the samples was calculated and the most highly variable genes were selected to produced PCA plots presented here, showing 250, 500, 1000 or 47,000 most variable genes. The legend accompanying each plot describes the data points (yellow: cNKs, red: ILC1s, blue: trNKs, triangle: liver and circle: uterine origin). Percentage of each principal component can be found in the brackets along the axis. MV: most variable, PCA: principal component analysis, PC1: principal component 1, PC2: principal component 2.

Thus, it was decided to continue with interpreting the most stringent version of the PCA plot, produced by selecting the top 250 MV, which looked very similar to the other PCA plots (**Fig. 4.2**). PCA confirmed the similarity of transcriptional profiles of hepatic and uterine

cNK cells, as well as CD49a^{+} uterine ILC1s and trNKs, as they clustered together. However, this unbiased analysis also highlighted unexpected differences between uterine and liver CD49a^{+}Eomes^{-} ILC1s, as they have not clustered as closely together as one might have anticipated on the basis of their similar surface phenotypes.

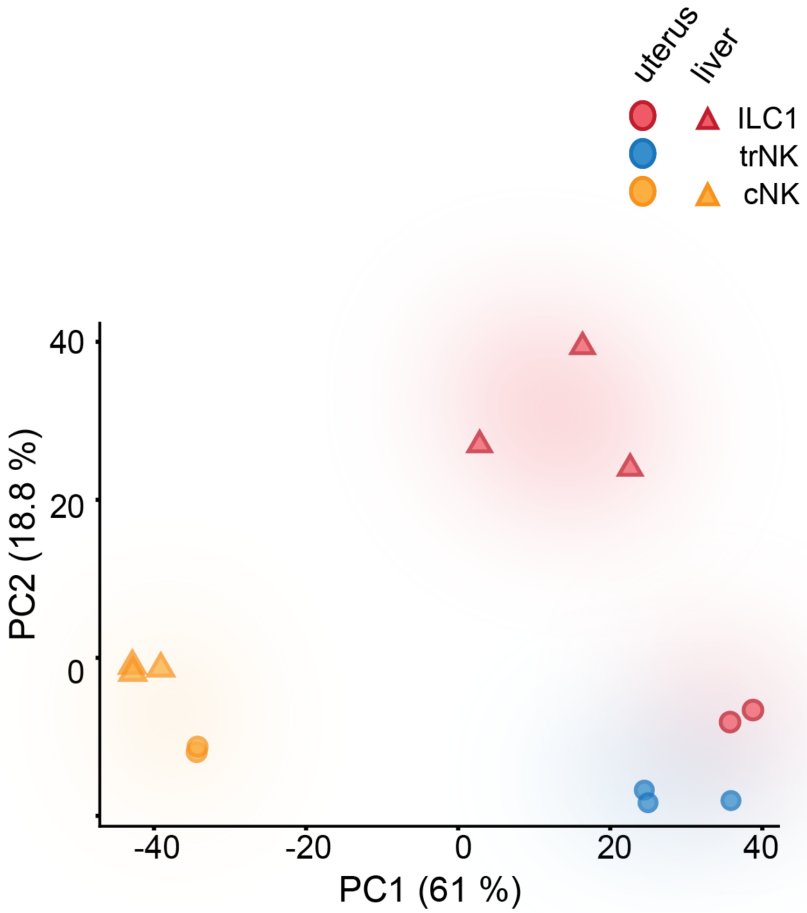

Figure 4.2. Final unbiased principal component analysis. The 250 most highly variable genes were selected to produce a PCA plot presented here. The legend accompanying the plot describes the data points (yellow: cNKs, red: ILC1s, blue: trNKs, triangle: liver and circle: uterine origin). Percentage of each principal component can be found in the brackets along the axis. MV: most variable, PCA: principal component analysis.

Hierarchical clustering of the 2 liver subsets and the 3 uterine subsets using only the differentially expressed genes with a log2 fold change cut-off ≥ 7.5 and p-value ≤ 0.01, confirmed that liver and uterine CD49a^{-}Eomes^{+} cNK cells were very similar (**Fig. 4.3**), while

the tissue of origin determined differences among the other subsets. Indeed, CD49a^{+}Eomes^{-} ILC1s from liver and uterus clustered apart, suggesting tissue-specific gene signatures even in these two cells types that were sorted using the same FACS panel and that are phenotypically very similar.

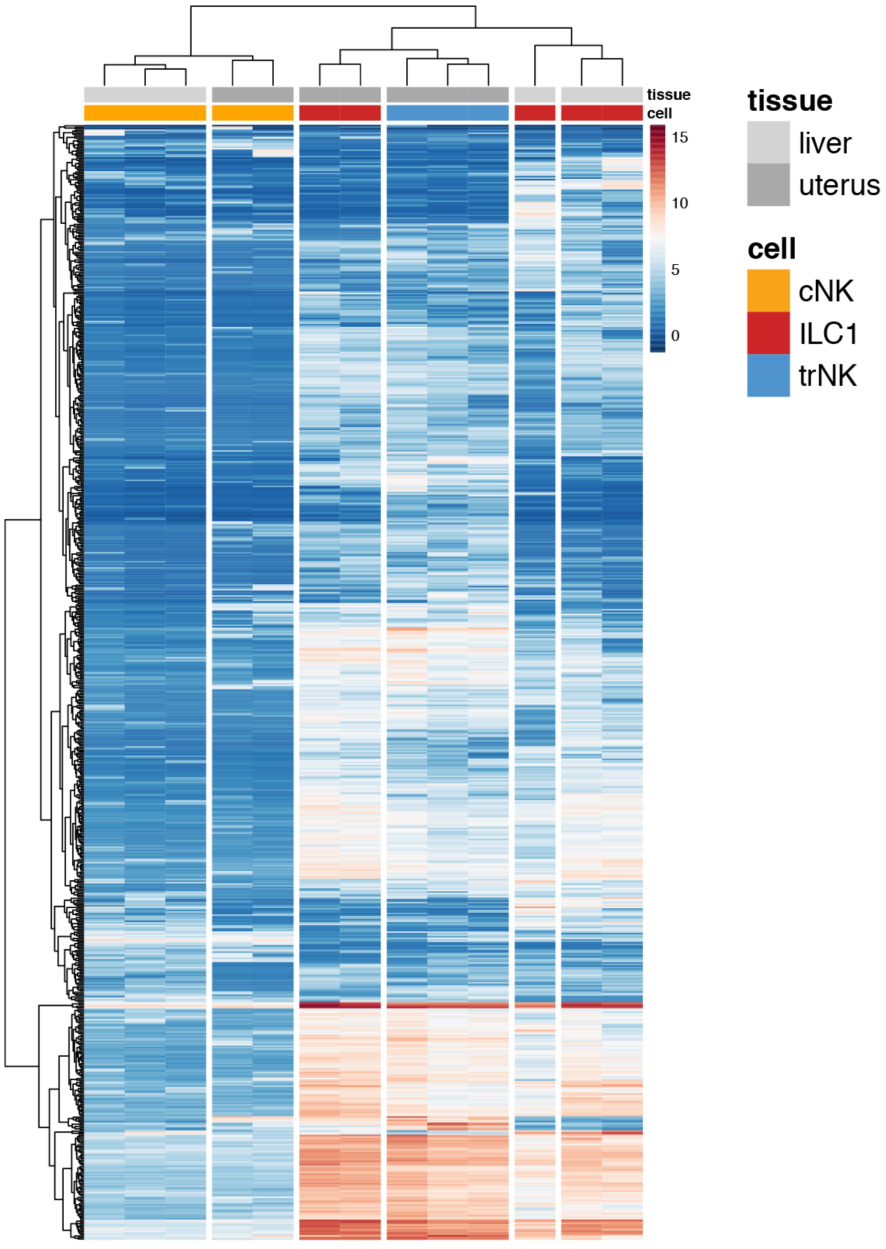

Figure 4.3. Heat map of differentially expressed genes confirms the difference between CD49a^{+} and CD49a^{-} subsets. Only the differentially expressed genes with a log2 fold change cut-off ≥ 7.5 and p-value ≤ 0.01 were selected to generate the heat map. These differentially expressed genes originate from pairwise comparisons explained later in this chapter, but with more stringent cut-off values. The legend accompanying the plot describes the data points (yellow: cNKs, red: ILC1s, blue: trNKs, light grey: liver and dark grey: uterine tissue).

The heat map presented in **Figure 4.3** was made using the differentially expressed gene lists described later in this chapter (with a more stringent log2fold change and p-value cut-off) and is used here only to confirm the PCA findings (**Fig. 4.2**), particularly the differences between ILC1s from two different tissues as well as similarities between cNKs from these two tissues.

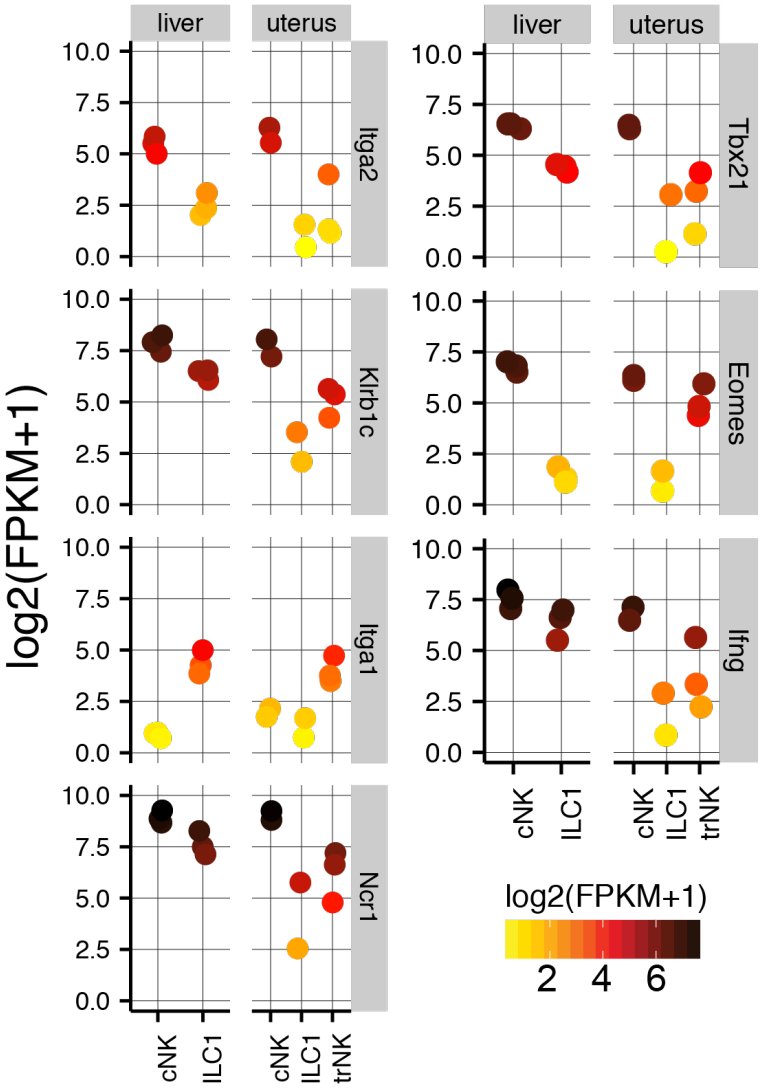

Figure 4.4. Individual gene expression of selected genes validates the FACS-sorting strategy. Expression levels of some genes encoding proteins that were used for the sorting of g1 ILCs from uterus and liver at mid-gestation for the RNA-seq experiments are shown, in addition to some other genes encoding various proteins important in development/functions of distinct subsets of g1 ILCs. The colour scale represents log2(FPKM+1) transformed normalised reads. FPKM: fragments per kilobase of exon model per million reads mapped.

Furthermore, all five subsets were confirmed to express *Klrb1c* (NK1.1), *Ncr1* (NKp46) – although this gene was found to be expressed at low levels in uterine ILC1s in a pattern similar to *Tbx21* (T-bet) and *Ifng* (IFNγ). The subsets were also distinguished according to expression of *Eomes*, *Itga1* (Cd49a) and *Itga2* (Cd49b) (**Fig. 4.4**). Validation through analysing the expression of individual genes in such manner indicated that the performed sorting was reliable.

4.2.2 Principal Component Analysis reveals novel transcripts in group 1 ILCs

Genes defining the two principal components used for clustering in **Figure 4.2** were explored in further detail. Principal component 1 (PC1) explained 61% of the variance between the subsets (**Fig. 4.2** and **4.5a**).

Some of the genes explaining this variance belonged to the C-type lectin domain families, such as *Clec7a* and *Clec4a3*, encoding DECTIN-1 and DCIR3, respectively, which were both significantly upregulated in both CD49a$^+$ ILC1s and trNKs compared to the cNK cells in the uterus, with a similar pattern of expression in liver CD49a$^+$Eomes$^-$ ILC1s (individual gene expression for these genes will not be presented here). It is also worth noting that although these genes were found to be upregulated in both CD49a$^+$ subsets in the uterus, they were more highly expressed in ILC1s compared to trNKs. Other genes defining PC1 were genes encoding surface-expressed TLR1 and intracellular TLR13, *Adgre1* encoding F4/80 and *Mertk* encoding MerTK, a member of the Tyro-3/Axl/Mer (TAM) family of receptor tyrosine kinases (RTKs). Similarly, these genes were upregulated in CD49a$^+$ subsets in both organs and showed a very low overall level of expression in cNK cells.

Principal component 2 (PC2) explained 18.8% of the variance (**Fig.4.2** and **4.5b**). Unlike in the uterus, genes found in PC2 were significantly upregulated in the liver ILC1s (expression of the individual genes will not be shown at this point), with low to almost no expression

observed in any of the other subsets, explaining in part why liver ILC1s do not cluster with uterine ILC1s. Surprisingly, several of the top genes defining the PC2 were associated with the gene signature of B-cells. In addition to genes encoding various domains of the light and heavy immunoglobulin chains, *CD79a, Blk* as well as *CD19* appeared to contribute to this variance. One of the rare genes upregulated in uterine ILC1s within PC2 was *CD200r2*, one of the receptors for CD200, type-1 immunoglobulin superfamily member (**Fig. 4.5b**).

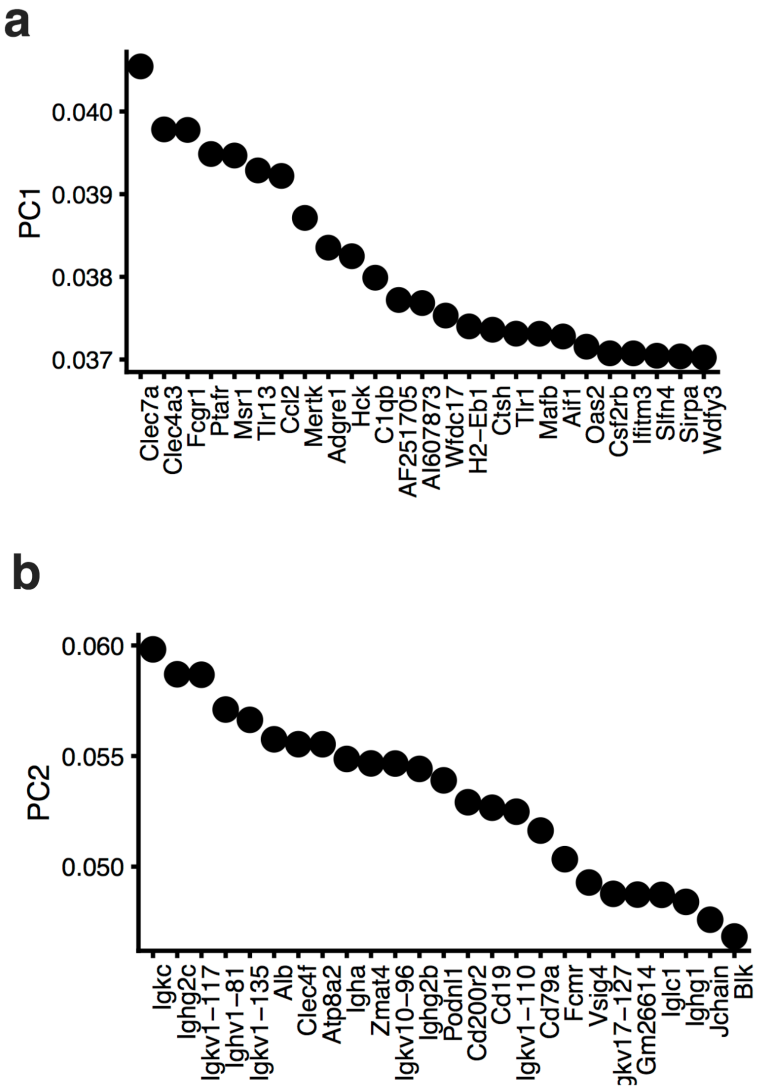

Figure 4.5. Principal components 1 and 2 reveal novel transcripts in g1 ILCs. Top genes which explain the variance within PC1 and PC2 are shown. (**a**) Top genes explaining the variance within PC1. (**b**) Top genes explaining the variance within PC2.

4.2.3 Exploration of newly identified transcripts in uterine group 1 ILCs

Flow cytometry experiments were performed to attempt to explore some of the transcripts that were identified through the analysis of the PC1 and PC2 on the protein level, as well as some other genes of interest. Only a few of numerous targets explored are presented in **Figure 4.6.**

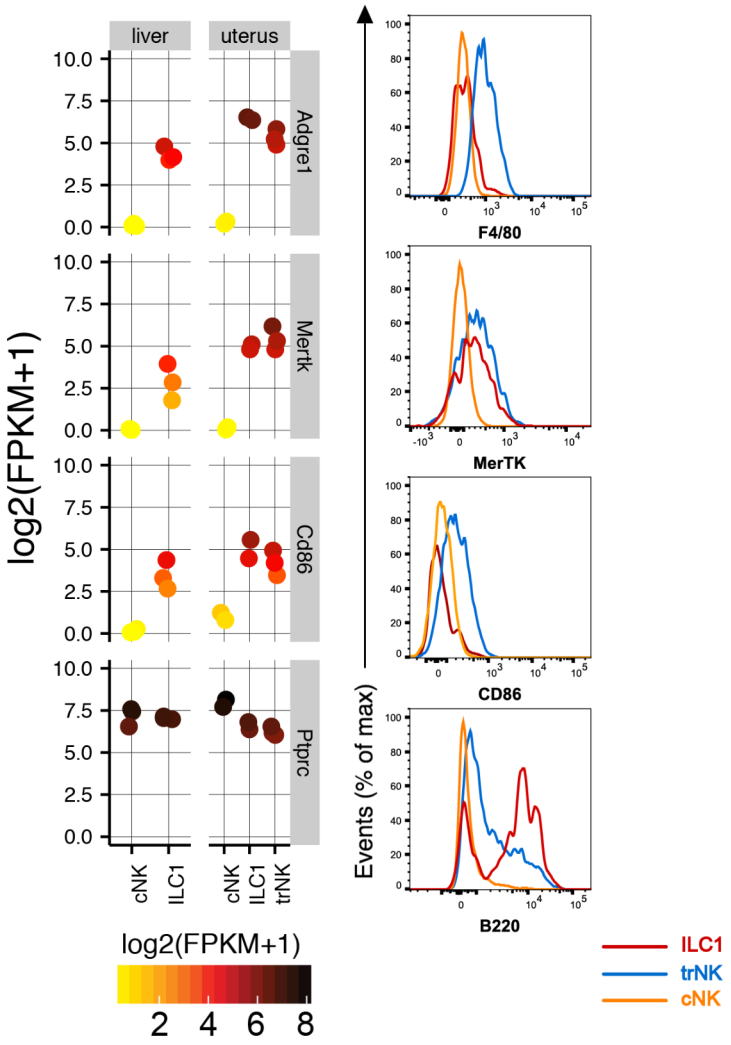

Figure 4.6. Protein expression confirmed some of the selected highly expressed transcripts. Plots on the left show expression levels of selected individual genes in uterine and liver g1 ILCs. Histograms to the right of each gene expression plot show the representative flow cytometry validation data of their protein products in the uterus at mid-gestation. Fluorescence minus one (FMO) and isotype controls were used to set the gates for the flow cytometry experiments as explained in Chapter 2. Data is representative of at least five independent experiments. Colour coding for g1 ILCs is the same as in all previous figures in this chapter. The colour scale represents log2(FPKM+1) transformed normalised reads. FPKM: fragments per kilobase of exon model per million reads mapped.

It was confirmed that F4/80, a protein encoded by *Adgre1*, was indeed expressed by uterine group 1 ILCs, as suggested by the RNA-seq data. However, although both ILC1s and trNKs had high levels of the transcript, protein was expressed only in trNKs. On the other hand, MerTK protein was expressed at similar levels in both ILC1s and trNKs of mid-gestation uterus. Some other genes that are characteristic of cells usually expressing MerTK and F4/80 (APCs) were also examined on the protein level. CD86 (also known as B7-2), for instance, a co-stimulatory molecule required to activate T cells by APCs, was found to be expressed on trNK cells. *Ptprc* gene was expressed equally high in all g1 ILCs in the uterus and liver, but there was a distinct pattern of its protein (B220) expression in uterine g1 ILCs, with ILC1s displaying almost a bimodal pattern of expression, trNKs displaying intermediate levels of it on their surface and cNKs not expressing any B220.

Figure 4.5b showed that *Cd19* was one of the top transcripts explaining the variance within PC2. Differential *Cd19* gene expression between the liver and the uterus (not shown) pointed to a higher level of *Cd19* transcript in the liver ILC1s compared to CD49a$^+$ subsets in the uterus. This was investigated further on the protein level by flow cytometry in the liver and uterus at mid-gestation, by excluding CD19 from the initial gating steps to eliminate lineage-negative cells and then continuing as previously described. However, on the protein level at mid-gestation (gd 9.5), there was not a significant difference in the percentage of CD19$^+$ cells between ILC1s and trNK and liver ILC1s (**Fig. 4.7a** and **b**), although a low percentage of CD19$^+$ cells was observed in both tissues at gd 9.5 in the ILC1 gate. Strikingly, CD19$^+$ cells were the most abundant early in gestation within ILC1s, at gd 5.5, when between 10-50% of ILC1s expressed CD19 (**Fig. 4.7a** and **b**). Even though their percentage was variable (**Fig. 4.7b**), it was always significantly higher than at gd 9.5. This was an observation highly specific to the uterus, since the same trend in liver ILC1s was not observed. Once it became

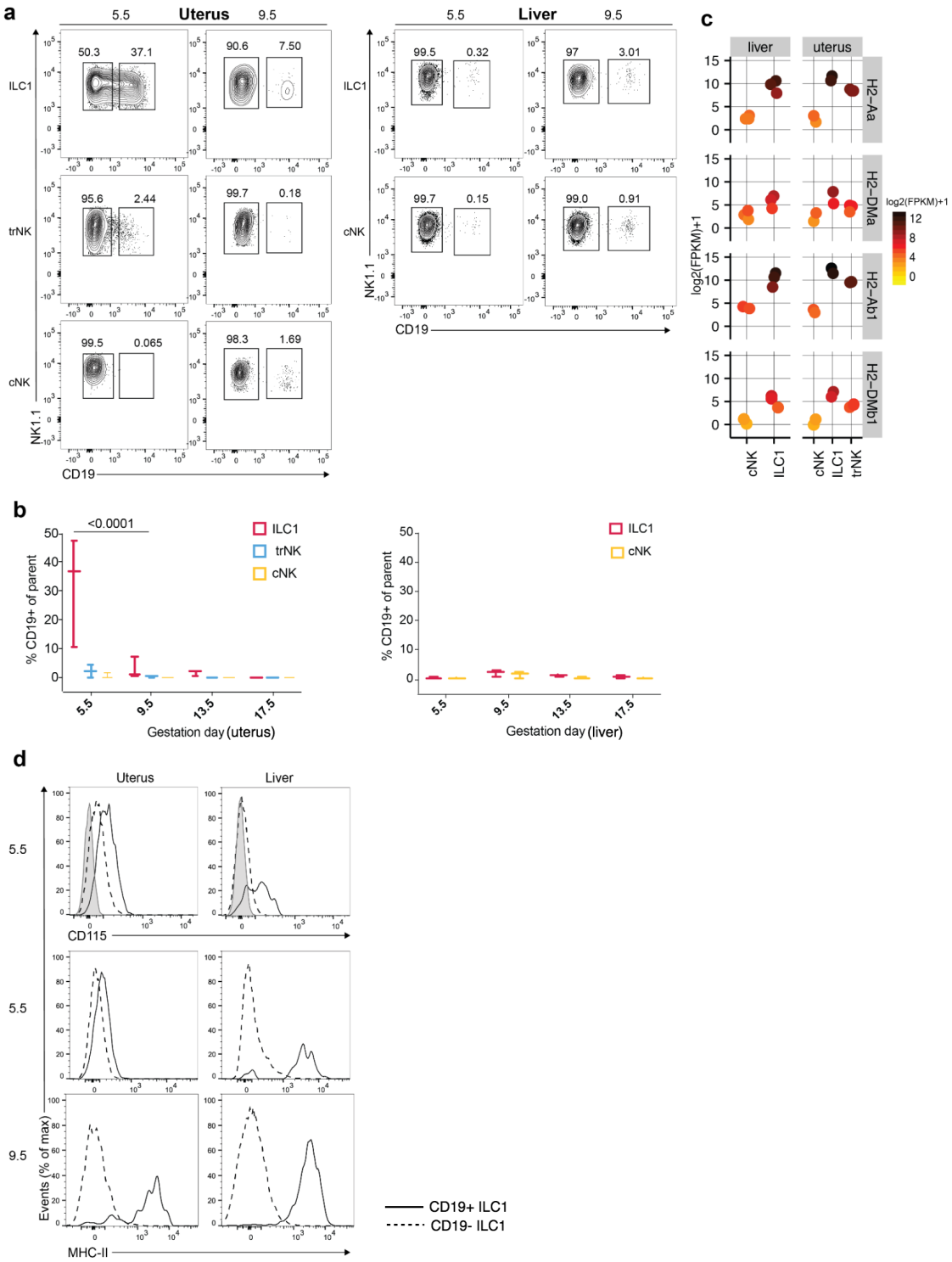

Figure 4.7.Some ILC1s express CD19 and MHC-II. (a) Representative flow cytometry plots showing CD19 expression on the g1 ILCs in the uterus and liver at gd 5.5 and gd 9.5 as indicated in the figure. ILC1s, trNKs, cNKs in both liver and uterus were gated as described in all previous figures. Gates were set using FMO and isotype controls as mentioned in the Chapter 2 and all other figures. Data is representative of at least 4 independent experiments. (**b)** Quantification of the CD19^{+} subsets within their parent populations during four gestation time-points and as gated in (a) in both uterus and liver. Only significant p-values are presented. Two-way ANOVA with multiple comparisons corrections was used to analyse the data for statistical significance. Error bars represent maximum and minimum values. (**c**) Expression levels of various genes encoding chains of

the MHC-II protein in uterine and liver g1 ILCs samples from the RNA-seq data. (**d**) Expression of CD115 at gd 5.5 and MHC-II at gd 5.5 and gd 9.5 on uterine and liver ILC1s, stratified by CD19 expression. CD115 data is representative of 2 independent experiments and MHC-II data is representative of at least 10 independent experiments. Dashed line: CD19- IL1s, full line: CD19+ ILC1s, grey-shaded histogram: isotype control for CD115. Colour coding for g1 ILCs is the same as in all previous figures in this chapter. The colour scale represents log2(FPKM+1) transformed normalised reads. FPKM: fragments per kilobase of exon model per million reads mapped.

evident that there are $CD19^+$ and $CD19^-$ ILC1s, expression of certain proteins of interest was further explored on the surface of these two subsets. One of these proteins was MHC-II, since it was observed in the RNA-seq dataset that several genes encoding various chains of the MHC-II molecule were upregulated in $C49a^+$ subsets in the liver and uterus, particularly *H2-Aa* and *H2-Ab* in both uterus and liver (**Fig. 4.7c**). While in the liver there was continuously a population of $MHC\text{-}II^+CD19^+$ ILC1s and $MHC\text{-}II^-CD19^-$ ILC1s, this was not the case in the uterus.

Only at gd 9.5 there was a significant shift in the level of expression of MHC-II on $CD19^+$ ILC1s compared to a very low expression early in gestation at gd 5.5, suggesting a dynamic regulation of the protein expression in the uterine microenvironment (**Fig. 4.7d**). In addition, the gene encoding macrophage-colony stimulating factor receptor (M-CSFR/CSF-R1/CD115) and mainly known as a receptor for the M-CSF and IL-34, came up as upregulated in $CD49a^+$ cells in the uterus and liver. As shown in **Fig. 4.7d**, CD115 was indeed expressed on both $CD19^+$ and $CD19^-$ ILC1s in the uterus at gd 5.5, but only on $CD19^+$ ILC1 in the liver at the same time-point. CD115 was not validated to be expressed on the uterine trNKs. Finally, when the pregnant uterus at gd 9.5 was dissected into two layers: decidua and myometrium/MLAp, there was a higher percentage of $CD19^+$ ILC1s identified in the decidua, closer to the site of interaction with the embryo, suggesting not only temporal but also a spatial organisation of $CD19^+$ ILC1s (**Fig.4.8**).

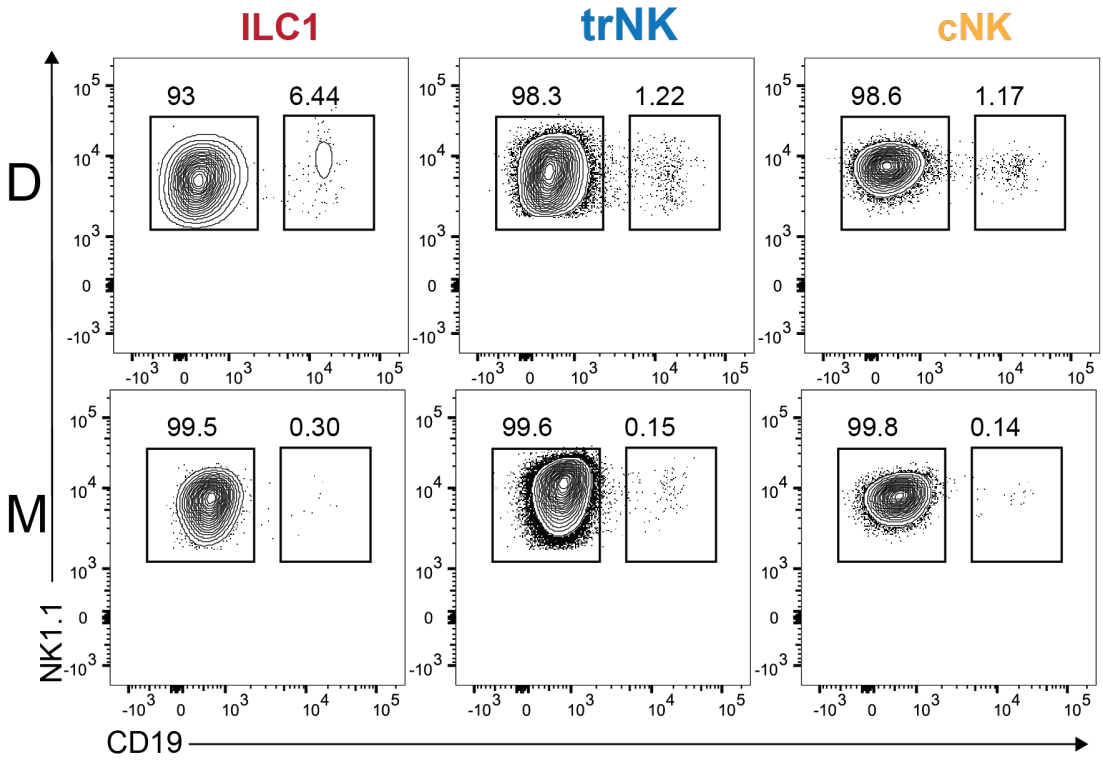

Figure 4.8. CD19$^+$ cells are more abundant in the decidua compared to the myometrium/MLAp at mid-gestation. As explained in the Materials and Methods (Chapter 2), decidua was separated from the myometrium/MLAp in order to assess the spatial organisation of CD19$^+$ subsets with a better resolution. The populations were sorted as single, live, CD45$^+$CD3$^-$NK1.1$^+$NKp46$^+$ and (1) Eomes$^-$CD49a$^+$ for ILC1s, (2) Eomes$^+$CD49a$^+$ for trNKs and (3) Eomes$^+$CD49a$^-$ for cNKs. These parent populations of distinct g1 ILCs were then gated as shown in the plots above for CD19 expression. Top row represents decidua and bottom row myometrium/MLAp. Plots are representative of two independent experiments. D: decidua, M: myometrium/MLAp.

4.2.4 Identifying the core gene signatures of uterine g1 ILCs

Ultimately, the goal of this study was to define the core gene signatures of uterine g1 ILCs that would represent a valuable resource for the future studies in the field of reproductive immunology. After lists of differentially expressed genes (DEGs) between subsets had been generated (with Russell Hamilton, see Statement of collaborative work), they were analysed using several approaches: (1) UpSet, (2) Gene Ontology (GO) and (3) exploring DEGs for the highest-fold change in genes (either up- or down-regulated).

UpSet is a computational tool which is superior over Venn diagrams as it allows visualisation of many intersections in a considerably less complex manner. Here, UpSet was used to summarise some of the findings from the DEG lists and identify genes only differentially expressed in a comparison of interest and nowhere else. This is because the input for the UpSet are the DEG lists. By data-mining through these lists, UpSet determines which genes (from which pairwise comparison, for instance), have not been identified in any of the other comparisons. Initially, 11 pairwise comparisons of the DEG lists were performed. However, 5 comparisons were finally selected for an in-depth analysis based upon primary objectives of this study: (a) what the differences between 'circulating' (Eomes^{+}CD49a^{-}) and 'tissue-resident' (Eomes^{+}CD49a^{+} and Eomes^{-}CD49a^{+}) between the two tissues are and (b) how these cells are different from each other within the uterus only.

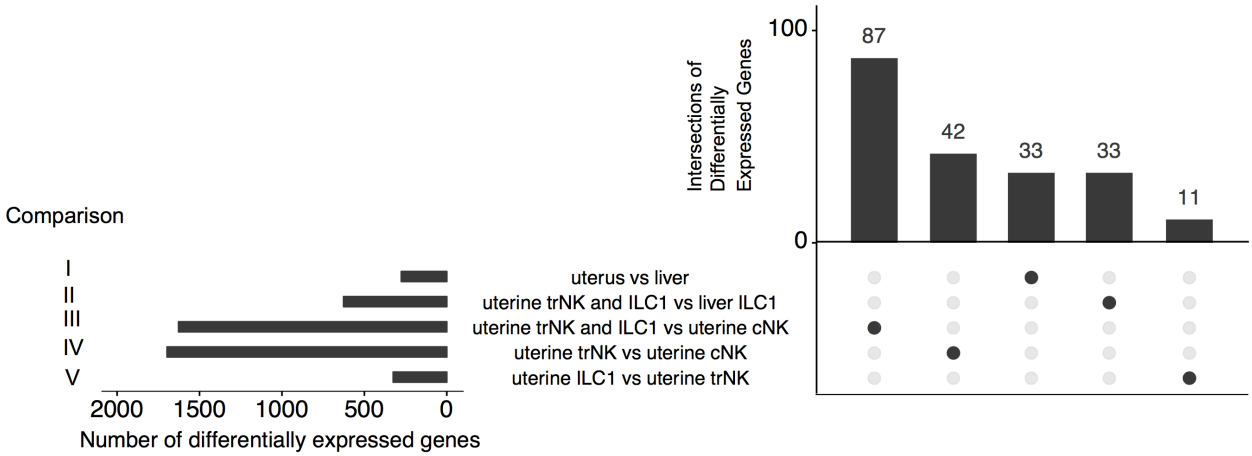

Figure 4.9. Summary of the differentially expressed genes in selected comparisons. UpSetR plot displayed here represents the summary of the comparisons of interest for the scope of this study. DEG lists were used for the UpSetR input and the comparison lists of genes which were used have been labelled in Roman numbers I-V and will be referred in such way throughout the text. The dots in the intersections on the plot on the right-hand side of the figure show how many unique genes were found in that particular comparison and none of the others.

To address the objective (a), two comparisons between DEG lists were made (summarised in **Fig. 4.9**):

I All uterine (**ILC1, trNK, cNK**) vs all liver subsets (**ILC1, cNK**);

II Uterine CD49a$^+$ (**ILC1, trNK**) vs liver CD49a$^+$ (**ILC1**).

To address the objective (b), 3 comparisons of DEG lists were performed:

III Uterine CD49a$^+$ (**ILC1, trNK**) vs uterine CD49a$^-$ (**cNK**);

IV Uterine Eomes$^+$CD49a$^+$ (**trNK**) vs uterine Eomes$^+$CD49a$^-$ (**cNK**);

V Uterine Eomes$^-$CD49a$^+$ (**ILC1**) vs uterine Eomes$^+$CD49a$^+$ (**trNK**).

The number of differentially expressed genes was variable, from about 250 to just over 1,500 detected genes with the adjusted p-value < 0.05 and log2 fold change two or above (**Fig. 4.9**).

Comparison I: Differences between all uterine and all liver g1 ILCs at mid-gestation

Functional annotation GO analysis of the differentially expressed genes between all uterine and all liver g1 ILCs pointed to vascular endothelial growth factor (VEGF) signalling and oxygen/gas transport as some of the most highly enriched biological pathways in all uterine g1 ILCs (Figure 4.10a) Specific genes involved in these pathways included *Kdr*, encoding VEGF receptor 2 and *Pdgfra*, alpha receptor for the plateled-derived growth factor (PDGF), found in the VEGF signalling pathway, but also haemoglobin chains within the oxygen and gas transport pathways (Hbb-Y, Hba-X, Hbb-BH1) (**Fig. 4.10a**). In total, 265 pathways were detected in this comparison. As many genes were involved in multiple pathways, some of them overlapped. For example, regulation of cellular response to TGF-β signalling, SMAD protein transduction and regulation of pathway-restricted SMAD protein phosphorylation (with upregulated *Dab2*, *Fbn1*, *Tgfb2*, *Inhba)* all pointed to the importance of tightly regulated TGF-β signalling in the uterine g1 ILCs. Other significantly enriched uterine pathways included response to hypoxia and decreased oxygen levels (*Ang*, *Hif3a*, *Hlf*, *Kdr*), extracellular matrix organisation (*Flrt2*, *Fbln1*, *Mmp9*, *Tgfbi*), as well as a number of

pathways relating to wound healing and the regulation of blood vessel development.

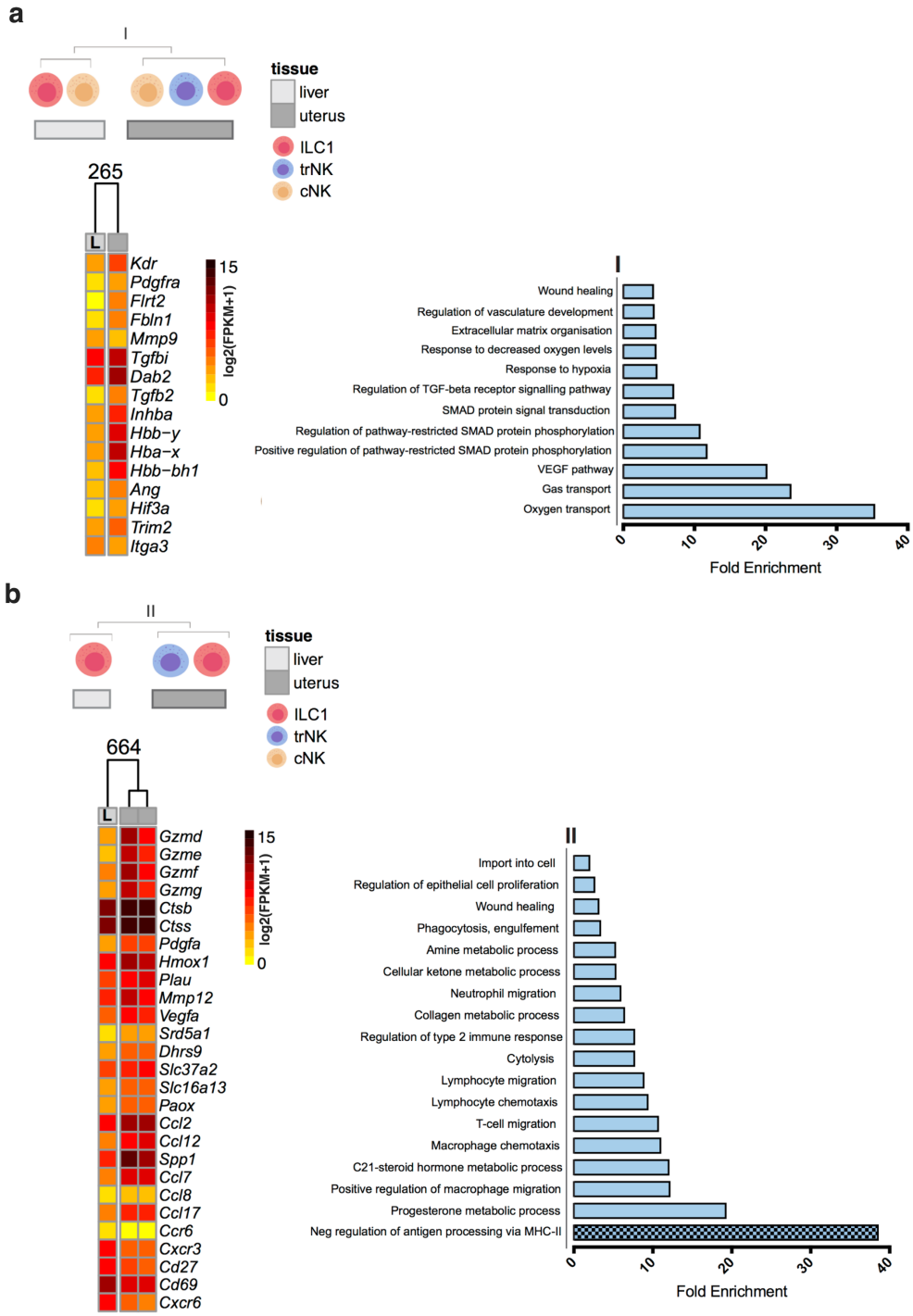

Figure 4.10. Genes determining the differences between uterine and liver g1 ILCs. Selected genes from the comparisons of interest are presented in the heat maps shown on the left (**a-b**). The genes in heat maps were selected from the analyses of Gene Ontology (GO) enriched pathways (shown to the right of each heat map), UpSetR data (Fig. 4.9) and DEG gene lists for highest fold change genes. (**a**) The heatmap and GO analysis for comparison I. (**b**) The heatmap and GO analysis for comparison II. Patterned bar indicates GO pathways enriched in liver ILC1s, while all other bars are pathways enriched in uterine subsets. The colour scale represents log2(FPKM+1) transformed normalised reads. FPKM: fragments per kilobase of exon model per million reads mapped.

Overall, the pathways enriched across uterine g1 ILCs relate to uterine physiology at mid-gestation, such as vascular remodelling. UpSet list of genes exclusively differentially expressed between all uterine and all liver subsets suggested *Itga3,* encoding CD49c, as the most highly expressed liver g1 ILC specific gene and *Trim2* as the uterine counterpart (**Fig. 4.10a**).

Comparison II: Differences between CD49a$^+$ cells in the uterus and liver at mid-gestation

Similarly to the previous comparison, but excluding cNK cells from the analysis, DEGs determining the differences between tissue-resident (CD49a$^+$) subsets in the uterus and liver were further analysed. The top enriched pathway (almost 40-fold) was negative regulation of antigen processing and presentation of peptide via MHC-II, with *H2-Oa* and *H2-Ob* as representative genes within this pathway. Both genes encode H2-O protein with a main function of inhibiting the H2-DM-mediated antigen-loading process (Walter et al., 2000). Both genes were upregulated in liver ILC1s compared to uterine trNK and ILC1s (**Fig. 4.10b**). Most highly upregulated genes in the uterine CD49a$^+$ cells were *Gzme*, *Gzmd*, *Gzmg*, *Gzmf*, encoding 'non-conventional' mouse granzymes, identified as a part of the highly enriched pathway of cytolysis via the GO. Steroid metabolic processes, including progesterone metabolism, were found to be almost 20-fold enriched in the uterus with genes such as *Srd5a1* and *Dhrs9.* Genes associated with macrophage chemotaxis, but also lymphocyte migration were enriched in uterine tissue-resident cells (*Ccl2*, *Ccl12, Ccl7*, *Ccl8*, *Ccl17*), suggesting that they may be involved in a crosstalk with myeloid and lymphoid cells and that this may be of more importance in the uterus compared to liver. This is emphasised by a high expression of *Spp1*, encoding ostepontin, which is important for neutrophil migration (Koh et al. ,2007) and reflected in about 6-fold enrichment of neutrophil migration pathway in CD49a$^+$ g1 ILCs (**Fig. 4.10b**). While lymphocyte migration in general was

characteristic of uterine CD49a$^+$ cells, liver ILC1s seemed to be equipped with the transcriptional machinery required to regulate T cell migration, through the upregulated genes *Cxcr3* and *Ccr6*. Collagen metabolism was also found to be upregulated in the uterus, with *Ctsb* and *Ctss* being the most highly expressed genes. Wound healing and ECM organisation (*Plau*, *Flrt3*, *Hmox1*, *Pdgfa*), as well as regulation of epithelial cell proliferation (*Vegfa*, *Mmp12*) coming up as enriched pathways showed it may be CD49a$^+$ cells rather than CD49a$^-$ cNK regulating these essential tissue-remodelling processes. Somewhat unexpected was the discovery of pathways like import into cell and phagocytosis, usually associated with the antigen-presenting cells (APCs). UpSet analysis pointed to *Ccr6* to be exclusively differentially expressed in liver ILC1s, but also pointed to *Slc16a13* as a uterine CD49a$^+$ specific gene. Among genes in the list of differentially expressed genes between uterine and liver CD49a$^+$ cells, *Cd27*, *Cd69* and *Cxcr6* appeared to be upregulated in liver ILC1s (**Fig. 4.10b**).

Comparison III: Differences between the tissue-resident and circulating g1 ILCs in the uterus at mid-gestation

As more detailed, individual comparisons were carried out in the following two comparisons, for the overall comparison of CD49a$^+$ (ILC1 and trNK) to CD49a$^-$ (cNK) g1 ILCs in the uterus, GO Slim was used (a cut-down version of the regular GO used elsewhere in this work). Main enriched pathway in uterine CD49a$^+$ cells compared to cNKs was the unsaturated fatty acid biosynthesis (genes *Mgst1*, *Mgst2*, *Alox5ap*) (**Fig. 4.11a**). Related to this, lipid metabolism came up as enriched in the 2 CD49a$^+$ uterine subsets (genes *Apoe*, *Psap*). The next most enriched pathway was the lysosomal transport (genes *Rab7b*, *Lamp2*, *CD68*, *Lamp1*). Response to IFN-γ was highly characteristic of these cells (through a very high expression of *Irf7* for instance). *S1pr5*, encoding sphingosine-1-phosphate receptor 5

and well-known receptor regulating egress of NK cells came up as the main uniquely differentially expressed gene between CD49a^{+} and CD49a^{-} cells, specifically upregulated in CD49a^{-} cNK cells.

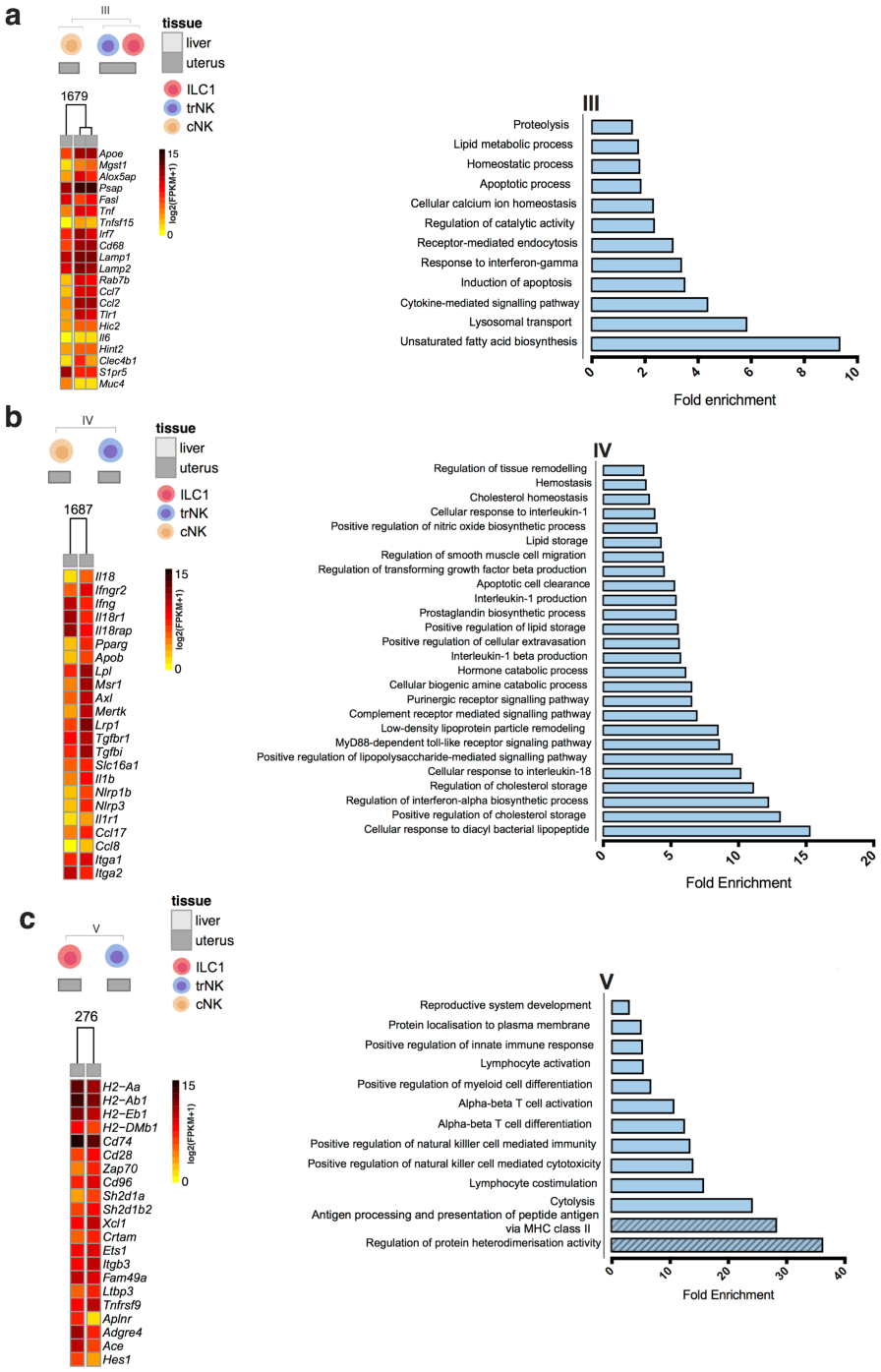

Figure 4.11. Genes determining the differences between uterine g1 ILCs. Selected genes from the comparisons of interest are presented in the heat maps shown on the left (**a-c**). The genes in heat maps were selected from the analyses of Gene Ontology (GO) enriched pathways (shown to the right of each heat map), UpSetR data (Fig. 4.9) and DEG gene lists for highest fold change genes. (**a**) The heatmap and GO analysis for comparison III. (**b**) The heatmap and GO analysis for comparison IV. (**c**) The heatmap and GO analysis for

comparison V. Patterned bar in (c) indicates GO pathways enriched in uterine ILC1s, while all other bars are pathways enriched in uterine trNKs. The colour scale represents log2(FPKM+1) transformed normalised reads. FPKM: fragments per kilobase of exon model per million reads mapped.

On the other hand, hypermethylated-in-cancer-2, encoded by *Hic2* appeared specific to uterine CD49a^{+} and no other cells. *Ccl7* was a gene with the highest fold change in the uterus, while it was almost not expressed at all in the liver ILC1s. *Ccl2* and *Tlr1* were some of the other very highly upregulated genes in trNK and ILC1, while cNK cells may be important sources of Mucin4 (*Muc4*) (**Fig. 4.11a**).

Comparison IV: Differences between the uterine trNK and cNK cells at mid-gestation

*Msr1***,** encoding macrophage-scavenger receptor 1 and *Clec7a*, encoding DECTIN-1, exhibited the highest fold change in trNK compared to cNK (about 300-500-fold, respectively) (**Fig 4.11b**). One of the genes upregulated almost 40-fold in trNKs was *Slc40a1*, encoding ferroportin (FPN1) (**Fig. 4.12**). Given that FPN1 is the main exporter of iron from the cells, this suggests iron metabolism may be of importance in uterine tissue-resident NK cells. This dataset showed a high expression of *Nfe2l2* (NRF2) and significantly upregulated *Nfe2l3* (NRF3) in trNKs (Chevillard & Blank, 2011). Both proteins can bind to antioxidant response elements and *Nfe2l3* locus has been shown to be associated with endometriosis through genome-wide association studies, with a p-value of 1.4×10^{-9} (Painter et al., 2010). Some other *Nrf2*-target genes such as *Hmox1* were all found to be highly upregulated in trNKs.

About 900 enriched pathways were detected in the trNKs through the GO analysis. Pathways relating to the cholesterol storage and homeostasis were among the most highly enriched pathways in trNKs with genes such as *Pparg*, *Apob* and *Lpl*. Genes associated with cellular response to IL-18 were also upregulated in a way that suggested crosstalk between trNKs and cNKs: trNK cells upregulated *Il18* and *Ifngr2*, while cNK cells upregulated *Il18r1* and

Il18rap as well as *Ifng*. Thus, cNK cells may be more responsive to IL-18 and a major source of IFN-γ, and trNK cells may be more important as producers of IL-18 and cells responsive to IFN-γ. In a similar manner, trNK cells were also found to potentially be involved in IL-1β production but to also be responsive to IL-1, through a high expression of genes such as *Nlrp1b*, *Nlrp3*, *Il1b*, (IL-1β production) and *Il1r1*, *Ccl1*, *Ccl17*, *Ccl8* (cellular response to IL-1). Interestingly, apoptotic cell clearance was among the enriched pathways, with genes like *Lrp1*, *Axl* and *Mertk* highly upregulated compared to cNK cells. As shown here, trNK (but also ILC1) may be highly responsive to TGF-β, sensing this cytokine's fluctuations through receptors such as *Lrp1*, but also *Tgfbr1* (**Fig. 4.11b**).

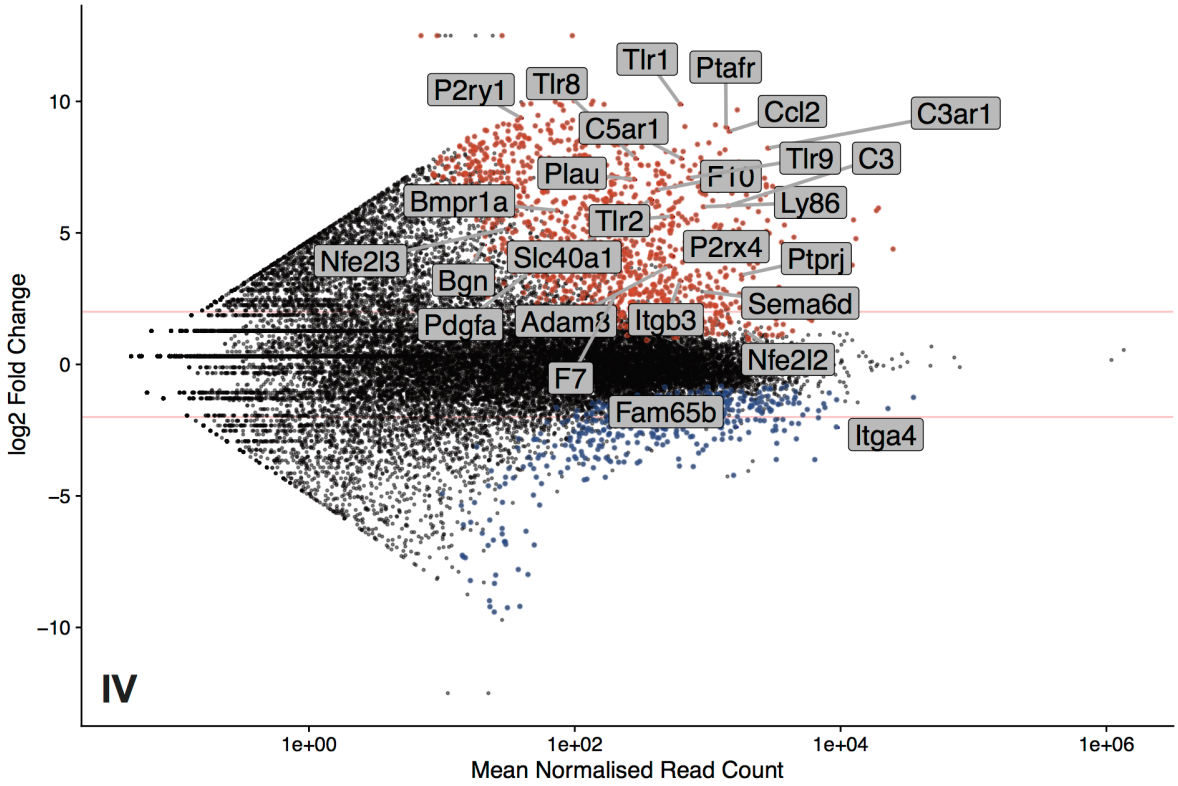

Figure 4.12. Differences between the uterine trNK and cNK cells at mid-gestation. Selected genes from the comparisons of interest are presented in the MA plot. The genes labelled on the plot were selected from the analyses of Gene Ontology (GO) enriched pathways and UpSetR data (Fig. 4.9), both derived from the DEG gene lists for highest fold change genes. Red lines represent the absolute cut-off value of the log2 fold change of 2 that was used to generate the DEG lists. Red dots are significantly upregulated genes in trNKs, while blue dots represent cNK upregulated genes.

In addition, *Tgfbi*, introduced in comparison I earlier as a significantly upregulated uterine-specific transcript, was upregulated in trNKs. UpSet pointed to *Slc16a1*, encoding MCT1, one of well characterized monocarboxylate transporters (lactate exporter) to be unique to trNK, suggesting the potential importance of distinct metabolic requirements for uterine CD49a^{+} trNK cells compared to other subsets. Some other unique genes in trNK compared to cNK were *Tlr9, Tlr1, Bgn* as well as various genes involved in the purinergic receptor signaling (*P2rx4*, *P2rx7*) pathways (**Fig. 4.11b** and **Fig. 4.12**).

Comparison V: Differences between the uterine ILC1 and trNK cells at mid-gestation

While there was a much lower number of DEGs between uterine ILC1 and trNK than in some other comparisons, the GO analysis between them uncovered subtle differences between these two subsets phenotypically different by Eomes expression. Most highly upregulated gene in ILC1s compared to trNK was *Aplnr*, encoding for APJ or apelin receptor, which responds to the adipokine apelin (**Fig. 4.11c**). Apelin receptor was shown before to be very highly expressed in the mouse endometrium by in situ hybridisation histochemistry, while no expression was observed in the myometrium (Pope et al., 2012).

Some other highly expressed genes in ILC1s included *Adgre4*, encoding F4/80 receptor as well as *Ace*, encoding angiotensin I-converting enzyme which is a part of the renin-angiotensin system. Protein heterodimerisation activity was the most highly enriched pathway in uterine ILC1s (gene *Hes1* for example). Genes *H2-Aa*, *H2-DMb1*, *H2-Ab1*, *H2-Eb1* and *CD74* were found to be expressed highly in both ILC1 and trNK, but to a higher extent in ILC1, resulting in pathways related to antigen processing and presentation of peptide via MHC class II to be among the most highly enriched pathways detected in ILC1s. However, most other detected DEGs were downregulated in ILC1s compared to trNKs. *Sh2d1a*, encoding signalling lymphocytic activation molecule (SLAM)-associated protein

(SAP) with a role in SLAM signalling, *Sh2d1b2*, encoding EAT-2B and also a member of SAP-family of adapters, as well as *CD96* were all upregulated in trNK. Similarly, *Crtam*, commonly recognised as a receptor for Nectin-like molecules (Arase et al., 2005) and *Xcl1*, encoding lymphotactin previously shown to be produced by the human uNK cells (Kennedy et al., 2016), both part of leukocyte-mediated cytotoxicity GO pathway, were found to be highly expressed in trNKs. In addition, a number of enriched pathways related to the lymphocyte activation and in particular differentiation/activation of T-cells was identified. Specific genes from these pathways upregulated in trNKs were *CD28* and *Zap70,* for instance. Not only was the trNK signature associated with interaction with lymphocytes, but it also suggested a potential regulation of myeloid cell differentiation, through genes such as *Ets1* and *Itgb3.* The only uniquely differentially upregulated gene in ILC1 as suggested by UpSet was *Fam49a*. trNK cells were marked by significantly upregulated expression of *Ltbp3* and *Tnfrsf9* among other genes (**Fig 4.11c**).

4.3 Summary

In this chapter, the RNA-seq dataset was explored in further detail. The overall aim was to interpret the findings, attempt to validate some of them and explore further biologically in order to demonstrate the usefulness of the dataset as a resource and finally, to identify the core gene signatures for the uterine g1 ILCs at mid-gestation.

Through PCA and hierarchical clustering of all 5 subsets from the uterus and liver, it became clear that what is referred to as 'tissue-residency', expression of CD49a surface marker, affects how the g1 ILC subsets will cluster. Based on the unbiased PCA clustering analysis taking into the account the most variable genes, Eomes^{-}CD49a^{-} cNKs from the liver and uterus clustered together and were clearly separated from all the other subsets. According to the heat map taking into the account only the DEG lists, Eomes^{-}CD49a^{+} ILC1s and Eomes^{+}

CD49a$^+$ trNKs from the uterus clustered with the liver ILC1s, while cNKs were separated from these 3 subsets, confirming that there are gene signatures that are specific to CD49a$^-$ or CD49a$^+$ subsets through unbiased clustering approaches. One should be careful when defining these cells as 'tissue-resident' or 'circulating'. Although these terms were used in this dissertation to refer to CD49a$^+$ cells as tissue-resident and CD49a$^-$ subsets as circulating/conventional/splenic-like cNK cells, this might not be a completely accurate interpretation. Original studies using the surgical mouse model of parabiosis showed that CD49a$^+$ liver NK cells were indeed tissue-resident because they were found only within the host immune compartment rather than in the other parabiont (Peng et al., 2013). This was later confirmed for the uterine and skin CD49a$^+$ cells (Sojka et al., 2014). It was, however, recently shown that CD49a$^+$ can be induced on human pbNK cells through the stimulation with IL-12 and IL-15 (Hydes et al., 2017). Therefore, one should be careful when using only one or several markers to describe cells as truly tissue-resident or circulating. It might be that these markers are upregulated as a consequence of their recruitment to distinct microenvironment. Thus, one should not use such limited information in order to make the assumptions about the origin of cells, for instance.

Looking in detail at the genes within the first two principal components that determined PCA clustering revealed several novel transcripts in both uterine and liver g1 ILCs that were previously unappreciated for this group of cells. One of these transcripts was *Mertk*, encoding the MerTK from the TAM receptor family of RTKs, shown here to be expressed by both trNK and ILC1s in the uterus and liver and this was explored further on the protein level by flow cytometry in the uterus at mid-gestation. This might be relevant to the biology of reproduction as it was previously shown that TAM-triple knockouts are infertile (Lu et al., 1999; Lemke, 2013). trNK cells express highly another TAM receptor, *Axl*. In addition, it was shown that one of the MerTK ligands, Gas6 is expressed by the mouse trophoblast

(Madeja et al., 2011). In other studies, TAM receptors have been shown to be in transmitting signals required for generation of functional and mature NK cells (Caraux et al., 2006), which could also be highly relevant to the g1 ILCs in the uterus. Another gene that was one of the top genes within the PC2 was *CD200r2*, one of the receptors for CD200. Interaction between CD200 and its receptors has been associated with immunosuppressive signals and CD200-deficient mice are susceptible to autoimmunity (Taylor et al., 2005). Interestingly, other receptors for CD200 were found to be expressed in the uterine subsets in this study, such as *CD200r1* and *CD200r4* (data not shown). It was shown that CD200 can exert different functions depending on the receptor it binds and that it is highly expressed in immune-privileged sites (Carson et al., 2006). With a very recent study that suggested the involvement of soluble CD200 in the predisposition and pathology of endometriosis (Clark et al., 2018), it might possible this is another candidate gene that deserves a further look into in order to define the tissue-specific functions of g1 ILCs. By confirming the expression of proteins such as CD86 and F4/80, it appeared that CD49a$^+$ cells in the uterus at mid-gestation display gene and protein signatures resembling cells of myeloid origin, and particularly of the antigen-presenting cells (i.e. macrophages). Although most of these genes were similarly upregulated in liver Eomes$^-$CD49a$^+$ ILC1s, there was no protein expression for any of the proteins stained for, suggesting a uterine-specific regulation of the gene expression.

It was also shown in this chapter that some g1 ILCs, predominantly in the uterus, express CD19, a typical B cell protein. CD19$^+$ ILC1s cells were present in significantly higher numbers at gd 5.5 compared to gd 9.5 and also expressed MHC-II. CD19 was previously described on a subset of human pbNK cells from B lymphoblastic leukemia (Soma et al., 2014). Another report confirmed the existence of a population of CD19$^+$CD56$^+$ NK cells that could be detected in a cohort of pediatric patients with various immunodeficiencies and was present at similar levels over a number of years (Korol et al., 2015). CD19 therefore, may

mark g1 ILCs with the APC-like signature. Along these lines, DECTIN-1 is a receptor for β-glucans commonly expressed on phagocytes and plays an important role in the antifungal response. Recent study has clarified that NK cells recognise β-1,3-glucan in order to stimulate the granule convergence and polarisation (Li et al., 2018) and therefore increased expression of the gene encoding DECTIN-1 in uterine CD49a^{+} subsets may affect their effector functions, too.

Analysing the lists of the DEGs through various approaches pointed to previously unappreciated enriched pathways and associated genes in distinct subsets of g1 ILCs. While the search for genes of interest discussed here is not an exhaustive list, it demonstrates the value of the RNA-seq resource generated and offers the opportunity to design novel research projects.

Overall, uterine trNK and ILC1s appeared to be marked by gene signatures that were not only characteristic of other ILCs and NK cells, but also all other subsets of immune cells, including certain cells of myeloid lineage such as antigen-presenting cells.

In order to analyse the generated data systematically, inter-tissue (2 uterine vs liver comparisons) and intra-tissue (3 uterine comparisons) were performed in this study.

From the inter-tissue comparisons between the uterus and liver, some of the most commonly identified enriched pathways pointed to a potentially essential role of the TGF-ß signalling in the function of uterine g1 ILCs. Both trNK and ILC1s in the uterus at mid-gestation were found to express a number of upregulated TGF-ß receptor transcripts (*Tgbr1*, *Tgfbr2*). They even expressed *Lrp1*, which can bind the TGF-ß in addition to other functions, such as being a haemoglobin scavenging receptor and involved in apoptotic cell clearance (Staudt et al., 2013; Cao et al., 2014). Importantly, one of the most highly upregulated transcripts overall in this RNA-seq dataset was the *Tgfbi*, encoding the TGF-ß induced protein, TGBI (also known as BIGH3). TGFBI is a secreted ECM protein. It was originally identified in human

adenocarcinoma cell line post-incubation with TGF-ß for 48 hours, thus the name (Skonier et al., 1992). It has since been described as a protein secreted in several tissue microenvironments, including tumour models, but it is now known that it can be induced by factors other than TGF-ß and jointly with other ECM components like fibronectin, as was shown for IL-4 in macrophages (Gratchev et al., 2001). For the field of reproductive biology, TGF-ß is very important as it had been shown to inhibit trophoblast proliferation and invasion, but different studies reported different downstream inhibition pathways (Staun-Ram & Shalev, 2005), as well as that the TGF-ß may promote the proliferation of mouse trophoblast stem cells (Erlebacher et al., 2004). Other work showed that the TGFBI expression was highest at gd 4 in the mouse uterus, coinciding with the most active period of trophoblast invasion, but it was found to reduce from gd 7 in the uterus, while increasing in the placenta. In a non-pregnant uterus, its expression was at its highest in estrus (Uekita et al., 2003). It is therefore tempting to speculate that the TGF-ß induces the secretion of TGFBI by uterine CD49a^{+} cells, which then may be regulating some of the essential downstream events ensuring a successful placentation. Based on the work of others summarised above, this may occur via regulation of the trophoblast invasion or vascular remodelling and should be investigated in the future studies.

The other common theme to uterine-resident subsets compared to liver was enrichment of pathways involved in regulation of the migration of various other immune cells. One of these was the 6-fold enrichment of neutrophil migration pathway, and *Spp1* was one of the transcripts specifically upregulated within this pathway, which is supported by previous studies (Koh et al., 2007). Recently, it was reported that the protein ostepontin, encoded by *Spp1*, was secreted by the uterine trNKs and influenced fetal growth (Fu et al., 2017).

In order to interpret these findings, the alymphoid mouse model $Rag2^{-/-}Il2rg^{-/-}$ was used as these animals lack all B cells, T cells, NK cells and other ILCs. In line with the data previously described in this chapter, alymphoid mice indeed had a significantly lower expression of *Spp1* transcript at mid gestation (**Fig. 4.13**, bottom), presumably due to the lack of trNK cells, although there was still a residual level of expression observed. This confirmed findings of the aforementioned study at mid-gestation (Fu et al., 2017), although in the non-pregnant females, there was no significant difference between the immunocompetent (B6) and alymphoid (immunocompromised) animals. This is important because there are other sources of ostepontin, such as uterine glands (Hempstock et al., 2004) and it is therefore essential to not make premature conclusions only on the basis of expression in one cell type. The study by Fu and colleagues has shown 2 other growth factors, *Ptn* (encoding pleiotropin) and *Ogn* (encoding osteoglycin) to be expressed by the uterine trNK cells, but these were not validated in the work presented in this dissertation neither through RNA-seq (not shown), nor RT-qPCR (**Fig. 4.13**, top and bottom) and contradicted published findings (Fu et al., 2017). Finally, a highly enriched pathway in uterine compared to liver g1 ILCs was the progesterone metabolism (**Fig. 4.10b**). Uterine NK cells do not express various progesterone and oestrogen receptors in humans and mice (King et al., 1996; Henderson et al., 2003), although there is evidence that uNK cells are progesterone-dependent cells (Oh & Croy, 2008). To test whether progesterone induction would have any effect on the distribution of the g1 ILCs, non-pregnant and non-sexually mature animals were injected consecutively for three days with progesterone (as explained in the Chapter 2 and previously described in (Tagliani et al., 2011)). Only first few time-points are presented in **Figure 4.14** (3w, 3w with progesterone injections and 5w and 8w when the animals reach sexual maturity).

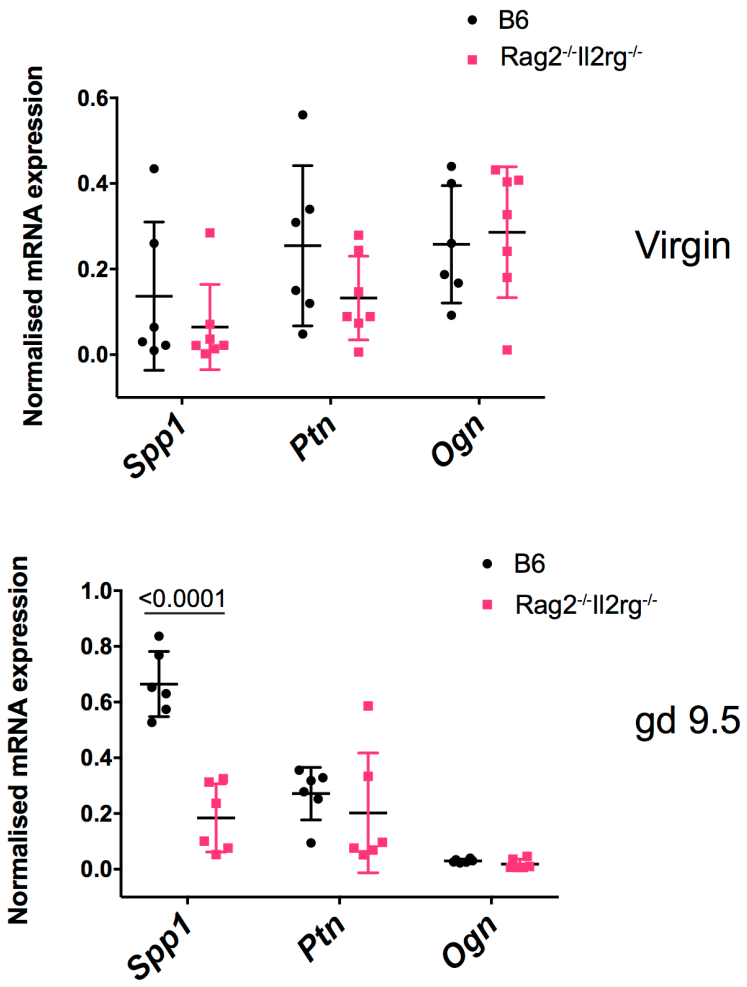

Figure 4.13. Gene expression of the growth factors in the uterus. Levels of the mRNA expression of Spp1, Ptn and Ogn were analysed by the RT-qPCR in the whole uterus of C57BL/6 (wild-type, B6) and Rag2$^{-/-}$Il2rg$^{-/-}$ females. Top: non-pregnant (virgin) expression of growth factor genes in the whole uterine tissue from 2 different strains of mice. Bottom: gd 9.5 (one implantation site per sample) expression of growth factor genes in the whole uterine tissue from 2 different strains of mice. Pink squares: Rag2$^{-/-}$Il2rg$^{-/-}$ data points, black dots: WT (C57BL/6) data points. Data are representative of 5 independent experiments and 4 technical replicates were used in each biological replicate. Two-way ANOVA with multiple comparisons correction was used for statistical significance testing. Error bars represent mean±SD.

While there was no effect observed in the liver between the females at 3w of age that were progesterone injected and those that were not (**Fig. 4.14b**), in the uterus there was a marked difference. Progesterone injections inverted the ratio of trNKs to cNKs, similarly what was observed later at 8w of age when the animals are sexually mature (**Fig 4.14a**), although the

percentages of both trNKs and cNKs remained much lower than at 8w of age due to a still high percentage of ILC1s at 3w of age. This data from the neonatal uterus suggested that progesterone may have important functions in shaping the landscape of g1 ILCs. Similarly to other studies mentioned earlier, none of the progesterone receptors were detected by the RNA-seq in this dissertation either, and therefore the progesterone actions would occur indirectly, presumably via crosstalk with other cells in the uterus.

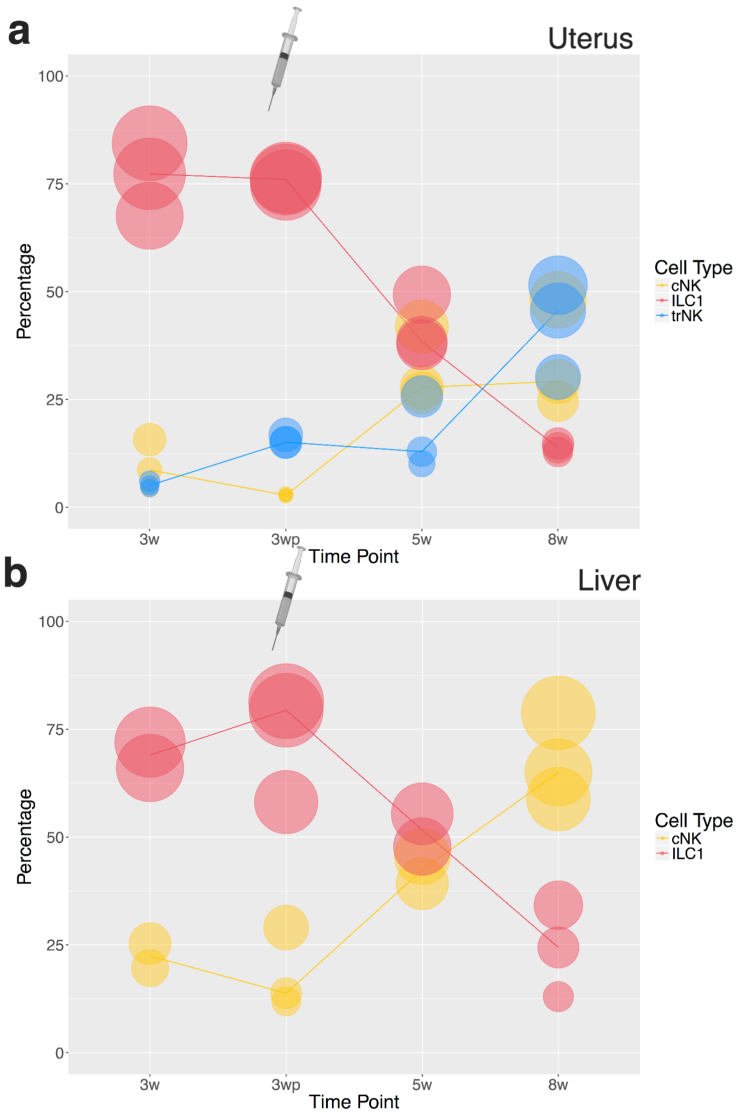

Figure 4.14. Progesterone injection alters the distribution of g1 ILCs in the uterus. Individual data points showing the percentages of g1 ILCs during reproductive life in the non-pregnant females in uterus and liver within their parent population of single, live, $CD45^{+}Lin^{-}NK1.1^{+}NKp46^{+}$ cells. Three time points were analysed: 3w, 5w and 8w with an additional time point indicated as 3wp to mark the progesterone-injected animas. (**a**) Distribution of g1 ILCs in the uterus at 3w, 3w-progesterone-injected, 5w and 8w. (**b**) Distribution of g1 ILCs in the liver at 3w, 3w-progesterone-injected, 5w and 8w. w: week.

The intra-tissue comparison of uterine subsets through analysis of DEG lists showed many different pathways that suggested that in particular uterine tissue-resident CD49a$^+$ g1 ILCs (ILC1s and trNK) are equipped with machinery to adapt quickly and respond to various factors originating from the microenvironment. This also suggested the essential function of the tight regulation of various subsets' immunometabolism in order to ensure they carry out their roles at the maternal-fetal interface.

Microsomal glutathione transferases (*Mgst1*, *Mgst2*) were here identified within the most enriched pathways related to the fatty acid metabolism in the uterine CD49a$^+$ g1 ILCs. These are enzymes which commonly detoxify reactive intermediates through glutathione-dependent transferase and peroxidase activities. They are usually activated by oxidative stress. In DCs fatty acids are essential for the development and function, and inhibition of the fatty-acid biosynthesis perturbed development of the DCs and decreased expression of MHC-II and costimulatory molecules (Rehman et al., 2013). Similar pathways were shown to be very important for reprogramming of the effector T cells and regulating the fate between Tregs and T helper cells (Berod et al., 2014). Thus, it would be of interest to investigate how alterations of the immunometabolism of g1 ILC through fatty acid modulation might affect their fate or function in the uterus. Recent work demonstrated that cytokine-stimulated NK cells upregulated SREBP proteins which promote the expression of genes involved in fatty-acid and cholesterol synthesis; this was essential for the metabolic reprogramming of NK cells (Gardiner & Finlay, 2017; Assmann et al., 2017). Although SREBP proteins may not have same functions in the uterine NK cells, other genes that might be uterine-specific were identified in this dissertation and deserve further analysis. *Slc16a13* encodes an orphan monocarboxylate transporter, MCT13, with mainly unknown functions (Halestrap, 2013). It is a proton-linked transporter of monocarboxylates such as lactate and pyruvate, transporting them out of the cell. Glycolysis is important for pbNK cell functions (Gardiner & Finlay,

2017) and the data generated in this study suggested that it may be equally essential for the uterine tissue-resident NK cells. Although lactate can be used up in many ways, it might be the case that uterine trNK and/or ILC1s produce lactate as a signal for the SA remodelling, in a manner analogous to angiogenesis, while inducing immunosuppression through acidosis in the tumour microenvironment (Romero-Garcia et al., 2016). It was shown that Warburg-like glycolysis is important for decidual development (Zuo et al., 2015). Tissue resident NK cells and ILC1s may provide lactate for the development of undifferentiated stromal cells in addition to other lactate soures which function through other MCTs (MCT4). It remains to be determined whether it is trNKs or ILC1s that are the main mediators of it, if such mechanism occurs at all. UpSet analysis pointed to *Slc16a1*, encoding MCT1, one of well characterized monocarboxylate transporters (lactate exporter) to be unique to trNKs (Velásquez et al., 2016). This does not exclude that both trNKs and ILC1s require metabolic fine-tuning for their functions, but via different transporters. Similarly, purinergic signalling may be of interest for the future studies regarding uterine g1 ILCs, because it was shown that in liver for example, nucleotides (i.e., ATP) can inhibit NK cell cytotoxicity. Scavenging of extracellular ATP increased NK activity and stimulated liver regeneration (Graubardt et al., 2013). Most recently, one of the genes identified in the RNA-seq here to be upregulated in uterine trNKs, *P2rx7*, was shown to be essential for the maintenance of tissue-resident memory T cells and most importantly, to regulate the tissue damage (Stark et al., 2018). This could prove to be important in the uterus, a tissue that regularly undergoes tissue remodelling.

5. The origin, plasticity and memory-like properties of uterine group 1 ILCs

5.1. Introduction

As described in much greater detail in Chapter 1, NK cells can be identified in a range of lymphoid but also non-lymphoid organs, including uterus. However, how NK cells develop in each one of these specific tissue niches is less clear and one of the longest standing questions in the reproductive immunology is: do uterine NK cells originate from in situ present precursors, or do they migrate there from blood?

Although human NKPs have been elusive for a long time, they have recently been identified for the first time in a range of tissues, including fetal liver and adult tonsil (Renoux et al., 2015). In general, current knowledge on the NK development in humans (with the exception of Renoux and colleagues) comes mainly from the studies on SLTs such as tonsils. In Chapter 1 it was also discussed in great detail how ILCs exhibit great plasticity and that almost all possible conversions can take place. One example that is highly relevant to the work in this chapter came from a finding that cells overlapping with NCR^{+}ILC3s and at the time called 'stage 3 immature NK cells' were identified in human PB and uterus, while expressing *Rorc* and producing IL-22. However, when they were cultured in vitro, they could give rise to mature NK cells (Male et al., 2010). Another study at a similar time discovered $CD34^{+}$ progenitors in the decidua that gave rise to functional NK cells, and although majority of the cells that developed from these progenitors were $CD56^{bright}CD16^{-}$, most of them did not express any decidual NK-specific KIRs or any other surface markers (Vacca et al., 2011). Before these, it was found that the culture of purified $CD16^{+}$ pbNK cells with TGF-β could give rise to $CD16^{-}CD9^{+}$ decidual NK-like cells, suggesting plasticity dependent on the local cues in the microenvironment (Keskin et al., 2007). This makes the study of ILC1 and cNK

differentiation much more complex, especially with a tissue that is not easily sampled, such as the uterus. The aim of Chapter 5 was to attempt to answer a question of the g1 ILC development, plasticity and whether they can adapt to such a dynamic microenvironment through developing memory.

5.2. Results

5.2.1 Identification of uterine NK progenitors in human and mouse uterus

Uterine g1 ILCs are abundant in human and murine uterus and it is still unknown whether these cells arise from peripheral NKPs found in the PB or in situ progenitors. In this study, using the same panel of markers for the identification of NKPs in adult tonsil (Renoux et al., 2015), NKPs were found for the first time in human decidua (**Fig. 5.1**). They were identified as $Lin^{-}CD34^{+}CD38^{+}CD123^{-}CD45RA^{+}CD7^{+}CD10^{+}CD127^{-}$ cells.

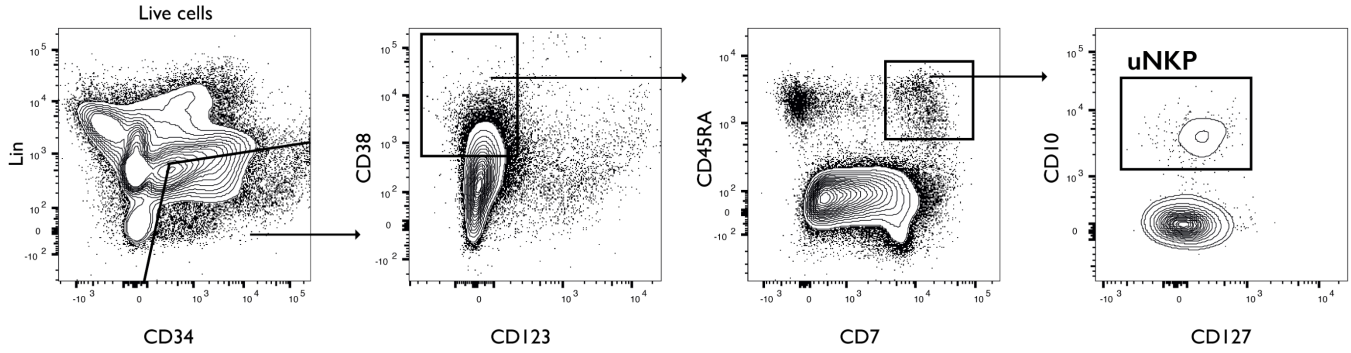

Figure 5.1. NKP exists in freshly isolated human decidua from the first trimester. Freshly isolated decidual leukocytes were immediately analysed by flow cytometry ex vivo. Gating strategy is presented. Final $CD10^{+}CD127^{-}$ gate represents the NKP population. Lineage channel included CD3, CD4, CD11b, CD11c, CD14, CD15, CD19, CD33, CD56, CD66b, CD235a. Data are representative of four independent experiments performed on samples of different gestational ages (one sample per independent experiment, n=4).

Frequency of NKPs ranged from 0.02-0.05% of $CD34^{+}$ cells in the decidua, similar to the frequency observed in the tonsil (Renoux et al., 2015). The lowest NKP frequency was

observed in the 10-week old decidual sample, while the highest frequency was detected in 8-week old decidua (data not shown). Fresh and frozen cells were compared and frozen samples appeared to have preserved the NKP phenotype and could be used in future experiments (data not shown). Once this progenitor was identified, the next step was to perform the index sorting and investigate whether these are indeed NK progenitors and whether they can exclusively give rise to uterine NK cells. However, due to the lack of clinical sample supply, it was not possible to perform these experiments.

Preliminary experiments performed in the group had pointed to the existence of the NKPs in the uterus of virgin mice, phenotypically identical to a previously defined mouse BM NKP (Rosmaraki et al., 2001) as $Lin^{-}CD45^{+}CD11b^{-}CD122^{+}NKG2D^{-}DX5^{-}NK1.1^{-}$ cell. They had also been found as much more frequent in the uterus than in the BM (unpublished observations by another group member). Thus, the aim was to design the experiments in which the developmental potential of these uterine NKPs would be compared to BM NKPs in vivo, by performing an adoptive transfer of NKPs into. Briefly (more details in Chapter 2), NKPs were isolated and FACS-sorted from C57BL/6 WT animals (CD45.2, donor) and injected via the tail vain in a PBS suspension into the alymphoid $Rag2^{-/-}Il2rg^{-/-}$ females (CD45.1, recipient), lacking all B cells, T cells, NK cells and ILCs, as they are double knockouts for the *Rag2* gene and common cytokine receptor chain gene (Mazurier et al., 1999). Originally, this experiment had been performed another group member with the BM NKPs in order to optimise the conditions. The readout in these optimising experiments was primarily the spleen as one would expect to see the donor cells present in the spleen. However, no NK cell engraftment had been observed, even in the spleen which should serve as a proxy for successful reconstitution, and therefore, this set of experiments had to be repeated (no data of the previous group member shown). These experiments were then repeated for this study and the number of injected cells was titrated. PBS-only, 300, 600 and

900 NKPs were injected into sexually mature (8-12w) $Rag2^{-/-}Il2rg^{-/-}$ females, but the NK cell engraftment still had a very low success rate in all the tissues assessed, including spleen (no data shown), at both 14 and 21 days post-transfer.

However, there were advances in the NK development research since the original paper describing NKPs used in previous experiments described here (Rosmaraki et al., 2001). In particular, the NKP stage has been refined further into an NK-committed progenitor (pre-NKP), a developmental intermediate between the CLP and the next stage, termed refined NKP (rNKP) (Fathman et al., 2011; Carotta et al., 2011). Therefore, it was decided to re-assess previous work performed and to examine whether these other intermediates were present in the mouse uterus. The same panel as used in the two aforementioned studies from 2011 was applied, and it was shown that indeed some of these progenitors exist in the mouse uterus (**Fig. 5.2a**). Results for the BM from the original studies were confirmed, as all three subsets: CLP ($Lin^-CD27^+CD244^+c\text{-}kit^-CD127^+Flt3^+CD122^-$), pre-NKP ($Lin^-CD27^+CD244^+c\text{-}kit^-CD127^+Flt3^-CD122^-$) and rNKP ($Lin^-CD27^+CD244^+c\text{-}kit^-CD127^+Flt3^-CD122^+$) were present in the BM. Uterus however, contained only the rNKP, rather than the first committed NK progenitor, pre-NKP (**Fig 5.2a**). After this was established, the adoptive transfer experiments were repeated, again using BM as source of progenitors in order to optimise the experiment prior to injecting the uterine progenitors into $Rag2^{-/-}Il2rg^{-/-}$ model system. C57BL/6 (WT) mouse was used as a control to confirm the presence of CD45.2 cells in the spleen as WT is a $CD45.2^+$ congenic which allows the identification of cells injected into $CD45.1^+$ $Rag2^{-/-}Il2rg^{-/-}$ animal (**Fig. 5.2b**, top row). As expected, in PBS-only injected animals (which were used here as another control) there were no $CD45.2^+$ donor cells identified in the uterus (**Fig 5.2b**, second row). Three other progenitor subsets were injected into $Rag2^{-/-}Il2rg^{-/-}$ animals: 10,000 lineage negative cells ($CD11b^-CD19^-CD3^-CD5^-B220^-Ter119^-Gr\text{-}1^-$), 1,500 CLPs or 1,000 rNKPs from the BM injected per animal. Samples were

analysed 14 days later. Lineage-negative-injected animals had the highest frequency of CD45.2^{+} cells that reached the uterus during this period and gave rise to cells of other lineages, as there were CD3^{+} and CD19^{+} cells present in the cell suspensions (**Fig 5.2b**, third row). CLPs injection resulted in a similar frequency of CD45.2^{+} cells, but there were no CD3^{+} cells detected (**Fig. 5.2b** fourth row).

Finally, rNKP from the BM, which was also shown to be the only NKP in the uterus (**Fig. 5.2a**) gave rise to exclusively CD3^{-}CD19^{-} cells and subsequently the highest frequency of Eomes^{+}NK1.1^{+} cells compared to other investigated samples. However, there was a notable lack of consistency between replicates in each of the independent experiments, since some Rag2$^{-/-}$Il2rg$^{-/-}$ animals had much lower percentages of CD45.2^{+} donor cells in their uteri, suggesting that the transferred cells were not reaching this organ. Finally, experiments using uterine rNKPs were not performed because it was not in line the Home Office Project Licence to use such large numbers of animals. Just one independent experiment with three biological replicates would have required the use of over 60 animals and given the lack of consistency with progenitors from a much more progenitor-rich organ (BM), this was not further pursued. In a manner similar to what was described about the human NKP work, index sorting and NK development from this newly identified uterine progenitor has not been investigated downstream and this work remains to be done.

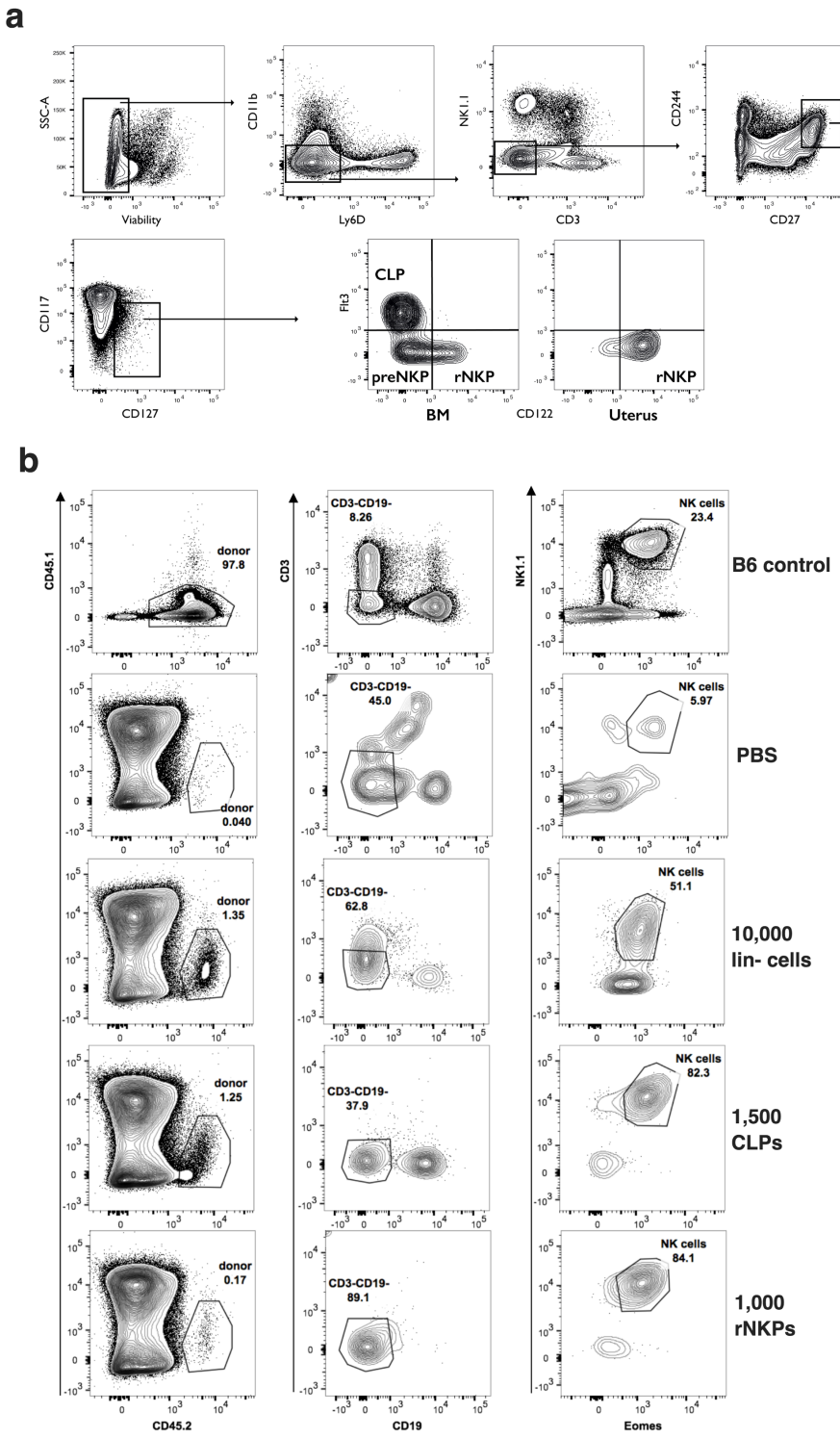

Figure 5.2. rNKP exists in the non-pregnant mouse uterus. (**a**) Freshly isolated cells from the bone marrow were immediately stained and analysed ex vivo for the presence of the NKPs. The gating strategy is presented. CLPs, pre-NKPs and rNKPs are indicated in the final plot in the BM and uterus of a non-pregnant female. Data is representative of two independent experiments and animals were pooled for each sample in order to obtain enough tissue. (**b**) Adoptive transfer of the cells isolated from the C57BL/6 (B6/CD45.2/donor) and injected intravenously into the tail vain of the $Rag2^{-/-}Il2rg^{-/-}$ (CD45.2/recipient). One representative row per each condition (number and type of injected progenitors) is shown out of three independent experiments and three replicates per experiments. Top row represents C57BL/6 control animal (spleen), while the remaining rows

represent $Rag2^{-/-}Il2rg^{-/-}$ injected with PBS only, 10,000 lineage negative cells/animal, 1,500 CLPs/animal or 1,000 rNKPs/animal. Lineage channel included CD11b, CD19, CD3, CD5, B220, Ter119 and Gr-1. All gates were set using appropriate FMO and isotype controls.

5.2.2 Plasticity of uterine group 1 ILCs

As explained in more detail in Chapter 1 (section 1.2.2.10), it is impossible to investigate the development of ILCs, and in particular the development of g1 ILCs, without accounting for a considerable level of plasticity between the subsets. Cells largely overlapping with NCR^{+}ILC3s have been identified in human PB and uterine mucosa and have been found to express *Rorc* while also giving rise to mature uNK cells (Male et al., 2010). Due to this overlap between ILC3s, ILC1s and various stages of NK cell development in both human and mice, the next aim was to investigate whether similar plasticity occurs in the mouse uterus. To examine the plasticity of ILC3s and g1 ILCs and dissect further the origin of ILC1 cells in the murine uterus, a RORγt-Cre fate-mapping mouse model was utilised. Transgenic mice expressing Cre-recombinase under the control of *Rorc* gene were bred with Rosa26R-EYFP reporter mice to generate RORγt-Cre/R26R-EYFP females. In R26R-EYFP animals, there is a LoxP-flanked stop cassette located upstream of EYFP. Therefore, when *Rorc* gene is expressed, it activates the Cre-recombinase which excises the stop cassette and subsequently activates the expression of YFP. Readout in these animals is the YFP expression when cells have been expressing *Rorc*. Every cell that has expressed RORγt at some point is traceable as YFP^{+}, even if the surface phenotype has changed and they do not express RORγt anymore and is commonly referred to as the ex-ILC3 if it stopped expressing the protein. Analysis of the uterus of these animals demonstrated that ex-ILC3s that were described in other tissues (Chapter 2, section 1.2.2.10) exist in the mouse uterus, too. All of the g1 ILCs expressed some YFP, with trNKs displaying the highest intensity of YFP, ILC1s lower and cNKs the lowest although still being YFP^{+} (**Fig. 5.3**).

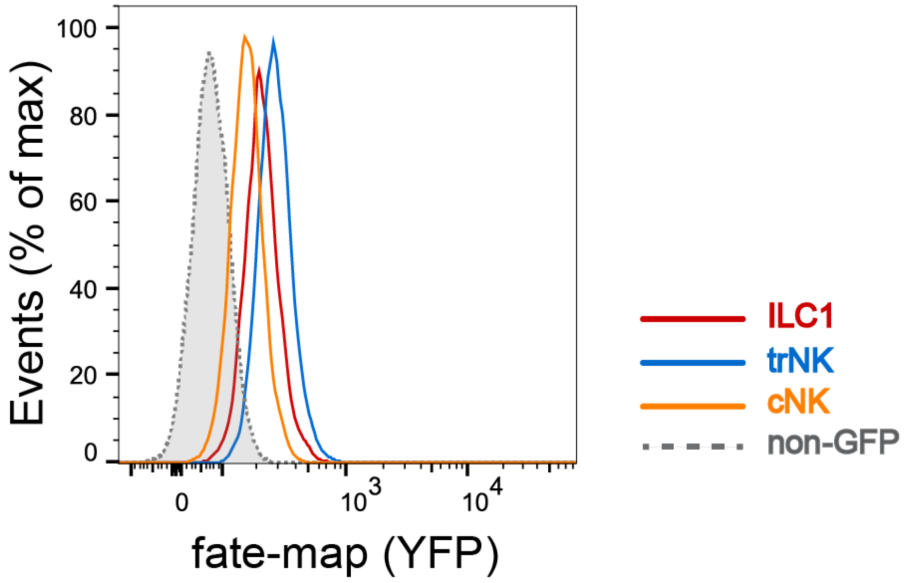

Figure 5.3. Fate-mapping of g1 ILCs. The uterus of RORγt-Cre/R26R-EYFP animals was analysed for the expression of YFP in each individual subset. All gates were set using appropriate FMO and isotype controls.

Rorc-expressing cells identified in a previous study in the human uterine mucosa which could also give rise to mature uNK cells were shown to produce IL-22, as described by Male and colleagues and referenced earlier. Therefore, it was investigated whether any of the g1 ILCs in the uterus could also produce IL-22.

trNK and cNK cells from the uterus at mid-gestation, as well as cNK from the spleen as a control, were sorted and incubated with either (1) PMA/I and protein transport inhibitors or (2) the control medium containing protein transport inhibitors only, but not PMA/I for stimulation. This experiment showed that trNK cells from the uterus at mid-gestation can also produce IL-22, regardless of stimulation (**Fig. 5.4a**). Almost 80% of trNK cells produced IL-22 when stimulated with PMA/I, but even without stimulation it was 60-70% of cells. The IL-22 MFI levels were also significantly elevated in the trNK cells compared to other g1 ILCs in the uterus and compared to the splenic cNK cells which could not produce any IL-22 (**Fig. 5.4b-c**).

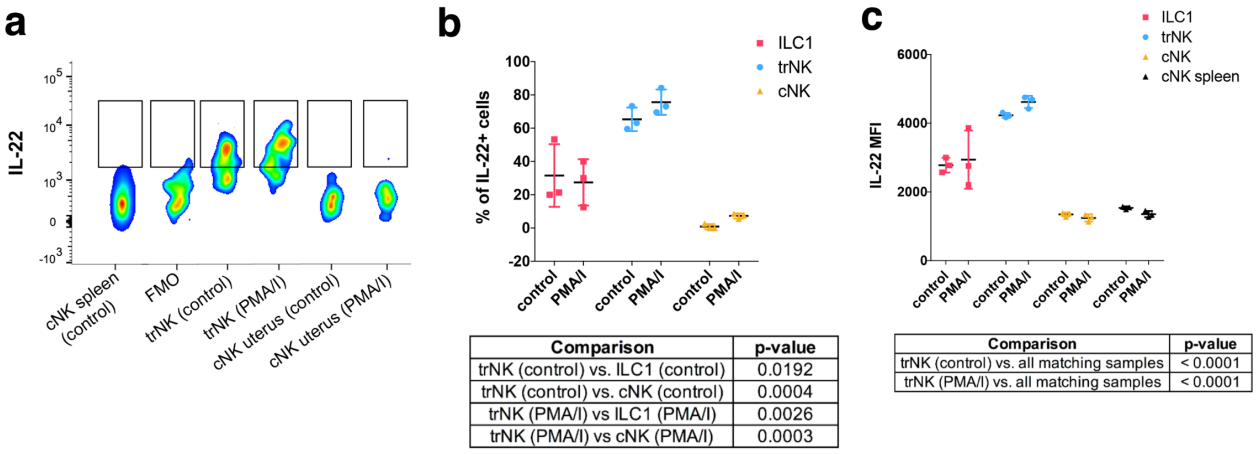

Comparison	p-value
trNK (control) vs. ILC1 (control)	0.0192
trNK (control) vs. cNK (control)	0.0004
trNK (PMA/I) vs ILC1 (PMA/I)	0.0026
trNK (PMA/I) vs cNK (PMA/I)	0.0003

Comparison	p-value
trNK (control) vs. all matching samples	< 0.0001
trNK (PMA/I) vs. all matching samples	< 0.0001

Figure 5.4. Uterine CD49a^{+}Eomes^{+} trNK cells produce IL-22 at mid-gestation. Uterine trNKs and cNKs from pregnant females at gd 9.5 were freshly isolated, FACS-sorted and then stimulated with PMA/Ionomycin Cocktail Mix containing protein transport inhibitors or just protein transport inhibitors. (**a**) Control wells were incubated with the medium that contained only the protein transport inhibitors. (**b**) Quantification of the data presented in (a), representing the percentage of IL-22-producing cells within each g1 ILC subset. (**c**) MFI levels of IL-22 expression measured by flow cytometry on g1 ILCs in the uterus and control samples from the spleen. All gates were set using appropriate FMO and isotype controls. Statistical significance was evaluated by two-way ANOVA with multiple comparisons correction. Tables under panels (**b**) and (**c**) summarise p-values for comparisons discussed in text. Error bars represent mean ± SD. MFI: mean fluorescence intensity

Recent study has identified plasticity between g1 ILC subsets in tumour microenvironment (Gao et al., 2017). This group has shown that in a tumour microenvironment, effector NK cells (phenotypically corresponding to cNK cells) can become non-cytotoxic ILC1s and that this happens via an intermediate that they termed ‘intermediate ILC1s’ but phenotypically they corresponded to uterine trNKs described here. Most importantly, this conversion was driven by the TGF-β. The model proposed by this study is summarised in **Fig 5.5a**. Since TGF-β signalling pathways were among the most highly enriched pathways in the RNA-seq dataset presented in Chapters 3 and 4, it was of interest for this study whether TGF-β would similarly influence the plasticity in the uterus. Firstly, an experiment from Gao and colleagues was recapitulated, where cNK cells that were FACS-sorted from both spleen (as a

control) and non-pregnant uterus were cultured for five days. They were cultured either with TGF-β and IL-15 or IL-15 alone. By performing this experiment it was observed that the uterine cNK fully converted into trNK cells, while with IL-15 there was minor population of CD49a and Eomes double negative population (**Fig. 5.5b**).

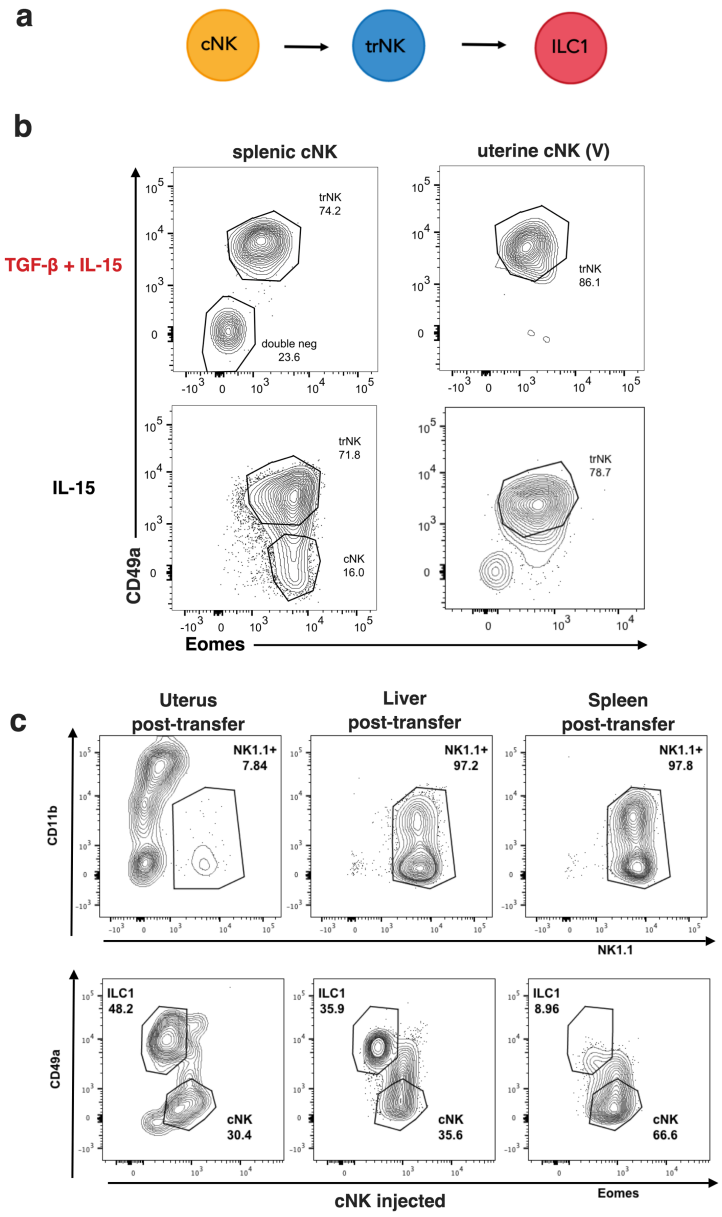

Figure 5.5 cNK cells from the uterus and spleen may display a tissue-specific plasticity. (**a**) Summary of the model proposed by (Gao et al., 2017) (**b**) Splenic and uterine cNK cells from non-pregnant females were FACS-sorted and cultured in either TGF-β with IL-15 (top row) or just IL-15 (bottom row). (**c**) C57BL/6 splenic cNK cells were FACS-sorted and adoptively transferred into Rag2$^{-/-}$Il2rg$^{-/-}$ females. 14 days post-transfer, uterus, spleen and liver were analysed by flow cytometry. Each bottom row plot derives from a corresponding top row plot. All gates were set using appropriate FMO and isotype controls.

Secondly, splenic cNK cells from B6 WT animals were sorted and injected into alymphoid $Rag2^{-/-}Il2rg^{-/-}$ females. 14 days post-transfer, uterus, liver and spleen were analysed for the presence of g1 ILCs. The highest frequency of ILC1s was observed in the uterus, compared to liver and especially spleen (**Fig. 5.5c**). However, it is important to observe that the lowest percentage and number (not shown here) of cNK cells reached the uterus measured by the percentage of $NK1.1^{+}$ cells, while liver and spleen appeared to have fully been reconstituted with transferred NK cells.

5.2.3 Second gestation is marked by the expansion of memory-like ILC1s

Since it has proven infeasible to attempt to dissect the development and plasticity of g1 ILCs in both mouse and human samples any further for the reasons described in the previous two sections of this chapter, another approach was undertaken in order to understand how g1 ILCs persist in the uterine microenvironment during and beyond first gestation which has been the subject of the study presented in this dissertation so far.

As discussed in Chapter 4, although *Cd19* gene came up as one of the top genes within PC2 (**Fig. 4.5**) and appeared upregulated in liver ILC1s compared to uterine ILC1s, on the protein level this was not the case. The CD19 protein was expressed on uterine ILC1s, despite a very low level of gene expression detected through the RNA-seq. As further explained in the analysis of various comparisons of DEG lists in Chapter 4, one of the genes that came up as specifically upregulated in liver ILC1s compared to uterine ILC1s and trNKs was *Cxcr6* (**Fig. 4.10b** and **Fig. 5.6a**). Since CXCR6 expression on the cell surface is known to mark memory NK and T cells in mice (Paust et al., 2010; Tse et al., 2014), levels of the protein were assessed on the surface of g1 ILCs. As shown in **Figure 5.6b**, uterine ILC1s expressed CXCR6 at mid-gestation at the levels comparable to liver ILC1s. cNKs did not express any CXCR6 in either of the organs, while uterine trNKs had low-to-intermediate levels of

CXCR6 expressed on their surface. These results confirmed previous data on liver ILC1s (Paust et al., 2010) and indicated that some subsets of uterine g1 ILC might be able to expand in response to gestation-specific signals in following pregnancies if CXCR6 is indeed a marker of memory-like, adaptive NK cells.

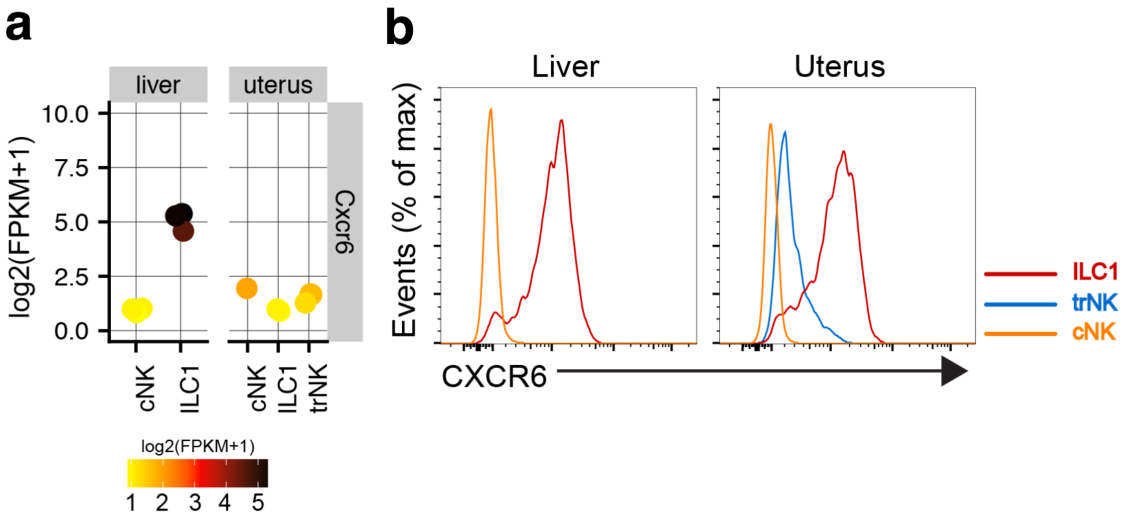

Figure 5.6. Uterine CD49a^{+}Eomes^{-} ILC1s express CXCR6. (**a**) Individual gene expression of *Cxcr6* gene in uterine and liver g1 ILCs. Scale represents log2(FPKM+1) normalised reads. (**b**) Protein expression measured by flow cytometry on g1 ILCs in the liver and the uterus. All gates were set using appropriate FMO and isotype controls. FPKM: fragments per kilobase of exon model per million reads mapped.

Thus, the distribution of g1 ILCs was compared between first and second gestation. Due to the feasibility challenges with setting up timed-pregnancies and ensuring that the data for first and second gestation g1 ILCs distribution was obtained in the same independent experiments, only two time points during gestation were investigated: gd 5.5 and gd 9.5. There was a marked increase in CD49a^{+}Eomes^{-} ILC1s in second gestation (**Fig 5.7a**). Although the percentage of ILC1s in the second gestation already increased by gd 5.5, it was highly significant at gd 9.5 (**Fig 5.7b**).

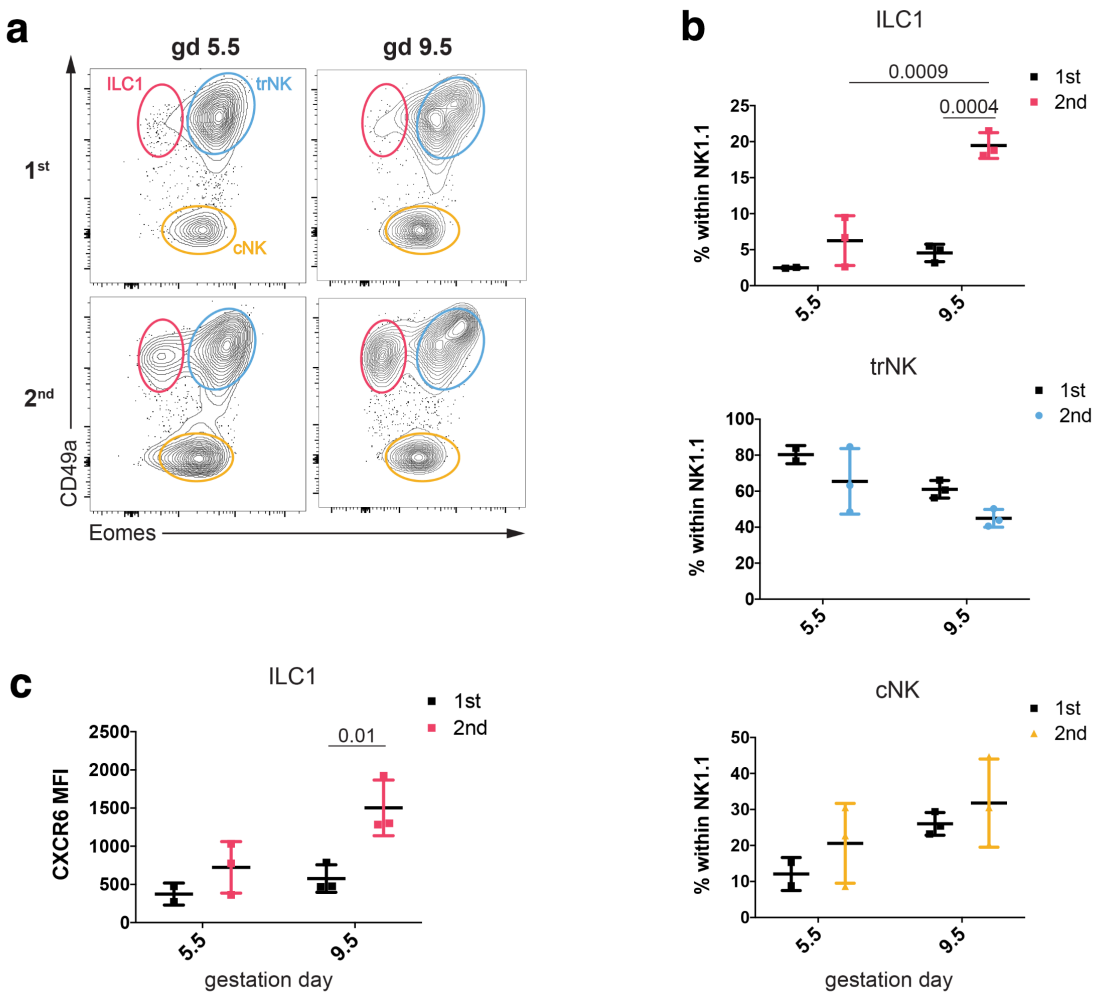

Figure 5.7. Uterine CD49a^{+}Eomes^{-} ILC1s expand in second gestation and express higher levels of CXCR6. (**a**) Representative plots showing the distribution of g1 ILCs in the uterus during the first gestation (top row) and second gestation (bottom row) at gd 5.5 and gd 9.5. Data is representative of two or three independent samples and three independent experiments. All gates were set using appropriate FMO and isotype controls. (**b**) Percentages of g1 ILC subsets in the first and second gestation at gd 5.5 and gd 9.5 as presented in (**a**). Statistical significance was determined by two-way ANOVA with multiple comparisons correction. Error bars represent mean ± SD. (**c**) MFI of CXCR6 protein on ILC1s in first and second gestation at gd 5.5 and gd 9.5 Statistical significance was evaluated by two-way ANOVA with multiple comparisons correction. Error bars represent mean ± SD. MFI: mean fluorescence intensity

There were no significant changes observed in percentages of trNKs and cNKs between first and second gestation (**Fig. 5.7b**). Not only did the ILC1 percentages increase in second gestation, but there was also a significant increase of CXCR6 expression levels on the surface of these expanded ILC1s in the second gestation at gd 9.5 (**Fig. 5.7c**). The trend that was

observed with increased percentages of ILC1s in the second gestation was mirrored by the investigation of absolute numbers. Only significant difference was in the absolute number of ILC1s in second gestation at 9.5 when they appeared highly increased in numbers (**Fig. 5.8a**). trNKs and cNKs did not exhibit any differences in numbers, similar to the percentage data in **Figure 5.7b** (**Fig. 5.8b-c**).

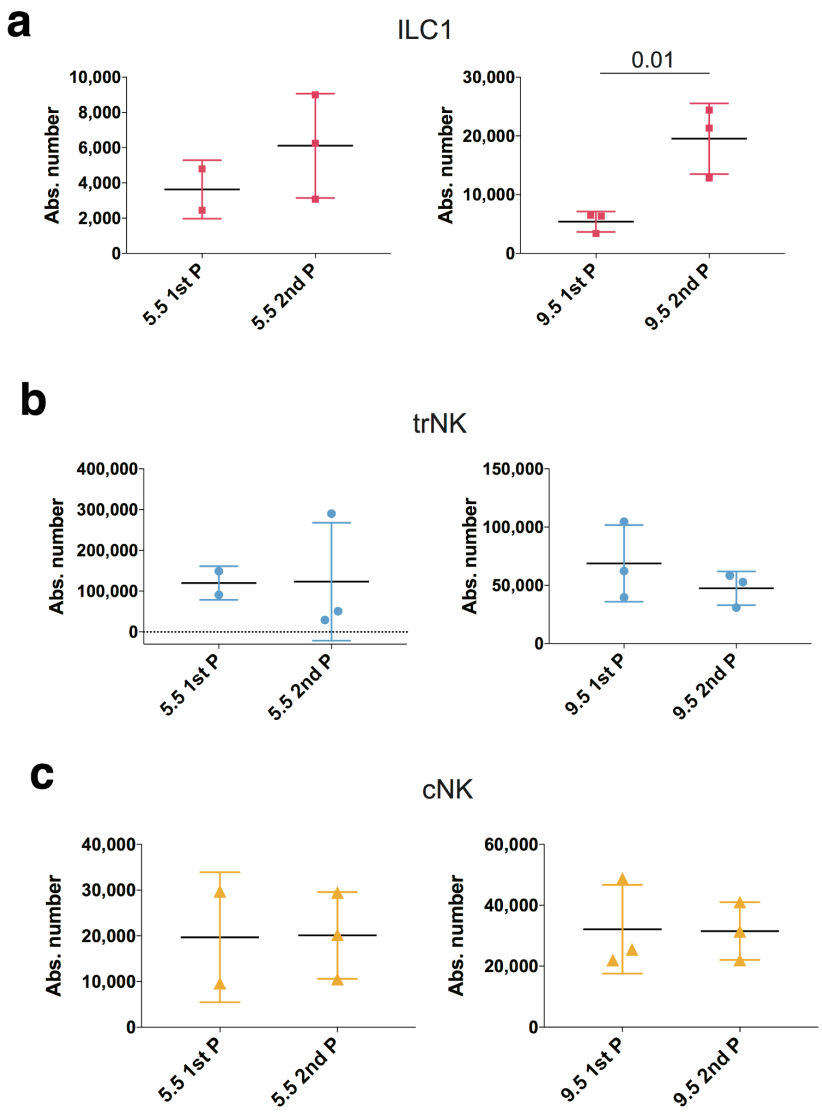

Figure 5.8. Uterine CD49a^{+}Eomes^{-} ILC1s are increased in absolute numbers in second gestation. The plots are showing absolute numbers of the distinct subsets of uterine g1 ILCs during the first gestation and second gestation at gd 5.5 and gd 9.5, for (**a**) ILC1s, (**b**) trNKs and (**c**) cNKs. Data is representative of two or three independent samples and three independent experiments. Statistical significance was evaluated by two-way ANOVA with multiple comparisons correction. Error bars represent mean ± SD.

Finally, it was of interest to investigate whether ligands for receptors detected previously in this chapter exist in the uterus. For this, the whole uterine tissue was prepared, total RNA isolated and then analysed for the expression of genes of interest by RT-qPCR (as explained in Chapter 2)

Although there was a limited number of samples available for this experiment, it appeared that *Tgfb1* transcript was already upregulated in first gestation at gd 9.5 compared to gd 5.5 (**Fig. 5.9a**) However, in the second gestation, its levels at gd 5.5 increased compared to the first gestation at the same time, but this increase did not occur at gd 9.5.

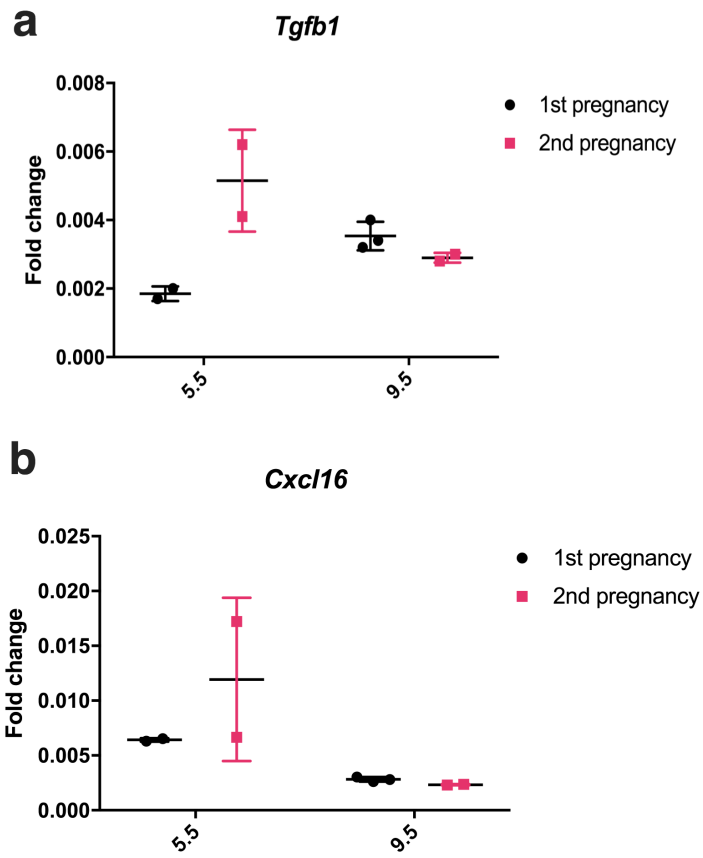

Figure 5.9. *Tgfb1* and *Cxcl16* transcripts appeared to increase at gd 5.5 in second gestation. Levels of the mRNA encoding genes of interest through first and second gestation at gd 5.5 and gd 9.5, analysed by the RT-qPCR in the whole uterus of C57BL/6 (wild-type, B6) females. (**a**) mRNA expression of *Tgfb1* during first and second gestation at two different time points. (**b**) mRNA expression of *Cxcl16* during first and second gestation at two different time points. Data are representative of two to three biological replicates, three independent experiments and 4 technical replicates were used for each biological replicate.

On the contrary, *Cxcl16*, encoding CXCL16, a ligand for CXCR6 was expressed at a very low level at all the time points investigated, except for gd 5.5 during second gestation when the expression appeared to increase (**Fig. 5.9b**). It was impossible to perform any statistical testing on this data due to a low number of samples and high level of variability particularly for *Cxcl16* expression.

5.3. Summary

Despite recent advances, the molecular mechanism of g1 ILC development in the uterus is unknown. The main purpose of this chapter was to understand the origins of the three subsets of uterine g1 ILCs and attempt to delineate the lineage relationships between them.

In this chapter, it was shown for the first time that NKPs exist in the first trimester human decidua. Frequency of NKPs within $CD34^+$ was found to be between 0.02% - 0.05%, which is in line with previously published data (Renoux et al., 2015). However, the NKP frequency appeared to decrease as the gestational age increased. Due to a limited number of samples available (each one of a different gestational age), a question of whether this frequency change was donor-specific or gestational age-specific remains to be answered in future studies. In addition to the human pregnant uterus, the NKP was identified in the mouse non-pregnant uterus here using a refined understanding of the NK cell development (Fathman et al., 2011; Carotta et al., 2011). This was an improvement compared to the previous attempts in the group using an older phenotypical definition of the NKP (Rosmaraki et al., 2001), because for the first time it was possible to find BM-derived cells of donor origin ($CD45.2^+$ cells) in the injected $Rag2^{-/-}Il2rg^{-/-}$ females. Interestingly, uterus only contained rNKPs, rather than the upstream pre-NKPs and CLPs that exist in the BM. This suggested that rather than the earliest committed NK progenitor (pre-NKP), it is perhaps more likely pre-NKPs home to the uterus where they finish their tissue-specific developmental pathways. For both human

and mouse experiments involving NKPs, there were tremendous challenges such as the lack of clinical samples to continue work on the human NKP, as well as an unjustifiable number of mice required to obtain a minimum number of progenitors to inject a group of animals that would yield statistically significant data. As stated in the results (section 5.2.1), there was a lack of consistency particularly in the uterine NK engraftment, suggesting that specifically injected rNKPs might not be reaching the uterus through a tail vein IV injection, as there was a much higher level of reconstitution consistency when CLPs and lineage-negative cells were injected into alymphoid mice. For these reasons, no further experiments were undertaken. However, now that the existence of the NKP has been established, future work should involve experiments such as index sorting and developmental assays in order to determine whether these are fully NK-committed progenitors as was described before (Renoux et al., 2015) as well as how functional they are. Endometrium should also be examined for the presence of NKPs as soon as the tissue sample collections continue in order to compare the findings to the data presented here describing NKP in the non-pregnant mouse uterus.

In context of the development and the fact that ILCs as a family of cells exhibit a high level of plasticity, fate-mapping experiments were performed that confirmed that there might be plasticity between 'ex-ILC3s' and g1 ILCs in the uterus, since most of the g1 ILCs, but particular trNKs, expressed RORγt during their development. In line with these findings, it was also shown that trNKs are capable of producing IL-22, similarly to what was demonstrated in earlier work on 'stage 3 immature NK cells' in the uterine mucosa (Male et al., 2010).

TGF-β signalling was another one of the highlights of this chapter as TGF-β-related pathways came up in the RNA-seq analysis in the Chapter 4 and previous work described the importance of TGF-β in regulating the plasticity of g1 ILCs in other tissues (Gao et al., 2017). In vitro culturing and adoptive transfer experiments here showed that uterine cNK

cells have the capacity to convert into trNK cells (in vitro) and that splenic cNK cells can contribute to reconstituting the ILC1 compartment in alymphoid mice (in vivo). However, similar to a manner observed in adoptive transfer experiments with the NKPs, cNK injections did not result in a detection of many donor cells in the recipients. Different routes of delivery of cells to be injected should be considered for the future experiments. In addition, there was a discrepancy between the findings of Gao and colleagues and in vitro culture of splenic cNK cells shown here in **Figure 5.5b**. In the study here, no conversion of splenic cNKs into ILC1s during a 5-day culture was observed, unlike in the paper from Gao and colleagues. It is unclear why this is, since the concentrations of the TGF-β and IL-15 used in the experiment here were identical to the one used in the aforementioned study. Gao and colleagues only showed the expression of ILC1-specific markers, rather than the representative plots of all cultured g1 ILCs harvested after a 5-day culture, as shown here in **Figure 5.5b**. It is still important to titrate the TGF-β concentration used in the future for uterine cNKs. It was technically not feasible to do within the scope of this study as the number of animals required was too high. In addition, levels of the TGF-β throughout gestation as well as before and after should be assessed, similarly to what was done in **Figure 5.9a** on a limited number of samples.

Finally, both liver and uterine ILC1s expressed high levels of memory-associated marker CXCR6 (Paust et al., 2010; Tse et al., 2014). This guided the study further with the aim to assess the distribution of g1 ILCs in second gestation in mouse. There was a significant expansion of ILC1s which were $CXCR6^{+}$ in second gestation. None of the other subsets expanded. This suggested the idea of pregnancy 'memory'. Ligand for CXCR6, CXCL16 is expressed by trophoblast cells (Huang et al., 2008) so this may be one of the drivers of the expansion. Very importantly, cells described as 'pregnancy-trained decidual NK cells' have

been described recently in humans (Gamliel et al., 2018), posing the question of the memory of pregnancy as an important one to address in future studies.

One elegant way to address the development and plasticity of g1 ILCs in the uterus in the future studies may be the $Ncr1^{iCre}Tbx21^{fl/fl}$ mouse model (in further text: T-bet cKO). This model was described recently (Cuff & Male, 2017). Since Cre-recombinase is induced in all Ncr1 (NKp46)-expressing cells, the original idea was to generate a mouse model in which T-bet, as a transcription factor important for the development of ILC1s would be knocked out of all $NKp46^{+}$ cells, generating an ILC1-specific conditional KO, while retaining cNKs. The study that reported this originally found that this was not an ILC1-specific KO model as there was an equivalent reduction in both cNKs and ILC1s in the liver, which was of interest to this group (Cuff & Male, 2017). However, a preliminary experiment was carried out in collaboration with Dr Victoria Male at the UCL to investigate the uterus of T-bet cKO females. Animals were collected from the UCL animal facility and the experiments downstream performed as described in all previous experiments carried out at the University of Cambridge. When g1 ILC distribution was assessed, liver findings were confirmed to be the same as in the original study, with the same ratio of ILC1s:cNK, showing that both subsets were similarly affected by the deletion of T-bet (**Fig. 5.10a**, top row). Slight discrepancy was observed in the spleen (**Fig. 5.10a**, middle row), where the control animal ($Ncr1^{WT}Tbx21^{fl/fl}$) appeared to have an abundance of ILC1s, but on the contrary the deletion in the T-bet cKO appeared to have been successful, unlike in the original study by Cuff and Male referenced earlier. Finally, the virgin uterus at 8-weeks of age was lacking both ILC1s and cNKs, suggesting that this might be of interest for the studies addressing uterine g1 ILC lineage relationships in the future (**Fig. 5.10a**, bottom row), as a trNK-only mouse model. It was however surprising to observe a much higher percentage of ILC1s in control animals

compared to what was observed previously (Chapter 3), but this might be due to the differences in animal facilities.

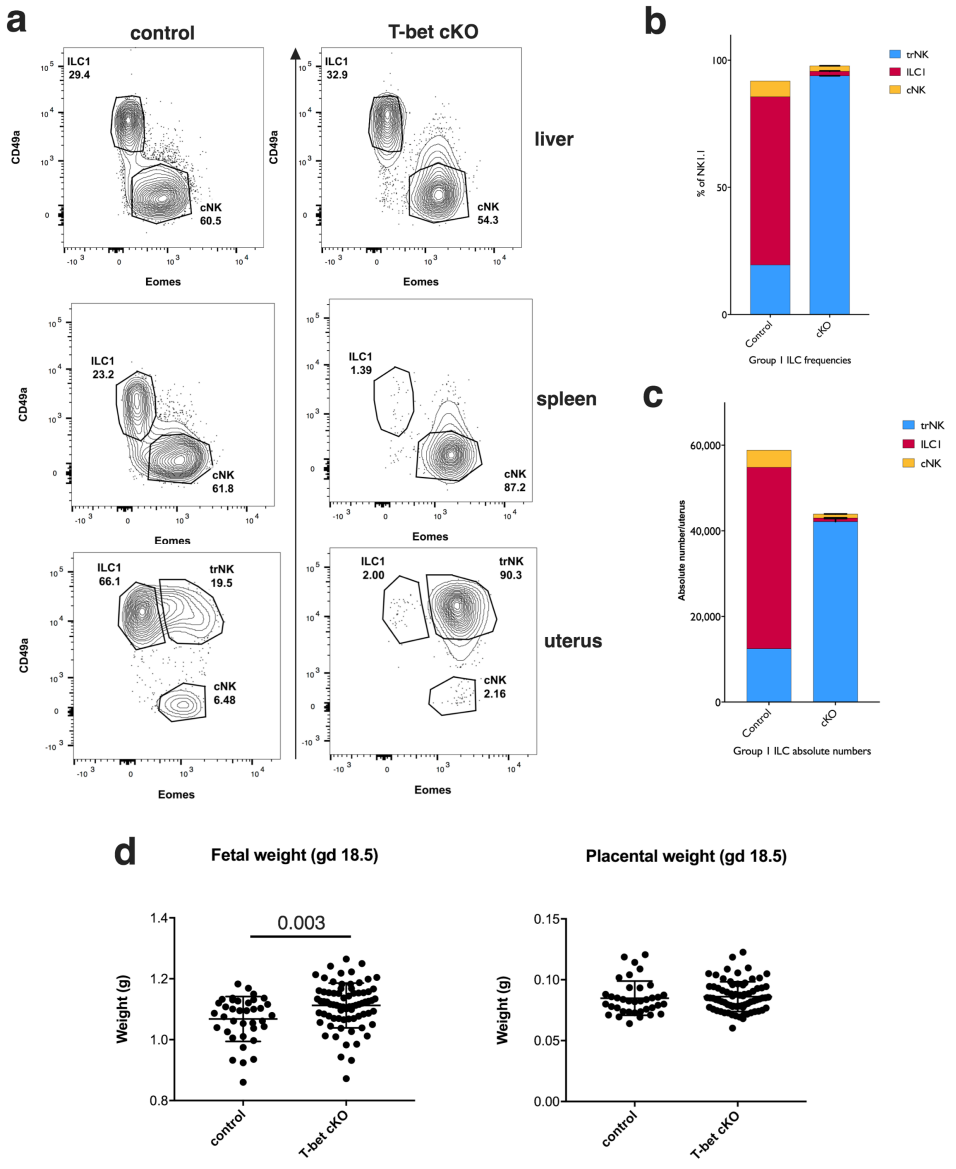

Figure 5.10. T-bet cKO animals have only uterine trNKs and display an increase in fetal weight in first gestation. (**a**) Representative plots showing distribution of g1 ILCs in liver (top row), spleen (middle row) and uterus (bottom row) of 8w old non-pregnant females. (**b**) Quantification of the data shown in (a), where each subset displayed as a percentage of within is parent population of g1 ILCs (all NK1.1% cells), (similar to the Fig. 3.2). (**c**) Quantification of the data shown in (a), where each subset displayed as an absolute number of cells within the uterus. (**d**) Fetal and placental weights of conceptuses from T-bet cKO females mated with WT males. Error bars represent mean ± SD. In order to evaluate the statistical significance of the data, two-tailed, unpaired t test was used. Only the significant values are displayed on the plot. Data are representative of 6-10 litters per cross. Means g: gram, gd: gestational day, w: week, T-bet cKO: $Ncr1^{iCre}Tbx21^{fl/fl}$ genotype, control: : $Ncr1^{WT}Tbx21^{fl/fl}$.

The data is preliminary and the quantification can be observed in **Fig. 5.10b** and **c**, where it is obvious that $Ncr1^{iCre}Tbx21^{fl/fl}$ animals have a much higher frequency and absolute numbers of trNK cells, respectively. In addition, measurements of the fetal and placental weights in crosses with the T-bet cKO female with the WT male showed that the fetal weight of the pups from these crosses is significantly higher compared to the control animals, while there was no significant differences in their placental weights (**Fig 5.10c**). However, most interesting experiments utilising these animals would involve investigation of second pregnancies as these animals lack ILC1s which were shown to expand specifically in second gestation earlier in this chapter.

6. Final conclusions and future directions

In conclusion, the data provided in this thesis has shown evidence required for a further understanding of the functions and development of the uterine g1 ILCs.

The data has been provided to demonstrate a dynamic distribution of the g1 ILCs in the uterine microenvironment during the key stages of the mouse reproductive life. Main observations from this set of experiments were that (1) ILC1 cells are the most abundant g1 ILCs before puberty, (2) trNK cells are the most abundant g1 ILCs early in gestation and (3) cNK cells become dominant later in gestation. These observations supported the ongoing hypothesis in the group that each of these uterine subsets developed distinct uterine-specific functions required in homeostasis during non-pregnant and pregnant state.

By using the RNA-seq, core gene signatures of the g1 ILCs in the uterus at mid-gestation were identified and together with the aforementioned data on the distribution of g1 ILCs, this dataset represents a valuable resource for future studies. Main focus in this thesis was to identify signatures that set uterine CD49a^{+} tissue-resident ILC1 and trNK cells apart from CD49a^{-} cNK cells, as well as to determine their tissue-specific signatures in comparison to the phenotypically similar cells in the liver. The lists of detected genes and enriched pathways are far too long to be summarised here and have in part been summarised in Chapter 4. Therefore, only some of the findings will be discussed here in order to justify the final conclusions.

For both uterine CD49a^{+} subsets, proteolysis-related terms represented a common theme within the enriched pathways. This suggested a protein processing activity by these cells during the extensive tissue remodelling taking place at mid-gestation in ILC1s and trNKs. Strikingly, genes that are not commonly associated with NKs and ILC1s were upregulated in CD49a^{+} cells. Some of these included *Adgre1*, *Cd86* and *Mertk*, all much more commonly

associated with APCs, and all of these were validated on the protein level on the surface of trNKs and/or ILC1 at mid-gestation.

According to this and DEG data, CD49a^{+}Eomes^{+} trNK cells appear to be the hub of the uterine g1 ILCs, as they were equipped with the transcriptome that may enable them to interact with the majority of other cells present at the maternal-fetal interface, including trophoblast cells, other leukocytes, secreted growth factors, smooth muscle cells, blood vessels and even other g1 ILCs. It will be essential in the future studies to address where these cells originate from. From the fate-mapping experiments shown in Chapter 5, they resembled ex-ILC3 cells, through *Rorc* expression at some point during development. They were also capable of producing IL-22, regardless of stimulation. This puts more emphasis on utilising mouse as a model for reproductive immunology research, since these findings were in line with what had previously been described in the human uterine mucosa (Male et al., 2010).

ILC1s, on the other hand, were only highly abundant before puberty and then again in the second gestation. During all the other stages, they were present at very low levels. It was still possible to gain an insight into what their functions may be through the RNA-sequencing at mid-gestation by investigating DEGs identified between ILC1s and trNKs. ILC1s may interact with the adipocytes, as they expressed the receptor for the adipocyte-derived factor apelin, which is highly expressed in the mouse uterus. One of the essential events during gestation is the SA remodelling and the appropriate regulation of blood pressure. ILC1s also expressed gene encoding angiotensin I-converting enzyme very highly and uniquely compared to all other subsets. Thus, they might be the essential regulators of this process, despite being present in very low percentages and numbers throughout all other stages. This however, depends on the rate of mRNA translation into a protein in a particular niche and

remains to be investigated further. Not only did the ILC1s (and trNKs) display APC-like gene signature, but a minor population of ILC1s was found to express CD19 and MHC-II, resembling not only APCs in general, but B cells in particular. Such information on ILC1s, however, fits the previous data shown in Chapter 4, such as the identification of the antigen-processing and presentation via MHC-II pathway as another highly upregulated pathway in the uterine CD49a^{+} cells. Therefore, the MHC-II expression might not necessarily indicate that there is an active antigen presentation to the T cells by ILCs, as was shown for ILC3s (Burg et al., 2014). It may simply reflect the fact that there is an ongoing protein processing following a potential engulfment of cells, since they expressed a range of genes associated with apoptotic cell clearance in a macrophage-like manner. Interestingly, high levels of CD19^{+}CD5^{+} cells were shown to be indicators of preeclampsia in humans (Jensen et al., 2012). These cells were not extensively phenotyped so they might represent a minor population similar to CD19^{+} g1 ILCs described in this thesis, rather than the B cells as they were termed in that report. A subset of NKp46^{+} NK cells resembling B cells which were CD19^{+} and produced immunoglobulins (termed NKB cells) was described in one report, although their existence was later disputed (Wang et al., 2016; Kerdiles et al., 2017) and therefore this is currently a controversial subject. However, more recently, NKB cells appeared in the literature again and were shown to be induced in the SIV and HIV infections (Manickam et al., 2018). Thus, this minor subset of CD19^{+}MHC-II^{+} ILC1s should not be dismissed and future studies should address what the biological functions of these cells are. More markers should be used to phenotype this subset in the future and not only at gd 5.5 and gd 9.5 as shown in this thesis but at the other stages before gestation, at all stages of gestation and during the post-partum period. One of the most interesting discoveries made in this thesis was that ILC1s expanded in both percentages and absolute numbers in second gestations. They also expressed higher levels of the memory-associated NK cell marker, CXCR6,

suggesting that these cells expand specifically in response to pregnancy-related cues, since CXCL16 can be produced by trophoblast (Huang et al., 2008) and *Cxcl16* gene expression was upregulated in second gestation in the whole uterus as shown in Chapter 5. Expansion of $CXCR6^+$ ILC1s was not observed in the matched liver or spleen. $CXCR6^+$ ILC1s were present in much higher numbers and percentages at gd 5.5 of the second gestation, but this increased significantly by gd 9.5. It is important to note that at gd 5.5 of the second gestation, this otherwise rare subset, was extremely abundant and this was very consistent, which will allow for easier FACS-sorting and subsequent in vitro manipulation in the future studies. That was one of the main challenges in the work presented in this thesis, since any in vitro manipulation of ILC1s required a high number of animals to be sacrificed, due to very low numbers before and during first gestation. It will also be essential to continue following the dynamics of the ILC1s after first gestation in order to determine when their expansion begins. This work represents an exciting direction for the future research, since decidual NK cells with memory properties and enhanced function have been identified in subsequent human gestations (Gamliel et al., 2018). In addition, there is a lower rate of pregnancy complications observed in second pregnancies and memory NK cells/ILC1s might be relevant in these cases (Hernandez-Diaz et al., 2009).

The third subset, cNK cells, starts increasing from mid-gestation but peaks in late gestation. Therefore, not only is it tempting to speculate that cNK cells are essential for a crosstalk with trNK cells at mid-gestation, but also that they might be essential for the immune protection of the fetus later in gestation after placenta has been established as they displayed more of a cytotoxic gene signature rather than the tissue-remodelling signature of the ILC1s and trNKs.

Certain genes identified in the distinct subsets of uterine g1 ILCs in this thesis had been

previously associated with disease in humans, by studying their mutations and polymorphisms. One example is the identification of *Scarb1* gene, highly upregulated in tissue-resident g1 ILCs. In humans, the polymorphism in *Scarb1* associates with the success of the IVF (Yates et al., 2011). *Mucin4* polymorphisms (*Mucin4* being highly upregulated in cNKs) were found to be associated with endometriosis-related infertility (Chang et al., 2011). It is also of importance to note that numerous genes in the UpSet lists did not have a canonical name and included pseudogenes, long non-coding RNA and antisense transcripts. Given the similarities of g1 ILCs in general, these may prove to be essential in cell-specific gene targeting as they may be master regulators of the gene expression in a subset of interest.

The prediction model ImmuCC for mouse tissues that allows the deconvolution of transcriptome data was used in order to attempt to identify what cell types were present in cell preparations for RNA-seq. Briefly, using the expression profiles of normal mouse immune cells obtained on Affymetrix Mouse Genome platform, a signature matrix was created to identify 25 immune cell types (Chen et al., 2017). By applying this matrix to the RNA-seq dataset described here, relative compositions of these immune cell types were inferred in the sorted samples. The close similarity of uterine and hepatic cNK cells was confirmed as their gene signatures aligned with NK and T cells. However, the $CD49a^{+}$ compartment was heterogeneous. While trNK and liver ILC1s had similar proportions of cell types represented (the highest being activated $CD8^{+}$ T cells, Th1 cells, activated NK cells with lower fraction of monocyte, activated DCs and M1 macrophages), uterine ILC1s were very different. The gene signatures of uterine ILC1s predicted cells as diverse as M0 and M1 macrophages, with the highest fraction being monocytes and activated DCs, which corroborated the data obtained through analyses in Chapters 4 and 5, suggesting again that these cells have a tissue-specific signature which resembles many other immune cell types

(**Fig. 6.1**). This may be a consequence of adaptation to the particular niche they are found in. It is worth noting that ImmuCC is in no way a perfect way for the data deconvolution since ILCs are not in the 25 immune cell types, but it did confirm the observations of the Chapters presented in this thesis.

Figure 6.1. A prediction model suggests unique features in uterine ILC1s and trNKs that the evidence was provided for within the scope of this thesis. The data is explained in the text.

Although liver and uterine g1 ILC subsets were very similar, phenotypically, on the transcriptome level that was not found to be the case according to the evidence presented in this thesis. Genes that were validated on the protein level in the uterus were in most independent experiments not validated in the matched livers, although cells originating from both tissues had equivalent levels of gene expression. This is an essential point, because a tendency of researchers when designing flow cytometry panels is to use the same fluorophore for the lineage channel in order to maximise the number of channels available for markers of interest for cell phenotyping. For example, F4/80 antibody is very commonly used in the lineage negative channel to exclude macrophages when NK cells are analysed, or to positively select for macrophages. Similarly, CD11c is often used in the lineage negative channels to exclude DCs as their conventional marker, although through this work it became evident that all g1 ILCs expressed very high levels of the CD11c protein (data not shown). However, with the advance in the flow cytometers that allow cell profiling using a much higher number of markers, these non-conventional markers should be used with care and their expression reassessed in each individual tissue investigated.

Finally, NK progenitors were identified in both human and mouse uterus, but it was not feasible to continue these projects due to the lack of samples and the need for a high number of animals, respectively. However, future projects should attempt to delineate the developmental trajectories of the uterine g1 ILCs by harnessing the power of much more advanced single-cell technologies available today.

In support of the findings in this thesis, several excellent single-cell resources were published recently. These include two reports describing the human maternal-fetal interface during the first trimester of pregnancy (Vento-Tormo et al., 2018; Suryawanshi et al., 2018)2. Vento-Tormo and colleagues described three subsets of decidual NK cells with distinct surface receptor profile and immunomodulatory properties and their data largely corroborates the

findings presented in this thesis. The resource presented in thesis here should be used alongside these novel human datasets when new experiments are designed. Quality of the data presented here was also confirmed by a single-cell study in which the Microwell-seq technique of single-cell RNA-seq was used to analyse over 400,000 cells from majority of mouse tissues, including uterus (Han et al., 2018). Notably, this was the data from a non-pregnant mouse, but the expression of many genes was similar to what was observed in this thesis on the mid-gestation samples.

Establishment of the novel resources to guide reproductive research will help clarify results presented in this thesis even further. For instance, recently established endometrial and trophoblast organoids may be instrumental in determining the lineage potential when incubated with NKPs from the human uterus (Turco et al., 2017; Turco et al., 2018). Since low numbers of NKPs can be obtained from the uterus and organoids have a very long-term life, these experiments would yield significant knowledge on how trophoblast or endometrium with various factor they produce affect NK cell development and plasticity and provide a much more physiological approach of testing. Synthetic biology approaches are available now as well, with the development of organs on chips. One example is the microfluidic culture model of the reproductive tract which can mimic the 28-day menstrual cycle (Xiao et al., 2017).

Through studying a cohort of patients with severe combined immunodeficiency (SCID), one recent study has suggested that ILCs are redundant (Vély et al., 2016), especially when the B and T cell compartment is preserved, with particular focus on the T cells' effector mechanisms that can compensate for the lack of ILCs. Of particular interest for the research presented in this thesis is a conclusion of the study that ILCs appear redundant for human reproduction, in addition to not being required during the disease, since 2 female *Jak3*-deficient patients had normal pregnancies resulting in healthy babies. However, such

conclusions cannot be made without analysis of a much larger cohort and taking into account all the clinical data, including the data related to the reproduction. As a recent essay proposed, immune system is based on equilibrium and constantly in a dynamic state between various antagonistic types of response (Eberl, 2016). These responses originate from both the internal and external environment and g1 ILCs in this thesis were shown to be equipped with the transcriptome to cope with signals of both origins.

In conclusion, a transcriptome atlas of uterine g1 ILCs is provided in this thesis. There is an obvious heterogeneity within the subsets that were sorted and RNA-sequenced, as some genes were detected at very low levels but there was a high protein expression and vice versa. Future work should focus on looking into distinct stages of reproductive life and single-cell analysis in order to capture the dynamic transcriptomic changes within each subset of the uterine g1 ILCs.

7. References

Akhanoba, F. et al., 2014. Severe systemic candidiasis following immunomodulation therapy in in vitro fertilisation-embryo transfer (IVF-ET). *BMJ Case Reports*, 2014(311), pp.1–4.

Aluvihare, V.R., Kallikourdis, M. & Betz, A.G., 2004. Regulatory T cells mediate maternal tolerance to the fetus. *Nature immunology*, 5(3), pp.266–271.

Amsalem, H. et al., 2014. Identification of a Novel Neutrophil Population: Proangiogenic Granulocytes in Second-Trimester Human Decidua. *The Journal of Immunology*, 193(6), pp.3070–3079.

Arase, N. et al., 2005. Heterotypic interaction of CRTAM with Necl2 induces cell adhesion on activated NK cells and CD8+ T cells. *International Immunology*, 17(9), pp.1227–1237.

Arenas-Hernandez, M. et al., 2015. Isolation of Leukocytes from the Murine Tissues at the Maternal-Fetal Interface. *Journal of Visualized Experiments*, (99), pp.1–12.

Ashkar, A.A., Di Santo, J.P. & Croy, B.A., 2000. Interferon γ Contributes to Initiation of Uterine Vascular Modification, Decidual Integrity, and Uterine Natural Killer Cell Maturation during Normal Murine Pregnancy. *Journal of Experimental Medicine*, 192(2), pp.259–270.

Assmann, N. et al., 2017. Srebp-controlled glucose metabolism is essential for NK cell functional responses. *Nature immunology*, 18(11), pp.1197–1206.

Baban, B. et al., 2018. Presence and Profile of Innate Lymphoid Cells in Human Breast Milk. *JAMA Pediatrics*, pp.1–3.

Balmas, E. et al., 2018. Maternal group 2 innate lymphoid cells control fetal growth and protect from endotoxin-induced abortion in mice. *bioRxiv*, pp.1–44.

Barber, E.M. & Pollard, J.W., 2003. The Uterine NK Cell Population Requires IL-15 but These Cells Are Not Required for Pregnancy nor the Resolution of a Listeria monocytogenes Infection. *The Journal of Immunology*, 171(1), pp.37–46.

Barker, D.J.P. & Osmond, C., 1986. Infant mortality, childhood nutrition, and ischaemic heart disease in England and Wales. *The Lancet*, pp.1–5.

Bellofiore, N. et al., 2018. Characterization of human-like menstruation in the spiny mouse: comparative studies with the human and induced mouse model. *Human reproduction (Oxford, England)*, 33(9), pp.1715–1726.

Bellofiore, N. et al., 2016. First evidence of a menstruating rodent: the spiny mouse (Acomys cahirinus). *The American Journal of Obstetrics & Gynecology*, 16(1), pp.1–26.

Benirschke, K., Burton, G.J. & Baergen, R.N., 2012. Placental Types. In *Pathology of the Human Placenta*. Berlin, Heidelberg: Springer Berlin Heidelberg, pp. 27–39.

Bernink, J.H. et al., 2013. Human type 1 innate lymphoid cells accumulate in inflamed mucosal tissues. *Nature immunology*, 14(3), pp.221–229.

Berod, L. et al., 2014. De novo fatty acid synthesis controls the fate between regulatory T and T helper 17 cells. *Nature Medicine*, 20(11), pp.1327–1333.

Bijovsky, A.T., Zorn, T.M.T. & Abrahamsohn, P.A., 1992. Remodeling of the Mouse Endometrial Stroma during the Preimplantation Period. *Acta Anatomy*, 144, pp.231–234.

Bisset, L.R. et al., 2004. Reference values for peripheral blood lymphocyte phenotypes applicable to the healthy adult population in Switzerland. *European Journal of Haematology*, 72, pp.1–10.

Björkström, N.K., Kekäläinen, E. & Mjösberg, J., 2013. Tissue-specific effector functions of innate lymphoid cells. *Immunology*, 139(4), pp.416–427.

Blackburn, D.G., 1998. Reconstructing the Evolution of Viviparity and Placentation. *Journal of Theoretical Biology*, pp.1–8.

Boulenouar, S. et al., 2016. The Residual Innate Lymphoid Cells in NFIL3-Deficient Mice Support Suboptimal Maternal Adaptations to Pregnancy. *Frontiers in Immunology*, 7(8), pp.1065–10.

Bronson, F.H., Dagg, C.P. & DG, S., 1966. *Reproduction* 1966 ed., New York: Dover Publications, Inc.

Brosens, I. et al., 2011. The "Great Obstetrical Syndromes" are associated with disorders of deep placentation. *The American Journal of Obstetrics & Gynecology*, 204(3), pp.193–201.

Brown, J.L. et al., 2018. Enrichment of Innate Lymphoid Cell Populations in Gingival Tissue. *Journal of Dental Research*, 196(77), pp.002203451878214–7.

Bulmer, J.N., Williams, P.J. & Lash, G.E., 2010. Immune cells in the placental bed. *The International Journal of Developmental Biology*, 54(2-3), pp.281–294.

Bulmer, J.N. & Sunderland C.A., 1984. Immunohistological characterisation of lymphoid cell populations in the early human placental bed. *Immunology*, 52 (1984), pp. 349-357

Burg, von, N. et al., 2014. Activated group 3 innate lymphoid cells promote T-cell-mediated immune responses. *Proceedings of the National Academy of Sciences*, 111(35), pp.12835–12840.

Burton, G.J. et al., 2002. Uterine Glands Provide Histiotrophic Nutrition for the Human Fetus during the First Trimester of Pregnancy. *The Journal of Clinical Endocrinology & Metabolism*, 87(6), pp.2954–2959.

Byers, S.L. et al., 2012. Mouse Estrous Cycle Identification Tool and Images. *PLoS ONE*, pp.1–5.

Cao, C. et al., 2014. Placental heme receptor LRP1 correlates with the heme exporter FLVCR1 and neonatal iron status. *Reproduction (Cambridge, England)*, 148(3), pp.295–302.

Caraux, A. et al., 2006. Natural killer cell differentiation driven by Tyro3 receptor tyrosine kinases. *Nature immunology*, 7(7), pp.747–754.

Carotta, S. et al., 2011. Identification of the earliest NK-cell precursor in the mouse BM. *Blood*, 117(20), pp.5449–5452.

Carson, M.J. et al., 2006. CNS immune privilege: hiding in plain sight. *Immunological Reviews*, 213, pp.1–18.

Carter, A.M., 2012. Evolution of placental function in mammals: the molecular basis of gas and nutrient transfer, hormone secretion, and immune responses. *Physiological reviews*, 92(4), pp.1543–1576.

Cella, M. et al., 2008. A human natural killer cell subset provides an innate source of IL-22 for mucosal immunity. *Nature*, 457(7230), pp.722–725.

Cella, M., Otero, K. & Colonna, M., 2010. Expansion of human NK-22 cells with IL-7, IL-2, and IL-1 reveals intrinsic functional plasticity. *Proceedings of the National Academy of Sciences*, 107(24), pp.10961–10966.

Chakraborty, D. et al., 2011. Natural killer cells direct hemochorial placentation by regulating hypoxia-inducible factor dependent trophoblast lineage decisions. *Proceedings of the National Academy of Sciences*, 108, pp.16295–16300.

Chang, C.Y.-Y. et al., 2011. MUC4 gene polymorphisms associate with endometriosis development and endometriosis- related infertility. *BMC Medicine*, 9(1), pp.1–10.

Charalambous, F., Elia, A. & Georgiades, P., 2012. Decidual spiral artery remodeling during early post-implantation period in mice: Investigation of associations with decidual uNK cells and invasive trophoblast. *Biochemical and Biophysical Research Communications*, 417(2), pp.847–852.

Chaturvedi, V. et al., 2015. CXCR3 blockade protects against Listeria monocytogenes infection–induced fetal wastage. *Journal of Clinical Investigation*, 125(4), pp.1713–1725.

Chaves, P. et al., 2018. Loss of Canonical Notch Signaling Affects Multiple Steps in NK Cell Development in Mice. *The Journal of Immunology*, 201(11), pp.1–14.

Chea, S. et al., 2016. Notch signaling in group 3 innate lymphoid cells modulates their plasticity. *Science signaling*, 9(426), pp.ra45–ra45.

Chen, Luxi et al., 2018. CD56 Expression Marks Human Group 2 Innate Lymphoid Cell Divergence from a Shared NK Cell and Group 3 Innate Lymphoid Cell Developmental Pathway. *Immunity*, 49, pp.1–18.

Chen, Zhilin, Zhang, J., Hatta, K., Lima, P.D.A., Yadi, H., Colucci, F., Yamada, A.T. & Croy, B.A., 2012a. DBA-Lectin Reactivity Defines Mouse Uterine Natural Killer Cell Subsets with Biased Gene Expression1. *Biology of Reproduction*, 87(4), pp.1–18.

Chen, Zhilin, Zhang, J., Hatta, K., Lima, P.D.A., Yadi, H., Colucci, F., Yamada, A.T. & Croy, B.A., 2012b. DBA-Lectin Reactivity Defines Mouse Uterine Natural Killer Cell Subsets with Biased Gene Expression. *Biology of Reproduction*, 87(4), pp.1–9.

Chen, Ziyi et al., 2017. Inference of immune cell composition on the expression profiles of mouse tissue. *Scientific Reports*, 7, pp.1–11.

Chevillard, G. & Blank, V., 2011. NFE2L3 (NRF3): the Cinderella of the Cap“n”Collar transcription factors. *Cellular and Molecular Life Sciences*, 68(20), pp.3337–3348.

Chiossone, L. et al., 2018. Natural killer cells and other innate lymphoid cells in cancer. *Nature Reviews Immunology*, 172(Suppl. 3), pp.1–18.

Cindrova-Davies, T. et al., 2017. RNA-seq reveals conservation of function among the yolk sacs of human, mouse, and chicken. *Proceedings of the National Academy of Sciences*, 114(24), pp.E4753–E4761.

Clark, D.A. et al., 2018. Soluble CD200 in secretory phase endometriosis endometrial venules may explain endometriosis pathophysiology and provide a novel treatment target. *Journal of Reproductive Immunology*, pp.1–36.

Cohen, E., Baerts, W. & van Bel, F., 2015. Brain-Sparing in Intrauterine Growth Restriction: Considerations for the Neonatologist. *Neonatology*, 108(4), pp.269–276.

Collins, M.K., Tay, C.-S. & Erlebacher, A., 2009. Dendritic cell entrapment within the pregnant uterus inhibits immune surveillance of the maternal/fetal interface in mice. *Journal of Clinical Investigation*, 119, pp.2062–2073.

Colucci, F., 2015. NK cells and other innate lymphoid cells at the maternal-fetal interface. *Journal of Reproductive Immunology*, 111, pp.4–5.

Constantinides, M.G. et al., 2014. A committed precursor to innate lymphoid cells. *Nature*, 000(7496), pp.1–14.

Constantinides, M.G. et al., 2015. PLZF expression maps the early stages of ILC1 lineage development. *Proceedings of the National Academy of Sciences*, 112(16), pp.5123–5128.

Cooper, C. et al., 1997. Growth in infancy and bone mass in later life. *Annals of the Rheumatic Diseases*, 56, pp.17–21.

Cortez, V. & Colonna, M., 2016. Diversity and function of group 1 innate lymphoid cells. *Immunology Letters*.

Cortez, V.S. et al., 2017. SMAD4 impedes the conversion of NK cells into ILC1-like cells by curtailing non-canonical TGF-β signaling. *Nature immunology*, 18(9), pp.995–1003.

Cortez, V.S. et al., 2016. Transforming Growth Factor-β Signaling Guides the Differentiation of Innate Lymphoid Cells in Salivary Glands. *Immunity*, 44, pp.1–13.

Croxatto, D. et al., 2016. Group 3 innate lymphoid cells regulate neutrophil migration and function in human decidua. *Mucosal immunology*, pp.1–12.

Croy, B.A. et al., 2002. Decidual natural killer cells: key regulators of placental development (a review). *Journal of Reproductive Immunology*, 57(1-2), pp.151–168.

Croy, B.A. et al., 2014. *The Guide to Investigation of Mouse Pregnancy* First Edition. A. Croy et al., eds., Elsevier GmbH.

Croy, B.A. et al., 2006. Uterine natural killer cells: a specialized differentiation regulated by ovarian hormones. *Immunological Reviews*, 214, pp.161–185.

Cuff, A.O. & Male, V., 2017. Conventional NK cells and ILC1 are partially ablated in the livers of Ncr1iCreTbx21fl/fl mice. *Wellcome Open Research*, 2, pp.39–11.

Cumano, A., Dieterien-Lievre, F. & Godin, I., 1996. Lymphoid Potential, Probed before Circulation in Mouse, Is Restricted to Caudal Intraembryonic Splanchnopleura. *Cell*, 86, pp.907–916.

Cupedo, T. et al., 2008. Human fetal lymphoid tissue–inducer cells are interleukin 17–producing precursors to RORC+ CD127+ natural killer–like cells. *Nature immunology*, 10(1), pp.66–74.

Daussy, C. et al., 2014. T-bet and Eomes instruct the development of two distinct natural killer cell lineages in the liver and in the bone marrow. *Journal of Experimental Medicine*, 211(3), pp.563–577.

De Leo, B. et al., 2017. Immunoprofiling of human uterine mast cells identifies three phenotypes and expression of ERβ and glucocorticoid receptor. *F1000Research*, 6, pp.667–19.

De, M. & Wood, G.W., 1989. Influence of oestrogen and progesterone on macrophage distribution in the mouse uterus. *Journal of Endocrinology*, 126, pp.417–424.

Di Renzo, G.C., 2009. The Great Obstetrical Syndromes. *The Journal of Maternal-Fetal & Neonatal Medicine*, 22(8), pp.633–635.

Doisne, J.M. et al., 2015. Composition, Development, and Function of Uterine Innate Lymphoid Cells. *The Journal of Immunology*, 195(8), pp.3937–3945.

Dulson, S.J., Harrington, L.E. & Zajac, A.J., 2018. Inscribing the core memories of killers. *Cellular and Molecular Immunology*, 457, pp.1–2.

Eberl, G., 2016. Immunity by equilibrium. *Nature Reviews Immunology*.

Eberl, G. & Littman, D.R., 2004. Thymic origin of intestinal alphabeta T cells revealed by fate mapping of RORgammat+ cells. *Science (New York, N.Y.)*, 305(5681), pp.248–251.

Eisenbarth, S.C., 2018. Dendritic cell subsets in T cell programming: location dictates function. *Nature Reviews Immunology*, 86, pp.1–15.

Erlebacher, A., 2013. Immunology of the Maternal-Fetal Interface. *Annual Review of Immunology*, 31(1), pp.387–411.

Erlebacher, A. et al., 2007. Constraints in antigen presentation severely restrict T cell recognition of the allogeneic fetus. *Journal of Clinical Investigation*, 117(5), pp.1399–1411.

Erlebacher, A., Price, K.A. & Glimcher, L.H., 2004. Maintenance of mouse trophoblast stem cell proliferation by TGF-?/activin. *Developmental Biology*, 275(1), pp.158–169.

Ewels, P. et al., 2016. MultiQC: summarize analysis results for multiple tools and samples in a single report. *Bioinformatics*, 32(19), pp.3047–3048.

Fallon, P.G. et al., 2006. Identification of an interleukin (IL)-25–dependent cell population that provides IL-4, IL-5, and IL-13 at the onset of helminth expulsion. *Journal of Experimental Medicine*, 203(4), pp.1105–1116.

Fathman, J.W. et al., 2011. Identification of the earliest natural killer cell-committed progenitor in murine bone marrow. *Blood*, 118(20), pp.5439–5447.

Filipovic, I. et al., 2018. Molecular definition of group 1 innate lymphoid cells in the mouse uterus. *Nature Communications*, 9(1), pp.1–13.

Firth, M.A. et al., 2013. Nfil3-independent lineage maintenance and antiviral response of natural killer cells. *Journal of Experimental Medicine*, 210(13), pp.2981–2990.

Fort, M.M. et al., 2001. IL-25 Induces IL-4, IL-5, and IL-13 and Th2-Associated Pathologies In Vivo. *Immunity*, 25, pp.985–995.

Freud, A.G. et al., 2016. NKp80 Defines a Critical Step during Human Natural Killer Cell Development. *Cell reports*, 16, pp.1–13.

Freud, A.G., Yu, J. & Caligiuri, M.A., 2014. Human natural killer cell development in secondary lymphoid tissues. *Seminars in Immunology*, 26(2), pp.1–6.

Fu, B. et al., 2017. Natural Killer Cells Promote Fetal Development through the Secretion of Growth-Promoting Factors. *Immunity*, 47(6), pp.1100–1113.e6.

Gaccioli, F. et al., 2017. Screening for fetal growth restriction using fetal biometry combined with maternal biomarkers. *The American Journal of Obstetrics & Gynecology*, 218(2), pp.1–13.

Gaccioli, F. et al., 2018. Screening for fetal growth restriction using ultrasound and the sFLT1/PlGF ratio in nulliparous women: a prospective cohort study. *The Lancet child and Adolescent Health*, 2(8), pp.1–13.

Gamliel, M. et al., 2018. Trained Memory of Human Uterine NK Cells Enhances Their Function in Subsequent Pregnancies. *Immunity*, 48(5), pp.951–962.e5.

Gao, Y. et al., 2017. Tumor immunoevasion by the conversion of effector NK cells into type 1 innate lymphoid cells. *Nature immunology*, 146, pp.3289–16.

Gardiner, C.M. & Finlay, D.K., 2017. What Fuels Natural Killers? Metabolism and NK Cell Responses. *Frontiers in Immunology*, 8(4), pp.536–8.

Gardner, L. & Moffett, A., 2003. Dendritic Cells in the Human Decidua. *Biology of Reproduction*, 69(4), pp.1438–1446.

Gascoyne, D.M. et al., 2009. The basic leucine zipper transcription factor E4BP4 is essential for natural killer cell development. *Nature immunology*, 10(10), pp.1118–1124.

Geiger, T.L. et al., 2014. Nfil3 is crucial for development of innate lymphoid cells and host protection against intestinal pathogens. *Journal of Experimental Medicine*, 211(9), pp.1723–1731.

Gekas, C. et al., 2005. The Placenta Is a Niche for Hematopoietic Stem Cells. *Developmental Cell*, 8(3), pp.365–375.

Gentek, R. et al., 2018. Hemogenic Endothelial Fate Mapping Reveals Dual Developmental Origin of Mast Cells. *Immunity*, 48(6), pp.1–18.

Georgiades, P., Ferguson-Smith, A.C. & Burton, G.J., 2002. Comparative Developmental Anatomy of the Murine and Human Definitive Placentae. *Placenta*, 23(1), pp.3–19.

Gratchev, A. et al., 2001. Alternatively Activated Macrophages Differentially Express Fibronectin and Its Splice Variants and the Extracellular Matrix Protein βIG-H3. *Scandinavian Journal of Immunology*, 53(4), pp.386–392.

Graubardt, N. et al., 2013. Promotion of liver regeneration by natural killer cells in a murine model is dependent on extracellular adenosine triphosphate phosphohydrolysis. *Hepatology*, 57(5), pp.1969–1979.

Guerin, L.R. et al., 2011. Seminal Fluid Regulates Accumulation of FOXP3+ Regulatory T Cells in the Preimplantation Mouse Uterus Through Expanding the FOXP3+ Cell Pool and CCL19-Mediated Recruitment1. *Biology of Reproduction*, 85(2), pp.397–408.

Guilliams, M. & Scott, C.L., 2017. Does niche competition determine the origin of tissue-resident macrophages? *Nature Reviews Immunology*, 17(7), pp.1–10.

Gumá, M. et al., 2006. Expansion of CD94/NKG2C+ NK cells in response to human cytomegalovirus-infected fibroblasts. *Blood*, 107, pp.1–9.

Guo, P. et al., 2009. Dual nature of the adaptive immune system in lampreys. *Nature*, 459(7248), pp.796–801.

Halestrap, A.P., 2013. The SLC16 gene family - Structure, role and regulation in health and disease. *Molecular Aspects of Medicine*, 34(2-3), pp.337–349.

Hamlett, W.C. & Wourms, J.P., 1984. Ultrastructure of the pre-implantation shark yolk sac placenta. *Tissue Cell*, 16, pp.613–625.

Hamlett, W.C., Wourms, J.P. & Hudson, J.S., 1985. Ultrastructure of the Full-Term Shark Yolk Sac Placenta. *Journal of Ultrastructure Research*, 91, pp.221–231.

Hammer, Q. et al., 2018. Adaptive Natural Killer Cells Integrate Interleukin-18 during Target-Cell Encounter. *Frontiers in Immunology*, 8, pp.1731–9.

Hamperl, H. and Hellweg, G, 1958. Granular endometrial stroma cells. Obstet Gynecol **11**, 379–387.

Han, X. et al., 2018. Mapping the Mouse Cell Atlas by Microwell-Seq. *Cell*, 172(5), pp.1091–1097.e17.

Hanna, J. et al., 2006. Decidual NK cells regulate key developmental processes at the human fetal-maternal interface. *Nature Medicine*, 12(9), pp.1065–1074.

Hedrich, H.J. & Bullock, G., 2004. *The Laboratory Mouse (Handbook of experimental animals)*, Elsevier.

Helige, C. et al., 2013. Distribution of decidual natural killer cells and macrophages in the neighbourhood of the trophoblast invasion front: a quantitative evaluation. *Human reproduction (Oxford, England)*, 29(1), pp.8–17.

Hempstock, J. et al., 2004. Endometrial glands as a source of nutrients, growth factors and cytokines during the first trimester of human pregnancy: A morphological and immunohistochemical study. *Reproductive Biology and Endocrinology*, 2(1), pp.58–14.

Henderson, T.A. et al., 2003. Steroid Receptor Expression in Uterine Natural Killer Cells. *The Journal of Clinical Endocrinology & Metabolism*, 88(1), pp.440–449.

Herberman, R.B., Nunn, M.E. & Lavrin, D.H., 1975. Natural cytotoxic reactivity of mouse lymphoid cells against syngeneic and allogeneic tumors. I. Distribution of reactivity and specificity. *International Journal of Cancer*, 16(2), pp.216–229.

Hernandez-Diaz, S., Toh, S. & Cnattingius, S., 2009. Risk of pre-eclampsia in first and subsequent pregnancies: prospective cohort study. *BMJ*, 338(jun18 1), pp.b2255–b2255.

Hiby, S.E. et al., 2014. Maternal KIR in Combination with Paternal HLA-C2 Regulate Human Birth Weight. *The Journal of Immunology*, 192(11), pp.5069–5073.

Hirano, M. et al., 2013. Evolutionary implications of a third lymphocyte lineage in lampreys. *Nature*, 000(7467), pp.1–5.

Houser, B.L. et al., 2011. Two Unique Human Decidual Macrophage Populations. *The Journal of Immunology*, 186(4), pp.2633–2642.

Huang, B. et al., 2016. Interleukin-33-induced expression of PIBF1 by decidual B cells protects against preterm labor. *Nature Genetics*, pp.1–10.

Huang, Y. et al., 2008. Human Trophoblasts Recruited T Lymphocytes and Monocytes into Decidua by Secretion of Chemokine CXCL16 and Interaction with CXCR6 in the First-Trimester Pregnancy. *The Journal of Immunology*, 180(4), pp.2367–2375.

Hug, L.A. et al., 2016. A new view of the tree of life. *Nature Microbiology*, 1(5), pp.1–6

Hughes, T. et al., 2014. The transcription Factor AHR prevents the differentiation of a stage 3 innate lymphoid cell subset to natural killer cells. *Cell reports*, 8(1), pp.150–162.

Hurst, S.D. et al., 2002. New IL-17 Family Members Promote Th1 or Th2 Responses in the Lung: In Vivo Function of the Novel Cytokine IL-25. *The Journal of Immunology*, 169(1), pp.443–453.

Hydes, T. et al., 2017. IL-12 and IL-15 induce the expression of CXCR6 and CD49a on peripheral natural killer cells. *Immunity, Inflammation and Disease*, 6(1), pp.34–46.

Jensen, F. et al., 2012. CD19+CD5+ Cells as Indicators of Preeclampsia. *Hypertension*, 59, pp.861–868.

Kazzaz, B.A., 1972. Specific endometrial granular cells. A semiquantitative study. *Eur J Obstet Gynecol,* 3, pp.77–84.

Kennedy, P.R. et al., 2016. Activating KIR2DS4 Is Expressed by Uterine NK Cells and Contributes to Successful Pregnancy. *The Journal of Immunology*, 197(11), pp.4292–4300.

Kerdiles, Y.M. et al., 2017. Natural-Killer-like B Cells Display the Phenotypic and Functional Characteristics of Conventional B Cells. *Immunity*, 47(2), pp.199–200.

Keskin, D.B. et al., 2007. TGF-beta promotes conversion of CD16+ peripheral blood NK cells into CD16- NK cells with similarities to decidual NK cells. *Proceedings of the National Academy of Sciences*, 104, pp.1–6.

Khalturin, K. et al., 2003. Urochordates and the origin of natural killer cells: Identification of a CD94 NKR-P1-related receptor in blood cells of Botryllus. *Proceedings of the National Academy of Sciences*, pp.1–6.

Kiessling, R., Klein, E. & Wigzell, H., 1975. "Natural" Killer cells in the mouse. I. Cytotoxic cells with specificity for mouse Moloney leukemia cells. Specificity and distribution according to genotype*. *European Journal of Immunology*, 5, pp.112–117.

Kiessling, R., Klein, E., Pross, H., et al., 1975. "Natural" killer cells in the mouse. II. Cytotoxic cells with specificity for mouse Moloney leukemia cells. Characteristics of the killer cell. *European Journal of Immunology*, 5(2), pp.117–121.

Kim, S.Y. et al., 2012. Methylome of Fetal and Maternal Monocytes and Macrophages at the Feto-Maternal Interface. *American Journal of Reproductive Immunology*, 68(1), pp.8–27.

Kindstedt, E. et al., 2018. Innate lymphoid cells are present in gingivitis and periodontitis. *Journal of Periodontology*, pp.1–24.

King, A., Birkby, C. & Loke, Y.W., 1989. Early Human Decidual Cells Exhibit NK Activity against the K562 Cell Line but Not against First Trimester Trophoblast. *Cellular immunology*, pp.1–8.

King, A., Gardner, L. & Loke, Y.W., 1996. Evaluation of oestrogen and progesterone receptor expression in uterine mucosal lymphocytes. 11, pp.1079–1082.

Klose, C.S.N. et al., 2014. Differentiation of Type 1 ILCs from a Common Progenitor to All Helper-like Innate Lymphoid Cell Lineages. *Cell*, 157(2), pp.340–356.

Koh, A. et al., 2007. Role of osteopontin in neutrophil function. *Immunology*, 122(4), pp.466–475.

Koopman, L.A. et al., 2003. Human Decidual Natural Killer Cells Are a Unique NK Cell Subset with Immunomodulatory Potential. *Journal of Experimental Medicine*, 198(8), pp.1201–1212.

Korol, C. et al., 2015. NK Cells Expressing the B Cell Antigen CD19: Expanding the Phenotypical Characterization and the Potential Consequences from Misinterpretation of This Subset Population. *Cytometry Part B Clinical Cytometry*, 88B, pp.358–360.

Kostrzewski, T. et al., 2018. Multiple Levels of Control Determine How E4bp4/Nfil3 Regulates NK Cell Development. *The Journal of Immunology*, 200(4), pp.1–17.

Krzewski, K. & Strominger, J.L., 2008. The killer's kiss: the many functions of NK cell immunological synapses. *Current opinion in cell biology*, 20(5), pp.597–605.

Kyoizumi, S. et al., 2017. Fate Decision Between Group 3 Innate Lymphoid and Conventional NK Cell Lineages by Notch Signaling in Human Circulating Hematopoietic Progenitors. *The Journal of Immunology*, 199(8), pp.1–18.

Lash, G.E. et al., 2016. Decidual macrophages: key regulators of vascular remodeling in human pregnancy. *Journal of Leukocyte Biology*, 100(2), pp.315–325.

Lau, C.M. et al., 2018. Epigenetic control of innate and adaptive immune memory. *Nature immunology*, 11, pp.1–16.

Lejeune, B., Van Hoeck, J. & Leroy, F., 1981. Transmitter role of the luminal uterine epithelium in the induction of decidualization in rats. *Journal of Reproduction and Fertility*, 61, pp.1–7.

Lemke, G., 2013. Biology of the TAM Receptors. *Cold Spring Harbor Perspectives in Biology*, 5(11), pp.a009076–a009076.

Lédée, N., Prat-Ellenberg, L., et al., 2018. Impact of prednisone in patients with repeated embryo implantation failures_ Beneficial or deleterious? *Journal of Reproductive Immunology*, 127, pp.11–15.

Lédée, N., Vasseur, C., et al., 2018. Intralipid® may represent a new hope for patients with reproductive failures and simultaneously an over-immune endometrial activation. *Journal of Reproductive Immunology*, 130, pp.1–16.

Li, S.S. et al., 2018. Identification of the fungal ligand triggering cytotoxic PRR-mediated NK cell killing of Cryptococcus and Candida. *Nature Communications*, 9(1), pp.1–13.

Li, Y. et al., 2018. Decidual-Placental Immune Landscape During Syngeneic Murine Pregnancy. *Frontiers in Immunology*, 9, pp.387–13.

Lima, J. et al., 2016. Characterization of B cells in healthy pregnant women from late pregnancy to post-partum: a prospective observational study. *BMC Pregnancy and Childbirth*, 16(1), pp.1–13.

Locksley, R.M., Killeen, N. & Lenardo, M.J., 2001. The TNF and TNF Receptor Superfamilies: Integrating Mammalian Biology. *Cell*, pp.1–15.

Long, E.O. et al., 2013. Controlling Natural Killer Cell Responses: Integration of Signals for Activation and Inhibition. *Annual Review of Immunology*, 31(1), pp.227–258.

Lu, Q. et al., 1999. Tyro-3 family receptors are essential regulators of mammalian spermatogenesis. *Nature*, 398, pp.1–6.

Luci, C. et al., 2008. Influence of the transcription factor RORγt on the development of NKp46+ cell populations in gut and skin. *Nature immunology*, 10(1), pp.75–82.

Madeja, Z. et al., 2011. Paternal MHC expression on mouse trophoblast affects uterine vascularization and fetal growth. *Proceedings of the National Academy of Sciences*, 108(10), pp.4012–4017.

Male, V. & Brady, H.J.M., 2014. Transcriptional control of NK cell differentiation and function. *Current topics in microbiology and immunology*, 381, pp.173–187.

Male, V. et al., 2010. Immature NK cells, capable of producing IL-22, are present in human uterine mucosa. *Journal of immunology (Baltimore, Md. : 1950)*, 185(7), pp.3913–3918.

Male, V. et al., 2014. The transcription factor E4bp4/Nfil3 controls commitment to the NK lineage and directly regulates Eomes and Id2 expression. *The Journal of Experimental Medicine*, 211(4), pp.635–642.

Manickam, C. et al., 2018. Progressive lentivirus infection induces natural killer cell receptor-expressing B cells in the gastrointestinal tract. *AIDS*, pp.1–23.

Marchand, F., 1895. Uber die sogenannten dezidualen Geschwulste im Anschlub an normale Gebert, Blasenmole und Extrauterinschwangerschaft. Mschr Geburtsh Gynak 1, 419.

Mayer, W.E. et al., 2002. Isolation and characterization of lymphocyte-like cells from a lamprey. *Proceedings of the National Academy of Sciences*, 99, pp.14350–14355.

Mazurier, F. et al., 1999. A Novel Immunodeficient Mouse Model-RAG2 gamma Cytokine Receptor Chain Double Mutants-Requiring Exogenous Cytokine Administration for Human Hematopoietic Stem Cell Engraftment Common. *Journal of Interferon & Cytokine Research*, 19(5), pp.533–541.

McGovern, N., Chan, J.K.Y. & Ginhoux, F., 2015. Dendritic cells in humans--from fetus to adult. *International Immunology*, 27(2), pp.65–72.

Mebius, R.E., Rennert, P. & Weissman, I.L., 1997. Developing Lymph Nodes Collect CD4+CD3-LTbeta+ Cells That Can Differentiate to APC, NK Cells and Follicular Cells but Not T or B Cells. *Immunity*, 7, pp.493–504.

Medawar, P.B., 1953. Some immunological and endocrinological problems raised by the evolution of viviparity in vertebrates. *Symp. Soc. Exp. Biol.*, 7, pp.320–338.

Meyer, N., Woidacki, K., Knöfler, M., et al., 2017. Chymase-producing cells of the innate immune system are required for decidual vascular remodeling and fetal growth. *Scientific Reports*, 7, pp.1–14.

Meyer, N., Woidacki, K., Maurer, M., et al., 2017. Safeguarding of Fetal Growth by Mast Cells and Natural Killer Cells: Deficiency of One Is Counterbalanced by the Other. *Frontiers in Immunology*, 8, pp.67–10.

Mifsud, W. & Sebire, N.J., 2014. Placental Pathology in Early-Onset and Late-Onset Fetal Growth Restriction. *Fetal Diagnosis and Therapy*, 36(2), pp.117–128.

Mikkola, H.K.A., 2006. The journey of developing hematopoietic stem cells. *Development*, 133(19), pp.3733–3744.

Mjösberg, J.M. et al., 2011. Human IL-25- and IL-33-responsive type 2 innate lymphoid cells are defined by expression of CRTH2 and CD161. *Nature immunology*, 12(11), pp.1055–1062.

Moffett, A. & Colucci, F., 2015. Co-evolution of NK receptors and HLA ligands in humans is driven by reproduction. *Immunologic Research*, 267, pp.283–297.

Moffett, A. & Colucci, F., 2014. Uterine NK cells: active regulators at the maternal-fetal interface. *Journal of Clinical Investigation*, 124(5), pp.1872–1879.

Moffett, A. & Loke, C., 2006. Immunology of placentation in eutherian mammals. *Nature Reviews Immunology*, 6(8), pp.584–594.

Moffett, A. & Male, V. H. NK cells and reproduction; in Natural Killer Cells 403–416 (Springer International Publishing, 2009). doi:10.1016/B978-0-12-370454-2.00030-2

Moffett, A. & Shreeve, N., 2015. First do no harm: uterine natural killer (NK) cells in assisted reproduction. *Human reproduction (Oxford, England)*, 30(7), pp.1519–1525.

Moffett, A., Regan, L. & Braude, P., 2004. Natural killer cells, miscarriage, and infertility. *BMJ*, 329, pp.1283–1285.

Moffett-King, A., 2002. Natural killer cells and pregnancy. *Nature Reviews Immunology*, 2(9), pp.656–663.

Mone, F., McAuliffe, F.M. & Ong, S., 2014. The clinical application of Doppler ultrasound in obstetrics. *The Obstetrician & Gynaecologist*, 17(1), pp.13–19.

Montaldo, E. et al., 2014. Human RORγt(+)CD34(+) cells are lineage-specified progenitors of group 3 RORγt(+) innate lymphoid cells. *Immunity*, 41(6), pp.988–1000.

Montaldo, E. et al., 2016. Unique Eomes+ NK Cell Subsets Are Present in Uterus and Decidua During Early Pregnancy. *Frontiers in Immunology*, 6(2), pp.145–11.

Moraru, M. et al., 2012. Intravenous Immunoglobulin Treatment Increased Live Birth Rate in a Spanish Cohort of Women with Recurrent Reproductive Failure and Expanded CD56+ Cells. *American Journal of Reproductive Immunology*, 68(1), pp.75–84.

Mori, M. et al., 2016. The decidua—the maternal bed embracing the embryo—maintains the pregnancy. *Seminars in Immunopathology*, pp.1–15.

Moro, K. et al., 2010. Innate production of TH2 cytokines by adipose tissue-associated c-Kit+Sca-1+ lymphoid cells. *Nature*, 463(7280), pp.540–544.

Muzzio, D.O. et al., 2014. B Cell Development Undergoes Profound Modifications and Adaptations During Pregnancy in Mice1. *Biology of Reproduction*, 91(5), pp.1930–11.

Nabekura, T. et al., 2014. Costimulatory Molecule DNAM-1 Is Essential for Optimal Differentiation of Memory Natural Killer Cells during Mouse Cytomegalovirus Infection. *Immunity*, 40(2), pp.225–234.

Nadkarni, S. et al., 2016. Neutrophils induce proangiogenic T cells with a regulatory phenotype in pregnancy. *Proceedings of the National Academy of Sciences*, 113(52), pp.E8415–E8424.

Nagamatsu, T. & Schust, D.J., 2010. The Contribution of Macrophages to Normal and Pathological Pregnancies. *American Journal of Reproductive Immunology*, 63(6), pp.460–471.

Nancy, P. et al., 2012. Chemokine Gene Silencing in Decidul Stromal Cells Limits T Cell Access to the Maternal-Fetal Interface. *Science (New York, N.Y.)*, 336, pp.1317–1321.

Neill, D.R. et al., 2010. Nuocytes represent a new innate effector leukocyte that mediates type-2 immunity. *Nature*, 464(7293), pp.1367–1370.

Niakan, K.K. et al., 2012. Human pre-implantation embryo development. *Development*, 139(5), pp.829–841.

Ogasawara, M. & Aoki, K., 2000. Successful Uterine Steroid Therapy in a Case with a History of Ten Miscarriages. *American Journal of Reproductive Immunology*, 44, pp.253–255.

Oh, M.-J. & Croy, B.A., 2008. A map of relationships between uterine natural killer cells and progesterone receptor expressing cells during mouse pregnancy. *Placenta*, 29(4), pp.317–323.

Ottersbach, K. & Dzierzak, E., 2005. The Murine Placenta Contains Hematopoietic Stem Cells within the Vascular Labyrinth Region. *Developmental Cell*, 8(3), pp.377–387.

O'Sullivan, T.E., Sun, J.C. & Lanier, L.L., 2015. Natural Killer Cell Memory. *Immunity*, 43(4), pp.634–645.

Paffaro, V.A., Jr et al., 2003. Subset Classification of Mouse Uterine Natural Killer Cells by DBA Lectin Reactivity. *Placenta*, 24(5), pp.479–488.

Painter, J.N. et al., 2010. Genome-wide association study identifies a locus at 7p15.2 associated with endometriosis. *Nature Genetics*, 43(1), pp.51–54.

Palis, J. & Yoder, M.C., 2001. Yolk-sac hematopoiesis: The first blood cells of mouse and man. *Experimental hematology*, pp.1–10.

Pancer, Z. et al., 2004. Somatic diversification of variable lymphocyte receptors in the agnathan sea lamprey. *Nature*, 430, pp.1–7.

Paust, S. et al., 2010. Critical role for the chemokine receptor CXCR6 in NK cell–mediated antigen-specific memory of haptens and viruses. *Nature immunology*, 11(12), pp.1127–1135.

Peng, H. et al., 2013. Liver-resident NK cells confer adaptive immunity in skin-contact inflammation. *Journal of Clinical Investigation*, 123(4), pp.1444–1456.

Perchet, T. et al., 2018. The Notch Signaling Pathway Is Balancing Type 1 Innate Lymphoid Cell Immune Functions. *Frontiers in Immunology*, 9.

Pijnenborg, R., Vercruysse, L. & Hanssens, M., 2006. The Uterine Spiral Arteries In Human Pregnancy: Facts and Controversies. *Placenta*, 27(9-10), pp.939–958.

Plaks, V. et al., 2008. Uterine DCs are crucial for decidua formation during embryo implantation in mice. *Journal of Clinical Investigation*, 118, pp.3954–3965.

Pope, G.R. et al., 2012. Central and peripheral apelin receptor distribution in the mouse: Species differences with rat. *Peptides*, 33(1), pp.139–148.

Price, A.E. et al., 2010. Systemically dispersed innate IL-13–expressing cells in type 2 immunity. *Proceedings of the National Academy of Sciences*, pp.1–6.

Purdy, A.K. & Campbell, K.S., 2009. Natural killer cells and cancer: regulation by the killer cell Ig-like receptors (KIR). *Cancer biology & therapy*, 8(23), pp.2211–2220.

Quenby, S. et al., 2005. Prednisolone reduces preconceptual endometrial natural killer cells in women with recurrent miscarriage. *Fertility and Sterility*, 84(4), pp.980–984.

Raghupathy, R. et al., 2000. Cytokine production by maternal lymphocytes during normal human pregnancy and in unexplained recurrent spontaneous abortion. *Human Reproduction*, 15, pp.713–718.

Rasweiler, J.J., 1991. Spontaneous Decidual Reactions and Menstruation in the Black Mastiff Bat, *Molossus ater*. *The American Journal of Anatomy*, 191, pp.1–22.

Ratsep, M.T. et al., 2014. Uterine natural killer cells: supervisors of vasculature construction in early decidua basalis. *Reproduction (Cambridge, England)*, 149(2), pp.R91–R102.

Reavey, J.J., Maybin, J.A. & Critchley, H.O.D., 2018. *Inherited Bleeding Disorders in Women* Second. J. J. Reavey, P. D. James, & C. A. Lee, eds., John Wley & Sons Ltd.

Rehman, A. et al., 2013. Role of Fatty-Acid Synthesis in Dendritic Cell Generation and Function. *The Journal of Immunology*, 190(9), pp.4640–4649.

Reisz, R.R., 1997. The origin and early evolutionary history of amniotes. *Trends in Ecology and Evolution*, pp.1–5.

Renoux, V.M. et al., 2015. Identification of a Human Natural Killer Cell Lineage-Restricted Progenitor in Fetal and Adult Tissues. *Immunity*, 43(2), pp.394–407.

Robinette, M.L. et al., 2015. Transcriptional programs define molecular characteristics of innate lymphoid cell classes and subsets. *Nature immunology*, 16(3), pp.306–317.

Romer, A.S., 1967. Major Steps in Vertebrate Evolution. *Science (New York, N.Y.)*, pp.1–10.

Romero, R., 2009. Prenatal medicine: The child is the father of the man*. *The Journal of Maternal-Fetal & Neonatal Medicine*, 22(8), pp.636–639.

Romero, R. et al., 2006. The preterm parturition syndrome. *BJOG an International Journal of Obstetrics and Gynaecology*, 113(Suppl 2), pp.17–42.

Romero-Garcia, S. et al., 2016. Lactate Contribution to the Tumor Microenvironment: Mechanisms, Effects on Immune Cells and Therapeutic Relevance. *Frontiers in Immunology*, 7(Pt 2), pp.R502–11.

Rosmaraki, E.E. et al., 2001. Identification of committed NK cell progenitors in adult murine bone marrow. *European Journal of Immunology*, 31, pp.1–10.

Rossant, J. & Cross, J.C., 2001. Placental development: Lessons from mouse mutants. *Nature Reviews Genetics*, 2, pp.538–548.

Rossant, J. & Tam, P.P.L., 2017. New Insights into Early Human Development: Lessons for Stem Cell Derivation and Differentiation. *Stem Cell*, 20(1), pp.18–28.

Rowe, J.H. et al., 2012. Pregnancy imprints regulatory memory that sustains anergy to fetal antigen. *Nature*, 490(7418), pp.1–6.

Ruiz, J.E. et al., 1996. Intravenous Immunoglobulin Inhibits Natural Killer Cell Activity In Vivo in Women With Recurrent Spontaneous Abortion. *American Journal of Reproductive Immunology*, 35, pp.370–375.

Sacks, G., 2015. Enough! Stop the arguments and get on with the science of natural killer cell testing. *Human reproduction (Oxford, England)*, 30(7), pp.1526–1531.

Samstein, R.M. et al., 2012. Extrathymic Generation of Regulatory T Cells in Placental Mammals Mitigates Maternal-Fetal Conflict. *Cell*, 150(1), pp.29–38.

Sander, P.M., 2012. Reproduction in Early Amniotes. *Science (New York, N.Y.)*, 337(6096), pp.806–808.

Sanos, S.L. et al., 2008. RORγt and commensal microflora are required for the differentiation of mucosal interleukin 22–producing NKp46+ cells. *Nature immunology*, 10(1), pp.83–91.

Sato, A. et al., 2003. Genes encoding putative natural killer cell C-type lectin receptors in teleostean fishes. *Proceedings of the National Academy of Sciences*, pp.1–6.

Satoh-Takayama, N. et al., 2010. IL-7 and IL-15 independently program the differentiation of intestinal CD3-NKp46+ cell subsets from Id2-dependent precursors. *Journal of Experimental Medicine*, 207(2), pp.273–280.

Satoh-Takayama, N. et al., 2008. Microbial Flora Drives Interleukin 22 Production in Intestinal NKp46+ Cells that Provide Innate Mucosal Immune Defense. *Immunity*, 29(6), pp.958–970.

Scarpellini, F. & Sbracia, M., 2009. Use of granulocyte colony-stimulating factor for the treatment of unexplained recurrent miscarriage: a randomised controlled trial. *Human reproduction (Oxford, England)*, 24(11), pp.2703–2708.

Schuijs, M.J., Hammad, H. & Lambrecht, B.N., 2018. Professional and "Amateur" Antigen-Presenting Cells In Type 2 Immunity. *Trends in Immunology*, 40(1), pp.1–13.

Scoville, S.D. et al., 2016. A Progenitor Cell Expressing Transcription Factor RORγt Generates All Human Innate Lymphoid Cell Subsets. *Immunity*, 44(5), pp.1140–1150.

Seillet, C. et al., 2016. Deciphering the Innate Lymphoid Cell Transcriptional Program. *Cell reports*, 17(2), pp.436–447.

Seillet, C. et al., 2014. Differential requirement for Nfil3 during NK cell development. *Journal of immunology (Baltimore, Md. : 1950)*, 192(6), pp.2667–2676.

Seshadri, S. & Sunkara, S.K., 2013. Natural killer cells in female infertility and recurrent miscarriage: a systematic review and meta-analysis. *Human Reproduction Update*, 20(3), pp.429–438.

Sharkey, D.J. et al., 2012. Seminal Fluid Induces Leukocyte Recruitment and Cytokine and Chemokine mRNA Expression in the Human Cervix after Coitus. *The Journal of Immunology*, 188(5), pp.2445–2454.

Skonier, J. et al., 1992. cDNA cloning and sequence analysis of beta ig-h3, a novel gene induced in a human adenocarcinoma cell line after treatment with transforming growth factor-beta. *DNA and cell biology*, 11(7), pp.511–522.

Sojka, D.K. et al., 2014. Tissue-resident natural killer (NK) cells are cell lineages distinct from thymic and conventional splenic NK cells. *eLife*, 3, p.e01659.

Soma, L. et al., 2014. Apparent CD19 expression by natural killer cells: A potential confounder for minimal residual disease detection by flow cytometry in B lymphoblastic leukemia. *Cytometry Part A*, 88(2), pp.145–147.

Spits, H. et al., 2013. Innate lymphoid cells — a proposal for uniform nomenclature. *Nature Reviews Immunology*, 13(2), pp.1–5.

Spits, H., Bernink, J.H. & Lanier, L., 2016. NK cells and type 1 innate lymphoid cells: partners in host defense. *Nature immunology*, 17(7), pp.758–764.

Stark, R. et al., 2018. Trm maintenance is regulated by tissue damage via P2RX7. *Science Immunology*, pp.1–12.

Staudt, N.D. et al., 2013. Myeloid Cell Receptor LRP1/CD91 Regulates Monocyte Recruitment and Angiogenesis in Tumors. *Cancer Research*, 73(13), pp.3902–3912.

Staun-Ram, E. & Shalev, E., 2005. **Human trophoblast function during the implantation process**. *Reproductive Biology and Endocrinology*, 3(1), pp.56–12.

Sun, J.C., Beilke, J.N. & Lanier, L.L., 2009. Adaptive immune features of natural killer cells. *Nature*, 457(7229), pp.557–561.

Suryawanshi, H. et al., 2018. A single-cell survey of the human first-trimester placenta and decidua. *Science Advances*, pp.1–13.

Svensson, J. et al., 2011. Macrophages at the Fetal-Maternal Interface Express Markers of Alternative Activation and Are Induced by M-CSF and IL-10. *The Journal of Immunology*, 187(7), pp.3671–3682.

Tagliani, E. et al., 2011. Coordinate regulation of tissue macrophage and dendritic cell population dynamics by CSF-1. *Journal of Experimental Medicine*, 208(9), pp.1901–1916.

Tait Wojno, E.D. & Artis, D., 2016. Emerging concepts and future challenges in innate lymphoid cell biology. *Journal of Experimental Medicine*, 213(11), pp.2229–2248.

Tam, P.P.L., 2004. Embryonic Axes: The Long and Short of It in the Mouse. *Current Biology*, 14(6), pp.R239–R241.

Tan, J. et al., 1999. Differential Uterine Expression of Estrogen and Progesterone Receptors Correlates with Uterine Preparation for Implantation and Decidualization in the Mouse*. *Endocrinology*, 140, pp.1–12.

Tang, W. W. C., Kobayashi, T., Irie, N., Dietmann, S. & Surani, M. A. Specification and epigenetic programming of the human germ line. Nat Rev Genet 17, 585–600 (2016).

Taylor, N. et al., 2005. Enhanced Tolerance to Autoimmune Uveitis in CD200-Deficient Mice Correlates with a Pronounced Th2 Switch in Response to Antigen Challenge. *The Journal of Immunology*, 174, pp.143–154.

Thompson, L.A. et al., 1992. The Leukocytic Reaction of the Human Uterine Cervix. *American Journal of Reproductive Immunology*, 28, pp.85–89.

Tilburgs, T. et al., 2006. Differential Distribution of CD4+CD25bright and CD8+CD28− T-cells in Decidua and Maternal Blood During Human Pregnancy. *Placenta*, 27, pp.47–53.

Tilburgs, T. et al., 2009. Fetal–maternal HLA-C mismatch is associated with decidual T cell activation and induction of functional T regulatory cells. *Journal of Reproductive Immunology*, 82(2), pp.148–157.

Trundley, A. & Moffett, A., 2004. Human uterine leukocytes and pregnancy. *Tissue Antigens*, 63, pp.1–12.

Tse, S.-W. et al., 2014. The Chemokine Receptor CXCR6 Is Required for the Maintenance of Liver Memory CD8+ T Cells Specific for Infectious Pathogens. *The Journal of Infectious Diseases*, 210(9), pp.1508–1516.

Turco, M.Y. et al., 2017. Long-term, hormone-responsive organoid cultures of human endometrium in a chemically defined medium. *Nature Cell Biology*, 19(5), pp.568–577.

Turco, M.Y. et al., 2018. Trophoblast organoids as a model for maternal–fetal interactions during human placentation. *Nature*, 564(7735), pp.1–19.

Uekita, T. et al., 2003. Dynamics of BIGH3 mRNA Expression During Pregnancy in the Uterus and the Placenta of the Mouse: A possible Regulatory factor for Trophoblastic Invasion. *Journal of Reproduction and Development*, pp.1–10.

Vacca, P. et al., 2011. CD34+ hematopoietic precursors are present in human decidua and differentiate into natural killer cells upon interaction with stromal cells. *Proceedings of the National Academy of Sciences*, 108(6), pp.2402–2407.

Vacca, P. et al., 2015. Identification of diverse innate lymphoid cells in human decidua. *Mucosal immunology*, 8(2), pp.254–264.

van der Horst, C.J., 1954. Elephantulus Going into Anoestrus; Menstruation and Abortion. *Philosophical Transactions of the Royal Society B: Biological Sciences*, 238(653), pp.27–61.

van Ebbenhorst Tengbergen, W.J.P.R., 1955. The Morphology of the Mouse Anterior Pituitary During the Oestrous Cycle. *Acta Endocrinologica*, 18, pp.213–218.

Velasco-Herrera, M.D.C. et al., 2018. A novel innate lymphoid cell delineates childhood autoimmune arthritis. *bioRxiv*, pp.1–22.

Velásquez, S.Y. et al., 2016. Short Term Hypoxia Synergizes with Interleukin 15 Priming in Driving Glycolytic Gene Transcription and Supports Human Natural Killer Cell Activities. *Journal of Biological Chemistry*, 291(25), pp.12960–12977.

Vento-Tormo, R. et al., 2018. Single-cell reconstruction of the early maternal–fetal interface in humans. *Nature*, 563(7731), pp.1–6.

Vély, F. et al., 2016. Evidence of innate lymphoid cell redundancy in humans. *Nature immunology*, pp.1–10.

Vivier, E. et al., 2008. Functions of natural killer cells. *Nature immunology*, 9(5), pp.503–510.

Vivier, E. et al., 2018. Innate Lymphoid Cells: 10 Years On. *Cell*, 174(5), pp.1054–1066.

Vivier, E. et al., 2011. Innate or adaptive immunity? The example of natural killer cells. *Science (New York, N.Y.)*, 331(6013), pp.44–49.

Vivier, E. et al., 2016. The evolution of innate lymphoid cells. *Nature immunology*, 17(7), pp.790–794.

Von Numers, C., 1953. On the specific granular cells (globular leukocytes) of the human endometrium. Acta Pathol Microbiol Scand 33, 250–256.

Vonarbourg, C. et al., 2010. Regulated Expression of Nuclear Receptor RORγt Confers Distinct Functional Fates to NK Cell Receptor-Expressing RORγt+ Innate Lymphocytes. *Immunity*, 33(5), pp.736–751.

Walter, W. et al., 2000. H2-M, a facilitator of MHC class II peptide loading, and its negative modulator H2-O are differentially expressed in response to proinflammatory cytokines. *Immunogenetics*, 51(10), pp.794–804.

Wang, S. et al., 2016. Natural Killer-like B Cells Prime Innate Lymphocytes against Microbial Infection. *Immunity*, pp.1–15.

Weill, P.,1921. Etudes sur les leukocytes I. Les cellules granuleuses des muqueuses intestinale et uterine. Arch Anat Microsc 17, 77–82.

Wilkens, J. et al., 2013. Uterine NK Cells Regulate Endometrial Bleeding in Women and Are Suppressed by the Progesterone Receptor Modulator Asoprisnil. *The Journal of Immunology*, 191(5), pp.2226–2235.

Wingett, S.W. & Andrews, S., 2018. FastQ Screen: A tool for multi-genome mapping and quality control. *F1000Research*, 7, pp.1338–13.

Woods, L., Perez-Garcia, V. & Hemberger, M., 2018. Regulation of Placental Development and Its Impact on Fetal Growth—New Insights From Mouse Models. *Frontiers in Endocrinology*, 9, pp.6–18.

Xiao, S. et al., 2017. A microfluidic culture model of the human reproductive tract and 28-day menstrual cycle. *Nature Communications*, 8, pp.1–13.

Xu, W. et al., 2015. NFIL3 Orchestrates the Emergence of Common Helper Innate Lymphoid Cell Precursors. *Cell reports*, 10(12), pp.2043–2054.

Yadi, H. et al., 2008. Unique Receptor Repertoire in Mouse Uterine NK cells. *The Journal of Immunology*, 181(9), pp.6140–6147.

Yang, Q. et al., 2015. TCF-1 upregulation identifies early innate lymphoid progenitors in the bone marrow. *Nature immunology*, 16(10), pp.1044–1050.

Yates, M. et al., 2011. Clinical impact of scavenger receptor class B type I gene polymorphisms on human female fertility. *Human reproduction (Oxford, England)*, 26(7), pp.1910–1916.

Yoder, J.A. & Litman, G.W., 2010. The phylogenetic origins of natural killer receptors and recognition: relationships, possibilities, and realities. *Immunogenetics*, 63(3), pp.123–141.

Yoshida, H. et al., 1999. IL-7 receptor alpha+ CD3- cells in the embryonic intestine induces the organizing center of Peyer's patches. *International Immunology*, pp.1–13.

Yu, X. et al., 2014. The basic leucine zipper transcription factor NFIL3 directs the development of a common innate lymphoid cell precursor. *eLife*, 3, pp.945–20.

Zhang, G. et al., 2017. Genetic Associations with Gestational Duration and Spontaneous Preterm Birth. *New England Journal of Medicine*, 377(12), pp.1156–1167.

Zhang, J. et al., 2012. Unusual timing of CD127 expression by mouse uterine natural killer cells. *Journal of Leukocyte Biology*, 91(3), pp.417–426.

Zhang, T. et al., 2017. Successful treatment with intrauterine delivery of dexamethasone for repeated implantation failure. *American Journal of Reproductive Immunology*, 78(6), pp.e12766–8.

Zhang, X. et al., 2007. Wild Fulvous Fruit Bats (Rousettus leschenaulti) Exhibit Human-Like Menstrual Cycle1. *Biology of Reproduction*, 77(2), pp.358–364.

Zhou, J.Z., Way, S.S. & Chen, K., 2018. Immunology of the Uterine and Vaginal Mucosae. *Trends in Immunology*, pp.1–13.

Zuo, R.-J. et al., 2015. Warburg-like Glycolysis and Lactate Shuttle in Mouse Decidua during Early Pregnancy. *The Journal of Biological Chemistry*, 290, pp.21280–21291.

Appendix

Table A.1. Comparison I. All differentially expressed genes from the comparison I: all uterine (ILC1, trNK, cNK) subsets vs all liver (ILC1, cNK) subsets. FC: fold change, padj: adjusted p-value.

Gene	FC	pvalue	padj
Hba-x	6,7928	1,47E-37	2,27E-33
Hbb-y	6,5059	1,68E-32	1,29E-28
Hbb-bh1	6,4695	1,83E-31	9,40E-28
H19	6,3382	5,97E-29	2,30E-25
A2m	6,1354	3,35E-28	1,03E-24
Prl8a2	5,5805	3,71E-20	7,14E-17
Peg3	4,8331	8,24E-16	1,41E-12
Prap1	4,6175	2,67E-12	2,94E-09
Serpinh1	4,2129	9,26E-11	6,49E-08
Sox11	4,1860	3,70E-10	2,28E-07
Fbln1	4,0091	3,32E-09	1,51E-06
Gzme	3,9693	5,62E-12	5,10E-09
Tgfb2	3,9322	5,20E-09	2,17E-06
Flrt3	3,8176	1,07E-09	5,89E-07
Retnla	3,7668	1,18E-09	6,26E-07
Map1b	3,6736	4,17E-09	1,84E-06
Igf2bp1	3,6649	1,41E-11	1,15E-08
Dab2	3,6532	1,11E-22	2,45E-19
Hebp1	3,5984	6,28E-09	2,48E-06
Ptn	3,5839	3,12E-08	9,83E-06
Mrc2	3,5677	1,87E-07	5,34E-05
Pdpn	3,4863	5,44E-08	1,68E-05
Flrt2	3,4834	3,39E-07	9,02E-05
Nrep	3,4778	3,66E-07	9,17E-05
F7	3,4759	2,68E-08	8,62E-06
Nrk	3,4223	7,66E-09	2,88E-06
Cryab	3,3339	9,44E-07	0,0001915
Gzmd	3,2738	2,59E-08	8,48E-06
Ms4a7	3,2332	1,73E-12	2,05E-09
Lin28b	3,2275	8,89E-07	0,0001852
Spsb1	3,2235	1,52E-06	0,000279
Grb10	3,2006	1,03E-06	0,0002072
Pf4	3,1673	5,49E-07	0,0001282
Igf2	3,1656	6,81E-07	0,0001458
Cpe	3,1549	4,42E-06	0,0006549
Arfgef3	3,1069	1,96E-06	0,0003439
Cd109	3,0490	5,55E-06	0,0007991
Zcchc3	3,0414	1,25E-06	0,0002467
Ahnak2	3,0322	1,71E-06	0,0003108
Pmepa1	3,0024	1,95E-09	9,72E-07
Gzmg	2,9813	6,77E-06	0,0009405
Fcrls	2,9006	2,09E-06	0,0003627
Hsd3b6	2,8932	1,15E-05	0,0014838
Ccl7	2,8841	5,70E-06	0,0008072
Vcan	2,8774	1,95E-10	1,25E-07
A530064D06Rik	2,8735	2,58E-09	1,24E-06
Gm15246	2,8720	2,29E-05	0,0024043
Speg	2,8647	2,64E-05	0,0027166
Afap1l1	2,8610	2,26E-05	0,0023852
Ccl12	2,8550	7,50E-06	0,0010141
Inhba	2,8517	2,11E-07	5,91E-05
Spp1	2,8400	5,82E-08	1,76E-05
Etv1	2,8388	1,23E-08	4,43E-06
Gab1	2,8280	2,80E-06	0,0004552
Uaca	2,8200	2,66E-05	0,0027166
Gm13899	2,8101	3,99E-05	0,0037093
Scn3b	2,8072	1,60E-05	0,0019072
Scin	2,8068	9,40E-07	0,0001915
Col4a1	2,7768	4,67E-06	0,0006859
Tpm2	2,7710	4,86E-05	0,0043318
Nes	2,7464	2,21E-05	0,0023498
Olr1	2,7458	5,81E-07	0,0001338
Gap43	2,7349	6,36E-05	0,0053026
9130008F23Rik	2,7202	1,98E-05	0,002215
Kank2	2,7150	2,26E-06	0,0003829
Mitf	2,7017	3,04E-06	0,0004778
Basp1	2,6692	5,57E-09	2,26E-06
Slco2b1	2,6558	2,86E-05	0,002861
Dusp9	2,6476	3,81E-05	0,0035795
Tmem119	2,6356	2,91E-05	0,0028761

Gene	FC	pvalue	padj
Trim71	2,6348	0,0001096	0,00785754
Hif3a	2,6140	9,47E-05	0,00715437
Lgmn	2,6045	4,80E-12	4,81E-09
Gpr31b	2,6016	0,0001347	0,00899237
Pla1a	2,5849	0,000149	0,00945524
Adamts1	2,5768	0,0001078	0,00776386
Ch25h	2,5531	0,0001565	0,0098306
Ms4a6d	2,5500	6,68E-08	1,94E-05
A130050O07Rik	2,5220	9,95E-05	0,00737309
Igf2bp3	2,5143	1,99E-05	0,00221501
Nefm	2,5105	0,0002348	0,01288916
Arhgap29	2,5040	4,38E-05	0,00402072
Plb1	2,4968	0,0001704	0,01049337
Dixdc1	2,4908	4,03E-06	0,00060273
Gzmf	2,4591	4,13E-05	0,00381415
C430049B03Rik	2,4529	0,0002664	0,01408653
Gm37354	2,4472	5,34E-05	0,004655
Gpr176	2,4469	0,0003325	0,01631997
Clec5a	2,4407	3,23E-06	0,00050228
Gdf15	2,4400	0,0001264	0,00862044
Fkbp9	2,4342	0,0002297	0,01273602
Tdrd9	2,4085	0,000447	0,01985914
Scamp1	2,4035	3,81E-07	9,18E-05
Snx24	2,3967	0,0001927	0,01129558
Lhfpl2	2,3955	3,87E-05	0,00361305
Lipt2	2,3907	0,0003086	0,01554739
Ms4a8a	2,3887	1,30E-05	0,00163271
Ms4a14	2,3886	0,0002247	0,01259301
Clec4d	2,3759	6,36E-05	0,00530259
Sh3pxd2b	2,3683	2,84E-09	1,33E-06
Fign	2,3592	0,0004958	0,0214071
Tlr5	2,3591	9,72E-05	0,007309
6330403L08Rik	2,3428	0,0005811	0,02408362
Rai14	2,3323	1,18E-05	0,0015042
Tgfbi	2,3265	1,85E-06	0,00032899
Layn	2,3255	0,00058	0,02408362
Fbn1	2,3194	0,0006992	0,0279987
Gja1	2,3117	0,0007215	0,02852328
Cdk5r1	2,2873	0,0004971	0,0214071
Ankrd66	2,2830	0,0008502	0,03143346
Ang	2,2789	0,0003541	0,01706063
3110043O21Rik	2,2555	0,0004387	0,01954713
Piwil4	2,2524	0,001034	0,0360667
Clec4n	2,2503	6,81E-05	0,00556337
Spata9	2,2340	0,0006559	0,02647101
Gdf3	2,2325	0,0001271	0,0086309
Tbc1d16	2,2322	0,000714	0,02846223
2210408F21Rik	2,2312	0,0010605	0,03682343
Zc3h12c	2,2306	0,0004812	0,02113362
Mgl2	2,2283	0,0001155	0,00809156
Gm14049	2,2266	0,00113	0,03787306
E330034L11Rik	2,2230	1,54E-05	0,00185703
Igsf10	2,2176	0,0011998	0,03935459
Ptgfrn	2,2157	0,0009944	0,03516093
Csf2rb2	2,2095	8,25E-07	0,00017422
Spic	2,2046	1,02E-09	5,84E-07
Adam15	2,2040	0,0001433	0,00928676
Il1rn	2,1985	1,90E-05	0,002202
Arhgef17	2,1945	0,0013026	0,04149168
Pdgfra	2,1883	0,0010721	0,03714325
Hmga2	2,1876	0,0002134	0,01229192
Prune2	2,1869	3,58E-05	0,00340643
Ermap	2,1858	0,001091	0,03745399
Ophn1	2,1853	0,0002558	0,0136908
Cxcl3	2,1843	0,0002456	0,0133318
Peg10	2,1803	0,0001736	0,01053794
Rab3il1	2,1801	0,00029	0,01480228
Lbp	2,1747	0,0003376	0,01641661
Aoc1	2,1733	0,0015028	0,04569851
Ms4a6c	2,1716	2,23E-06	0,00038122

Gene	FC	pvalue	padj
Rhag	2,1697	0,0010125	0,035558937
Ly6c1	2,1622	0,0001045	0,007671589
Gm37747	2,1622	3,18E-05	0,003068783
Met	2,1617	0,0003342	0,016319967
Gm26947	2,1589	0,0001074	0,007763858
Pigz	2,1489	0,0016842	0,049647539
Marcks	2,1385	1,43E-08	5,03E-06
Tnfsf4	2,1298	0,0011855	0,039053844
C3ar1	2,1244	0,0001259	0,008620436
Kdr	2,1241	0,000437	0,019529969
Gm10484	2,1219	0,0001934	0,011295578
Slfn4	2,1210	0,0002254	0,012593006
Spint1	2,1105	0,0007164	0,028462229
Gm36992	2,1020	0,0008405	0,031301244
AA467197	2,1011	5,31E-06	0,000772124
Gm16267	2,0957	0,001395	0,043184773
Trim2	2,0903	0,0007152	0,028462229
Siglec1	2,0851	6,14E-07	0,000139168
Slfn1	2,0693	4,42E-05	0,004022778
Plet1	2,0506	0,0007344	0,028883565
Mest	2,0494	0,0011026	0,037531195
Gm10177	2,0381	0,0005553	0,023382863
9430020K01Rik	2,0368	0,0005686	0,023755512
Ednrb	2,0281	0,0009444	0,033939116
Stab1	2,0165	0,0002547	0,013690799
Fstl1	2,0100	6,39E-11	4,69E-08
Papss2	2,0047	0,0002288	0,012734675
Rab3a	-2,0232	0,0001434	0,009286762
2810001G20Rik	-2,0268	0,0001569	0,009830602
Itga3	-2,0319	0,0008788	0,032030428
Gm527	-2,0640	0,0015135	0,045932255
Sox6	-2,0817	0,0013347	0,042090539
Bcl11b	-2,0855	0,0002349	0,012889159
Cxcr5	-2,0860	0,0012483	0,040472805
Gm42870	-2,0934	0,001275	0,041036878
Ltb	-2,1283	0,0005969	0,024640322
Alad	-2,1303	3,13E-05	0,003033872
Sult1a1	-2,1343	0,0015658	0,047250645
Trdv4	-2,1419	6,82E-05	0,005563374
Tg	-2,1474	0,0016443	0,048844902
Itih4	-2,1478	0,001664	0,049239319
Axin2	-2,1515	0,0009063	0,032875609
Dnajc25	-2,1688	4,30E-09	1,84E-06
Tle2	-2,1694	0,0011414	0,038007383
Alas2	-2,1720	0,0002674	0,014086527
Il20ra	-2,1727	0,001335	0,042090539
Cdon	-2,1789	0,0003706	0,017472599
Gm6934	-2,2068	0,0006032	0,024796689
Rln3	-2,2119	0,0010928	0,037453994
Gm44175	-2,2144	0,000785	0,030105421
Plekhf1	-2,2157	6,91E-05	0,005581747
Ciart	-2,2264	0,000379	0,017813707
Fabp1	-2,2316	0,0010574	0,036797638
Ngp	-2,2392	0,000872	0,031882046
Gm44645	-2,2440	0,0009652	0,034444964
4930589O11Rik	-2,2542	0,0008502	0,031433459
Gm16565	-2,2736	9,17E-05	0,006996908
Ahsg	-2,2846	0,0007731	0,029722333
Ambp	-2,2997	0,0007491	0,029238599
Hist4h4	-2,3001	2,79E-05	0,002806303
Pck1	-2,3002	0,0004282	0,019191941
Apob	-2,3033	0,0002452	0,013331799
Hspa2	-2,3133	2,36E-08	7,90E-06
Bend5	-2,3310	0,0006352	0,025703851
Cbx6	-2,3346	2,92E-07	7,90E-05
Zfp239	-2,3363	0,0001794	0,010719557
Cd7	-2,3431	2,75E-06	0,000450723
Map7	-2,3444	1,95E-05	0,002211937
AI661453	-2,3459	0,0001362	0,009048411
Mmp9	-2,3494	0,0003181	0,0157686

Gene	FC	pvalue	padj
Tldc1	-2,3572	0,000148199	0,009441866
Cd22	-2,3663	1,49E-06	0,000276384
5830454E08Rik	-2,3743	0,000198053	0,011478909
Tcrg-C1	-2,3942	0,000270608	0,014094476
Gm16602	-2,4173	0,000395274	0,018410697
Gpr55	-2,4440	2,12E-05	0,002284688
Ighg2c	-2,4554	0,0003142	0,015625865
Rgs12	-2,4675	1,73E-05	0,002032801
Msrb2	-2,4747	1,63E-05	0,00193167
2610524H06Rik	-2,4938	2,67E-06	0,000442717
Sult2b1	-2,4997	0,000118046	0,008197816
Nlgn2	-2,5014	0,000160315	0,010006395
Ift27	-2,5026	3,11E-05	0,003032399
Gm26640	-2,5401	0,000139254	0,009166429
Prss12	-2,5451	8,21E-06	0,001091661
Gstt2	-2,5481	1,36E-06	0,00026185
Rflnb	-2,5669	1,19E-08	4,38E-06
Klk8	-2,5755	4,64E-05	0,004157351
Slc25a2	-2,5897	1,86E-06	0,000328991
Gm26614	-2,6162	0,000123217	0,00851856
1700029I15Rik	-2,6286	6,92E-05	0,005581747
Gm26802	-2,6330	0,000102382	0,007552254
Trgj4	-2,6560	6,97E-05	0,005599001
Cd8a	-2,6781	7,43E-06	0,001014098
Cxcr3	-2,7134	1,09E-10	7,29E-08
Gm20743	-2,7304	4,33E-07	0,000102744
Aqp9	-2,7362	3,90E-06	0,000589118
Sema4f	-2,7553	3,32E-05	0,00317561
Fga	-2,7702	3,78E-05	0,003571802
Gpr182	-2,7825	2,00E-05	0,002215011
Art2b	-2,8197	2,89E-06	0,000463683
A1bg	-2,8614	2,97E-05	0,002912888
Chad	-2,8630	2,01E-05	0,002215011
Slc27a6	-2,8838	1,26E-06	0,000246716
Bcl2l15	-2,9125	5,71E-06	0,000807167
Jchain	-2,9274	3,31E-06	0,000510392
Pzp	-2,9445	1,52E-05	0,001843142
Apol11b	-2,9532	1,45E-05	0,001805009
Serpina3k	-3,0126	1,01E-05	0,001303347
Nat8f1	-3,1210	2,31E-06	0,000386636
Tcrg-C4	-3,1320	5,05E-11	3,90E-08
Ccdc136	-3,1894	3,72E-07	9,17E-05
Paqr9	-3,2128	1,47E-06	0,000276384
Bmp7	-3,3393	1,28E-09	6,60E-07
Trgv2	-3,3901	3,59E-07	9,17E-05
Dtx1	-3,4042	6,43E-23	1,65E-19
Scd1	-3,4317	1,02E-09	5,84E-07
Gm19590	-3,4376	3,68E-07	9,17E-05
Nfe2l3	-3,4388	2,25E-08	7,71E-06
Hlf	-3,5283	6,00E-08	1,78E-05
Igha	-3,8681	5,00E-12	4,81E-09
Cd79a	-4,1643	6,47E-12	5,54E-09
Igkc	-4,3942	2,02E-15	2,83E-12
Podnl1	-4,6955	1,06E-15	1,63E-12
Alb	-4,8107	2,08E-14	2,67E-11

Table A.2. Comparison II. All differentially expressed genes from the comparison II: uterine CD49a^{+} (ILC1, trNK) subsets vs liver (ILC1) subset. FC: fold change, padj: adjusted p-value.

Gene	FC	pval	padj
Gzme	8,1801	8,87E-17	2,62E-13
Pdpn	7,6743	2,26E-12	1,25E-09
Gzmd	7,5979	2,06E-13	1,60E-10
Cd109	7,5240	5,33E-11	2,17E-08
Gzmg	7,2735	1,18E-10	4,48E-08
Plb1	7,1975	1,16E-09	3,05E-07
Gzmf	7,1576	1,07E-14	1,07E-11
Flrt3	6,9055	3,63E-16	6,89E-13
A2m	6,8499	1,22E-09	3,13E-07
Spsb1	6,7024	1,40E-09	3,46E-07
Arfgef3	6,3856	1,76E-09	4,23E-07
Speg	6,2710	1,06E-07	1,35E-05
Tdrd9	6,1883	2,48E-07	2,72E-05
Dixdc1	6,1206	4,98E-10	1,52E-07
Retnla	6,0417	3,93E-15	5,59E-12
Rhov	6,0136	6,17E-07	5,82E-05
Ahnak2	5,9917	5,64E-10	1,63E-07
Clip3	5,9262	1,24E-08	2,13E-06
Afap1l1	5,8658	3,25E-07	3,34E-05
Sox11	5,8531	1,32E-06	0,000105996
Lin28b	5,8489	1,07E-08	1,89E-06
Ddx3y	5,7947	1,38E-06	0,000110679
Inhba	5,7800	1,44E-09	3,51E-07
Olfml2b	5,7780	3,77E-06	0,000250208
Ccl7	5,6874	1,42E-16	3,47E-13
Fkbp9	5,5238	1,70E-07	2,01E-05
Igf2bp1	5,4808	1,76E-11	7,91E-09
Erv3	5,4461	1,79E-06	0,000138026
Ednrb	5,4247	1,10E-17	6,26E-14
Hif3a	5,4196	5,19E-06	0,000327996
Tal1	5,3709	1,06E-06	8,95E-05
Pf4	5,3565	7,70E-13	5,05E-10
Hemgn	5,3503	2,46E-08	3,78E-06
Scin	5,3343	5,24E-08	7,51E-06
Ankrd66	5,3339	1,73E-06	0,000134243
Piwil4	5,3206	1,38E-05	0,000712524
Rnase2a	5,2811	3,52E-05	0,001505755
A630012P03Rik	5,2644	3,64E-05	0,001547128
Gm44205	5,2024	1,45E-05	0,000739511
Igsf10	5,2023	6,13E-06	0,000372362
Dpysl5	5,1759	3,42E-07	3,46E-05
Khdc1c	5,1657	4,01E-06	0,000264284
Cped1	5,0987	4,38E-05	0,001819225
Serpinh1	5,0885	2,38E-05	0,001110741
Flrt2	5,0105	0,000165949	0,004831718
Ch25h	4,9939	1,92E-07	2,20E-05
Spp1	4,9801	2,77E-09	5,99E-07
Col1a1	4,9722	6,52E-05	0,002434655
Lipg	4,9602	2,78E-05	0,00126333
Prap1	4,9592	6,11E-05	0,002347765
Syngr1	4,9303	9,40E-05	0,003246248
Thsd7a	4,9281	9,56E-05	0,003295617
Prl8a2	4,8839	4,50E-05	0,001851401
Gm14011	4,8737	0,000153859	0,004605843
Gpnmb	4,8556	2,67E-12	1,43E-09
Rhag	4,8480	2,34E-06	0,000173094
Klk1b11	4,8378	0,000106764	0,003573239
Eya4	4,8350	0,000265891	0,006982292
Tgfb2	4,8064	0,000145529	0,004439936
A230028O05Rik	4,7733	8,64E-05	0,003046591
Fut10	4,7550	0,000281686	0,007329426
Fcrl6	4,6420	1,23E-09	3,13E-07
Dsc2	4,6338	1,16E-05	0,000617051
Hebp1	4,6231	4,79E-07	4,62E-05
Kif26b	4,6171	0,000301224	0,007708533
Prokr1	4,6096	0,000214146	0,005905097
Ccl8	4,5794	6,13E-05	0,002352183
Tmprss4	4,5411	0,000505623	0,01126694
Ccl12	4,5409	1,77E-08	2,85E-06
Asns	4,5357	1,51E-05	0,000765003

Gene	FC	pval	padj
Dusp9	4,5214	0,000107915	0,003597646
Adamts1	4,4948	1,05E-06	8,86E-05
Rab15	4,4928	0,000891749	0,017045089
Tmsb15a	4,4884	1,65E-05	0,000823539
Rps6ka6	4,4767	0,000249207	0,006657134
Gpr176	4,4679	0,000660179	0,013592993
Eif2s3y	4,4119	0,000726271	0,01463603
Adam33	4,4004	1,03E-06	8,76E-05
Akr1c18	4,3790	0,001216559	0,021353343
Pard3	4,3687	0,000610698	0,012900986
Tnfaip8l3	4,3567	0,000450165	0,010272553
Ccdc122	4,3342	0,000134763	0,00422067
Mak	4,3143	0,000949112	0,017900982
Basp1	4,2978	7,02E-20	1,20E-15
Fcrlb	4,2900	0,000300962	0,007708533
Afp	4,2740	0,000585414	0,012514471
Dsp	4,2700	0,000186099	0,005303052
Ptgfrn	4,2562	4,43E-06	0,000285399
Coprs	4,2505	0,000143316	0,004391843
Emp1	4,2271	2,62E-10	8,75E-08
Gm20056	4,2264	0,001189695	0,020956565
Klhl30	4,2214	5,61E-07	5,35E-05
Fbln1	4,2086	0,000970463	0,018102318
Slco2b1	4,1908	9,94E-09	1,79E-06
Lhfpl2	4,1643	5,33E-06	0,000333588
Prtg	4,1480	0,000209425	0,005793651
Ifnlr1	4,1060	0,000324189	0,00818346
Gm15246	4,0918	0,001064285	0,019346413
6330403L08Rik	4,0769	0,000138864	0,004294213
Bag2	4,0765	0,000515296	0,011408019
Cbr2	4,0526	1,96E-05	0,000944633
Hsd3b6	4,0244	0,000406112	0,009495785
Mtcl1	4,0146	0,002462816	0,035564973
Car6	4,0074	0,00117723	0,02080138
Gm43717	4,0055	0,000941275	0,01777281
Tsacc	3,9922	0,002677833	0,037619699
Bace2	3,9848	0,002653818	0,037486783
Peg3	3,9755	0,001888879	0,029552045
Rbfox2	3,9740	0,00226132	0,033593093
Slc39a2	3,9567	0,00185338	0,029132315
Tnfsf4	3,9508	0,000585802	0,012514471
Stmn2	3,9444	0,002094734	0,031682721
Vegfa	3,9425	3,58E-15	5,56E-12
B4galnt2	3,9383	0,0017889	0,028383054
Nt5dc2	3,9337	0,001067984	0,019354931
Gm42632	3,9264	0,00267538	0,037618927
4930533B01Rik	3,9195	0,00032828	0,008192116
Dab2	3,9094	1,27E-07	1,59E-05
Anxa9	3,8966	0,000344515	0,008473376
Srd5a1	3,8780	0,000976041	0,018148192
Kdr	3,8718	4,01E-10	1,27E-07
Mgat3	3,8643	0,000654008	0,013522804
Gm24273	3,8546	0,002675574	0,037618927
Gm13899	3,8467	0,001648532	0,026927082
Ctsg	3,8293	0,000718249	0,01450863
C3ar1	3,8292	6,94E-15	8,27E-12
Des	3,8262	0,001544604	0,025597652
Nefm	3,8254	0,002015367	0,030963366
Tm4sf19	3,8242	0,003484012	0,045111803
Epb41l1	3,7963	7,42E-06	0,000437019
Hmcn2	3,7623	0,003262733	0,043398048
Ctnnd2	3,7566	1,91E-05	0,00093233
Cacna1b	3,7431	0,000542346	0,011868342
Fcrls	3,7382	6,46E-05	0,002422468
Lyve1	3,7359	2,21E-06	0,000166065
Vipr2	3,7194	9,30E-05	0,003230084
Apol9b	3,7043	0,002518003	0,036043928
Uaca	3,6980	0,001852211	0,029132315
Gm13650	3,6935	0,000327641	0,008188156
Ebf3	3,6450	0,001815784	0,028751041

Gene	FC	pval	padj
Arhgap29	3,6339	4,91E-07	4,71E-05
Plxna1	3,6227	9,12E-10	2,43E-07
Peg10	3,6211	4,11E-06	0,000268727
Htra1	3,6169	0,000898382	0,017106673
Pnp2	3,6159	0,000612759	0,012912577
Zcchc3	3,6113	0,000800542	0,01572434
Clec4d	3,6011	3,63E-05	0,001543539
Fat1	3,5999	0,000558837	0,012095861
Nrk	3,5932	0,000351331	0,008579202
Atp6v0d2	3,5719	0,00296806	0,040561902
Gpr87	3,5617	0,003259058	0,043398048
Ly6c1	3,5410	8,24E-07	7,44E-05
Gm5345	3,5270	0,003082328	0,041623618
Gm15635	3,5124	0,001068213	0,019354931
Arg2	3,4974	0,000418808	0,009673379
Lrp12	3,4812	0,000118877	0,003821401
Cd300lf	3,4672	9,20E-17	2,62E-13
Piwil2	3,4541	0,002567274	0,036537402
Sapcd2	3,4257	2,67E-05	0,001230291
Gm43844	3,4206	0,000112347	0,003699937
Stab1	3,4128	8,35E-07	7,44E-05
Sh2d1b2	3,4063	5,63E-05	0,002202861
Spry4	3,3875	0,000764618	0,015193562
Tubb2b	3,3598	0,000410737	0,009549012
Dnmt3aos	3,3583	0,002172586	0,032673016
Tdo2	3,3569	0,000355797	0,008615606
Ccl2	3,3491	4,11E-09	8,45E-07
Ankrd33b	3,3353	0,000343392	0,00845794
Ninj1	3,3279	6,22E-08	8,71E-06
Gm38345	3,3127	0,00010781	0,003597646
Igf2bp3	3,3125	0,000194482	0,005459887
Ccr1	3,3052	8,16E-06	0,000460975
Nhsl1	3,3045	0,000316049	0,008027734
Gas6	3,2981	4,04E-06	0,000264986
Olr1	3,2589	9,61E-06	0,000526475
Tmem171	3,2557	2,94E-05	0,001315173
Clec4n	3,2474	6,38E-06	0,000385721
Gm38001	3,2456	0,003929212	0,049205955
Cdk20	3,2388	0,00336071	0,0441227
Col1a2	3,2387	0,003808069	0,048005856
Eomes	3,2141	4,98E-05	0,002014764
8030453O22Rik	3,2018	0,002512364	0,036042993
Fnip2	3,1929	4,48E-09	9,00E-07
Prune2	3,1889	2,34E-07	2,60E-05
Gm26797	3,1836	0,000378302	0,008989444
AA467197	3,1779	1,46E-05	0,000739511
Ms4a7	3,1551	2,01E-05	0,000964595
Npl	3,1511	1,12E-06	9,32E-05
Dcn	3,1452	0,001000124	0,018429417
Mreg	3,1426	0,002090456	0,031661041
Gm26781	3,1309	0,001364451	0,023207582
Slc7a2	3,1267	6,60E-06	0,000394984
Kcnn4	3,1184	5,81E-05	0,002238078
Il1f9	3,1092	2,80E-05	0,001268121
Gm15531	3,1087	0,003233893	0,04315819
Lpl	3,1079	2,03E-12	1,20E-09
9130204K15Rik	3,1069	0,002046748	0,031164979
Gdf15	3,1018	9,60E-05	0,003295617
Reps2	3,0954	8,26E-05	0,002954115
Slfn4	3,0913	5,68E-05	0,002207158
Gzmc	3,0871	0,000520822	0,011500529
Snx24	3,0792	0,0020956	0,031682721
Mt2	3,0684	0,000729561	0,014684996
Gdf3	3,0642	8,25E-06	0,000463134
Hmox1	3,0598	3,75E-06	0,000250129
Cstb	3,0597	8,90E-16	1,52E-12
Rai14	3,0065	9,70E-05	0,003318033
Fsd1l	2,9991	0,00055755	0,012092523
Tmem119	2,9652	0,002151652	0,032443944
Mgl2	2,9495	0,000131864	0,004152753

Gene	FC	pval	padj
Slc7a5	2,9417	1,84E-12	1,12E-09
Lgmn	2,9407	1,63E-07	1,96E-05
Gab1	2,9303	0,003560911	0,045700147
Thbs1	2,9286	3,50E-09	7,37E-07
Epas1	2,9255	0,000145913	0,004439936
Mboat1	2,9223	0,002608402	0,037009821
Plau	2,8987	4,43E-07	4,30E-05
Ecm1	2,8925	0,000288356	0,007457485
Ms4a14	2,8864	0,001098366	0,019797271
C5ar1	2,8746	1,90E-08	3,01E-06
Gm20712	2,8572	0,000162972	0,004787898
Tjp1	2,8565	0,00014835	0,004481755
Rab3il1	2,8488	2,71E-05	0,001241566
Dnph1	2,8449	0,001393558	0,023597851
Dhrs9	2,8378	0,000704559	0,014316808
Anpep	2,8375	1,94E-05	0,000942206
Anxa4	2,8173	1,85E-11	7,91E-09
Scamp1	2,8171	3,00E-05	0,001334308
Mmp12	2,8118	1,98E-08	3,10E-06
Ptafr	2,8115	2,05E-07	2,33E-05
Cd63	2,7888	0,000751959	0,01497689
Psrc1	2,7875	3,72E-05	0,001571131
Kif5c	2,7863	0,003303926	0,043750746
Sh3pxd2b	2,7674	4,97E-05	0,00201355
Snx7	2,7670	7,65E-05	0,002790577
Rhou	2,7467	0,000471292	0,01059879
Ccl17	2,7409	0,003995018	0,049766317
Mmp14	2,7360	9,63E-06	0,000526475
Cd93	2,7337	4,17E-07	4,07E-05
Gpt2	2,7272	0,003763988	0,047661354
Gm37534	2,7264	0,003424077	0,044512995
Rnase4	2,7014	0,000661032	0,013594161
Fabp5	2,7000	1,72E-05	0,000854705
Fam20c	2,6999	9,28E-07	8,10E-05
Mfsd12	2,6913	0,000254261	0,006743319
F10	2,6788	4,36E-09	8,85E-07
Klra4	2,6769	0,000129035	0,004101494
Gm16353	2,6512	0,000158796	0,00470824
Tln2	2,6500	7,76E-06	0,000449221
A530064D06Rik	2,6481	0,000114494	0,003750415
Bst1	2,6463	8,07E-06	0,000460284
Fth1	2,6307	8,25E-11	3,20E-08
Fcgr1	2,6266	7,43E-07	6,77E-05
Myo10	2,6250	0,002425533	0,035235246
Dhrs3	2,6170	5,83E-06	0,000360468
Paox	2,6138	0,001120475	0,02004758
1700084C06Rik	2,6098	0,003821795	0,048072381
Ms4a6d	2,6005	0,000158337	0,00470824
Spon1	2,5881	0,000285926	0,007417133
Myo1b	2,5833	0,000859652	0,016580121
Atp6v0a1	2,5827	1,27E-06	0,000102692
Slc16a13	2,5748	0,002044277	0,031155145
Plet1	2,5721	0,003705374	0,047093837
Hpgds	2,5516	6,77E-09	1,28E-06
Rgs16	2,5488	0,001452605	0,024452184
Klrg1	2,5448	0,000791162	0,015593924
Apbb2	2,5443	0,001721002	0,027721488
Coq7	2,5305	0,001142188	0,020329515
Gm37354	2,5295	0,001211657	0,02129945
Clcn5	2,5268	1,35E-10	4,80E-08
Mthfr	2,5242	6,19E-05	0,002356516
9430076C15Rik	2,5143	3,30E-05	0,001427451
Srxn1	2,5129	9,64E-05	0,003305001
Gpr157	2,5114	8,99E-05	0,003136894
Ophn1	2,5088	0,003799954	0,047938967
Naglu	2,5038	0,000191084	0,005391088
Vcam1	2,4956	6,85E-08	9,43E-06
Mfsd11	2,4938	9,22E-06	0,000512685
C5ar2	2,4882	1,84E-05	0,000902001
Ctsb	2,4547	5,44E-15	7,14E-12

Gene	FC	pval	padj
Ifit3b	2,4435	9,80E-05	0,0033348
Crtap	2,4239	0,002079014	0,031526284
Lgals3	2,4138	4,59E-06	0,000294815
Tlr5	2,4137	0,001628701	0,026782567
Pdgfa	2,4106	0,002640341	0,037376609
Grn	2,4002	3,77E-07	3,75E-05
Spic	2,3960	1,35E-08	2,30E-06
Igfbp4	2,3955	1,65E-07	1,97E-05
Slc7a11	2,3952	7,91E-05	0,002868054
Ctla2a	2,3938	3,86E-06	0,000255472
Fam129b	2,3929	0,000102753	0,003445767
Arg1	2,3873	0,000749721	0,014965823
Mt1	2,3826	0,000535106	0,011755114
Mrc1	2,3603	0,001154949	0,020535237
Sh2d1a	2,3594	0,002768909	0,038518746
Olfml3	2,3590	0,00159214	0,026237542
Rgl1	2,3503	7,63E-10	2,14E-07
Tex264	2,3421	0,000271573	0,007086748
Mertk	2,3240	3,43E-05	0,001471545
Slc7a8	2,3131	7,50E-06	0,000439975
Cndp2	2,3121	1,84E-13	1,49E-10
Dmxl2	2,2896	0,000355586	0,008615606
Ms4a8a	2,2845	0,002732494	0,038178105
Trim30c	2,2842	0,00173957	0,027959253
Gm37795	2,2827	0,002734731	0,038178105
Rsad2	2,2799	9,31E-05	0,003230084
Klra8	2,2743	0,003222502	0,043039818
Osbpl1a	2,2634	0,000588825	0,012541732
Chst14	2,2620	0,002640822	0,037376609
Litaf	2,2608	2,80E-11	1,16E-08
Rab7b	2,2601	0,000130329	0,004127244
Eps8	2,2497	2,70E-05	0,001241566
Fstl1	2,2431	6,87E-05	0,002554734
Cdkn1a	2,2402	2,84E-05	0,001282941
Gm43775	2,2313	0,001343146	0,022903262
Gas2l3	2,2228	0,000217018	0,005947131
Cpd	2,2165	2,48E-07	2,72E-05
Stra6l	2,2110	0,002037254	0,031123888
Osm	2,2077	2,17E-05	0,001032422
Clec4a2	2,2053	0,001677873	0,027344256
Lmna	2,2048	0,00169611	0,027519876
Tlr2	2,2028	0,002695555	0,037806432
Plxnc1	2,2011	6,77E-06	0,000404012
Gna12	2,1956	1,38E-09	3,45E-07
Prdx1	2,1788	4,58E-14	3,91E-11
4930430E12Rik	2,1430	3,10E-05	0,001366951
Stard8	2,1407	1,32E-05	0,000690915
Ctsl	2,1407	3,18E-07	3,29E-05
Ly6c2	2,1327	0,00176111	0,028172809
Nckap1	2,1315	0,003046298	0,041333279
Slfn1	2,1290	0,003479548	0,045096743
Ctsz	2,0947	6,22E-05	0,002359301
Gdpd1	2,0923	0,002448194	0,035438785
Scimp	2,0824	0,000149675	0,00450582
Slc37a2	2,0750	0,000651077	0,01348693
Tax1bp3	2,0593	0,00326284	0,043398048
Gusb	2,0553	1,94E-06	0,000148795
Msr1	2,0540	0,000100734	0,003391379
Arl11	2,0532	0,000635077	0,013268214
Atp6v1c1	2,0494	1,83E-11	7,91E-09
Fcgr2b	2,0466	0,000307901	0,007855848
Lxn	2,0425	3,36E-07	3,42E-05
Usp18	2,0421	5,52E-05	0,002165191
Akip1	2,0262	0,001784356	0,028383054
Ly6a	2,0249	0,003072278	0,041586608
Tspan3	2,0235	0,000834247	0,016227448
Ms4a4c	2,0193	0,001952651	0,030244828
Wfdc17	2,0096	8,16E-05	0,002930993
Lap3	2,0079	0,000365329	0,008782829
Ctss	2,0076	2,87E-06	0,000206876

Gene	FC	pval	padj
Xcr1	-2,0039	0,003499868	0,045257005
Tspyl3	-2,0166	0,000226636	0,006159945
Plppr3	-2,0238	1,18E-06	9,69E-05
Gm44130	-2,0267	0,002449925	0,035438785
Jakmip1	-2,0530	0,00029078	0,007503421
Gramd1a	-2,0535	8,25E-06	0,000463134
Ubash3a	-2,0566	0,003076225	0,041595745
Gpr18	-2,0639	0,000589283	0,012541732
Rab6b	-2,0646	0,000595559	0,012643766
Zfp707	-2,0726	0,003876796	0,048672742
Ptpn4	-2,0782	1,04E-05	0,000561335
Phf1	-2,0806	8,48E-07	7,50E-05
Leng9	-2,0808	0,001183961	0,020894078
Klrk1	-2,0831	9,94E-06	0,000539461
Nxpe3	-2,0842	1,15E-05	0,000613725
Cd3d	-2,0877	0,000687397	0,014034895
Klrc3	-2,0878	0,001323712	0,022707972
Gm36940	-2,0891	4,48E-05	0,0018512
Gm19557	-2,0968	9,75E-05	0,00332964
1700096K18Rik	-2,0981	0,003042792	0,041318544
Dusp10	-2,1039	0,000146948	0,004463078
Atp2a3	-2,1062	0,000142584	0,004385157
Stat4	-2,1098	1,05E-05	0,000565887
Farp1	-2,1217	0,000806993	0,015832835
Itgb7	-2,1263	6,11E-07	5,79E-05
Clcf1	-2,1362	0,00068259	0,013970178
Klrb1f	-2,1379	2,07E-06	0,000157622
Lrrc75a	-2,1391	0,000125716	0,004003445
E430024P14Rik	-2,1494	0,000710636	0,014388911
Gm37842	-2,1638	0,003246985	0,043299046
Pde7a	-2,2077	7,40E-12	3,51E-09
Prkce	-2,2120	8,33E-05	0,002964203
Klra5	-2,2122	0,003551287	0,045610923
Snord104	-2,2182	0,00055125	0,012016971
Tox	-2,2205	0,000324184	0,00818346
Cyp2e1	-2,2371	0,000590867	0,012559794
Rasgrp2	-2,2473	1,17E-06	9,64E-05
Rab3a	-2,2546	0,003893424	0,048829426
Ets1	-2,2579	0,000200822	0,005596243
D130040H23Rik	-2,2588	0,000405675	0,009495785
Gimap8	-2,2610	0,000872846	0,016740006
Peg13	-2,2630	3,14E-05	0,00136878
Rnf122	-2,2969	0,001285767	0,022242433
Cdyl2	-2,3056	4,55E-05	0,001865036
Klrb1	-2,3121	0,002196381	0,032862192
Grasp	-2,3180	0,001321506	0,022707972
Gm26189	-2,3196	0,000863513	0,016605805
Cacna1e	-2,3396	3,14E-06	0,000220717
Gem	-2,3408	0,000109368	0,003631397
Gm38243	-2,3446	0,000861049	0,016588309
Tlr12	-2,3569	0,000465702	0,010514634
9430087J23Rik	-2,3578	0,000587682	0,012538928
Tnfrsf18	-2,3586	0,000217064	0,005947131
Cd69	-2,3599	2,76E-07	2,95E-05
Cbx7	-2,3609	0,000990417	0,018320877
Grap2	-2,3651	1,17E-05	0,000617656
Gm7967	-2,3682	0,000329398	0,008208012
Ugt3a1	-2,3789	0,002186877	0,03277244
1700023H06Rik	-2,3804	0,002200733	0,032893442
Gimap4	-2,4032	8,94E-05	0,003126262
Gm37352	-2,4058	8,07E-05	0,002912495
Mgst2	-2,4097	0,000196538	0,005490515
Gm37090	-2,4139	0,002735475	0,038178105
Chrne	-2,4169	0,002704134	0,037895624
Gm29438	-2,4171	0,002196717	0,032862192
Rfx2	-2,4247	0,002022349	0,031042698
Fosb	-2,4304	0,000168662	0,004896074
Pitpnm2	-2,4629	0,000175233	0,005052446
Ppp1r15a	-2,4695	3,59E-06	0,000243488
Ipcef1	-2,4715	6,05E-12	2,95E-09

Gene	FC	pval	padj
Afmid	-2,4788	0,003325062	0,043928391
F2rl1	-2,4936	0,001592483	0,026237542
Ifng	-2,4959	0,001069289	0,019354931
Katnb1	-2,5005	5,20E-05	0,002087221
Lrrk2	-2,5024	0,001068672	0,019354931
Myo6	-2,5060	1,95E-05	0,000944633
Ccl4	-2,5126	4,94E-06	0,000314819
Dennd5b	-2,5292	0,000207992	0,005763335
Slc25a53	-2,5342	7,42E-07	6,77E-05
Tspan15	-2,5398	0,001924275	0,029976273
L1cam	-2,5467	1,21E-08	2,10E-06
Ccl5	-2,5521	9,96E-06	0,000539461
Osgin1	-2,5527	0,001708271	0,027612194
Gdf11	-2,5647	5,98E-08	8,44E-06
Plekhf1	-2,5687	0,001753172	0,028124901
Dgka	-2,5741	2,17E-07	2,45E-05
Gm26724	-2,5795	0,000210107	0,005803113
E430021H15Rik	-2,5798	0,001411703	0,023857786
Gm37023	-2,5885	0,003541923	0,045563301
Baiap3	-2,5886	0,000179931	0,005153092
Gm36724	-2,5918	8,43E-05	0,002991291
Adrb2	-2,5930	8,29E-07	7,44E-05
Cnrip1	-2,6021	1,44E-05	0,000736651
Klrb1a	-2,6172	1,09E-05	0,000582479
Izumo4	-2,6212	0,000544816	0,011907118
Akap12	-2,6397	0,000459973	0,010420842
Rora	-2,6513	5,65E-06	0,000350673
Zfp831	-2,6533	6,15E-05	0,002353271
Aff3	-2,6805	0,001308815	0,022537169
Serpina3f	-2,6833	9,48E-06	0,000521859
Traf3ip2	-2,6834	1,12E-07	1,43E-05
Gm38126	-2,6892	0,000961075	0,018053138
B130055M24Rik	-2,7053	0,000369789	0,008877539
Serpini1	-2,7276	1,75E-05	0,000865434
Cers4	-2,7321	1,54E-07	1,86E-05
Trbc2	-2,7348	4,49E-05	0,0018512
Hdc	-2,7402	0,000378744	0,008989444
Acpp	-2,7604	1,21E-05	0,000635586
Cd27	-2,7633	8,10E-05	0,002918646
Bcl11b	-2,7690	0,000508177	0,011279685
AI661453	-2,7777	0,002415004	0,035172108
Mir6924	-2,7844	0,003399309	0,044387004
Gbp10	-2,7877	0,003363431	0,0441227
Gimap3	-2,7899	1,36E-05	0,000706795
Tob1	-2,7967	9,92E-08	1,28E-05
Pdzd2	-2,7996	0,000382269	0,009047498
Adgrg5	-2,8049	2,19E-05	0,001040406
Gm37469	-2,8058	0,001019569	0,01869282
4930532G15Rik	-2,8069	0,000175898	0,005063079
Gm37215	-2,8237	0,002034038	0,031123888
Astl	-2,8285	0,000526472	0,011595298
A630072L19Rik	-2,8550	0,003117214	0,041928861
Llgl2	-2,8635	0,000101649	0,00341543
Slc10a1	-2,8667	2,22E-05	0,001048739
Gm26616	-2,8854	0,003108623	0,041879306
Gm16845	-2,8869	0,000228577	0,006182538
Gm4956	-2,9446	1,91E-05	0,00093233
Ltb	-2,9555	0,003149916	0,042335371
Cd226	-2,9658	1,11E-06	9,31E-05
Gm16575	-2,9687	1,80E-05	0,000886777
Gm11769	-2,9739	0,002659475	0,037486783
Gjb2	-3,0002	5,52E-05	0,002165191
Rasgrf1	-3,0006	0,000113708	0,003732469
Hspa1b	-3,0300	0,00032286	0,00817641
1700019D03Rik	-3,0341	0,00073327	0,014729412
Gm17334	-3,0382	0,001019164	0,01869282
Gm15890	-3,0601	0,000994548	0,018372227
Rapgef4	-3,0736	0,001110191	0,019926241
Gm37176	-3,0745	0,003595832	0,04607902
Abi3bp	-3,0927	0,001634066	0,026796721

Gene	FC	pval	padj
Xlr4a	-3,1038	0,000468908	0,010573047
Apol7e	-3,1148	2,07E-05	0,000987377
Lat	-3,1197	1,12E-06	9,32E-05
Tasp1	-3,1357	5,55E-10	1,63E-07
Arl4d	-3,1364	6,75E-07	6,30E-05
2610024D14Rik	-3,1438	0,000215309	0,005927602
Rab11fip4	-3,1455	2,39E-09	5,23E-07
Gm44175	-3,1544	0,003549375	0,045610923
Gm26884	-3,1556	0,000170014	0,00492694
Angptl1	-3,1565	0,001167218	0,02071023
Klri1	-3,1645	1,96E-09	4,59E-07
Adgrl4	-3,1914	0,000416525	0,009659872
Fgl1	-3,1977	2,15E-05	0,001026739
Heatr9	-3,2527	1,23E-06	0,000100191
Gm4312	-3,2626	6,31E-05	0,002384098
Aim1l	-3,2646	1,85E-07	2,16E-05
Gm28053	-3,2747	0,000559768	0,012095861
Gm15872	-3,3037	0,000147719	0,004470592
2810468N07Rik	-3,3440	0,001789218	0,028383054
Gm24616	-3,3651	0,003674154	0,046769901
Cd163	-3,3673	3,30E-05	0,001427451
Gm21909	-3,3712	4,26E-06	0,000277221
Ttn	-3,3830	3,75E-07	3,75E-05
Ddx43	-3,3931	9,16E-08	1,19E-05
Clec1b	-3,4041	0,002997837	0,040838049
Ebf1	-3,4077	7,60E-05	0,002779528
Klrc1	-3,4275	1,01E-08	1,80E-06
Cyp2d22	-3,4286	0,003397921	0,044387004
C330011M18Rik	-3,4302	1,19E-07	1,49E-05
Gm6506	-3,4417	0,000136649	0,004256304
Gm27240	-3,4422	3,17E-06	0,00022156
Gm36028	-3,4791	0,003614194	0,046259644
Ms4a1	-3,4820	1,41E-12	8,90E-10
H2-Oa	-3,4878	0,000614804	0,012939701
Lrrn4	-3,4976	0,001636989	0,026815521
Pik3c2b	-3,5012	2,94E-06	0,000211132
Adgrl1	-3,5125	5,77E-10	1,64E-07
Trac	-3,5168	8,05E-06	0,000460284
Cd7	-3,5274	2,11E-09	4,74E-07
Cyp17a1	-3,5431	0,002798272	0,038825857
Gm37802	-3,5496	0,000374152	0,008957087
Slc25a2	-3,5503	1,53E-05	0,000771767
Klrc2	-3,5517	4,81E-08	6,96E-06
Cd160	-3,5537	7,12E-08	9,64E-06
Xkrx	-3,5584	0,00035585	0,008615606
Cd3e	-3,5650	0,001454854	0,024465916
Prlr	-3,5708	0,000431116	0,009917409
Gm42870	-3,5879	0,000397466	0,009331971
Gm37447	-3,6302	0,003301267	0,043749479
Gm22101	-3,6604	0,001825614	0,028879894
Gm10874	-3,6780	0,003631983	0,046368222
Sema4f	-3,6792	0,00126744	0,022075448
Cd8a	-3,6816	0,000187154	0,00532321
2010005H15Rik	-3,7019	0,003953557	0,049474532
Cpne7	-3,7306	5,77E-05	0,002230973
Gm42684	-3,7348	3,91E-10	1,26E-07
Gm20743	-3,7392	2,96E-07	3,10E-05
Gm23442	-3,7609	0,003051671	0,041373297
Cr2	-3,7812	0,000114694	0,003750415
Cdh17	-3,7953	0,000115172	0,003758819
Dtx1	-3,8106	1,81E-08	2,88E-06
Cxcr3	-3,8220	6,39E-09	1,23E-06
Ighd	-3,8383	1,41E-06	0,0001124
Gm45108	-3,8584	0,001786577	0,028383054
Mmp9	-3,8599	5,34E-05	0,002111763
Apol11b	-3,8747	0,002568476	0,036537402
Tcrg-C2	-3,8867	0,000298522	0,007673897
Cxcr5	-3,8917	0,000130649	0,00412972
Pax5	-3,8943	0,001139991	0,020311598
Cyp4b1	-3,9025	0,003154229	0,042359985

Gene	FC	pval	padj
Fam124b	-3,9079	0,001758817	0,028162521
Ccdc136	-3,9207	0,000144335	0,004415141
Art2b	-3,9352	4,70E-06	0,000300228
G0s2	-3,9753	0,000642159	0,01337887
Gm43081	-3,9763	0,001862811	0,029224558
Gm9694	-3,9904	0,001751474	0,028124095
Gramd2	-4,0263	0,00353729	0,045563301
Chp2	-4,0298	0,00354224	0,045563301
Acsm1	-4,0388	0,003420414	0,044509208
Snord43	-4,0401	0,000409951	0,009546313
Ighv1-55	-4,0549	0,003341605	0,04397944
Kcnh6	-4,0577	0,003207338	0,042938075
P4htm	-4,0708	0,000778508	0,015415724
Gm35339	-4,0869	0,000654393	0,013522804
Prrt1	-4,0981	5,65E-09	1,10E-06
Pou2af1	-4,1143	0,000158881	0,00470824
Nat8f1	-4,1228	0,000422036	0,009734771
Btla	-4,1256	1,50E-06	0,000117379
Igkv2-112	-4,1306	0,002800084	0,038825857
Cxcr6	-4,1633	1,87E-09	4,44E-07
Hic1	-4,1761	8,60E-05	0,003039472
Igkv8-24	-4,1945	0,002341025	0,034329
Pdgfrb	-4,2093	0,002249637	0,033477816
Gm19590	-4,2234	0,001244167	0,021758897
Scd1	-4,2281	2,94E-05	0,001315173
Btbd11	-4,2460	2,70E-13	2,00E-10
Zfp683	-4,2624	9,30E-07	8,10E-05
Ighv3-6	-4,2689	0,001969412	0,030449083
Fga	-4,3144	0,00025442	0,006743319
Tnfrsf13c	-4,3228	4,84E-09	9,60E-07
Ccr6	-4,4031	0,000990695	0,018320877
Paqr9	-4,4084	0,000291011	0,007503421
Rln3	-4,4896	0,000766572	0,015214667
Dmpk	-4,5020	6,22E-05	0,002359301
Apol7b	-4,5103	2,74E-05	0,001252267
Fcer2a	-4,5331	3,23E-08	4,92E-06
Dysf	-4,5357	0,001025559	0,018782468
Glp1r	-4,5460	0,00026845	0,007038658
Gm26640	-4,5519	7,69E-05	0,002793744
Gm16602	-4,5954	0,000520363	0,011500529
Zfp93	-4,6288	6,06E-06	0,00036955
Mzb1	-4,7031	0,000347145	0,00851352
Pck1	-4,7128	9,90E-07	8,53E-05
Iglc3	-4,7496	1,36E-05	0,000706795
Gm25106	-4,7701	5,87E-06	0,000360468
Sdpr	-4,7960	0,000135339	0,004230948
Blk	-4,7995	2,29E-05	0,001070915
Igkv17-121	-4,8072	0,000161505	0,004752973
Pzp	-4,8430	0,000202459	0,005628293
Gm10505	-4,8471	0,000118879	0,003821401
H2-Ob	-4,8580	5,52E-13	3,77E-10
Ighv10-1	-4,8638	0,000392556	0,009229387
Gm26802	-4,8728	3,99E-05	0,001668406
Ambp	-4,8908	0,000161041	0,00474751
Kcna2	-4,9051	7,39E-09	1,39E-06
Serpina3k	-4,9807	9,59E-05	0,003295617
Bend5	-4,9916	0,000178079	0,005117213
Ccdc80	-4,9928	2,94E-05	0,001315173
Ighv1-64	-5,0112	0,000216489	0,005947131
Axin2	-5,0227	3,47E-08	5,25E-06
Igkv6-32	-5,0685	0,000139124	0,004294213
Cdc42ep1	-5,1057	1,37E-07	1,70E-05
Igkv3-10	-5,1095	0,000163986	0,004808243
Id3	-5,1440	2,61E-14	2,34E-11
Zmat4	-5,1743	2,15E-06	0,000162886
Tat	-5,3073	8,25E-05	0,002954115
Igkv3-2	-5,3089	6,31E-05	0,002384098
Tcrg-C4	-5,3770	3,38E-17	1,44E-13
Igkv8-30	-5,3996	7,40E-05	0,002714931
Ablim2	-5,5393	5,85E-06	0,000360468

Gene	FC	pval	padj
Trgv2	-5,5902	4,33E-06	0,000281065
Trgj4	-5,5938	8,37E-07	7,44E-05
A1bg	-5,6016	7,58E-06	0,000442471
Adh1	-5,6250	2,71E-05	0,001241566
Igkv12-98	-5,6433	9,36E-06	0,000518598
C6	-5,6663	2,19E-06	0,000165641
Igkv2-109	-5,6690	2,40E-05	0,001115255
Igha	-5,6870	4,61E-08	6,73E-06
Chad	-5,7139	8,94E-07	7,86E-05
Ahsg	-5,7398	9,45E-06	0,000521859
Gm26614	-5,7774	3,70E-06	0,000248503
Cd200r2	-5,7856	7,03E-08	9,59E-06
Vsig4	-5,7988	7,39E-06	0,00043627
Tcrg-C1	-5,8053	3,14E-09	6,69E-07
Igkc	-6,0199	3,83E-08	5,74E-06
Cd40lg	-6,0216	2,84E-06	0,000205703
Gm6934	-6,1252	5,33E-10	1,60E-07
Ngp	-6,1417	3,84E-09	8,00E-07
Hlf	-6,2732	3,90E-08	5,79E-06
Itih4	-6,3431	1,62E-08	2,67E-06
Iglc1	-6,5732	1,62E-08	2,67E-06
Podnl1	-6,5955	3,93E-12	1,97E-09
Ighg2c	-6,6177	2,78E-07	2,95E-05
Ltf	-6,8146	2,14E-09	4,74E-07
Atp8a2	-6,8275	1,51E-11	6,95E-09
Alb	-6,9565	2,11E-09	4,74E-07
Jchain	-6,9871	9,59E-18	6,26E-14
Igkv17-127	-7,1033	2,00E-09	4,62E-07
Cd79a	-7,2156	7,27E-15	8,27E-12
Cd19	-7,4659	1,73E-16	3,68E-13
St6galnac3	-7,5245	1,04E-14	1,07E-11
Igkv1-135	-7,7226	2,13E-12	1,21E-09
Igkv10-96	-7,7543	1,68E-14	1,60E-11
Clec4f	-8,0141	1,29E-10	4,68E-08

Table A.3. Comparison III. All differentially expressed genes from the comparison III: uterine CD49a^{+} (ILC1, trNK) subsets vs uterine CD49a^{-} (cNK) subset. FC: fold change, padj: adjusted p-value.

Gene	FC	pval	padj
Ccl7	7,6916	1,75E-14	5,91E-11
Pf4	7,3764	2,97E-10	1,07E-07
Cd109	7,3175	1,06E-08	1,79E-06
C3ar1	7,2746	4,47E-14	9,43E-11
Kdr	7,2540	8,20E-11	3,64E-08
Tlr1	7,0754	5,67E-10	1,77E-07
Ptafr	6,9619	3,06E-10	1,07E-07
Ccl2	6,9266	2,91E-10	1,07E-07
Msr1	6,8975	1,13E-09	3,07E-07
Slco2b1	6,7718	6,31E-08	7,60E-06
Flrt3	6,7663	2,96E-12	3,33E-09
Ctnnd2	6,7396	3,86E-08	5,09E-06
Adam33	6,7207	9,75E-09	1,66E-06
Fcgr1	6,6940	3,90E-09	8,23E-07
C5ar1	6,6837	5,37E-10	1,71E-07
Ccl12	6,6717	3,28E-08	4,49E-06
Mfsd12	6,6694	3,01E-19	5,08E-15
Pltp	6,6538	2,99E-10	1,07E-07
Fam114a1	6,6314	1,18E-08	1,93E-06
Ch25h	6,6158	1,12E-07	1,13E-05
Lpcat2	6,6151	1,38E-10	5,69E-08
Tmem86a	6,6126	2,05E-09	5,01E-07
Nectin4	6,5694	4,64E-12	4,89E-09
Fkbp9	6,4991	2,94E-07	2,42E-05
Psd3	6,4966	4,41E-09	8,85E-07
Stxbp1	6,4908	9,56E-10	2,69E-07
Tal1	6,4448	3,14E-07	2,51E-05
Lacc1	6,4392	9,76E-10	2,70E-07
Ahnak2	6,4089	4,94E-08	6,32E-06
Ass1	6,3975	2,09E-11	1,41E-08
Rnf144b	6,3899	2,24E-09	5,33E-07
Lyve1	6,3693	8,23E-08	9,20E-06
Retnla	6,3666	5,12E-11	2,70E-08
Rab7b	6,3189	5,76E-08	7,14E-06
Ptgfrn	6,3150	5,33E-07	3,70E-05
Pde7b	6,3040	1,36E-08	2,18E-06
Itga9	6,2488	2,21E-08	3,27E-06
Plb1	6,2416	6,77E-07	4,39E-05
Rab3il1	6,2179	6,49E-07	4,30E-05
Cebpa	6,2156	3,83E-08	5,09E-06
Pdpn	6,2077	9,54E-09	1,64E-06
Ecm1	6,1989	2,79E-09	6,27E-07
Gas6	6,1716	1,31E-07	1,28E-05
Cxcl16	6,1664	7,72E-11	3,52E-08
Plxna1	6,1507	1,15E-09	3,08E-07
Clec7a	6,1454	2,53E-07	2,17E-05
Gzmf	6,1420	4,78E-09	9,48E-07
Fzd7	6,1270	2,70E-08	3,80E-06
Egln3	6,1224	3,02E-07	2,43E-05
Wfdc17	6,1147	7,08E-08	8,14E-06
Rgs10	6,1105	2,70E-08	3,80E-06
Trim30c	6,0985	2,51E-08	3,65E-06
Reps2	6,0816	1,86E-07	1,70E-05
Lipg	6,0561	3,51E-06	0,000152327
Tnip3	6,0530	2,89E-08	4,03E-06
Stra6l	6,0511	8,20E-08	9,20E-06
Mertk	6,0213	5,98E-07	4,09E-05
Tiam1	6,0203	1,51E-08	2,38E-06
Mafb	6,0189	9,66E-08	1,02E-05
Plau	6,0116	3,31E-09	7,15E-07
Arl11	6,0075	4,52E-08	5,81E-06
Havcr2	5,9932	9,81E-08	1,02E-05
Mmp14	5,9610	9,17E-08	9,79E-06
Etv5	5,9499	3,58E-14	8,64E-11
Ier3	5,9475	1,94E-07	1,74E-05
Ninj1	5,9389	5,26E-12	5,22E-09
Apbb2	5,9327	4,60E-10	1,51E-07
C1qb	5,9299	3,19E-07	2,51E-05
Cdkl2	5,9226	4,60E-07	3,32E-05
Gpnmb	5,9102	1,51E-11	1,16E-08

Gene	FC	pval	padj
Rin2	5,9022	5,77E-07	3,97E-05
Nr1h3	5,8917	1,62E-07	1,52E-05
Rhov	5,8875	9,52E-06	0,000326269
Vcam1	5,8835	2,61E-08	3,76E-06
Wdfy4	5,8801	9,01E-08	9,68E-06
H2-DMb1	5,8770	2,45E-07	2,14E-05
Ankrd66	5,8525	4,21E-06	0,000176364
Ctsh	5,8456	4,06E-07	3,03E-05
Anxa3	5,8445	4,24E-07	3,15E-05
Cysltr1	5,8351	4,37E-07	3,20E-05
Atp6v0a1	5,8336	1,54E-08	2,40E-06
Tlr13	5,8201	8,91E-07	5,32E-05
P2ry13	5,8163	1,60E-06	8,37E-05
Gdpd1	5,8063	1,43E-06	7,78E-05
Axl	5,8024	3,88E-07	2,95E-05
Zscan12	5,7961	6,54E-07	4,30E-05
Zak	5,7731	6,01E-09	1,13E-06
Gdf3	5,7717	1,84E-07	1,69E-05
Pld4	5,7479	1,09E-06	6,18E-05
Acvrl1	5,7468	2,65E-06	0,000122576
Spi1	5,7410	1,24E-06	6,88E-05
Oas2	5,7312	8,91E-07	5,32E-05
Thbs1	5,7293	1,50E-08	2,38E-06
Cd68	5,7258	3,55E-10	1,22E-07
Tdrd9	5,7219	1,41E-05	0,000443537
Gzmd	5,7205	2,15E-08	3,21E-06
Fam20c	5,7086	8,61E-07	5,26E-05
Matn2	5,6992	2,64E-06	0,000122576
Gas2l1	5,6962	8,68E-07	5,28E-05
Ddx3y	5,6949	1,68E-05	0,000507713
Adap2	5,6931	2,72E-06	0,000124473
Igsf10	5,6928	1,19E-05	0,000389832
Cd93	5,6917	8,61E-10	2,51E-07
Eps8	5,6916	3,47E-07	2,70E-05
Arg1	5,6824	2,67E-09	6,09E-07
Ednrb	5,6743	3,30E-14	8,64E-11
Nrp1	5,6727	9,36E-13	1,43E-09
Dsc2	5,6722	6,85E-06	0,000252388
Adgre1	5,6700	1,85E-06	9,19E-05
Apoe	5,6688	1,32E-07	1,28E-05
Ltbr	5,6667	5,56E-06	0,000215169
Tlr7	5,6646	1,90E-07	1,73E-05
Sdc3	5,6556	7,10E-08	8,14E-06
Gm44205	5,6452	2,56E-05	0,00070061
Il7r	5,6418	9,10E-11	3,93E-08
Olfml2b	5,6357	3,78E-05	0,000953299
F10	5,6278	9,54E-09	1,64E-06
Gm43768	5,6171	4,55E-06	0,000187226
Ccl6	5,5985	1,31E-07	1,28E-05
Gm13650	5,5918	1,87E-05	0,000552791
Ifitm1	5,5885	5,37E-06	0,00020972
Tgm2	5,5843	9,34E-10	2,67E-07
Pfkfb4	5,5706	5,79E-06	0,000220911
Slfn4	5,5648	9,40E-07	5,55E-05
Rnf217	5,5608	5,76E-06	0,000220715
Cttnbp2nl	5,5582	3,08E-06	0,000138234
Lifr	5,5396	7,74E-07	4,87E-05
Cd33	5,5339	2,47E-07	2,15E-05
Siglec1	5,5327	1,46E-06	7,89E-05
Ly86	5,5300	3,56E-07	2,74E-05
P2ry1	5,5297	1,47E-05	0,000458873
Gpr84	5,5164	9,90E-06	0,000337399
Clec4n	5,5121	1,98E-06	9,63E-05
Adamts1	5,5115	2,43E-06	0,000114901
Tlr9	5,5069	4,94E-06	0,000198682
Cmtm3	5,4899	1,31E-07	1,28E-05
Csf2rb	5,4884	3,59E-06	0,000155394
Mgat3	5,4871	2,87E-05	0,000767964
Mgl2	5,4852	6,29E-07	4,22E-05
Sirpa	5,4848	1,70E-06	8,67E-05

Gene	FC	pval	padj
Ankrd33b	5,4817	2,96E-05	0,000786609
Clec10a	5,4816	2,35E-05	0,000652462
Arhgap24	5,4790	2,76E-06	0,000125356
Hmox1	5,4702	3,49E-07	2,70E-05
Coprs	5,4654	3,96E-05	0,000988275
Clec4a1	5,4642	5,65E-06	0,000217539
C1qc	5,4490	2,30E-06	0,000110328
Tmem256	5,4352	1,81E-06	9,10E-05
Apba1	5,4283	5,92E-06	0,000224731
Ifi207	5,4277	2,62E-06	0,000122289
Gzmg	5,4272	4,36E-07	3,20E-05
Fmn1	5,4202	8,85E-06	0,000308962
Cp	5,4168	7,01E-09	1,27E-06
Il1r2	5,4146	1,49E-05	0,000462847
Plbd1	5,3980	1,67E-06	8,58E-05
Pla2g7	5,3925	9,34E-06	0,000322163
H2-Eb1	5,3905	8,59E-06	0,000303524
Igf1	5,3892	1,94E-07	1,74E-05
Rab32	5,3838	7,67E-11	3,52E-08
Tmtc3	5,3824	4,39E-07	3,20E-05
Adora2b	5,3811	2,04E-05	0,000592181
Cdc42bpb	5,3772	5,88E-06	0,000223818
H2-Ab1	5,3760	5,02E-06	0,000200316
Tnfrsf11a	5,3711	7,06E-07	4,51E-05
Dcn	5,3708	2,98E-05	0,000790673
Aif1	5,3673	9,28E-06	0,000320782
Lrp1	5,3663	6,34E-07	4,25E-05
Slc7a7	5,3579	6,00E-08	7,33E-06
Nt5dc2	5,3578	4,05E-05	0,001006251
Csf1r	5,3557	3,64E-06	0,000156879
Ccr1	5,3531	2,83E-07	2,35E-05
Slc15a3	5,3527	5,02E-07	3,58E-05
Plscr3	5,3433	8,78E-06	0,000308439
Gm38357	5,3385	4,17E-09	8,47E-07
Lpl	5,3259	1,17E-09	3,08E-07
Trem2	5,3241	1,14E-05	0,000375158
Afp	5,3140	3,73E-05	0,000944305
Ifi204	5,3084	3,45E-07	2,69E-05
Cd74	5,2991	5,00E-06	0,000199739
Mefv	5,2796	1,17E-05	0,000383745
Stom	5,2781	3,34E-11	1,94E-08
Hp	5,2774	3,79E-06	0,000161987
C130050O18Rik	5,2761	1,57E-05	0,000483011
Pafah2	5,2692	1,10E-05	0,000362876
Shtn1	5,2677	6,95E-06	0,000255269
Sh2b2	5,2550	2,59E-06	0,000121473
Anpep	5,2475	1,87E-06	9,23E-05
Fggy	5,2464	4,24E-05	0,00104479
Cd180	5,2421	7,15E-06	0,000260237
Csf2ra	5,2418	6,24E-07	4,21E-05
Myof	5,2388	2,31E-06	0,000110434
Ccl8	5,2362	4,86E-05	0,001160286
P2ry6	5,2321	6,46E-06	0,000240686
Cebpd	5,2292	3,24E-05	0,000842043
Gm15635	5,2225	7,08E-05	0,001580211
Tbc1d8	5,2208	4,45E-07	3,22E-05
Arhgap29	5,2159	9,55E-07	5,55E-05
Acvrl1	5,2070	3,25E-05	0,000844547
Lsr	5,2027	1,21E-05	0,000395264
Rhou	5,2003	1,07E-05	0,000356462
Dhrs9	5,1956	3,73E-06	0,000159957
A230028O05Rik	5,1935	0,000120065	0,002373984
Vipr2	5,1896	2,87E-05	0,000767989
Flt1	5,1889	1,22E-05	0,000395663
Spsb1	5,1887	1,64E-06	8,51E-05
4930533B01Rik	5,1767	7,54E-05	0,001657037
Mtss1	5,1747	3,68E-07	2,82E-05
P2rx7	5,1744	8,82E-06	0,000308962
Cds1	5,1717	5,92E-05	0,001362975
Gdf15	5,1672	4,94E-05	0,001176974

Gene	FC	pval	padj
Zfp385a	5,1670	3,90E-05	0,000977737
Igfbp5	5,1649	9,21E-05	0,001937896
Rnase2a	5,1621	0,000203815	0,003554858
Cacna1d	5,1604	1,14E-05	0,000375158
Cd36	5,1530	4,65E-06	0,000189974
Ptk2	5,1522	6,68E-05	0,001513232
A630012P03Rik	5,1490	0,000208258	0,003608715
Avil	5,1482	1,56E-06	8,20E-05
Mmp19	5,1458	3,99E-05	0,000993102
Lmo2	5,1362	1,63E-05	0,000494791
Hacd4	5,1302	1,83E-05	0,000544503
Lhfpl2	5,1280	1,09E-05	0,000362876
Inhba	5,1259	1,34E-06	7,42E-05
Ifitm3	5,1255	2,03E-05	0,000590897
Slc7a8	5,1254	1,49E-06	7,93E-05
Atml1	5,1240	4,60E-05	0,001116859
Arhgef39	5,1235	2,10E-05	0,000599909
Parp12	5,1225	1,59E-07	1,50E-05
Alox5ap	5,1181	2,86E-05	0,000766311
Tlr3	5,1169	5,31E-07	3,70E-05
Tifab	5,1147	3,36E-05	0,000867196
Slc8a1	5,1139	5,73E-05	0,001328196
H2-Aa	5,1091	2,12E-05	0,000602302
Tmem144	5,1067	7,17E-05	0,001595542
Nfix	5,0972	3,79E-05	0,000953299
Vdr	5,0963	6,01E-05	0,001380384
Cryl1	5,0953	3,42E-06	0,000149113
Cxcl2	5,0889	2,39E-05	0,000659725
Emp1	5,0854	1,08E-11	8,69E-09
Ctss	5,0830	2,65E-08	3,79E-06
Ly6a	5,0777	2,01E-06	9,78E-05
Fcrl5	5,0765	2,08E-05	0,000595236
Pparg	5,0738	6,83E-05	0,001542607
Aph1c	5,0602	1,51E-06	8,02E-05
3110082I17Rik	5,0595	3,09E-06	0,0001383
Aph1b	5,0590	4,95E-05	0,001177371
Atp6v0d2	5,0558	4,25E-05	0,001044924
Hgf	5,0554	8,39E-05	0,001798488
Stard8	5,0515	1,04E-15	8,76E-12
Stau2	5,0457	1,12E-08	1,86E-06
Ms4a6d	5,0345	6,57E-06	0,000243988
Cped1	5,0295	0,0002231	0,0038085
Cttn	5,0284	0,00014693	0,00278128
Cfh	5,0283	7,47E-06	0,000270264
App	5,0129	6,39E-06	0,000238516
C3	5,0085	1,20E-06	6,77E-05
Wdfy3	5,0042	4,04E-05	0,001004265
Plxnb2	5,0001	1,81E-06	9,10E-05
Olr1	4,9998	2,04E-05	0,000592181
Gm37648	4,9997	5,21E-06	0,000206639
Dusp4	4,9888	5,68E-05	0,001318758
Adgrg6	4,9885	0,00011066	0,002240564
Ctsg	4,9824	0,000173711	0,003163933
Gsn	4,9810	5,85E-07	4,01E-05
6430548M08Rik	4,9784	6,76E-05	0,001530115
Ago4	4,9784	4,84E-06	0,000195123
Il18	4,9767	0,0001121	0,002262648
Mrm2	4,9736	1,22E-05	0,00039717
Ccdc122	4,9637	0,000120413	0,002378079
Gm16353	4,9621	8,55E-07	5,24E-05
Pde8b	4,9443	8,07E-05	0,001747545
Sncg1	4,9392	2,80E-05	0,000754044
Pid1	4,9321	2,09E-05	0,000597773
Gpr19	4,9309	1,61E-05	0,000491761
St8sia6	4,9298	0,000124879	0,002454792
Ifngr2	4,9292	3,77E-06	0,000161227
Il1a	4,9286	7,06E-05	0,001578345
Cd83	4,9252	3,45E-08	4,69E-06
2210406H18Rik	4,9249	6,58E-08	7,81E-06
9130204K15Rik	4,9218	0,000126199	0,002458821

Gene	FC	pval	padj
Ms4a4a	4,9157	9,28E-06	0,000320782
Arfgef3	4,9147	2,94E-06	0,000132519
Mreg	4,9044	3,48E-05	0,00089416
Prokr1	4,9009	0,00035651	0,005526557
Hpgds	4,8988	1,57E-12	2,20E-09
Plaur	4,8950	6,38E-06	0,000238516
Kcnk6	4,8940	7,65E-08	8,66E-06
Gspt2	4,8923	0,000127272	0,002467314
Tifa	4,8899	0,000118398	0,002352055
Copz2	4,8861	1,11E-05	0,000366162
Kdelc1	4,8857	1,51E-05	0,000467016
Clec4a2	4,8830	4,14E-06	0,000174834
Tnf	4,8796	2,61E-06	0,00012191
Gstm4	4,8789	7,55E-05	0,001658663
Grn	4,8756	4,87E-09	9,55E-07
Rubcnl	4,8725	8,04E-05	0,001745428
Thsd7a	4,8633	0,000406719	0,006075934
Slamf8	4,8629	9,20E-05	0,001937508
Twnk	4,8542	7,97E-07	4,96E-05
Mpeg1	4,8528	2,12E-05	0,000602302
Cyp4f18	4,8517	0,000102584	0,002112547
Batf3	4,8371	5,64E-05	0,001315333
Plin2	4,8286	7,78E-12	6,91E-09
Aqp9	4,8208	3,31E-05	0,000856972
Marcks	4,8200	9,37E-06	0,000322584
Rassf4	4,8194	5,08E-06	0,000202243
Sh3bp4	4,8079	0,000103323	0,002117441
Gm6377	4,8026	0,000170573	0,003122974
Vkorc1	4,8020	3,42E-06	0,000149113
Ppfibp2	4,8000	0,000108756	0,002212648
Tmem26	4,7937	0,000186157	0,00334726
Klk1b11	4,7919	0,000426677	0,006282037
Lgmn	4,7882	7,88E-07	4,94E-05
Gm14011	4,7878	0,000613773	0,008120285
Fn1	4,7858	3,18E-06	0,000140699
Tmem106a	4,7804	1,47E-07	1,41E-05
I830077J02R	4,7787	0,000103164	0,002116744
Abcc3	4,7784	0,000101843	0,002099859
Tlr6	4,7775	4,40E-07	3,20E-05
Ap1s1	4,7713	5,99E-05	0,001379092
F11r	4,7711	4,06E-05	0,001006999
Scamp1	4,7701	2,42E-05	0,000668626
Cd4	4,7667	0,000127145	0,002467314
Klra2	4,7643	8,76E-05	0,001863234
Ak4	4,7637	0,000241103	0,004054286
Laptm4b	4,7599	6,99E-06	0,000256302
Rusc2	4,7568	0,000166793	0,003077819
Slc6a12	4,7507	0,000197654	0,003490713
Clec4d	4,7467	3,41E-05	0,000878602
Pla2g15	4,7414	1,36E-06	7,51E-05
Tmem176b	4,7379	9,00E-05	0,001905201
Lyz2	4,7378	4,54E-05	0,001107102
Gm45041	4,7369	0,000161013	0,002987513
Cybb	4,7272	9,37E-05	0,001960148
Mt1	4,7244	5,47E-06	0,00021196
Gm5345	4,7124	0,000592093	0,007925592
Gm16316	4,7120	7,82E-05	0,001706976
Upp1	4,7039	0,000572542	0,007768699
Sgms1	4,6990	3,20E-05	0,000835145
P2ry12	4,6945	4,65E-05	0,001122033
Ms4a7	4,6917	1,38E-05	0,000435307
Mfsd7a	4,6906	0,000384304	0,005828848
Eya4	4,6902	0,001053333	0,012190786
Ugt1a7c	4,6820	1,85E-06	9,19E-05
Kif13a	4,6811	2,47E-05	0,000678727
Htra3	4,6760	0,000202115	0,003537333
Gm20658	4,6756	0,000571947	0,007766868
Isg15	4,6711	3,18E-06	0,000140699
Slc7a2	4,6709	9,83E-08	1,02E-05
Rcn3	4,6705	0,000294596	0,004763806

Gene	FC	pval	padj
Nlrp3	4,6676	0,000235161	0,003974176
Gzme	4,6617	2,54E-06	0,00011979
Gpt2	4,6616	7,61E-06	0,000274203
Siglece	4,6609	0,000182285	0,003288149
Gm13710	4,6594	0,000566124	0,007705757
Gpr35	4,6592	5,68E-05	0,001318758
Fut10	4,6560	0,001011918	0,011827451
Gm23722	4,6537	0,000171741	0,003134826
Ctsz	4,6484	1,91E-07	1,73E-05
Tgfbi	4,6469	5,63E-05	0,001314161
Fpr2	4,6457	0,000217257	0,003731421
Epb41l1	4,6417	1,71E-06	8,67E-05
Sestd1	4,6401	5,20E-05	0,00122786
Ifit3b	4,6400	2,59E-06	0,000121491
Rnf150	4,6368	5,00E-06	0,000199739
Tnfaip2	4,6332	0,000242841	0,004079443
Rps4l	4,6325	5,44E-05	0,001273546
Cd300a	4,6306	2,36E-05	0,000654147
Arhgef10l	4,6290	0,000219783	0,003763305
Alox5	4,6183	0,000126331	0,002458821
Clec4a3	4,6154	0,000441644	0,006461316
Plekho1	4,6142	2,90E-06	0,000131341
Spic	4,6140	1,21E-06	6,78E-05
Tmem221	4,6045	0,00055528	0,007624047
Gm42603	4,6038	0,00078623	0,009757588
Gm2a	4,6013	3,41E-06	0,000149113
E130102H24Rik	4,5999	0,000255077	0,00423855
Tbxas1	4,5995	3,19E-06	0,000140699
Bag2	4,5949	0,000452217	0,006597833
Pdgfc	4,5944	0,000281235	0,004609632
Oasl2	4,5924	5,23E-06	0,000206639
Bex6	4,5908	0,000640693	0,008396211
Stab1	4,5904	8,52E-07	5,24E-05
Mrc1	4,5901	2,30E-05	0,000643208
Kcnk13	4,5872	0,000291632	0,004738591
Zfyve9	4,5819	0,000155619	0,002903403
Tlr2	4,5650	5,65E-05	0,001316549
Bmpr1a	4,5622	1,94E-05	0,000569917
Vill	4,5594	0,000175201	0,003180782
Ifi211	4,5590	1,60E-06	8,37E-05
Lst1	4,5589	0,000149675	0,002817436
Fap	4,5588	0,000452667	0,006598685
C1qa	4,5531	0,000193956	0,003445666
Lrrc25	4,5389	0,000558607	0,007647293
Gm26797	4,5363	7,28E-05	0,001615388
Gm17068	4,5317	0,000461436	0,006697568
Zfp467	4,5314	3,18E-07	2,51E-05
Adap2os	4,5289	0,000307398	0,004910586
Ypel2	4,5254	0,000357448	0,005530931
2810025M15Rik	4,5229	6,97E-05	0,001565593
Ctsb	4,5187	1,12E-10	4,71E-08
Spats2	4,5161	0,000682713	0,008796487
Pdia5	4,5137	0,000566533	0,007705757
Kif26b	4,5135	0,001254069	0,013933555
Dab2	4,5134	3,41E-06	0,000149113
Ly6i	4,5043	0,000117405	0,002343375
Dmxl2	4,5013	1,39E-05	0,000438033
Tgm1	4,4963	0,000497691	0,007065705
Gm15531	4,4916	0,00029223	0,004739181
Gm2396	4,4852	0,000606927	0,00806654
Gm13391	4,4842	0,000937148	0,011107472
Rtn1	4,4821	0,000557522	0,007644844
Dynlt1a	4,4819	0,000194325	0,003446351
Reep6	4,4819	0,000819935	0,01008682
Tns3	4,4793	4,66E-05	0,00112319
Gm37199	4,4730	0,000819658	0,01008682
Apobec1	4,4727	2,82E-07	2,35E-05
Tmprss4	4,4724	0,001537236	0,016214528
Fat1	4,4643	0,000575258	0,007776338
Paox	4,4606	1,88E-06	9,23E-05

Gene	FC	pval	padj
Akap1	4,4570	0,000757751	0,009516248
Cdk5rap1	4,4535	2,18E-06	0,000105114
Rps6ka2	4,4500	0,000219608	0,003763305
Tfec	4,4492	0,001060244	0,012239614
Sfmbt2	4,4480	0,000289377	0,00471103
Gm26603	4,4456	0,0008872	0,01065777
St6gal1	4,4455	0,000130209	0,002512703
Ifi203-ps	4,4421	0,000181539	0,003278202
Zfp608	4,4380	9,83E-07	5,66E-05
Rnf180	4,4334	0,001097499	0,012575011
Lgals3	4,4328	7,04E-08	8,14E-06
Dock1	4,4197	0,000626987	0,008248643
Gria3	4,4103	0,000523939	0,007299273
Gm15448	4,4103	0,000986175	0,011585157
Clec4b1	4,4094	0,000840974	0,010275365
Gm33370	4,4065	0,00061386	0,008120285
Siglecf	4,4028	0,001500418	0,015965967
Rab13	4,4027	0,000564639	0,007692411
Mcemp1	4,4002	0,00025055	0,004179804
Ralgds	4,3991	3,58E-08	4,83E-06
C5ar2	4,3978	9,49E-07	5,55E-05
Neil2	4,3968	0,00074185	0,00938638
Mmp13	4,3963	0,000555553	0,007624047
Tdo2	4,3959	8,39E-05	0,001798488
Tmcc2	4,3929	0,000214537	0,003695899
Gm17034	4,3911	0,000833066	0,010203698
Armc6	4,3881	0,000389348	0,005881434
Kcnj2	4,3866	0,000327814	0,00514796
Clec12a	4,3858	8,10E-05	0,001750758
Gm44981	4,3821	0,001193037	0,01345038
Gm15503	4,3763	0,001085897	0,01247598
Thop1	4,3754	0,000450084	0,006572401
1700071M16Rik	4,3716	0,001103529	0,01261839
Jag1	4,3711	0,000315382	0,0050087
Kank3	4,3660	0,000646832	0,008456953
Hck	4,3655	0,001046124	0,012159837
Mfsd7b	4,3646	4,02E-09	8,37E-07
Apol9b	4,3641	0,001307066	0,014380287
Mctp1	4,3607	0,000754871	0,00950123
Hk2	4,3596	8,72E-07	5,28E-05
Tbc1d32	4,3582	1,60E-05	0,000489401
Spint1	4,3565	0,000695964	0,008908592
Stmn2	4,3551	0,001856974	0,018676039
Mtap7d3	4,3494	0,000682408	0,008796487
Il6ra	4,3479	0,000256042	0,0042504
RP23-292C5.8	4,3459	1,78E-05	0,000531061
Gm16120	4,3432	0,00033667	0,005257656
4930512H18Rik	4,3410	0,001866955	0,018754055
Rbfox2	4,3401	0,002206511	0,021277884
Klhl13	4,3393	0,001098514	0,012578101
Gm24273	4,3389	0,001980107	0,019564436
Ppfia4	4,3331	0,000876643	0,010578309
Slc11a1	4,3317	9,13E-05	0,001927428
Pard3	4,3264	0,001765748	0,018049158
Nlrp1c-ps	4,3254	0,000605599	0,008061592
Nostrin	4,3214	0,000592073	0,007925592
Ehd1	4,3170	3,15E-09	6,90E-07
Pmp22	4,3168	0,000659921	0,008596882
Ifi205	4,3168	0,000107154	0,002185323
Nr1d1	4,3153	0,000300857	0,004828111
Rab15	4,3131	0,002973208	0,026434437
RP23-323L3.1	4,3129	3,00E-05	0,000796878
F13a1	4,3100	0,000157781	0,002937234
Gm15964	4,3099	0,000875366	0,010575879
Hlx	4,3052	0,000198336	0,003494628
Gm15987	4,3037	0,000195448	0,003458992
Bace2	4,2963	0,002737961	0,024989552
Kctd17	4,2943	0,000422215	0,006252041
Tmem176a	4,2924	0,000173027	0,003154894
Flrt2	4,2836	0,00032027	0,005067232

Gene	FC	pval	padj
Trib1	4,2803	8,69E-05	0,001856672
Pira2	4,2790	0,001251501	0,013914189
Ift22	4,2775	7,45E-05	0,00163983
Scin	4,2755	3,53E-05	0,000901854
Asah1	4,2739	4,07E-08	5,28E-06
Bcl2a1d	4,2735	2,94E-05	0,000784548
Arhgap23	4,2712	2,83E-07	2,35E-05
Ralb	4,2710	6,16E-07	4,17E-05
Tlr5	4,2699	0,000532778	0,007371486
Gm5431	4,2694	8,13E-05	0,001752575
Plxnd1	4,2688	0,000679321	0,008786373
Homer3	4,2642	0,001580833	0,016570746
Amz1	4,2633	0,000371041	0,005668451
Cdk20	4,2628	0,000530951	0,007358274
Atf3	4,2599	1,09E-05	0,000362876
Cacna1b	4,2595	0,000489961	0,006988924
Ptpro	4,2594	0,0005884	0,007894957
Eid2b	4,2553	0,000113252	0,002279367
Bcl2a1a	4,2441	0,001849849	0,018637722
Lyz1	4,2440	0,001379042	0,014890473
6330403L08Rik	4,2438	0,000404633	0,006050121
Sirpb1b	4,2409	0,000520459	0,007279177
Mtus1	4,2292	0,000201945	0,003537333
Agpat9	4,2234	0,000505394	0,007127072
Prss16	4,2229	0,001319204	0,014455322
Card9	4,2219	0,001542768	0,016252548
Akr1c18	4,2203	0,003667442	0,030958496
Sqrdl	4,2198	1,24E-05	0,00040045
Pirb	4,2174	9,69E-05	0,002015982
Nuak1	4,2153	0,000296708	0,004784211
Rasgrp4	4,2116	0,00040823	0,006093109
Nlrc4	4,2104	0,000575541	0,007776338
Slfn1	4,2074	8,98E-05	0,001902091
Fnip2	4,1991	1,48E-09	3,73E-07
Gm20056	4,1955	0,002874301	0,025781491
P2ry2	4,1936	0,002840174	0,025575213
B4galt4	4,1839	0,001996851	0,019718316
Abca3	4,1815	3,08E-05	0,000810729
Speg	4,1781	0,000275351	0,004530799
Il6	4,1700	0,003387352	0,029167996
Grk3	4,1700	0,000899568	0,010760369
Ptgs2	4,1694	0,000852407	0,010372802
Ifit3	4,1669	2,05E-05	0,000593224
Aldh3b1	4,1633	0,001371207	0,014824854
Nme4	4,1600	0,001730833	0,01777846
Cd300lb	4,1540	0,001041001	0,012116995
Slmo1	4,1529	0,001716308	0,017683114
Gm44860	4,1519	0,000779306	0,009688265
Ifi30	4,1417	6,25E-06	0,000234639
Gpr87	4,1399	0,002871736	0,025776849
Kirrel	4,1384	0,0033722	0,029107229
Ceacam1	4,1373	0,000383717	0,005825175
C4b	4,1336	0,001405858	0,015096937
Snx24	4,1318	0,001161552	0,013183534
Il1b	4,1185	0,000715658	0,00912342
Pnp2	4,1153	0,000506119	0,007131337
4933440N22Rik	4,1147	0,000265678	0,004393063
Aatk	4,1115	0,001421491	0,015222141
2610203C22Rik	4,1109	0,001570754	0,016475335
Gm20548	4,1070	0,000126316	0,002458821
AA467197	4,1055	4,24E-05	0,001044485
Syngr1	4,1027	0,002358352	0,022359958
Cd63	4,1023	0,000106533	0,002177918
Adk	4,0998	0,000289683	0,004711475
Hcar2	4,0987	0,000504662	0,007122708
Arhgef11	4,0972	0,000145473	0,002759894
Ckap4	4,0943	0,00019824	0,003494628
Folr2	4,0931	0,001447501	0,015461403
Cxcl10	4,0927	9,29E-05	0,001949714
Prune2	4,0859	1,46E-06	7,89E-05

Gene	FC	pval	padj
Slfn5	4,0820	4,72E-05	0,001131453
Fpr1	4,0813	0,001040911	0,012116995
Pdxk	4,0766	9,10E-09	1,60E-06
1500005C15Rik	4,0764	0,001229411	0,013722858
Smo	4,0752	0,001745023	0,017858955
Rnf128	4,0721	0,001346924	0,014627963
Rab20	4,0678	8,78E-05	0,001865411
Pilra	4,0662	0,000612474	0,008114679
Dnase1l3	4,0633	0,000441711	0,006461316
Ccdc184	4,0622	0,004501011	0,036218539
Eng	4,0615	0,00225985	0,021582463
Apob	4,0572	0,000901452	0,010775261
Psrc1	4,0572	6,65E-08	7,84E-06
Serpinb8	4,0566	0,000276902	0,004551875
Olfml3	4,0518	9,47E-07	5,55E-05
Dpep2	4,0453	1,21E-05	0,000395264
Dgat2	4,0392	0,002941216	0,026212468
Gm12454	4,0390	0,000396821	0,005964681
Galm	4,0387	0,000626739	0,008248643
Gm42934	4,0331	0,002414689	0,022701305
Lrrk2	4,0329	0,000524097	0,007299273
Catsperg1	4,0302	0,002940884	0,026212468
Gm15374	4,0301	0,001926724	0,019217106
Igf2bp2	4,0258	0,000112254	0,002262648
Gm14548	4,0226	0,003436702	0,029512939
Ttc30a1	4,0224	0,00149277	0,015894603
Gm43775	4,0223	1,03E-06	5,90E-05
Asns	4,0205	0,000642339	0,008406985
8430408G22Rik	4,0165	0,003131026	0,027461202
Gm15922	4,0090	0,003565527	0,030341162
C78197	4,0085	0,001313552	0,014442217
Abcc2	4,0076	0,001361035	0,014733774
Fth1	4,0046	4,46E-11	2,51E-08
Pstpip2	4,0042	0,001998188	0,019719979
Gm16094	4,0031	0,000671734	0,008708274
Stxbp6	4,0009	0,000906276	0,010809935
Gngt2	3,9972	0,000126396	0,002458821
Themis2	3,9948	2,21E-05	0,00062437
Rgmb	3,9929	0,002451233	0,022968052
Ldhb	3,9890	0,001227732	0,013722695
Rnase4	3,9877	0,000109562	0,002224177
Gm17359	3,9867	0,003875832	0,032249526
Carmil1	3,9863	0,001849779	0,018637722
Cd276	3,9858	0,002731109	0,024958504
A530064D06Rik	3,9856	0,00014843	0,002797117
Lyl1	3,9809	0,002176429	0,021096349
Ugt1a6a	3,9804	0,000401092	0,006007832
Tcp11l1	3,9781	0,000236738	0,003993358
Med29	3,9772	2,12E-05	0,000602837
8030453O22Rik	3,9687	0,0015627	0,016403514
Dnmt3aos	3,9679	0,001294315	0,014295953
Daglb	3,9636	1,41E-07	1,36E-05
Mtcl1	3,9595	0,005529874	0,041507279
Nek4	3,9552	5,47E-05	0,001279227
Gda	3,9533	0,000119258	0,002366366
Cfp	3,9521	4,77E-05	0,001140582
Sbf2	3,9518	2,11E-05	0,000602302
Gm43068	3,9515	0,004287811	0,034980878
Zfp629	3,9510	2,69E-06	0,000123657
Thefg	3,9474	0,001086686	0,012476541
Batf2	3,9464	0,004031715	0,033267569
Rnf149	3,9451	1,84E-06	9,19E-05
Gm15931	3,9440	0,003188798	0,02787427
Glrx	3,9419	4,27E-10	1,44E-07
Ms4a4c	3,9418	2,04E-05	0,000592181
Apip	3,9382	1,01E-05	0,000341917
Slc16a10	3,9359	1,65E-05	0,000500283
Btbd3	3,9350	0,000494815	0,007035618
Fabp5	3,9347	1,55E-05	0,000476779
Tsacc	3,9327	0,005971559	0,043907354

Gene	FC	pval	padj
Adck1	3,9300	3,68E-06	0,000158524
Ms4a14	3,9213	0,0054797	0,041309402
Trim47	3,9208	0,003817847	0,03190723
Abca9	3,9208	0,001777699	0,018116513
BC028528	3,9188	0,000542638	0,007465029
Spon1	3,9183	5,46E-06	0,00021196
Ncf2	3,9173	5,85E-05	0,001351333
Asph	3,9144	0,000148211	0,002796108
Dppa3	3,9135	0,005131919	0,039613247
Hebp1	3,9115	2,35E-05	0,000652462
Slc36a3os	3,9055	0,003800112	0,031806255
Nacc2	3,9038	8,41E-08	9,33E-06
Cd24a	3,9037	2,15E-08	3,21E-06
Rbm47	3,9025	0,000766253	0,009586451
P2rx4	3,9016	2,71E-06	0,000124343
Tbc1d4	3,9009	0,000152098	0,002855687
Gm21057	3,8995	0,003490964	0,029887616
Bst1	3,8984	1,15E-05	0,000378897
Map3k15	3,8965	0,000302282	0,004841674
Naaa	3,8962	1,58E-05	0,000486029
Clcn7	3,8953	2,74E-10	1,05E-07
Ifi27l2a	3,8949	0,000239701	0,004034725
Gm42793	3,8937	0,002738094	0,024989552
Gm10693	3,8888	0,004371786	0,035432262
Tmem119	3,8882	0,001372439	0,014828671
Tnfrsf21	3,8846	0,000428703	0,006303835
Tlr8	3,8837	0,00439491	0,035602572
Car6	3,8831	0,003756932	0,031524581
Rgs7bp	3,8827	0,000334232	0,005234127
Rai14	3,8770	0,000159827	0,002972043
Klra17	3,8753	0,001643851	0,017072159
Il15	3,8750	2,15E-05	0,000608269
Sh3bp5	3,8747	9,49E-06	0,000325823
Adgb	3,8741	0,00306637	0,027063
Gm12689	3,8732	0,005307743	0,040525303
Abcd2	3,8728	0,000386014	0,005844272
Irf6	3,8723	0,00253436	0,023576675
Cd300c2	3,8716	0,004750256	0,037455735
Tst	3,8668	0,003307261	0,028664062
Mgst1	3,8622	0,003146459	0,027567885
Fam198b	3,8615	0,000300617	0,004828111
Cacnb1	3,8609	0,002542464	0,023626008
Ube2l6	3,8609	5,67E-07	3,92E-05
Melk	3,8559	8,87E-05	0,001882417
D430018E03Rik	3,8557	0,006658025	0,047441592
Gm37498	3,8429	0,003726365	0,031328144
Gm37347	3,8391	0,003622168	0,030683823
Gm6264	3,8313	0,000776467	0,009671071
Mfap3l	3,8281	0,004993495	0,038918805
Fcrls	3,8276	0,000495092	0,007035618
Myo10	3,8271	0,000484356	0,006923003
Src	3,8262	0,005652339	0,042070766
Tns4	3,8247	0,000522171	0,007290515
Cdc42ep2	3,8168	0,00464842	0,036963817
Fuom	3,8159	0,006100604	0,04465833
Clec4e	3,8152	0,001049547	0,012182835
Gm37168	3,8152	0,005650665	0,042070766
Wfdc18	3,8151	0,006495139	0,046604316
Clec5a	3,8139	0,001325342	0,014483674
Gm43221	3,8114	0,003954419	0,032757971
Spp1	3,8067	2,03E-05	0,000590897
Mmp27	3,8039	0,005271778	0,04032372
Npl	3,8014	1,12E-06	6,36E-05
Tnfrsf8	3,7943	0,006323105	0,045852946
Cd300e	3,7927	0,004838916	0,037941961
Hist1h2bc	3,7868	6,18E-05	0,001416317
Dok3	3,7849	0,004030376	0,033267569
Tctex1d2	3,7810	0,001330674	0,014507526
Scpep1	3,7731	2,33E-05	0,000649811
Ccl9	3,7688	7,80E-06	0,000279976

Gene	FC	pval	padj
Dck	3,7670	2,44E-12	3,12E-09
Msrb2	3,7624	0,00019994	0,003509046
Igf2bp1	3,7608	6,72E-08	7,87E-06
Gm19719	3,7606	0,006398152	0,046236853
Tnfsf15	3,7603	0,005190269	0,039923553
Gm17084	3,7493	0,004778611	0,03759144
2010300C02Rik	3,7470	0,001272852	0,014095811
Tmem67	3,7468	8,92E-07	5,32E-05
Gm15551	3,7455	0,005962243	0,043873991
Psap	3,7444	1,44E-06	7,83E-05
Plxdc1	3,7425	0,005158538	0,03972781
Renbp	3,7415	4,04E-06	0,00017153
Acta2	3,7411	0,00656033	0,046943796
Pusl1	3,7406	0,000156383	0,002914418
Tnfsf18	3,7387	0,004528707	0,036373381
Gzmc	3,7346	0,000623843	0,008232966
Deptor	3,7338	0,000326499	0,005132087
5730508B09Rik	3,7331	0,000426744	0,006282037
Gm28404	3,7285	0,002288248	0,021804284
Nucb2	3,7283	0,00214181	0,020844641
Nfam1	3,7272	0,002235039	0,021467065
Ms4a8a	3,7264	0,001892892	0,018969413
Ppic	3,7237	0,003381501	0,029167996
Fcrl6	3,7230	3,18E-05	0,000830735
Gys1	3,7218	6,22E-05	0,001421497
Gm44079	3,7213	0,00659987	0,047119804
Afap1l1	3,7171	0,000467348	0,006743452
Ophn1	3,7155	0,000925603	0,011001564
Bco2	3,7113	0,005436159	0,041164348
Gm15530	3,7066	0,006716224	0,047725413
Gm42868	3,7010	0,006479511	0,046543199
Xxylt1	3,6996	0,001616894	0,016864893
Mir5104	3,6993	0,004447724	0,035978569
Enkd1	3,6968	0,004331438	0,035238111
Zfp750	3,6959	0,005640808	0,042070766
Il1rl2	3,6914	9,45E-07	5,55E-05
Angptl4	3,6906	0,003294577	0,028583503
Zcchc14	3,6893	0,002607792	0,024092116
Pilrb1	3,6864	0,001446095	0,015456174
Gm13207	3,6857	0,006487395	0,046579997
Ptrhd1	3,6847	0,000194082	0,003445666
Hpse	3,6842	1,90E-05	0,000560843
Fcgr4	3,6841	0,006460402	0,046485129
Gm38156	3,6785	0,004947235	0,03864755
Gm43149	3,6757	0,003662396	0,030931385
Ramp1	3,6735	0,001832347	0,018549433
Cebpb	3,6716	8,37E-07	5,17E-05
Nlrp1a	3,6666	0,00567136	0,042137958
Sdhaf1	3,6645	0,000117882	0,002348247
Cpq	3,6591	7,09E-06	0,000258782
BC049715	3,6580	0,000875245	0,010575879
Snx9	3,6564	2,26E-06	0,000109003
Cd40	3,6563	4,72E-05	0,001131453
Tnfsf13b	3,6544	0,002894212	0,025895906
Nudt12	3,6540	0,005657907	0,04209363
Mmp12	3,6520	1,05E-07	1,08E-05
Mx2	3,6491	0,000695229	0,008908592
Oas1g	3,6459	0,000683123	0,008796487
Arnt2	3,6456	0,004777475	0,03759144
Arrdc4	3,6419	4,64E-10	1,51E-07
Tspyl4	3,6401	5,31E-06	0,000208622
Pls3	3,6401	0,005084193	0,039352913
Dna2	3,6387	1,26E-05	0,000404076
Fam213b	3,6374	0,00507322	0,039322119
Gm26387	3,6371	0,001338442	0,014573376
Lin7a	3,6369	0,006222746	0,045277322
Ptgr1	3,6280	1,33E-05	0,000424263
Basp1	3,6264	1,27E-14	5,91E-11
Spdl1	3,6249	8,33E-05	0,001789181
Ctsk	3,6246	0,000507795	0,007142214

Gene	FC	pval	padj
Mapt	3,6236	0,006967075	0,049083828
Gm15356	3,6233	0,002494478	0,023282716
Smpdl3b	3,6216	0,002076524	0,020350181
Tarm1	3,6106	0,0025496	0,023655293
Zfp503	3,6098	0,005077473	0,039337002
Wdr60	3,6088	0,003841287	0,032056977
C1rl	3,6069	0,00326467	0,028382434
Fabp4	3,6020	0,006036795	0,044248845
Gm12971	3,5959	0,006939986	0,048954334
Cd86	3,5957	0,001720852	0,017719107
Epcam	3,5945	0,006323607	0,045852946
Scarb1	3,5938	0,000152215	0,002855687
Gm37468	3,5872	0,007107171	0,049759047
Plxdc2	3,5850	0,003777083	0,031677916
Adam15	3,5800	0,001935534	0,019236723
Rragd	3,5795	0,003451941	0,029598594
Lrp5	3,5795	0,000439882	0,006445743
Sh3pxd2b	3,5773	0,000139744	0,00267224
Zeb2os	3,5757	0,000137817	0,002641382
Hsf2	3,5738	6,51E-07	4,30E-05
Igsf6	3,5738	0,001406219	0,015096937
Ccrl2	3,5701	4,29E-06	0,000178458
Rasgrp3	3,5689	0,00069083	0,00886723
Gas2l3	3,5642	1,14E-08	1,88E-06
9430076C15Rik	3,5619	2,23E-05	0,000626615
Car9	3,5616	0,004736583	0,037387137
Slc27a1	3,5613	9,99E-05	0,002070944
Gm128	3,5487	0,006479307	0,046543199
Piwil4	3,5470	0,004567011	0,036540425
Fblim1	3,5470	0,003321834	0,028760806
Hfe	3,5425	0,001179961	0,013347562
Serping1	3,5398	0,006274774	0,045596872
Marcksl1	3,5396	0,000739301	0,009361145
Zfp704	3,5371	6,42E-08	7,68E-06
Gm16464	3,5370	0,000300862	0,004828111
Asb2	3,5360	0,001335807	0,014554085
Parvb	3,5327	3,87E-05	0,000970732
Gstt3	3,5309	0,005806962	0,042975085
Ryr1	3,5282	0,006398483	0,046236853
Dram1	3,5262	0,00021419	0,003693796
Ptprj	3,5245	8,96E-06	0,000311452
6430573P05Rik	3,5201	0,00667969	0,047555344
Chchd4	3,5187	1,93E-05	0,000567353
Rab11fip5	3,5133	0,003649959	0,030872725
Ampd3	3,5075	0,000562441	0,007671206
B830042I05Rik	3,5059	1,60E-05	0,000489401
Ang	3,5036	0,005261216	0,040297762
Ifitm2	3,4995	0,003849494	0,032077849
Cd101	3,4981	0,004872046	0,038130827
Scel	3,4943	0,000659419	0,008596882
Piwil2	3,4930	0,006686395	0,047563365
Acsl1	3,4929	6,22E-06	0,000234293
Cst3	3,4853	0,00018092	0,003270515
Col15a1	3,4850	0,005800766	0,042966936
Fcgr2b	3,4809	2,10E-06	0,00010177
Cisd1	3,4789	1,86E-05	0,000550855
Lin28b	3,4783	0,000270473	0,004461907
Slc27a6	3,4777	0,002294444	0,021850986
Dapk1	3,4771	0,00461391	0,036788342
Tusc1	3,4751	4,05E-07	3,03E-05
Anxa5	3,4699	3,70E-13	6,93E-10
Oas3	3,4637	3,72E-07	2,84E-05
Gm44270	3,4562	0,005306202	0,040525303
Fmnl2	3,4517	0,001359198	0,014723338
Gm37058	3,4498	0,001654782	0,017175111
Art2a-ps	3,4462	0,001787374	0,018182054
Rsad2	3,4450	1,47E-05	0,000458781
Plac8	3,4445	0,001319886	0,014455322
Ethe1	3,4421	0,001684042	0,017406994
Plk2	3,4421	4,50E-05	0,001098771

Gene	FC	pval	padj
Fancb	3,4397	0,005803875	0,042971099
Bst2	3,4355	1,16E-07	1,16E-05
Lilrb4a	3,4312	0,000400985	0,006007832
Gm17705	3,4304	0,00381956	0,03190723
Cdh1	3,4303	0,002144451	0,020858306
Lima1	3,4292	0,003331806	0,028832349
Slc7a11	3,4220	5,90E-05	0,001361217
Tmem106c	3,4211	0,000189779	0,003394282
Acp2	3,4196	4,72E-06	0,000191642
Cpd	3,4180	6,43E-11	3,19E-08
Pgap1	3,4073	0,000726442	0,009239834
Gm4951	3,4067	0,006729822	0,04777154
Dpp7	3,4028	0,000209866	0,003630352
Kmo	3,3969	0,005399488	0,040947739
Slc16a7	3,3932	0,002658655	0,024452787
Nid2	3,3863	0,002026386	0,019951558
Gm42515	3,3847	0,000335253	0,005245243
Angptl2	3,3847	0,000636534	0,008348192
Atp1a3	3,3835	0,00045373	0,006608477
Gm44949	3,3741	0,005322286	0,040602982
Sash1	3,3665	0,006682448	0,047555344
B3gnt3	3,3653	0,002660433	0,024452787
Bcl2a1b	3,3636	0,000520734	0,007279177
Dhx58	3,3625	5,60E-06	0,00021604
Rasa4	3,3566	0,000116515	0,002331137
Rogdi	3,3490	0,004260362	0,034830473
Dtx4	3,3459	0,005437814	0,041164348
2810002D19Rik	3,3424	1,04E-05	0,000349617
Cdkn1a	3,3387	1,03E-06	5,90E-05
Ctif	3,3387	0,001318939	0,014455322
Hk3	3,3372	0,000136588	0,002626779
Cln6	3,3307	4,72E-05	0,001131453
E230016K23Rik	3,3203	0,000841354	0,010275365
Ccnd1	3,3158	0,002385787	0,022504852
Tfe3	3,3126	1,31E-09	3,39E-07
Alas1	3,3113	1,67E-05	0,000505004
2900005J15Rik	3,3083	0,003441405	0,029538292
Evi2a	3,3072	2,70E-05	0,000732559
Ftl1	3,3071	6,68E-07	4,37E-05
Tbc1d9	3,2949	0,003448706	0,029585896
Ckb	3,2915	0,005105713	0,039465149
Msra	3,2900	4,36E-06	0,000181176
Pkib	3,2886	9,83E-05	0,002039862
Mt2	3,2880	0,00221855	0,021357342
Ifit2	3,2843	0,000130557	0,002516533
Mfsd11	3,2833	1,98E-07	1,77E-05
C920021L13Rik	3,2787	0,005289288	0,040439319
Hexa	3,2783	2,23E-07	1,96E-05
Bnip3	3,2759	0,000147368	0,002786441
5730409E04Rik	3,2736	0,000738647	0,009359893
Dnase2a	3,2652	0,000248798	0,004167063
AW209491	3,2568	0,000180088	0,003258983
Ctsl	3,2537	1,46E-06	7,89E-05
Ccl17	3,2483	0,004180421	0,034279241
Slc35f6	3,2428	2,91E-07	2,41E-05
Mx1	3,2422	8,51E-06	0,000301367
P4ha1	3,2356	7,19E-12	6,74E-09
Ppp2r2c	3,2307	0,00173753	0,017825534
Zfp516	3,2289	0,003360676	0,029037478
Fndc3b	3,2270	3,12E-05	0,000820536
Nectin3	3,2268	0,000373093	0,005694651
Gpr55	3,2247	0,002991489	0,026554976
Cep85l	3,2238	0,003238537	0,028213411
Blnk	3,2208	0,001624948	0,016917511
Gm44104	3,2188	0,003281763	0,028501656
Tceal8	3,2182	0,004282093	0,034974232
Tmem9	3,2138	5,17E-07	3,65E-05
Tanc2	3,2112	2,66E-05	0,000723117
Gm37354	3,2105	0,002794508	0,025353506
Tpd52	3,2099	0,000198497	0,003494628

Gene	FC	pval	padj
Gm9888	3,2081	0,00147885	0,015756334
Gatm	3,2050	0,005253493	0,040256888
Galc	3,1966	6,00E-06	0,00022749
Mvk	3,1962	0,000628087	0,008256678
Slc9a6	3,1952	7,98E-05	0,00173427
Tmem51	3,1762	0,000502309	0,007113298
Cd2ap	3,1754	0,000463629	0,006712081
Irf7	3,1747	5,04E-05	0,001198048
Dnase1l1	3,1685	0,000356952	0,005528335
Snx7	3,1682	6,39E-05	0,001452709
Sgcb	3,1677	0,001317587	0,014455322
Irak3	3,1575	0,003404606	0,029296979
Wdr41	3,1520	8,35E-10	2,51E-07
B430306N03Rik	3,1489	0,000847251	0,010317495
Stx3	3,1459	2,22E-07	1,96E-05
6820402A03Rik	3,1448	1,30E-05	0,000414844
Gm28727	3,1446	0,007051961	0,049413531
Pygl	3,1426	0,00210318	0,020551695
Gins2	3,1348	3,60E-05	0,000915022
B4galt6	3,1300	2,48E-05	0,000680155
Cmpk2	3,1266	6,69E-06	0,000247337
Pdgfa	3,1215	0,001730464	0,01777846
Ccdc18	3,1202	0,002276256	0,021714554
Fam46c	3,1122	5,31E-11	2,71E-08
Cep170b	3,1104	0,006974015	0,049112208
Pars2	3,1068	0,005088485	0,039368072
Cxcl3	3,1045	0,005830117	0,043127522
Dock7	3,1009	0,002095662	0,02049011
Tbc1d19	3,0969	0,007140185	0,049845346
Eepd1	3,0940	0,002209756	0,021297
Idh1	3,0891	0,00012766	0,002469301
Ifit1	3,0861	0,001510653	0,016054613
Myo5a	3,0824	0,000349346	0,005430482
Smox	3,0790	8,08E-09	1,45E-06
Rhbdf2	3,0744	0,000538472	0,00742589
Oxnad1	3,0689	0,000228849	0,003894827
F630040K05Rik	3,0667	3,92E-05	0,000981982
Fcgr3	3,0644	1,68E-06	8,64E-05
2310022B05Rik	3,0634	0,002007936	0,019804588
Cd302	3,0567	0,004972949	0,03879452
Pros1	3,0544	0,002570449	0,02383353
Gm42989	3,0527	0,000476739	0,006837307
Lpxn	3,0501	0,000127163	0,002467314
Vcan	3,0458	0,006329844	0,045878447
Nxpe5	3,0441	0,000288486	0,004701061
Gm42462	3,0404	0,005147972	0,039664551
Wrb	3,0380	1,29E-05	0,000411271
Prdx4	3,0378	0,000554509	0,00762212
Ncf1	3,0330	0,000119507	0,00236852
Cpne2	3,0319	0,000254541	0,004233818
Cstb	3,0179	2,25E-11	1,46E-08
Hbegf	3,0129	0,000315068	0,005008431
Coq3	3,0116	0,000831236	0,010188681
Rhag	3,0104	0,003559934	0,030308858
Gm38236	3,0031	0,002254299	0,021555786
Fdps	2,9979	0,001227467	0,013722695
1700030K09Rik	2,9966	0,001444127	0,015444925
Hvcn1	2,9895	3,61E-05	0,00091579
Tacc2	2,9860	0,001858168	0,018676909
5031439G07Rik	2,9820	0,001036222	0,012078037
Slc8a3	2,9816	0,007009709	0,049315097
Phf11d	2,9793	3,42E-05	0,000880143
Tada2a	2,9751	0,000583276	0,007857452
Lamp1	2,9695	4,63E-11	2,52E-08
Adamtsl4	2,9665	0,000284978	0,004661919
Arhgap19	2,9617	1,81E-11	1,27E-08
Mpp1	2,9610	2,83E-09	6,29E-07
Irf5	2,9555	0,001381857	0,014911327
4930539J05Rik	2,9508	0,006881953	0,048687508
Hsd17b7	2,9492	0,000292798	0,00474383

Gene	FC	pval	padj
Gm15832	2,9472	0,002090617	0,02045487
Dock4	2,9411	0,005144105	0,039652868
Tns1	2,9380	0,002682595	0,02462964
Mfsd13a	2,9332	0,002146943	0,020870518
Tdrkh	2,9293	0,002254501	0,021555786
Hdac9	2,9279	0,001832875	0,018549433
Mob3b	2,9240	0,001236107	0,013770261
Cd99l2	2,9237	0,000423812	0,006270182
Coq7	2,9233	0,000991805	0,011624584
Nudt1	2,9173	0,001053846	0,012190786
Tgfbr1	2,9166	7,29E-05	0,001615388
Wdr11	2,9148	0,000296458	0,004784211
Pik3r2	2,9128	0,000467067	0,006743452
Gpam	2,9088	0,003727949	0,031328144
Tmem50b	2,9063	2,23E-05	0,000627458
Cln8	2,9061	0,001065725	0,012286065
Pik3r6	2,9050	0,002762385	0,025129661
Gart	2,9049	2,62E-11	1,64E-08
Pgpep1	2,9040	0,000362197	0,005567705
Stard9	2,8998	0,003167389	0,027736856
Slfn3	2,8991	0,004926581	0,038504035
Aifm2	2,8837	0,001931005	0,019223637
H2-DMa	2,8796	0,005370756	0,040821619
Hsd17b11	2,8760	1,28E-05	0,000410899
Maf	2,8681	1,67E-06	8,58E-05
Cul7	2,8626	0,005325139	0,040602982
Skap2	2,8606	5,30E-06	0,000208622
Trpm2	2,8580	0,002408661	0,02265727
Chst14	2,8521	0,000726981	0,009239834
Fos	2,8506	0,000515842	0,007244123
Pwwp2b	2,8504	0,002070723	0,020318756
Nxt2	2,8436	1,04E-05	0,000349577
Cd300lf	2,8352	8,63E-10	2,51E-07
Pnp	2,8351	2,11E-07	1,87E-05
Npc2	2,8294	2,15E-08	3,21E-06
Lrrtm2	2,8286	0,001182043	0,013362154
Il2ra	2,8261	0,001199843	0,013500031
Gm12185	2,8188	0,001733392	0,017793905
Mgat4b	2,8131	3,15E-05	0,000828097
Tmem156	2,8070	0,000835079	0,01021352
1500011B03Rik	2,7944	0,004320124	0,03518262
Sat1	2,7907	0,00028428	0,004655014
Ptgs1	2,7890	0,001384116	0,014926151
Peli2	2,7856	0,007006573	0,049315097
Soat1	2,7855	3,45E-07	2,69E-05
Uevld	2,7839	0,000339667	0,005299553
Nfxl1	2,7761	1,15E-05	0,000378897
Loxl3	2,7757	0,005123951	0,039569849
Sh3tc1	2,7704	0,000391311	0,005892725
St3gal2	2,7615	0,000611623	0,008109776
Gm7160	2,7556	0,001601029	0,016730458
Sap30	2,7515	0,000203097	0,003546001
Bri3bp	2,7498	2,72E-05	0,000737003
Trpm4	2,7479	7,39E-05	0,001629842
Rnf141	2,7424	8,49E-12	7,16E-09
Gm37780	2,7422	0,002223791	0,021395586
Hint2	2,7398	0,006844523	0,048504087
Cndp2	2,7389	1,54E-14	5,91E-11
Arhgef12	2,7383	0,005271216	0,04032372
Anxa4	2,7378	4,07E-08	5,28E-06
Gaa	2,7330	4,64E-05	0,001121943
Nme6	2,7329	0,000830763	0,010188681
Eef1akmt1	2,7309	0,004664764	0,037057067
Abhd12	2,7291	5,36E-06	0,00020972
Fads1	2,7271	0,000184844	0,003327191
Ext1	2,7265	0,00695385	0,049031623
Zfp992	2,7242	3,29E-05	0,000853259
Lair1	2,7237	0,000122705	0,002417689
Mlh3	2,7207	0,007093346	0,049682879
Ppargc1b	2,7195	0,003870579	0,032237619

Gene	FC	pval	padj
Alcam	2,7109	0,000142127	0,002711664
Il1f9	2,7103	0,000878621	0,010578309
Msrb1	2,7035	0,000800007	0,00987769
Ifih1	2,7009	0,001537216	0,016214528
Ccdc88a	2,6899	0,00023235	0,003946444
Lyrm2	2,6850	8,75E-05	0,001863234
Tmem206	2,6841	4,02E-07	3,03E-05
H1f0	2,6812	0,000843172	0,010282677
Cd22	2,6809	0,002526627	0,023517706
Ogfrl1	2,6808	0,004524591	0,036373381
Yae1d1	2,6799	1,76E-10	7,07E-08
Ell2	2,6793	1,72E-05	0,000516062
Nol4l	2,6779	0,000142363	0,002713099
Cenpn	2,6729	0,003253384	0,028313509
Cyth3	2,6715	0,000245839	0,004125692
Galk1	2,6714	0,004540897	0,036417864
Nrp2	2,6675	0,003342896	0,028913482
Lap3	2,6563	2,05E-05	0,000592419
Mcfd2	2,6531	4,97E-06	0,000199492
Oas1a	2,6427	0,001175007	0,013300454
Creg1	2,6409	0,000385754	0,005844272
Rasal2	2,6386	0,005649585	0,042070766
Ddx60	2,6303	0,000779496	0,009688265
Gusb	2,6260	4,37E-07	3,20E-05
Tmem220	2,6169	0,00651563	0,04672305
Mpv17l2	2,6091	0,000583984	0,00786071
Sgk3	2,6078	0,001670187	0,017292436
Hexb	2,5992	8,95E-08	9,68E-06
Bpifc	2,5981	0,004659896	0,037037606
Sult6b1	2,5948	0,00299667	0,026572994
Xylt1	2,5944	4,39E-06	0,000181766
Mtmr10	2,5889	5,37E-06	0,00020972
Gpr146	2,5884	0,000277567	0,004558363
Cacna2d4	2,5876	0,000540634	0,007443536
Selenop	2,5875	3,00E-07	2,43E-05
Ly6e	2,5812	1,03E-05	0,000347348
Zfp839	2,5734	0,000189545	0,003394282
Stat2	2,5712	2,56E-05	0,00070061
Adam9	2,5677	1,06E-05	0,000355946
Rbpj	2,5673	0,000389515	0,005881434
Nagpa	2,5488	4,26E-06	0,000177845
Filip1l	2,5420	0,000490211	0,006988924
Atpif1	2,5416	4,53E-06	0,00018673
Wwc2	2,5410	0,002377799	0,022479793
Ero1l	2,5397	6,97E-07	4,47E-05
Vwa5a	2,5337	1,19E-07	1,19E-05
Cyfip1	2,5322	2,67E-06	0,000122922
Lamp2	2,5288	6,38E-05	0,001452709
Dnajc25	2,5268	1,02E-05	0,000345407
Plin3	2,5255	0,002381671	0,022491191
Mospd2	2,5228	0,001821793	0,01847646
Dse	2,5227	1,53E-07	1,46E-05
Trf	2,5185	0,00247409	0,023122939
Ano10	2,5181	0,000807006	0,009949536
Aldh6a1	2,5158	0,002441847	0,022905557
Ctsc	2,5099	3,51E-05	0,000897558
Pomk	2,5038	0,000688226	0,008840537
Eef1e1	2,5011	0,00023677	0,003993358
Trip13	2,4977	0,00264219	0,024391447
Gch1	2,4952	2,30E-05	0,000643208
Slc45a4	2,4928	1,46E-05	0,000457855
Nit2	2,4871	0,005216745	0,040048078
Milr1	2,4850	0,002815909	0,025465477
Lipa	2,4813	2,05E-09	5,01E-07
Atp6ap2	2,4786	9,66E-07	5,58E-05
Trappc6a	2,4772	0,001809717	0,018376087
Txndc15	2,4751	0,001305716	0,014380287
Ubac1	2,4693	0,00275587	0,025111023
Erbb3	2,4683	0,001204455	0,013542895
4931406C07Rik	2,4673	0,00484948	0,037989472

Gene	FC	pval	padj
Snx20	2,4575	0,000732005	0,009289694
Pfdn1	2,4498	0,002691806	0,024687333
Nkiras2	2,4427	0,002125104	0,020717919
Slamf6	2,4350	0,000959143	0,011320442
Emilin2	2,4243	0,00052487	0,007300376
Dram2	2,4195	9,64E-05	0,002008001
Swap70	2,4193	0,000687119	0,008833044
Umps	2,4172	7,03E-06	0,000257333
Gpx1	2,4152	0,007017445	0,049315097
Nadk	2,4117	0,000728097	0,009247056
Sgpl1	2,4086	6,55E-07	4,30E-05
Slc25a45	2,3981	8,11E-05	0,001751271
Igfbp4	2,3979	8,35E-06	0,000297022
Dclre1c	2,3915	3,00E-07	2,43E-05
Cep70	2,3862	0,001271345	0,014088374
Skp2	2,3807	8,74E-07	5,28E-05
Map4k3	2,3802	0,000874832	0,010575879
Hs1bp3	2,3792	0,00220648	0,021277884
Klc4	2,3791	0,001297779	0,014324829
Akap7	2,3781	0,006373339	0,046114429
Ocrl	2,3774	2,74E-05	0,00074046
Vps26a	2,3770	2,44E-10	9,56E-08
Specc1	2,3737	0,00024642	0,004131335
Mfsd1	2,3733	2,59E-12	3,12E-09
Prkcd	2,3686	0,001839548	0,018589464
Itgb3	2,3641	0,005385866	0,040918029
Dennd1a	2,3639	2,24E-08	3,28E-06
Dnhd1	2,3616	0,001948398	0,019330401
Coq4	2,3595	0,001557404	0,016365841
Smim13	2,3571	0,002503926	0,023345065
Cep76	2,3567	3,21E-05	0,000835924
Ets2	2,3513	2,06E-05	0,000593405
Slc43a2	2,3458	0,000574403	0,007776338
Nampt	2,3455	0,001084833	0,012472249
Chml	2,3443	0,003604145	0,030593943
Nek6	2,3411	0,000790486	0,009785599
Slc31a2	2,3383	0,001224547	0,013713951
Mthfr	2,3366	0,001535008	0,016214528
Dnajc4	2,3364	0,000681516	0,008796487
Il1rl1	2,3362	0,006897757	0,048742439
Fgd6	2,3323	0,000238996	0,004026888
Mcmdc2	2,3317	0,006268255	0,045569132
Serpinb6a	2,3279	0,000102979	0,002115516
Gla	2,3268	1,20E-07	1,19E-05
Ifit1bl1	2,3192	0,005355198	0,040758473
AI413582	2,3187	0,00031798	0,005035724
Pak4	2,3141	0,000170337	0,003122716
Blvra	2,3132	0,000634358	0,008328993
Frmd4b	2,3125	7,39E-06	0,000268046
Hic2	2,3123	0,006778633	0,048097781
Fam151b	2,3117	0,006653062	0,047426265
Dusp6	2,3066	0,000824796	0,01013922
Tln2	2,3023	0,000286034	0,004670134
Gm17259	2,3022	0,004469109	0,036114743
Amica1	2,2998	0,001205408	0,013544579
Frmd4a	2,2982	0,000254492	0,004233818
Prdx1	2,2973	1,62E-11	1,19E-08
Tep1	2,2939	0,000897494	0,01074318
Gm5615	2,2899	0,002115361	0,020646808
Smim3	2,2898	8,05E-05	0,001745583
Arl5c	2,2875	0,00217256	0,021070961
Naa40	2,2861	0,000987754	0,011585157
Cnpy3	2,2846	0,000520928	0,007279177
Abcg1	2,2841	5,52E-08	6,95E-06
Aacs	2,2826	0,000594374	0,007942211
Pofut2	2,2818	3,03E-05	0,000802324
Snx2	2,2770	3,90E-07	2,95E-05
Fam129b	2,2742	0,001743601	0,017855238
Dstyk	2,2626	0,0022529	0,021555786
Slc29a3	2,2622	0,001345208	0,014618735

Gene	FC	pval	padj
Heatr5a	2,2561	6,02E-09	1,13E-06
Fgd4	2,2556	0,00660169	0,047119804
Litaf	2,2533	5,62E-08	7,02E-06
Ctu1	2,2468	0,001066797	0,01229003
Dexi	2,2425	0,006074888	0,044508713
Ndrg1	2,2386	0,000222894	0,0038085
Hspbap1	2,2343	0,00540443	0,040966795
G6pdx	2,2301	3,50E-05	0,000896275
Rell1	2,2273	3,51E-06	0,000152327
Ssfa2	2,2248	2,21E-05	0,00062454
Zfp324	2,2245	0,002374268	0,022459006
Khk	2,2151	0,002864682	0,025740935
Bach1	2,2107	0,00098333	0,011565437
Abcg3	2,2087	0,006874372	0,048654281
Fam84b	2,2038	0,000324689	0,005113169
Cables1	2,1990	0,002698136	0,024731932
Pgd	2,1978	1,27E-08	2,06E-06
Treml2	2,1923	0,003973364	0,032882607
Erlin1	2,1810	0,00545478	0,041237258
Rab31	2,1795	0,000776966	0,009671071
Smim4	2,1760	0,001792496	0,018212188
Mtmr4	2,1672	0,000508162	0,007142214
Cyp4f13	2,1659	0,006411131	0,046288585
Svbp	2,1658	0,000397504	0,005964681
Nceh1	2,1652	0,000717133	0,009135319
Slc25a13	2,1632	0,001875937	0,018821866
Akr1a1	2,1624	3,11E-08	4,31E-06
Gm15601	2,1620	0,002391588	0,022546963
Tmem65	2,1601	8,84E-06	0,000308962
Brca2	2,1554	0,001845875	0,01863715
Erp29	2,1436	0,000205374	0,003574655
Cpped1	2,1405	5,69E-06	0,000218582
Tmem104	2,1381	0,001839098	0,018589464
Rflnb	2,1375	0,005554478	0,041636364
Tor3a	2,1358	0,000877454	0,010578309
Slc30a1	2,1340	8,01E-07	4,96E-05
Synj2	2,1316	0,006905595	0,048772935
Tspan3	2,1274	0,002514628	0,023418949
Lyn	2,1265	0,000755971	0,009507989
Mthfd2	2,1262	0,004666932	0,037057067
Sema4b	2,1246	3,09E-11	1,86E-08
Itpripl2	2,1244	9,54E-05	0,001991913
Smpdl3a	2,1237	0,003039749	0,026856159
Smad1	2,1223	0,003015685	0,026713521
Pank1	2,1215	0,000860794	0,010467307
Il4ra	2,1202	2,65E-05	0,00071982
D630030B08Rik	2,1191	0,002462773	0,023037786
Rnh1	2,1184	5,25E-07	3,69E-05
Tbcc	2,1157	0,005646729	0,042070766
Cd274	2,1103	0,000454232	0,006610072
Qpct	2,1046	0,003429521	0,029481294
Dhrs4	2,1001	0,002324651	0,022101221
Tmem55b	2,0990	0,001631209	0,016961757
Rpain	2,0936	0,000414634	0,006164088
Hilpda	2,0898	0,000669308	0,008696877
Serp1	2,0881	2,07E-05	0,000595236
Osbpl1a	2,0844	0,005743291	0,04261608
Agpat5	2,0790	0,001146042	0,013033813
Ifi213	2,0767	0,006496309	0,046604316
Minpp1	2,0733	6,93E-05	0,001559548
Gpr157	2,0696	0,003823049	0,031920569
Klhl5	2,0681	3,16E-06	0,000140438
Slc11a2	2,0653	9,57E-07	5,55E-05
Rtp4	2,0651	0,006966008	0,049083828
Syce2	2,0603	0,0003482	0,005417654
Ctsa	2,0573	0,000170721	0,003122974
Taldo1	2,0539	8,71E-05	0,001857097
Fam102b	2,0364	0,000498993	0,007078236
Atp6v1c1	2,0350	5,16E-08	6,55E-06
Ctso	2,0338	1,86E-06	9,19E-05

Gene	FC	pval	padj
Abhd4	2,0310	0,001852053	0,018647524
Slc6a6	2,0304	1,85E-06	9,19E-05
Jup	2,0300	2,40E-09	5,55E-07
Tbl3	2,0295	0,003033777	0,02683151
Gpr137b	2,0276	2,77E-05	0,000747297
Ahcyl2	2,0231	0,001977096	0,019554664
Tmcc3	2,0229	0,000963224	0,011352713
Myadm	2,0180	0,003783688	0,03171754
Atp6v1b2	2,0166	1,72E-06	8,69E-05
Zfp235	-2,0003	0,006446108	0,046441713
Mfsd4a	-2,0011	3,35E-09	7,15E-07
Znrf3	-2,0017	0,002199136	0,021231039
Ms4a4b	-2,0083	0,002824533	0,025529785
P2ry10	-2,0188	0,002510536	0,023393761
Gse1	-2,0229	0,000224395	0,003822881
Gm27271	-2,0235	0,001743437	0,017855238
Gm37387	-2,0265	0,005948502	0,043830244
Tsr3	-2,0312	0,000664603	0,008649071
Tas1r3	-2,0339	0,004960951	0,038718831
Tspan32	-2,0447	3,17E-05	0,000830376
Cers4	-2,0462	0,000757756	0,009516248
Chsy1	-2,0539	0,002044601	0,020107432
Snord104	-2,0626	0,004209045	0,034444326
Orm2	-2,0631	0,00563287	0,042038665
Asrgl1	-2,0796	3,84E-05	0,000965562
9430087J23Rik	-2,0873	0,007041807	0,049403961
Fam122b	-2,0917	0,000602248	0,00802965
Gm16575	-2,1047	0,007028646	0,049332144
Gramd4	-2,1151	0,001783491	0,018153503
Gem	-2,1203	0,002687946	0,024665341
Tmco6	-2,1229	0,005470037	0,041282117
Gimap6	-2,1248	0,004731182	0,037375233
Trbc2	-2,1275	0,00594546	0,043830244
Hmces	-2,1293	0,000321695	0,005085009
Agap2	-2,1299	0,000571046	0,007760892
Epha1	-2,1433	0,000532715	0,007371486
Lsm11	-2,1453	0,00404711	0,033361955
Fyn	-2,1565	0,000634576	0,008328993
Chst11	-2,1568	0,00123222	0,013745116
Mctp2	-2,1610	0,002177769	0,021097216
Zscan20	-2,1611	0,001475333	0,015738748
Scfd2	-2,1617	0,000333114	0,005221462
Poc5	-2,1681	0,000674501	0,00873072
Zdhhc18	-2,1771	3,07E-05	0,000810729
Klhl12	-2,1854	9,01E-08	9,68E-06
Zfp212	-2,1895	1,57E-07	1,48E-05
Snx33	-2,1918	0,001266156	0,014040094
Pdcd4	-2,1934	1,81E-07	1,68E-05
Jakmip1	-2,1967	0,000891701	0,010688999
Zbtb16	-2,1978	0,005297491	0,040483678
Sp4	-2,2004	8,94E-06	0,000311452
Ipcef1	-2,2152	7,67E-07	4,85E-05
Gm37912	-2,2166	0,001325399	0,014483674
Bach2	-2,2202	1,27E-06	7,03E-05
Rasal3	-2,2232	5,43E-05	0,001273546
Gm44226	-2,2299	0,001588126	0,016626531
Gimap5	-2,2328	0,001724589	0,01774675
Ablim1	-2,2330	0,002197747	0,021231039
Mxd4	-2,2348	1,25E-05	0,000404076
Tmtc4	-2,2354	2,48E-07	2,15E-05
Mmgt2	-2,2388	0,000313716	0,004996345
Ccnd2	-2,2395	7,43E-08	8,46E-06
Gm14300	-2,2461	0,003574686	0,03039863
Tulp4	-2,2489	4,16E-06	0,000175466
Gm18988	-2,2513	0,002367376	0,022418956
Card6	-2,2521	4,77E-06	0,000193411
Kif21b	-2,2541	3,61E-08	4,83E-06
1700025G04Rik	-2,2542	0,004533457	0,036392806
Fzd5	-2,2558	0,003219255	0,028088955
Pde7a	-2,2559	4,15E-09	8,47E-07

Gene	FC	pval	padj
Adamts10	-2,2600	0,000105686	0,002163221
Gm15232	-2,2624	0,005271174	0,04032372
Fasl	-2,2636	0,004488828	0,036137741
Smad3	-2,2717	0,000387614	0,005863228
Vps37b	-2,2744	0,00041396	0,006163311
Spata13	-2,2811	1,83E-05	0,000544781
B130055M24Rik	-2,2832	0,006703091	0,047662032
Sh2d3c	-2,2882	9,58E-07	5,55E-05
Gm26189	-2,2928	0,003387798	0,029167996
Glcci1	-2,2976	0,001255291	0,013937949
Cbarp	-2,2998	0,001519498	0,016117162
Phf1	-2,3133	1,76E-06	8,89E-05
Hcst	-2,3144	0,002648696	0,024438137
Rfx3	-2,3178	8,85E-08	9,68E-06
Gigyf1	-2,3193	0,000167236	0,003082632
Gm36940	-2,3215	0,000122646	0,002417689
Mag	-2,3215	0,004363556	0,035416803
Prkcq	-2,3233	0,005065053	0,03927706
Gabbr1	-2,3322	0,002598835	0,024043859
Plekhg2	-2,3368	1,22E-06	6,83E-05
Polm	-2,3405	0,000507426	0,007142214
Gpr174	-2,3420	0,001031483	0,012039441
Plppr3	-2,3438	2,39E-06	0,000113776
Adora2a	-2,3457	0,001709251	0,017631943
Abtb2	-2,3459	0,001365625	0,014773976
Scml4	-2,3462	0,004764616	0,037527065
Arap2	-2,3546	0,000783179	0,009726876
Farp1	-2,3559	0,00139967	0,015056893
Asap2	-2,3566	0,00011685	0,002335053
Dgka	-2,3576	4,33E-05	0,001064074
4833403J16Rik	-2,3711	0,00687423	0,048654281
Gm38384	-2,3713	0,000293097	0,004744125
Dusp2	-2,3731	2,65E-05	0,00071982
Serpinb9	-2,3785	0,00353235	0,030184484
Gm10125	-2,3818	0,000164387	0,003036741
Enpp5	-2,3856	0,003709454	0,031219388
Lax1	-2,3964	0,004671133	0,037057067
Tmc8	-2,4020	1,83E-05	0,000544781
Rasgrp2	-2,4150	1,71E-05	0,000514664
Setbp1	-2,4156	0,000468614	0,006755258
Klri2	-2,4185	0,006898387	0,048742439
B3gnt7	-2,4250	0,000454903	0,006614128
Ikzf3	-2,4307	0,000322781	0,005097402
Gm7967	-2,4362	0,001188182	0,013413574
Nlrc3	-2,4368	0,000665532	0,008654481
Gadd45gip1	-2,4409	0,003891399	0,032363086
Apol7e	-2,4415	0,005539358	0,041559966
Gm12763	-2,4437	0,002786721	0,025323725
Cnrip1	-2,4480	0,000358759	0,005537776
Tob1	-2,4484	4,11E-05	0,001015684
Ndnf	-2,4659	0,001070358	0,012314231
Eml2	-2,4703	0,006159931	0,044994972
Hip1r	-2,4766	1,95E-05	0,000571167
Gm37963	-2,4824	0,00551533	0,041443469
Ccnd3	-2,4842	3,32E-05	0,000857085
Hs3st3b1	-2,4858	0,000350825	0,005448453
Gm28100	-2,4902	0,004471388	0,036114743
Galntl6	-2,4907	0,000843146	0,010282677
Zhx2	-2,4925	7,85E-05	0,001711561
Atxn7l2	-2,4973	0,000683698	0,008796487
Cd247	-2,4990	0,006862014	0,048607611
Zdhhc15	-2,5014	0,003433101	0,029497038
Pim2	-2,5067	1,64E-06	8,51E-05
Gfod1	-2,5085	0,001185594	0,013393321
Cbx7	-2,5108	0,002765813	0,025147281
Klre1	-2,5115	0,003575885	0,03039863
Nxpe3	-2,5139	1,07E-05	0,000358192
Ubxn11	-2,5222	0,00152714	0,0161687
Itgb7	-2,5223	2,30E-06	0,000110328
B930095G15Rik	-2,5259	0,001872378	0,018797335

Gene	FC	pval	padj
Acap1	-2,5372	0,002084618	0,020417633
Pear1	-2,5381	0,004504372	0,036228294
Zfp420	-2,5476	0,000145134	0,002757286
Lrrc75a	-2,5479	0,000292116	0,004739181
Gm43062	-2,5483	0,000670054	0,008699865
Ptpn4	-2,5559	3,28E-06	0,000144303
Slc2a4rg-ps	-2,5567	0,000287283	0,004685998
Rundc3b	-2,5570	0,002256548	0,021563139
Zfhx2	-2,5661	5,28E-07	3,70E-05
S1pr4	-2,5672	0,001620789	0,016895072
Fam184a	-2,5690	0,002183981	0,021145248
Rab37	-2,5776	0,00367757	0,031028465
Ets1	-2,5802	0,000410616	0,006123295
Spry2	-2,5843	0,001352185	0,014666203
F2rl1	-2,5848	0,004910885	0,038399158
Vopp1	-2,5883	3,01E-06	0,000135457
Gm37034	-2,5927	0,003894873	0,032376008
Fam65b	-2,5936	6,14E-06	0,000232376
Zfp300	-2,5954	0,001853033	0,018647524
Lpin1	-2,6020	0,000370298	0,005662229
6330409D20Rik	-2,6069	0,003235765	0,028203838
C030034L19Rik	-2,6086	0,004811659	0,037780931
Atp2a3	-2,6125	0,000140772	0,002688865
Tbc1d10c	-2,6142	0,002234263	0,021467065
Tmem71	-2,6146	0,000190652	0,003406281
Gimap8	-2,6159	0,00100266	0,011727362
Ccdc88c	-2,6186	6,79E-05	0,001534207
Izumo4	-2,6205	0,002605005	0,024087726
Zfp275	-2,6211	3,50E-05	0,000896275
Dpy19l3	-2,6212	5,88E-08	7,24E-06
Rab11fip4	-2,6245	4,82E-06	0,000195123
Gimap4	-2,6334	0,000297826	0,004797641
Gm36932	-2,6461	0,005521014	0,041459224
Sorbs1	-2,6462	0,006315817	0,045835874
Syne3	-2,6479	0,00082999	0,010188681
Sorcs2	-2,6504	0,005251116	0,040256888
Hsd11b1	-2,6531	0,002608336	0,024092116
Satb1	-2,6555	0,001904233	0,019037814
Gm11346	-2,6566	0,001278021	0,014134491
Sbk1	-2,6587	0,003348468	0,028946831
Zfp937	-2,6614	6,47E-07	4,30E-05
Gm19585	-2,6617	0,00030209	0,004841674
Gimap3	-2,6746	0,000390633	0,005887775
Phf21b	-2,6818	0,001977959	0,019554664
Gm26762	-2,6828	7,31E-05	0,001618872
Fcho1	-2,6886	2,82E-05	0,000759875
Amigo1	-2,6931	8,39E-06	0,000297915
Gm38224	-2,6959	1,70E-06	8,67E-05
Slc25a53	-2,6991	9,14E-06	0,000317079
Ddx43	-2,7161	0,00036473	0,005587917
Gm38126	-2,7247	0,003661908	0,030931385
Prkca	-2,7294	0,000154584	0,002890476
Borcs7	-2,7472	0,000374248	0,005707109
Ncr1	-2,7587	0,000581162	0,007841503
H2-Ob	-2,7596	0,005396804	0,040947739
Gm42822	-2,7621	0,000171547	0,003134685
Zdhhc12	-2,7624	0,00114016	0,012975665
Raver2	-2,7726	0,000415135	0,006164088
Ifng	-2,7755	0,002127237	0,020726736
Klrb1f	-2,7787	2,79E-07	2,35E-05
6030443J06Rik	-2,7820	0,00140841	0,015101231
Klra9	-2,7888	0,000280098	0,004595464
Dyrk2	-2,7973	6,55E-13	1,11E-09
2810039B14Rik	-2,8023	0,000586734	0,007878867
Gm42684	-2,8033	5,11E-05	0,001210684
Rnf157	-2,8039	0,000210426	0,003636325
Gm37368	-2,8091	0,003544053	0,030246721
Aknaos	-2,8117	1,37E-05	0,000433426
Cd27	-2,8144	0,000626856	0,008248643
Ryr3	-2,8162	0,005363723	0,040804938

Gene	FC	pval	padj
Amotl1	-2,8176	0,000719775	0,009162063
Gm12216	-2,8290	4,10E-06	0,000173651
Mgst2	-2,8322	0,000145172	0,002757286
Nkg7	-2,8449	0,001215933	0,013626529
Gm14276	-2,8462	0,005029351	0,039143993
Adamts14	-2,8502	0,001148735	0,013046842
Pias3	-2,8602	0,000167925	0,003091953
Spn	-2,8622	1,57E-06	8,26E-05
Klrd1	-2,8640	6,32E-05	0,001442291
Gsta3	-2,8739	0,005794557	0,042939809
Klrb1c	-2,8860	0,00016848	0,003098779
Gm19557	-2,8943	1,48E-06	7,91E-05
Gm43753	-2,8962	0,00615743	0,044994972
Gpc1	-2,9001	0,000472371	0,006803597
Skap1	-2,9016	0,000902241	0,010777052
Slc26a10	-2,9186	0,000196287	0,003470199
Gm36931	-2,9218	0,000223725	0,003815316
Bcl9l	-2,9279	2,58E-06	0,000121446
Camk2n1	-2,9356	0,000523258	0,007299273
Gm37023	-2,9371	0,002666202	0,02449246
Klrk1	-2,9466	6,93E-07	4,46E-05
Plcb4	-2,9469	2,76E-06	0,000125356
Lrrn4cl	-2,9482	0,001339478	0,014575246
Il12rb2	-2,9508	1,25E-05	0,000404076
Cfap74	-2,9538	0,005773599	0,042803305
Gm38243	-2,9615	0,000112287	0,002262648
Srpk3	-2,9651	0,005039564	0,039151212
Elovl7	-2,9716	0,005211121	0,040048078
Zpbp	-2,9719	0,0029269	0,026132925
D8Ertd82e	-2,9775	1,43E-05	0,000449383
A930024E05Rik	-2,9824	0,001956796	0,01938651
Sell	-2,9841	0,000562628	0,007671206
Gm29237	-2,9843	0,001849222	0,018637722
Dnah8	-2,9860	0,002252181	0,021555786
Aff3	-2,9865	0,002458534	0,023023668
Rbm46os	-2,9882	0,005954369	0,043835177
Mir6924	-2,9928	0,00417922	0,034279241
Tmtc1	-3,0047	0,000884548	0,010633491
Dab2ip	-3,0111	0,000311767	0,004974702
Gm4956	-3,0119	0,000169889	0,003117897
F2rl2	-3,0162	9,62E-05	0,002004686
Gm42572	-3,0176	6,78E-06	0,000250175
Thefc	-3,0222	0,000143643	0,002734398
Gm4759	-3,0256	0,000137749	0,002641382
A430078G23Rik	-3,0299	7,92E-07	4,95E-05
Zfp473	-3,0306	0,000594748	0,007942211
4930577N17Rik	-3,0377	0,002280394	0,021741733
Stat4	-3,0381	2,82E-07	2,35E-05
D130040H23Rik	-3,0412	4,61E-05	0,001116859
Gm16334	-3,0441	0,000951444	0,011237433
B3gnt5	-3,0484	3,15E-07	2,51E-05
Zfp831	-3,0497	0,000101749	0,002099859
Gzma	-3,0503	0,000918247	0,010929485
Klri1	-3,0534	2,77E-07	2,35E-05
Klra13-ps	-3,0556	0,000934387	0,011089226
Gm37469	-3,0667	0,001417246	0,015186327
Arhgef18	-3,0762	2,66E-06	0,000122843
Chrne	-3,0843	0,000746432	0,0094302
Katnb1	-3,1021	4,59E-05	0,001116311
Sytl3	-3,1024	7,38E-05	0,001629842
Llgl2	-3,1043	0,000361638	0,005565139
Dlg3	-3,1060	1,09E-05	0,000362876
Traip	-3,1175	0,005646145	0,042070766
Klra14-ps	-3,1181	0,005904759	0,043583456
Theam	-3,1228	0,000787575	0,009767088
Itgam	-3,1275	0,002418897	0,022728201
Gm17552	-3,1393	0,006441942	0,046431539
Cdk5rl	-3,1566	0,003816682	0,03190723
Gm38228	-3,1567	0,004548112	0,036441073
Cuedc1	-3,1581	0,002597091	0,024040906

Gene	FC	pval	padj
C230085N15Rik	-3,1584	0,001060987	0,012239815
Tpmt	-3,1676	0,00554738	0,041601651
Rfx2	-3,1713	0,000753546	0,009491642
Mcam	-3,1889	0,006170168	0,045030744
Mirt1	-3,2021	6,82E-07	4,41E-05
Klra6	-3,2052	0,000683754	0,008796487
Nkd1	-3,2065	0,006000305	0,044038795
AI847159	-3,2176	6,09E-07	4,14E-05
Zfp174	-3,2265	0,000744464	0,009412393
Kcnj8	-3,2275	0,003421379	0,029426303
Tbx21	-3,2584	0,000482147	0,006897272
Gm44775	-3,2623	0,007126941	0,04981475
Zfp78	-3,2667	0,001553875	0,016338942
Gm13807	-3,3030	0,00029967	0,004822743
Rnf125	-3,3281	0,000390538	0,005887775
Gm16239	-3,3301	0,001327284	0,014489298
Lat	-3,3363	8,60E-06	0,000303524
Cdc20b	-3,3374	0,006205809	0,045188555
Gm11212	-3,3486	0,001282945	0,014179649
Scn3b	-3,3522	0,002314933	0,022021241
E430014B02Rik	-3,3599	2,30E-05	0,000643208
Gm37520	-3,3623	0,001100118	0,012587915
Gm26792	-3,3633	0,00303666	0,026842933
Pxylp1	-3,3658	0,000455491	0,006616976
Rab6b	-3,3677	1,52E-06	8,02E-05
Pde2a	-3,3799	0,001124469	0,012817108
Cspg5	-3,3856	0,000874587	0,010575879
Gm37766	-3,3884	0,00705047	0,049413531
Gm16845	-3,3931	7,64E-05	0,001673521
Itga2	-3,4299	0,000790808	0,009785599
Dnase1	-3,4399	0,004323136	0,03519016
Gm29123	-3,4493	5,34E-05	0,001256154
Gm37248	-3,4546	0,000232617	0,003946997
Bach2it1	-3,4637	0,000107048	0,002185323
1700007L15Rik	-3,4644	0,002198308	0,021231039
Gm43647	-3,4701	0,000575113	0,007776338
1700105P06Rik	-3,4732	0,005065078	0,03927706
Gm38118	-3,4837	8,71E-05	0,001857097
Gm24119	-3,4915	0,000878703	0,010578309
Klf12	-3,5213	0,005460429	0,041261469
Mss51	-3,5310	7,73E-05	0,001690112
Adgrl4	-3,5421	0,000604742	0,008056541
Gm37452	-3,5562	0,002249897	0,021555786
Gm37266	-3,6046	4,42E-05	0,001081011
Qprt	-3,6333	2,50E-07	2,15E-05
Gm38026	-3,6687	7,46E-11	3,52E-08
Il18rap	-3,6876	0,000127667	0,002469301
Gm27240	-3,6975	8,00E-06	0,000285953
Tshz3	-3,7046	7,63E-07	4,84E-05
Gm10490	-3,7227	0,005951767	0,043835154
Gm37856	-3,7237	0,000617795	0,008165929
Il18r1	-3,7249	0,000353624	0,005486868
Ccl5	-3,7268	1,96E-06	9,60E-05
Klrc3	-3,7289	6,39E-06	0,000238516
Klrc1	-3,7419	9,63E-08	1,02E-05
Gm43858	-3,7476	0,000100272	0,002075076
Arl4d	-3,7639	3,11E-06	0,000138966
Heatr9	-3,7718	2,33E-06	0,000111109
Gm29155	-3,7721	0,001520361	0,016117162
Gm26580	-3,7824	0,000530699	0,007358274
Slc2a10	-3,7876	0,002854147	0,025673627
Baiap3	-3,7900	5,23E-06	0,000206639
Bmx	-3,7967	0,006157123	0,044994972
Gm28277	-3,8091	0,004800377	0,037727473
Proca1	-3,8112	0,00360793	0,030593943
Ap3s1-ps2	-3,8193	0,00616676	0,04502536
Rac3	-3,8304	0,00384593	0,032074109
Plekhg5	-3,8433	1,41E-06	7,69E-05
S1pr5	-3,8528	7,08E-05	0,001580211
C330011M18Rik	-3,8535	2,96E-07	2,42E-05

Gene	FC	pval	padj
Gm16479	-3,8803	3,17E-05	0,000830735
Gm43967	-3,8934	0,003541061	0,030239762
St6galnac2	-3,8970	0,002366617	0,022418956
Cacna2d2	-3,9093	0,000275121	0,004530799
Scn11a	-3,9104	0,004737123	0,037387137
Klrb1a	-3,9106	1,18E-06	6,66E-05
A630072L19Rik	-3,9410	0,000161778	0,002994523
2010300F17Rik	-3,9508	0,000362465	0,005567705
Gm15854	-3,9771	0,001048014	0,012173417
Gm25106	-3,9846	0,000585039	0,007864401
Slc5a11	-3,9850	0,003557623	0,030308858
Gm29157	-3,9885	0,000977661	0,011506795
Btbd11	-3,9893	6,12E-09	1,13E-06
Gm43203	-3,9989	0,00069509	0,008908592
Sync	-4,0100	0,004640145	0,036950275
Gm22779	-4,0156	0,004021109	0,033212551
Gm10130	-4,0317	0,000918891	0,010929485
RP24-462O14.2	-4,0429	0,00205206	0,02016902
Gm5395	-4,0483	0,005216538	0,040048078
Gm8482	-4,0677	0,005907256	0,043583456
Gm38309	-4,0683	4,38E-05	0,001073343
Kcnc1	-4,0885	0,000216157	0,003716321
Gm44280	-4,1261	0,004528881	0,036373381
Clnkos	-4,1977	0,000987167	0,011585157
Gm24616	-4,2094	0,000503739	0,007122534
Unc5cl	-4,2357	0,002839498	0,025575213
Klrc2	-4,2430	6,87E-09	1,26E-06
Prss27	-4,2561	0,002888945	0,025876237
Gm614	-4,2576	0,000494188	0,007035618
Grhl2	-4,2696	0,001846477	0,01863715
Gm43172	-4,2778	0,002503265	0,023345065
Gm44081	-4,2817	0,003613664	0,030627161
Serpini1	-4,3080	8,82E-08	9,68E-06
Gm15556	-4,3334	0,002942025	0,026212468
Bmp10	-4,3340	0,000377284	0,00574822
Gm37261	-4,3406	0,002790196	0,02532801
Cldnd2	-4,3661	0,000175943	0,003190811
Gm21909	-4,3749	6,17E-08	7,49E-06
Gm37176	-4,3865	7,39E-05	0,001629842
4930447F24Rik	-4,3972	0,002827389	0,02554191
5430400D12Rik	-4,4881	0,002333397	0,022158831
Sspo	-4,5466	0,001163149	0,013186997
Klrb1	-4,5679	8,89E-07	5,32E-05
Camsap3	-4,5932	0,000250053	0,004175638
Dpf3	-4,6181	0,000610612	0,008107581
Gm43913	-4,7193	1,47E-05	0,000458271
Gm37593	-4,7815	1,01E-05	0,000343127
Gm26744	-4,8260	0,000189589	0,003394282
Muc4	-4,8310	2,29E-05	0,000641541
Cyp17a1	-4,8839	0,000192745	0,003436411
E230020A03Rik	-4,8899	6,86E-05	0,001547413
G0s2	-4,8961	0,000137352	0,002638481
Gm45107	-4,9157	0,000702219	0,008972448
Gm10505	-4,9823	0,000295173	0,004768565
2810468N07Rik	-5,0317	8,31E-05	0,001788622
Gm25635	-5,0351	7,14E-05	0,001591478
St6galnac3	-5,0677	4,70E-05	0,001131453
Gm6934	-5,0965	1,47E-06	7,91E-05
Wdr86	-5,2021	5,11E-05	0,001210684
Gm13375	-5,2803	1,94E-05	0,000569297
Fibcd1	-5,3396	0,000234316	0,00397183
Cdc42ep1	-5,3751	3,14E-07	2,51E-05
Fam132b	-5,4068	3,03E-05	0,000801185
Gpr63	-5,8914	1,95E-05	0,000571167
Fam124b	-6,0189	8,22E-06	0,000293271
Cym	-6,0304	7,67E-06	0,00027591
D830036C21Rik	-6,4157	4,21E-06	0,000176364
Nap1l5	-6,5811	1,07E-07	1,10E-05
Tmem74b	-6,7548	7,32E-07	4,66E-05

Table A.4. Comparison IV. All differentially expressed genes from the comparison IV: uterine Eomes^{+}CD49a^{+} (trNK) subset vs uterine Eomes^{+}CD49a^{-} (cNK) subset. FC: fold change, padj: adjusted p-value.

Gene	FC	pval	padj
Msr1	8,9447	2,05E-38	8,35E-35
Tlr1	8,4375	3,27E-25	1,30E-22
Clec7a	8,3704	3,17E-32	4,70E-29
Ptafr	8,3361	2,78E-31	3,24E-28
Mertk	8,3072	9,34E-29	6,63E-26
Tfec	8,2760	8,46E-16	1,05E-13
Ccl2	8,1743	1,94E-28	1,32E-25
Kdr	7,9454	7,78E-17	1,13E-14
Fcgr1	7,8447	8,27E-32	1,04E-28
Adap2	7,8357	6,39E-29	4,74E-26
Fmn1	7,8109	2,34E-24	8,10E-22
Ccl7	7,8036	3,87E-18	6,79E-16
C3ar1	7,7980	1,52E-36	4,96E-33
Cd109	7,7791	6,31E-11	3,63E-09
Mafb	7,7463	3,38E-53	5,51E-49
Slco2b1	7,6934	2,31E-12	1,62E-10
Rab7b	7,6169	6,46E-19	1,21E-16
Tlr13	7,5709	3,68E-28	2,31E-25
P2ry13	7,5662	3,06E-22	8,32E-20
Havcr2	7,5475	1,88E-21	4,49E-19
Cebpa	7,5472	6,09E-20	1,24E-17
Itga9	7,5421	1,24E-33	2,88E-30
Atrnl1	7,4969	2,69E-15	3,09E-13
Slc8a1	7,4545	4,20E-13	3,55E-11
Cd300c2	7,4541	5,07E-19	9,61E-17
Plb1	7,3793	9,91E-12	6,49E-10
Hck	7,3716	9,90E-26	4,48E-23
Gdpd1	7,3617	7,02E-14	6,47E-12
Hgf	7,3465	1,05E-12	8,34E-11
Wfdc17	7,3462	5,88E-28	3,55E-25
Ifitm1	7,3438	1,60E-12	1,18E-10
C5ar1	7,3242	3,18E-28	2,08E-25
Oas2	7,2879	8,77E-34	2,39E-30
Ahnak2	7,2839	1,64E-12	1,21E-10
Adgre1	7,2719	1,18E-42	9,64E-39
Wdfy3	7,2473	5,83E-42	3,17E-38
Rab3il1	7,1989	1,83E-11	1,12E-09
Lpcat2	7,1984	5,16E-30	4,67E-27
Lrp12	7,1336	5,52E-09	2,30E-07
Plxna1	7,1234	1,39E-23	4,44E-21
Stra6l	7,1141	5,50E-14	5,18E-12
C1qb	7,1126	1,81E-33	3,28E-30
Ctnnd2	7,1093	8,22E-10	4,03E-08
Ctsh	7,1003	1,54E-33	3,13E-30
Zfp385a	7,0836	2,99E-12	2,07E-10
Fam20c	7,0804	1,59E-17	2,45E-15
Rin2	7,0714	1,38E-16	1,94E-14
Flrt3	7,0249	6,59E-14	6,14E-12
Nlrp3	7,0179	1,41E-15	1,68E-13
Anxa3	7,0171	1,63E-23	5,12E-21
Lyve1	6,9838	7,55E-11	4,26E-09
Tlr8	6,9575	3,63E-18	6,43E-16
Pparg	6,9428	1,07E-12	8,47E-11
Cttnbp2nl	6,9368	1,32E-20	2,86E-18
Vcam1	6,9336	1,49E-27	8,38E-25
Rnf144b	6,9333	2,49E-13	2,15E-11
Pla2g7	6,9005	2,14E-16	2,86E-14
Csf2rb	6,8868	2,50E-29	2,15E-26
Fkbp9	6,8677	1,12E-08	4,39E-07
Lacc1	6,8511	4,86E-21	1,12E-18
Pltp	6,8345	1,67E-13	1,51E-11
Eps8	6,8243	7,61E-25	2,82E-22
Pld4	6,8175	2,62E-25	1,07E-22
Mmp14	6,7887	1,44E-16	2,00E-14
Psd3	6,7770	8,37E-12	5,53E-10
Pf4	6,7765	1,03E-09	4,94E-08
Acvr1	6,7657	2,07E-10	1,11E-08
Sirpa	6,7639	4,57E-32	6,21E-29
Gpnmb	6,7617	3,89E-26	1,86E-23
Tnfaip2	6,7610	1,22E-15	1,47E-13

Gene	FC	pval	padj
Pdpn	6,7391	6,77E-12	4,55E-10
Clec4a3	6,7297	2,36E-25	9,87E-23
Axl	6,7168	5,47E-31	5,95E-28
Lyz1	6,7109	1,00E-09	4,83E-08
Gzmf	6,7063	1,12E-10	6,21E-09
Plekhg1	6,7060	3,10E-11	1,85E-09
Fzd7	6,6991	1,15E-12	8,86E-11
Spi1	6,6975	7,44E-14	6,81E-12
Atp6v0a1	6,6968	1,48E-21	3,60E-19
Stxbp1	6,6862	1,09E-11	7,07E-10
H2-Eb1	6,6777	4,87E-33	7,95E-30
Reps2	6,6472	1,84E-10	9,89E-09
Tnip3	6,6460	1,18E-12	9,05E-11
Mefv	6,6459	3,45E-13	2,95E-11
Mgat3	6,6338	6,72E-08	2,31E-06
Cdkl2	6,6336	1,42E-09	6,62E-08
P2ry1	6,6296	9,32E-09	3,71E-07
Cd33	6,6224	1,46E-25	6,27E-23
Hmox1	6,6153	5,11E-22	1,37E-19
Thbs1	6,5927	1,37E-27	7,95E-25
Ecm1	6,5869	1,74E-11	1,09E-09
Gpr84	6,5786	4,72E-11	2,74E-09
Anpep	6,5614	4,50E-26	2,10E-23
Arl11	6,5585	1,10E-12	8,63E-11
P2rx7	6,5476	3,54E-17	5,25E-15
Gzmd	6,5432	3,34E-15	3,78E-13
Tifa	6,5418	1,31E-14	1,38E-12
Aif1	6,5349	3,21E-20	6,63E-18
Tmem86a	6,5340	1,39E-11	8,95E-10
Cd36	6,5309	4,60E-21	1,07E-18
Gas6	6,5270	3,23E-10	1,71E-08
Myof	6,5161	1,22E-25	5,38E-23
C1qc	6,4961	5,63E-23	1,64E-20
Fam114a1	6,4934	3,73E-09	1,62E-07
Cd4	6,4658	3,75E-11	2,21E-09
Dock1	6,4638	7,56E-15	8,16E-13
Acvrl1	6,4496	3,51E-10	1,83E-08
Lrp1	6,4367	9,23E-23	2,64E-20
Plau	6,4260	1,24E-16	1,76E-14
Clec4n	6,4218	4,66E-14	4,49E-12
Gm37199	6,4091	5,16E-08	1,81E-06
Mfsd12	6,4074	2,78E-17	4,16E-15
Gm44205	6,4008	5,02E-07	1,40E-05
Rgs10	6,3914	2,43E-13	2,11E-11
Wdfy4	6,3847	3,73E-16	4,75E-14
Abcc3	6,3838	1,58E-11	1,01E-09
Ankrd33b	6,3836	1,66E-07	5,19E-06
Ltbr	6,3799	5,11E-09	2,16E-07
Ear2	6,3747	4,83E-13	4,02E-11
Csf1r	6,3718	4,79E-25	1,86E-22
Cd180	6,3692	2,17E-22	6,01E-20
Clec10a	6,3650	6,44E-09	2,66E-07
Cxcl16	6,3536	1,90E-21	4,49E-19
Kif26b	6,3276	1,20E-07	3,91E-06
Alox5ap	6,3269	2,41E-14	2,49E-12
Il7r	6,3260	2,58E-17	3,90E-15
Fabp4	6,3182	4,25E-10	2,18E-08
Retnla	6,3174	2,77E-11	1,67E-09
Pde7b	6,3093	1,28E-10	7,05E-09
Ass1	6,3021	4,04E-14	3,92E-12
F10	6,2986	2,48E-24	8,42E-22
Apoe	6,2968	5,45E-17	8,01E-15
Tlr9	6,2802	3,68E-14	3,64E-12
Ppfibp2	6,2562	1,76E-12	1,27E-10
Zak	6,2488	8,65E-20	1,72E-17
Tifab	6,2451	1,72E-19	3,35E-17
Tdrd9	6,2441	8,42E-07	2,23E-05
Igf1	6,2378	5,73E-15	6,32E-13
Ifi207	6,2310	7,16E-21	1,60E-18
Trim30c	6,2142	9,15E-14	8,29E-12

Gene	FC	pval	padj
Slfn4	6,2103	3,16E-12	2,17E-10
Tnfrsf11a	6,2019	5,96E-25	2,26E-22
Flt1	6,1940	4,90E-14	4,65E-12
Siglec1	6,1929	2,81E-26	1,43E-23
Cd68	6,1839	3,85E-29	3,14E-26
Lhfpl2	6,1838	1,59E-11	1,01E-09
Plxnd1	6,1780	1,22E-19	2,40E-17
Tmem26	6,1748	1,76E-09	8,07E-08
Ccl12	6,1665	2,66E-07	7,85E-06
Tmtc3	6,1461	4,23E-18	7,19E-16
Epcam	6,1435	3,36E-10	1,76E-08
Tlr7	6,1047	5,68E-18	9,26E-16
Mmp13	6,1024	1,11E-10	6,15E-09
Nr1h3	6,0857	3,27E-10	1,72E-08
Gm26603	6,0805	4,23E-07	1,20E-05
Rusc2	6,0788	4,51E-08	1,60E-06
Mmp19	6,0665	2,43E-08	8,98E-07
Pde8b	6,0652	8,42E-08	2,80E-06
Adgrg6	6,0544	9,29E-08	3,08E-06
Lmo2	6,0490	5,71E-13	4,68E-11
Cd300ld	6,0478	1,29E-20	2,84E-18
Pdgfc	6,0365	7,20E-09	2,92E-07
Slc15a3	6,0213	1,16E-18	2,13E-16
Tal1	6,0206	1,53E-06	3,78E-05
Inhba	6,0174	5,62E-13	4,63E-11
Ptgfrn	6,0118	9,09E-07	2,39E-05
Cdc42bpb	6,0060	1,10E-08	4,32E-07
Arg1	6,0007	1,67E-12	1,22E-10
Adgb	6,0001	6,23E-09	2,58E-07
Clec4a1	5,9973	1,71E-16	2,34E-14
Gm6377	5,9973	7,92E-10	3,94E-08
Ifitm3	5,9928	9,50E-18	1,52E-15
Cd300e	5,9889	2,75E-15	3,14E-13
Rhou	5,9841	1,85E-09	8,45E-08
Tiam1	5,9805	5,20E-10	2,64E-08
Il1rn	5,9796	2,73E-14	2,75E-12
H2-Ab1	5,9649	2,36E-23	7,13E-21
Apbb2	5,9593	6,43E-10	3,23E-08
Avil	5,9577	1,65E-09	7,59E-08
Slc7a8	5,9553	3,01E-26	1,49E-23
Cxcl9	5,9531	3,89E-10	2,02E-08
Cxcl2	5,9513	2,84E-08	1,04E-06
Dsc2	5,9495	4,78E-06	0,00010395
Pfkfb4	5,9449	3,81E-08	1,37E-06
Cyp4f18	5,9365	1,49E-09	6,89E-08
Ccl6	5,9338	1,14E-15	1,39E-13
Hacd4	5,9232	1,56E-16	2,15E-14
Lpl	5,9189	3,49E-30	3,56E-27
Treml4	5,9100	1,03E-11	6,74E-10
Nectin4	5,9098	5,35E-10	2,70E-08
Gzmg	5,8917	6,89E-08	2,35E-06
Vipr2	5,8896	4,46E-07	1,27E-05
Cd93	5,8893	9,89E-19	1,83E-16
Ptk2	5,8888	4,05E-07	1,16E-05
Siglece	5,8867	2,97E-12	2,07E-10
Sdc3	5,8855	1,09E-21	2,72E-19
Il1a	5,8804	4,52E-08	1,60E-06
Csf2ra	5,8725	8,99E-18	1,45E-15
Olr1	5,8714	9,32E-13	7,49E-11
Lrrc25	5,8679	1,55E-07	4,89E-06
Ms4a14	5,8672	5,76E-08	2,01E-06
Nlrp1c-ps	5,8605	2,14E-10	1,14E-08
Ednrb	5,8597	1,14E-14	1,21E-12
Mid2	5,8543	6,30E-06	0,00013197
Cttn	5,8525	3,92E-06	8,67E-05
Ppfia4	5,8507	5,00E-11	2,89E-09
Dusp4	5,8417	7,83E-07	2,10E-05
Akap1	5,8417	8,69E-07	2,30E-05
Alox5	5,8372	2,51E-09	1,13E-07
Cysltr1	5,8341	1,75E-11	1,09E-09

Gene	FC	pval	padj
H2-DMb1	5,8322	7,05E-12	4,71E-10
Cybb	5,8319	3,58E-23	1,06E-20
Nlrp1b	5,8297	9,65E-12	6,35E-10
Sgms1	5,8290	2,45E-16	3,22E-14
Zscan12	5,8265	3,20E-07	9,34E-06
Ptgs2	5,8191	3,36E-12	2,30E-10
Gm38357	5,8135	9,25E-15	9,92E-13
1700071M16Rik	5,8064	9,17E-07	2,40E-05
Adam33	5,8061	4,18E-07	1,19E-05
F630028O10Rik	5,8040	2,01E-08	7,56E-07
Ak4	5,8035	1,29E-06	3,27E-05
Il18	5,7951	3,71E-08	1,34E-06
Tmem132a	5,7788	8,56E-10	4,17E-08
Trem2	5,7689	2,55E-07	7,59E-06
Thbgf	5,7589	4,15E-18	7,19E-16
Cds1	5,7435	2,81E-07	8,29E-06
Mgst1	5,7302	3,18E-07	9,30E-06
Nrp1	5,7215	1,14E-24	4,12E-22
Ier3	5,7199	1,42E-06	3,56E-05
P2ry6	5,7172	1,25E-17	1,96E-15
Gpr141	5,7155	1,41E-11	9,08E-10
Olfml2b	5,7091	2,46E-05	0,00043567
App	5,7034	2,22E-23	6,83E-21
H2-Aa	5,7017	5,37E-21	1,22E-18
F11r	5,7014	1,84E-16	2,50E-14
Kcnj2	5,7000	2,00E-15	2,34E-13
Shtn1	5,6879	7,23E-09	2,93E-07
6430548M08Rik	5,6815	2,34E-07	7,11E-06
Matn2	5,6767	1,98E-06	4,75E-05
Apba1	5,6755	6,88E-09	2,82E-07
Scamp1	5,6703	2,53E-16	3,30E-14
Tgm2	5,6648	2,05E-27	1,12E-24
Cd74	5,6446	6,08E-22	1,60E-19
Slamf8	5,6445	3,48E-09	1,52E-07
Pid1	5,6294	2,66E-14	2,69E-12
Gdf3	5,6283	6,73E-11	3,87E-09
Ctsg	5,6094	1,24E-05	0,00023843
Plaur	5,6051	1,75E-12	1,27E-10
Mpeg1	5,5992	2,18E-20	4,64E-18
Plbd1	5,5952	1,10E-17	1,75E-15
Sirpb1c	5,5834	1,43E-07	4,58E-06
Ch25h	5,5784	3,17E-06	7,20E-05
Fat1	5,5646	1,42E-06	3,56E-05
Rtn1	5,5605	5,85E-07	1,61E-05
C3	5,5423	1,95E-14	2,02E-12
Ly86	5,5371	2,43E-15	2,81E-13
Il1r2	5,5347	1,35E-06	3,40E-05
Lyz2	5,5163	4,32E-18	7,26E-16
Cacna1d	5,5085	1,04E-07	3,40E-06
Gdf15	5,5058	6,62E-07	1,80E-05
Rab15	5,4996	8,75E-05	0,00130277
Mtss1	5,4983	5,01E-10	2,56E-08
Clec4d	5,4913	6,00E-09	2,49E-07
Nfix	5,4867	3,35E-07	9,76E-06
Gm37347	5,4860	7,27E-08	2,46E-06
Emp1	5,4802	1,81E-14	1,89E-12
Aqp9	5,4790	3,97E-07	1,13E-05
Cmtm3	5,4782	2,98E-11	1,79E-09
Htra3	5,4766	6,45E-07	1,76E-05
Gm5150	5,4755	4,42E-09	1,89E-07
Thbd	5,4716	1,29E-10	7,06E-09
Rps6ka2	5,4674	5,32E-08	1,87E-06
Slc7a2	5,4632	2,22E-16	2,95E-14
Lifr	5,4577	3,88E-15	4,37E-13
Spats2	5,4556	1,37E-05	0,00025861
Apob	5,4547	7,10E-07	1,92E-05
3110082I17Rik	5,4545	1,58E-11	1,01E-09
Tmem144	5,4537	7,96E-06	0,00016291
Gpr87	5,4490	1,88E-05	0,00034512
Cd300lb	5,4476	8,32E-10	4,06E-08

Gene	FC	pval	padj
Pafah2	5,4457	4,47E-06	9,77E-05
Fcrl5	5,4392	7,85E-08	2,64E-06
Ninj1	5,4375	1,77E-10	9,53E-09
Gm42934	5,4364	3,02E-06	6,94E-05
Aph1b	5,4339	3,92E-06	8,67E-05
Sh2b2	5,4240	2,17E-07	6,65E-06
Gzme	5,4205	1,00E-12	7,96E-11
Etv5	5,4092	6,98E-14	6,47E-12
Prokr1	5,4042	5,90E-05	0,00093385
Dhrs9	5,3847	8,21E-07	2,18E-05
Hpgd	5,3844	5,77E-13	4,71E-11
Cd200	5,3834	2,44E-05	0,00043467
Ifi204	5,3776	9,11E-14	8,29E-12
Slamf9	5,3769	1,28E-06	3,25E-05
Rnase2a	5,3635	9,50E-05	0,00139894
Arfgef3	5,3460	1,47E-07	4,66E-06
Mreg	5,3315	4,74E-06	0,00010313
Grk3	5,3283	1,73E-11	1,09E-09
Ms4a6d	5,3279	7,20E-15	7,88E-13
Kif13a	5,3270	3,83E-14	3,74E-12
Smo	5,3194	3,19E-07	9,33E-06
Rubcnl	5,3181	3,72E-07	1,07E-05
Fn1	5,3174	4,30E-29	3,34E-26
Gm14548	5,3165	2,13E-05	0,00038323
Gm42632	5,3130	6,77E-05	0,00104416
Dcn	5,3106	2,90E-05	0,0005024
Slc40a1	5,3093	5,43E-08	1,90E-06
Adamts1	5,3076	7,21E-06	0,00014854
F13a1	5,3033	3,87E-16	4,89E-14
Ctss	5,2974	4,47E-24	1,49E-21
Pdia5	5,2880	2,42E-05	0,00043082
Nostrin	5,2853	4,05E-08	1,44E-06
Egln3	5,2782	8,93E-06	0,00017967
Dmxl2	5,2492	1,24E-12	9,39E-11
Nxpe4	5,2491	4,73E-10	2,42E-08
Ccr1	5,2479	3,33E-08	1,21E-06
Bcl2a1a	5,2466	6,16E-06	0,00012947
Aph1c	5,2444	3,35E-08	1,21E-06
Adamdec1	5,2311	1,65E-06	4,03E-05
Rab32	5,2279	3,12E-18	5,59E-16
Gm15931	5,2114	1,76E-06	4,28E-05
Pilrb2	5,2111	8,66E-10	4,20E-08
Arhgap29	5,2099	3,61E-07	1,05E-05
Parp12	5,2074	1,58E-26	8,33E-24
Tnf	5,2060	2,13E-13	1,89E-11
Kcnk6	5,1997	2,86E-16	3,71E-14
Gm2396	5,1995	7,00E-06	0,00014536
Stom	5,1992	3,27E-11	1,95E-09
Gpr35	5,1983	2,30E-13	2,01E-11
Ifngr2	5,1908	2,65E-14	2,69E-12
Atp6v0d2	5,1871	7,68E-05	0,00116806
Slc6a12	5,1822	2,01E-05	0,00036563
P2ry12	5,1724	4,94E-12	3,35E-10
Tns3	5,1694	2,25E-13	1,98E-11
Amz1	5,1665	1,79E-07	5,60E-06
Adora2b	5,1615	1,50E-05	0,00028162
Stard8	5,1578	6,55E-22	1,70E-19
Mctp1	5,1534	1,79E-05	0,00033247
C1qa	5,1468	1,34E-07	4,34E-06
Tlr2	5,1448	1,51E-10	8,16E-09
Klra2	5,1393	1,92E-16	2,59E-14
Hp	5,1340	6,33E-08	2,18E-06
Ankrd66	5,1193	9,53E-05	0,001401
Ptpro	5,1101	6,88E-11	3,94E-09
Mfsd7a	5,1091	3,41E-05	0,0005795
Cd300a	5,1074	9,89E-23	2,78E-20
Rnf217	5,1005	2,65E-05	0,00046436
Marcks	5,0994	8,45E-22	2,15E-19
Gm13650	5,0993	8,24E-05	0,00123817
Lilra5	5,0945	1,37E-09	6,41E-08

Gene	FC	pval	padj
Cebpd	5,0853	1,35E-05	0,00025694
Stau2	5,0835	2,05E-08	7,69E-07
Plxnb2	5,0795	1,28E-12	9,64E-11
Tgfbi	5,0762	7,35E-12	4,89E-10
Twnk	5,0758	1,49E-07	4,74E-06
Pla2g15	5,0676	7,30E-15	7,94E-13
Cfh	5,0631	5,90E-08	2,05E-06
Grn	5,0546	1,80E-17	2,74E-15
Jag1	5,0495	8,85E-06	0,00017826
Lyl1	5,0469	4,00E-08	1,43E-06
Fgd2	5,0448	2,01E-12	1,43E-10
Scin	5,0338	1,96E-09	8,91E-08
Slc7a7	5,0243	1,58E-07	4,97E-06
Fpr2	5,0217	1,36E-08	5,25E-07
Plin2	5,0211	2,32E-20	4,85E-18
I830077J02Rik	5,0201	4,08E-10	2,11E-08
Hpgds	5,0109	1,47E-18	2,67E-16
Gm15531	5,0094	4,05E-05	0,00067337
Il6ra	5,0006	5,34E-13	4,42E-11
Rnf128	4,9991	3,06E-05	0,00052538
Mt1	4,9981	2,61E-08	9,60E-07
Ago4	4,9948	5,48E-06	0,00011738
Cd83	4,9937	4,28E-12	2,91E-10
Lgmn	4,9927	1,27E-24	4,50E-22
Adap2os	4,9905	3,10E-06	7,06E-05
A230028O05Rik	4,9797	0,00024774	0,00315205
Kdelc1	4,9768	1,47E-06	3,66E-05
Gm26813	4,9735	3,07E-05	0,00052612
Carmil1	4,9690	4,56E-06	9,97E-05
Vill	4,9528	1,31E-06	3,32E-05
Tmem176b	4,9506	5,02E-15	5,60E-13
Arhgef10l	4,9459	6,93E-06	0,00014419
Coprs	4,9392	0,0002364	0,00303854
Rbm47	4,9317	2,09E-15	2,43E-13
Arnt2	4,9316	1,92E-05	0,00035103
Ctla4	4,9235	1,17E-06	2,98E-05
Neil2	4,9234	7,89E-05	0,00119411
Ypel2	4,9202	5,83E-05	0,00092639
Afp	4,9175	0,00039079	0,00463914
Tcf7l2	4,9154	1,20E-11	7,79E-10
Gpr19	4,9123	7,53E-06	0,00015449
Zfyve9	4,9082	1,22E-06	3,10E-05
Il1b	4,9067	1,30E-12	9,69E-11
Dab2	4,9001	2,19E-20	4,64E-18
Mrc1	4,8956	1,57E-09	7,24E-08
Arhgap24	4,8896	2,99E-05	0,00051628
Nlrc4	4,8751	7,87E-08	2,64E-06
Igf2bp2	4,8640	1,16E-08	4,52E-07
Ralgds	4,8578	6,61E-16	8,30E-14
Tbc1d8	4,8516	4,66E-09	1,98E-07
Snx24	4,8425	6,06E-06	0,00012823
AA467197	4,8408	1,26E-12	9,53E-11
Gm13710	4,8403	0,00020689	0,00272363
Rnf180	4,8369	0,0002178	0,00283527
Spic	4,8217	5,66E-24	1,85E-21
Cdc42ep2	4,8208	4,79E-05	0,00078048
Stab1	4,8195	4,17E-09	1,79E-07
Mmp27	4,8177	0,00023098	0,00298063
Ms4a7	4,8142	2,28E-13	2,00E-11
Bace2	4,8093	0,00062902	0,00688592
Myo10	4,8071	3,13E-09	1,38E-07
Mrm2	4,8069	2,10E-05	0,00037952
Col15a1	4,8012	1,57E-08	6,02E-07
Ctsz	4,7937	2,04E-13	1,82E-11
Plscr3	4,7928	6,07E-05	0,00095414
B4galt4	4,7870	1,05E-05	0,00020773
Gm44860	4,7812	1,40E-08	5,38E-07
Gm43768	4,7799	0,00012272	0,00173752
Pstpip2	4,7795	1,43E-06	3,58E-05
Ugt1a7c	4,7765	2,33E-06	5,51E-05

Gene	FC	pval	padj
Gas2l1	4,7730	2,76E-05	0,00047958
Rassf4	4,7720	1,00E-15	1,23E-13
Tbxas1	4,7674	1,19E-12	9,08E-11
Dapk1	4,7656	2,49E-11	1,52E-09
Ly6a	4,7545	1,49E-10	8,15E-09
Arhgef39	4,7486	9,51E-05	0,00139894
Hcar2	4,7324	3,01E-07	8,87E-06
Ifi203-ps	4,7280	2,08E-08	7,78E-07
C130050O18Rik	4,7264	3,55E-05	0,0006015
Ldhb	4,7254	2,89E-05	0,0005001
Gpt2	4,7142	1,46E-05	0,00027516
Abca9	4,7114	9,90E-13	7,92E-11
Gm15374	4,7086	0,00017781	0,00238901
Soga1	4,7010	9,91E-08	3,28E-06
Ms4a4a	4,6995	1,58E-08	6,05E-07
Slc11a1	4,6990	1,80E-12	1,29E-10
Fcgr4	4,6989	4,61E-09	1,97E-07
Tlr3	4,6915	9,25E-09	3,69E-07
Rnf150	4,6876	3,13E-12	2,16E-10
Tmem106a	4,6860	6,21E-10	3,13E-08
Gsn	4,6824	1,00E-09	4,83E-08
Ctsb	4,6809	4,22E-30	4,05E-27
P2ry2	4,6783	0,00064913	0,00705396
Mak	4,6735	0,00053319	0,00601979
Tlr6	4,6707	1,12E-09	5,30E-08
Cep170b	4,6655	5,28E-18	8,70E-16
C4b	4,6629	1,28E-05	0,00024469
Adgrg1	4,6554	6,08E-05	0,00095414
Lgals3	4,6552	1,52E-12	1,12E-10
Lst1	4,6539	2,20E-08	8,18E-07
St6gal1	4,6500	3,54E-06	7,94E-05
Igsf10	4,6396	0,00049029	0,00561993
Oasl2	4,6341	3,31E-16	4,26E-14
Skint3	4,6328	1,99E-05	0,00036329
Spint1	4,6317	6,26E-06	0,00013139
2810025M15Rik	4,6311	1,97E-05	0,00035889
Vkorc1	4,6276	1,13E-05	0,00022136
Trib1	4,6248	4,16E-11	2,43E-09
Kcnk13	4,6245	0,00019895	0,00263397
Gzmc	4,6234	9,76E-09	3,85E-07
Cd320	4,6231	0,00010452	0,00150998
Timd4	4,6197	0,00035884	0,00431643
Fut10	4,6181	0,00106682	0,01055241
Bex6	4,6180	0,00012903	0,00181431
Gspt2	4,6151	0,00027991	0,00349317
Clec4e	4,6037	1,84E-07	5,73E-06
Gm37648	4,5987	4,43E-05	0,00072769
Gm37168	4,5948	0,00052933	0,00599162
Nt5dc2	4,5941	0,00035843	0,00431467
Cp	4,5900	2,64E-07	7,82E-06
Sirpb1a	4,5864	6,99E-09	2,86E-07
Slpi	4,5822	0,00033701	0,00408701
Gm15448	4,5748	0,00028696	0,00355179
Upp1	4,5657	0,0008705	0,00892439
Mgl2	4,5624	3,18E-08	1,15E-06
Gm45041	4,5619	0,00024146	0,00309146
Siglecf	4,5596	0,00084398	0,00872938
Mtus1	4,5580	7,37E-06	0,00015146
Lrrk2	4,5563	4,21E-07	1,20E-05
Tnfrsf8	4,5521	0,00085988	0,00885451
Mtap7d3	4,5519	4,83E-05	0,00078493
4930533B01Rik	4,5473	0,00067499	0,00728412
Slc6a9	4,5413	0,00108001	0,01063773
Sfmbt2	4,5301	8,78E-06	0,00017726
Cyp26b1	4,5300	0,0010891	0,01070788
Fnip2	4,5273	1,30E-12	9,69E-11
Gm20658	4,5272	0,00059972	0,00665448
Cd63	4,5217	3,08E-06	7,03E-05
Dok3	4,5186	3,37E-05	0,00057346
Plxdc1	4,5164	0,00029495	0,00364186

Gene	FC	pval	padj
Tmem256	4,5134	6,43E-05	0,00100269
Kynu	4,5102	3,57E-06	8,00E-05
Ddx3y	4,5083	0,00088457	0,00906294
Igfbp5	4,5020	0,0008025	0,00836927
Eya4	4,4968	0,0015564	0,01434261
Pira2	4,4967	0,00023908	0,00307062
Ceacam1	4,4960	3,09E-08	1,13E-06
Fap	4,4913	0,00042483	0,00497439
Dnmt3aos	4,4826	0,00017611	0,00236805
Ms4a8a	4,4704	2,03E-08	7,62E-07
Nuak1	4,4695	3,10E-05	0,00053101
Art3	4,4683	0,00026681	0,00335026
Plpp3	4,4655	0,00068757	0,00739287
Card9	4,4653	0,00011276	0,00161199
Eng	4,4638	0,00020898	0,00274233
Tcp11l1	4,4610	4,49E-07	1,27E-05
Slc27a6	4,4594	1,54E-05	0,00028884
Gm128	4,4584	0,00040235	0,00474873
Tbc1d32	4,4572	1,21E-07	3,92E-06
Copz2	4,4519	5,25E-05	0,00084594
1500005C15Rik	4,4342	0,00019751	0,0026171
Ifi211	4,4340	1,03E-14	1,10E-12
Aldh3b1	4,4219	0,00016408	0,00223205
9130204K15Rik	4,4172	0,00078345	0,00819686
Ifit3b	4,4155	2,42E-09	1,09E-07
Apobec1	4,4058	2,96E-19	5,68E-17
Flrt2	4,3992	0,00025639	0,00323935
D330045A20Rik	4,3983	0,00038736	0,00460846
Gm10693	4,3963	0,00063773	0,00696253
Clec12a	4,3952	2,75E-12	1,92E-10
Arvcf	4,3924	0,00083288	0,00863646
Mcemp1	4,3913	4,25E-05	0,00070259
Cxcl1	4,3893	0,00082498	0,00855995
Fcrl6	4,3795	7,11E-09	2,89E-07
Fvt	4,3785	5,98E-06	0,00012685
Serpinb8	4,3780	5,00E-07	1,40E-05
Gm20548	4,3761	4,26E-06	9,33E-05
Rbfox2	4,3737	0,00193784	0,01725337
Abca3	4,3714	2,36E-08	8,78E-07
2010300C02Rik	4,3706	8,28E-05	0,00124308
Asph	4,3662	5,25E-09	2,20E-07
Gm43068	4,3659	0,00089774	0,00917488
Trim47	4,3645	0,00063849	0,00696452
Gm21057	4,3531	0,0005082	0,00579666
Cd276	4,3517	0,00032875	0,00400467
Ppic	4,3491	0,00030029	0,00369792
Ifi205	4,3481	9,91E-09	3,89E-07
Ralb	4,3477	6,89E-09	2,82E-07
Hk2	4,3466	3,18E-10	1,68E-08
Arhgap23	4,3434	5,24E-07	1,46E-05
Asns	4,3430	0,00024145	0,00309146
Laptm4b	4,3415	7,87E-05	0,00119202
Ly6i	4,3415	2,33E-07	7,08E-06
Aatk	4,3375	0,00035107	0,00423232
Spp1	4,3308	5,47E-08	1,91E-06
Cdh1	4,3284	7,13E-08	2,43E-06
Cdk20	4,3273	0,00061322	0,00675828
St8sia6	4,3262	0,00013776	0,00191887
Ccl24	4,3229	0,00111735	0,01090674
Fabp5	4,3189	8,27E-09	3,33E-07
Gm16353	4,3160	1,79E-06	4,33E-05
Cd14	4,3153	1,37E-06	3,46E-05
Gm11440	4,3074	0,00140736	0,01322668
Reep6	4,3055	0,00129129	0,01230181
Klhl13	4,3054	0,00100974	0,01011658
Mfsd7b	4,3030	7,98E-10	3,96E-08
Ckap4	4,3022	2,04E-05	0,00036934
4933416M07Rik	4,3016	0,00113926	0,01107417
Ehd1	4,2974	6,70E-09	2,76E-07
1700047K16Rik	4,2942	0,00032565	0,00397583

Gene	FC	pval	padj
B4galnt2	4,2920	0,0014124	0,01326289
Hlx	4,2912	0,00025421	0,00321673
Ceacam19	4,2902	0,00161955	0,01479914
Gm14011	4,2888	0,00239221	0,02040759
Spsb1	4,2841	0,00011857	0,00168323
Thop1	4,2836	0,00066711	0,00721566
Bmpr1a	4,2824	6,20E-05	0,0009712
Gm33370	4,2784	0,00099305	0,00997394
RP23-292C5.8	4,2762	7,17E-05	0,00109799
Ctsk	4,2738	1,02E-05	0,00020281
8430408G22Rik	4,2710	0,00076625	0,00807737
Epb41l1	4,2695	2,97E-05	0,00051334
Zfp467	4,2691	3,49E-06	7,86E-05
Tmprss4	4,2633	0,0026194	0,02190021
Adgre4	4,2606	4,32E-09	1,85E-07
Cdk5rap1	4,2587	1,14E-05	0,00022242
Elavl4	4,2568	0,00273463	0,02265336
Fth1	4,2559	5,01E-18	8,33E-16
Gm20633	4,2542	0,00020576	0,00271093
Pirb	4,2527	1,79E-12	1,28E-10
Fblim1	4,2525	4,04E-05	0,00067244
Gm26811	4,2468	0,00279116	0,02300489
Acod1	4,2378	5,58E-05	0,00089153
Rai14	4,2353	2,64E-07	7,82E-06
Clec5a	4,2337	2,97E-08	1,09E-06
Rasgrp3	4,2221	3,97E-09	1,71E-07
Syngr1	4,2211	0,00204859	0,01810107
Gm26797	4,2201	0,00027277	0,00341193
Ccl8	4,2174	0,00190533	0,01702897
Dnase1l3	4,2163	5,04E-08	1,78E-06
Tlr5	4,2156	4,65E-05	0,00075874
C5ar2	4,2140	6,49E-08	2,23E-06
Sbf2	4,2074	6,26E-20	1,26E-17
Vdr	4,2063	0,00095777	0,00968887
Gm13391	4,2052	0,00212629	0,01856632
Lsr	4,2051	0,00039872	0,00472068
Scamp5	4,2025	0,00042176	0,00494705
Gm12589	4,1956	0,00154175	0,01427003
Eid2b	4,1902	0,00025822	0,00325995
Fcrl1	4,1861	0,00085142	0,00878961
Bst1	4,1775	3,03E-09	1,35E-07
Vwf	4,1719	2,30E-05	0,00041142
Sestd1	4,1718	0,00086161	0,0088667
Gm43593	4,1697	0,00076109	0,00804547
Speg	4,1695	0,00057305	0,00639335
Lipg	4,1690	0,00335187	0,02663034
Clec4a2	4,1690	9,64E-09	3,82E-07
Zfp503	4,1644	0,0008224	0,00854402
Atf3	4,1619	3,98E-08	1,42E-06
Ccl1	4,1595	0,00076436	0,0080696
Cacna1b	4,1567	0,00109573	0,01075359
Btbd3	4,1538	2,96E-05	0,00051201
Tdo2	4,1519	0,00043318	0,00506131
Melk	4,1509	4,13E-05	0,00068463
Slfn5	4,1501	7,81E-11	4,38E-09
Ttc30a1	4,1462	0,00103117	0,01028707
Angptl4	4,1462	0,00071075	0,00759702
Gm15503	4,1398	0,00109088	0,01071887
Tarm1	4,1367	3,85E-05	0,00064389
Gm5345	4,1330	0,0029842	0,02426487
Mcoln3	4,1321	0,00288566	0,02355754
Gm44861	4,1285	7,25E-07	1,96E-05
Cryl1	4,1274	0,00019992	0,00264249
Rab20	4,1245	4,05E-05	0,00067337
Gm15356	4,1234	1,62E-07	5,06E-06
Asb2	4,1200	6,06E-08	2,09E-06
M1ap	4,1135	0,00117167	0,01131507
Homer3	4,1126	0,00222671	0,01927807
Plekho1	4,1102	1,42E-07	4,55E-06
Sh3pxd2b	4,1076	1,12E-12	8,75E-11

Gene	FC	pval	padj
Zfp608	4,1056	1,57E-07	4,93E-06
Nucb2	4,1054	1,09E-06	2,81E-05
Nr1d1	4,1010	0,00064174	0,00699231
Gm15964	4,0990	0,0005579	0,00626283
Dusp14	4,0951	0,00375737	0,02906648
Mmp12	4,0928	2,57E-14	2,64E-12
Gm5431	4,0915	3,72E-11	2,20E-09
Catsperg1	4,0914	0,00254391	0,02144377
Nlrp1a	4,0864	0,00020963	0,00274861
Il1r1	4,0852	0,00167579	0,01525323
Lrrc18	4,0791	0,00029863	0,00368454
Gstm4	4,0788	0,00119373	0,0114737
Fmnl2	4,0766	5,87E-06	0,00012499
Gngt2	4,0725	3,14E-09	1,38E-07
Gm12454	4,0701	0,00054884	0,00617393
Batf2	4,0688	0,00167766	0,0152617
Sh3bp5	4,0563	1,25E-10	6,87E-09
Ly6g5b	4,0514	0,0025506	0,02147155
Gm17230	4,0509	0,00261253	0,02186402
Igf2bp1	4,0509	1,11E-08	4,33E-07
Trem1	4,0504	0,00165981	0,01513314
Wipi1	4,0492	0,00094793	0,00961544
Gm16316	4,0491	0,00065322	0,00708889
S1pr3	4,0431	0,00331754	0,02640917
Slc7a11	4,0429	3,47E-12	2,37E-10
Hist1h2bc	4,0382	2,83E-05	0,0004923
Chchd4	4,0370	2,51E-07	7,50E-06
Piwil2	4,0336	0,00103722	0,01033809
Sirpb1b	4,0301	2,66E-05	0,00046564
RP23-323L3.1	4,0296	0,00020481	0,00270058
Tnfsf13b	4,0279	9,41E-05	0,00138932
P2rx4	4,0278	4,22E-18	7,19E-16
Tmcc2	4,0213	0,00049224	0,0056383
Ugt1a6a	4,0169	0,00063698	0,00695895
Csf1	4,0112	1,32E-06	3,33E-05
Tnfrsf21	4,0096	7,46E-08	2,52E-06
Prune2	4,0029	1,87E-07	5,79E-06
Cxcl10	3,9965	1,16E-07	3,80E-06
Slc16a10	3,9959	7,95E-07	2,13E-05
BC049715	3,9946	0,00022637	0,00293045
Stxbp6	3,9941	6,61E-05	0,00102361
Zfp750	3,9894	0,00243541	0,0207328
Gm9733	3,9862	0,00110522	0,01081422
Slc27a1	3,9789	3,84E-06	8,55E-05
Spdl1	3,9741	1,58E-05	0,00029576
Tgm1	3,9727	0,00226308	0,01953074
Gm42793	3,9711	0,00250947	0,0212303
Olfml3	3,9660	7,70E-06	0,0001577
Tmem119	3,9654	0,00014316	0,00198404
Flt4	3,9633	0,00201059	0,01780383
Bcl2a1d	3,9629	6,78E-06	0,00014144
Gm12543	3,9629	0,00167884	0,01526393
Cd86	3,9552	7,55E-10	3,77E-08
Ifi30	3,9533	1,30E-15	1,56E-13
Nfam1	3,9520	1,53E-06	3,78E-05
4930599N23Rik	3,9513	0,00494904	0,03590914
Gm43800	3,9504	0,00470934	0,03444574
Rnf149	3,9492	2,65E-11	1,60E-09
Lima1	3,9449	4,81E-07	1,35E-05
Gm15635	3,9434	0,00246626	0,02095164
Zfp629	3,9433	1,22E-05	0,00023491
Gm17068	3,9399	0,00241218	0,02056724
Tspyl4	3,9342	4,90E-07	1,37E-05
Mapt	3,9333	0,00348785	0,02746999
Gys1	3,9304	4,38E-05	0,00072032
Slfn1	3,9297	2,15E-07	6,60E-06
Asah1	3,9287	7,98E-16	9,94E-14
Tmem221	3,9277	0,0035025	0,02755875
Rasd2	3,9239	0,00447071	0,03314625
Glrx	3,9212	4,72E-14	4,51E-12

Gene	FC	pval	padj
Ceacam18	3,9205	0,00201416	0,01782577
Gm42603	3,9186	0,00430473	0,0322825
Sqrdl	3,9161	1,26E-07	4,10E-06
Fggy	3,9154	0,00253409	0,02139418
Pdxk	3,9148	1,09E-09	5,17E-08
1700095J12Rik	3,9130	0,00407951	0,0309925
Ptgr1	3,9123	2,95E-06	6,80E-05
Ifit3	3,9066	1,02E-06	2,65E-05
Clcn7	3,9049	1,03E-09	4,95E-08
Gm2a	3,8960	8,49E-09	3,41E-07
Sash1	3,8937	2,52E-05	0,00044558
Mfap3l	3,8893	0,00279006	0,02300489
Rgl3	3,8876	0,00645135	0,0437538
Dnah12	3,8789	5,08E-05	0,0008216
4930532G15Rik	3,8777	0,00072172	0,00770421
Rab11fip5	3,8751	0,00022115	0,00287656
Gm37498	3,8738	0,00254246	0,0214426
Ap1s1	3,8701	0,00089222	0,00912721
Pilra	3,8653	2,23E-10	1,18E-08
Sh3bp4	3,8639	0,00218014	0,01895537
Igsf6	3,8626	4,30E-13	3,62E-11
Gm5970	3,8548	0,00227843	0,01962164
Slc39a2	3,8531	0,00401208	0,03063717
Cd24a	3,8482	5,79E-08	2,01E-06
Ncf2	3,8478	2,64E-09	1,18E-07
Ampd3	3,8464	6,11E-06	0,00012882
4930512H18Rik	3,8464	0,00633023	0,04318378
Thsd7a	3,8411	0,00651937	0,04405032
1500009L16Rik	3,8389	0,00679392	0,04545386
Mt2	3,8381	6,86E-05	0,00105253
Cd209a	3,8377	0,00118486	0,01142213
2210406H18Rik	3,8373	8,41E-06	0,00017155
Gm17169	3,8361	0,00118959	0,01145257
Acta2	3,8356	0,00560992	0,03959475
B3galnt1	3,8330	0,00129182	0,01230181
Stmn2	3,8310	0,00682225	0,04558691
Irf6	3,8309	0,00287563	0,02349923
Ctsf	3,8258	0,00344892	0,02720277
Gm37468	3,8238	0,00046641	0,0053916
Apip	3,8222	2,45E-05	0,00043531
Gas2l3	3,8218	1,29E-09	6,04E-08
Gad1-ps	3,8211	0,00219787	0,01907902
Dppa3	3,8185	0,00395341	0,0302742
Zdhhc14	3,8175	0,00342688	0,02705612
Dtx4	3,8174	2,02E-05	0,00036636
Adcy4	3,8163	0,00069884	0,00748936
Plxdc2	3,8161	1,62E-05	0,00030266
Rab44	3,8143	0,00554634	0,03929903
Angptl2	3,8087	0,00011101	0,00159256
Ppp2r2c	3,8072	5,86E-05	0,00092958
Dpep2	3,8022	1,38E-07	4,45E-06
Nid2	3,8001	0,00015028	0,0020633
Pnp2	3,7995	0,00228603	0,01967672
Met	3,7974	1,10E-05	0,00021666
Rgs7bp	3,7882	0,00107975	0,01063773
Ckb	3,7847	8,15E-10	4,01E-08
Renbp	3,7818	2,41E-07	7,29E-06
Dynlt1a	3,7803	0,00212019	0,01854285
Med29	3,7763	0,00016032	0,00218454
Nme4	3,7729	0,00433827	0,03241482
Abcd2	3,7722	8,21E-07	2,18E-05
Il1rl2	3,7717	1,75E-06	4,27E-05
Daglb	3,7714	8,16E-07	2,18E-05
Arhgef11	3,7707	9,69E-05	0,00141684
Msrb2	3,7671	0,00021627	0,00282209
Ang	3,7629	0,00041735	0,00490801
Paox	3,7620	0,00014866	0,00204616
Rnase4	3,7618	8,63E-05	0,00128859
Afap1l1	3,7595	0,00121002	0,01158254
Mgarp	3,7586	0,00362719	0,02828066

Gene	FC	pval	padj
Nxnl2	3,7541	0,00728139	0,04779347
Gm43775	3,7532	2,20E-05	0,00039389
Adck1	3,7473	3,32E-05	0,00056585
Rgmb	3,7438	0,0034233	0,02705301
Psrc1	3,7393	3,68E-06	8,21E-05
Tst	3,7389	0,00516469	0,03712387
Tmem106c	3,7349	5,17E-05	0,00083256
Chdh	3,7345	0,004249	0,03198217
Gm17705	3,7304	0,00071041	0,00759702
Tmem67	3,7282	1,74E-06	4,25E-05
Pgap1	3,7219	5,39E-06	0,00011559
Nupr1	3,7202	0,00029049	0,00359219
Ccdc122	3,7187	0,00579483	0,04051416
Lilrb4a	3,7183	1,70E-12	1,24E-10
Rps6ka6	3,7158	0,00403567	0,03076778
Tmem176a	3,7083	8,31E-08	2,77E-06
A530099J19Rik	3,7068	0,00656531	0,04426903
Nacc2	3,7047	2,75E-06	6,40E-05
Gm14023	3,7046	0,00044664	0,00518896
Rps4l	3,7037	0,00111929	0,01091309
Gm19719	3,7006	0,00660127	0,044438
Fcrls	3,6999	0,00018941	0,00252652
Gm44079	3,6938	0,00446908	0,03314625
Dnah2	3,6890	0,00050425	0,00576373
Gbp2b	3,6865	0,00069508	0,00746371
Gm42967	3,6846	0,0053486	0,0380965
Gm8378	3,6801	0,00678492	0,04543057
Adk	3,6760	0,00250872	0,0212303
Tceal8	3,6747	0,00021148	0,00276845
Scpep1	3,6741	4,18E-06	9,21E-05
Ebi3	3,6736	0,00299792	0,02433316
Syn1	3,6701	0,00089252	0,00912721
Tbc1d4	3,6646	0,00056416	0,00632002
Ptgir	3,6626	0,00232695	0,01995521
Gm23722	3,6609	0,00311653	0,02520262
Parvb	3,6542	1,76E-08	6,67E-07
Batf3	3,6523	0,00143391	0,01341083
Deptor	3,6513	3,55E-07	1,03E-05
Basp1	3,6484	3,49E-14	3,47E-12
Acot1	3,6428	0,00666478	0,04479163
Cep290	3,6427	5,01E-06	0,00010846
Neo1	3,6407	0,00313165	0,02526363
Gm9974	3,6352	0,00516653	0,03712387
Zfp704	3,6338	1,03E-07	3,39E-06
Erg	3,6323	0,00144713	0,01351896
Rasgrp4	3,6297	9,42E-06	0,00018836
Fam196a	3,6290	0,00648533	0,04392948
Nectin3	3,6285	9,10E-05	0,00134871
Hsf2	3,6284	9,24E-07	2,42E-05
Cxcl3	3,6266	8,35E-05	0,00125234
Cfp	3,6212	8,53E-13	6,89E-11
Ctnnd1	3,6175	8,61E-06	0,00017454
Slc43a1	3,6151	0,00617092	0,04242731
9530085L11Rik	3,6149	0,00519291	0,03723144
Lilra6	3,6143	0,00021032	0,00275541
2900005J15Rik	3,6119	0,00184874	0,01664947
Dio2	3,6107	0,00702975	0,04660102
Arrdc4	3,6048	1,81E-08	6,86E-07
Galm	3,6032	0,00367732	0,02861677
Psap	3,6010	1,08E-09	5,12E-08
BC028528	3,5976	4,22E-06	9,26E-05
2810002D19Rik	3,5966	5,17E-06	0,00011144
Cd5l	3,5940	0,00417361	0,03153115
Hif3a	3,5939	0,00233782	0,02002278
A530064D06Rik	3,5928	5,26E-07	1,46E-05
5730508B09Rik	3,5904	0,00026406	0,00331824
8030453O22Rik	3,5903	0,00639117	0,0434798
Nudt12	3,5902	0,00681642	0,04556667
Gm43221	3,5851	0,00310138	0,02510504
Fkbpl	3,5779	0,0075553	0,04912283

Gene	FC	pval	padj
Mx2	3,5703	2,46E-06	5,81E-05
Nek4	3,5696	0,00032681	0,00398428
Gm9888	3,5653	0,00059123	0,00656917
Ccl9	3,5642	4,74E-07	1,33E-05
Gm42515	3,5621	8,46E-05	0,0012664
Abcc2	3,5540	0,0032487	0,02606907
Gda	3,5504	8,66E-05	0,00129057
Lrp5	3,5499	7,38E-08	2,50E-06
Il17rd	3,5489	0,00521389	0,03733261
Ifitm2	3,5484	7,82E-05	0,00118568
Wdr60	3,5480	0,00581342	0,04062669
Rcn3	3,5462	0,0068411	0,04566306
Acsl1	3,5413	6,25E-07	1,71E-05
Dnase2a	3,5343	1,53E-08	5,89E-07
Ghb	3,5330	0,00457478	0,03370337
Snx7	3,5244	7,05E-06	0,0001462
Bmyc	3,5226	0,00639229	0,0434798
Fam198b	3,5203	0,00077816	0,00816246
Ctif	3,5197	0,00039911	0,00472068
H2-M2	3,5156	0,00370503	0,02877747
Sdhaf1	3,5107	0,00074306	0,00788038
Plk2	3,5080	1,86E-05	0,00034195
Smpdl3b	3,5059	0,00104484	0,01037964
Hebp1	3,5053	0,00026162	0,00329077
Themis2	3,4986	1,19E-09	5,57E-08
Cpd	3,4981	3,90E-11	2,29E-09
Myo5a	3,4977	1,26E-08	4,88E-07
Blnk	3,4963	6,74E-08	2,31E-06
Tada2a	3,4919	3,17E-05	0,00054173
Ltb4r1	3,4908	0,00711833	0,04710226
Bgn	3,4907	0,00412737	0,03129776
Gm43914	3,4845	0,00626837	0,04290531
Il15	3,4838	3,07E-06	7,02E-05
9430076C15Rik	3,4833	9,06E-07	2,39E-05
Tmem9	3,4748	3,05E-07	8,96E-06
Tctex1d2	3,4704	0,00034687	0,0041878
Gm6264	3,4677	0,00267728	0,02229154
Oas1g	3,4614	2,95E-06	6,80E-05
Slc13a3	3,4597	0,00517928	0,0371949
Gm4951	3,4570	0,00160554	0,01469585
Ramp1	3,4552	0,00256153	0,02154772
Anxa5	3,4525	1,33E-17	2,06E-15
Snx9	3,4517	2,49E-07	7,46E-06
Pilrb1	3,4510	2,92E-06	6,75E-05
Hk3	3,4505	5,09E-05	0,00082244
Adam8	3,4471	2,63E-05	0,00046028
Map3k15	3,4436	0,0006313	0,00690616
E130102H24Rik	3,4427	0,00722668	0,04764211
Fpr1	3,4400	0,00269881	0,02241358
Dck	3,4307	2,38E-11	1,46E-09
Adam15	3,4306	0,00023046	0,00297622
Tanc2	3,4282	1,24E-05	0,00023844
Chil3	3,4236	0,00399855	0,0305482
Pusl1	3,4160	0,00129195	0,01230181
Nfe2l3	3,4119	0,00250884	0,0212303
Pip5k1b	3,4079	0,00497897	0,03603017
Ace	3,4052	2,02E-05	0,00036636
Sult2b1	3,4045	0,00414614	0,03139635
Dock7	3,3952	1,89E-08	7,15E-07
Gm16139	3,3940	0,00438251	0,03264072
4933440N22Rik	3,3888	0,00351716	0,02766074
1810055G02Rik	3,3830	0,00444296	0,03297045
AW209491	3,3823	0,00025377	0,00321374
Gm23731	3,3682	0,00727667	0,04778173
Frmd5	3,3637	0,00151657	0,01410309
Cebpb	3,3604	2,88E-08	1,06E-06
Rsad2	3,3533	2,12E-06	5,08E-05
Tusc1	3,3523	8,61E-06	0,00017454
Vcan	3,3519	7,16E-11	4,07E-09
Tbc1d9	3,3468	0,00063561	0,00694871

Gene	FC	pval	padj
Mvk	3,3363	0,00077078	0,00811629
Ethe1	3,3361	0,002762	0,02282217
Dixdc1	3,3308	3,53E-05	0,00059932
Cisd1	3,3285	0,00017247	0,00232686
Hbegf	3,3273	4,65E-05	0,00075874
Hvcn1	3,3271	5,08E-06	0,00010997
Dll1	3,3257	0,00430846	0,03229566
Clec9a	3,3033	0,00119671	0,01148883
Lin28b	3,3026	0,00142249	0,01334229
Npl	3,3020	8,11E-05	0,00122151
Ptprj	3,3009	4,46E-13	3,73E-11
Gm28727	3,2989	0,00645465	0,04375801
Hpse	3,2976	7,09E-07	1,92E-05
Eepd1	3,2974	0,00062598	0,0068572
Gab1	3,2881	0,00058719	0,00653255
Dsg2	3,2874	0,00574221	0,04023245
Il2ra	3,2757	2,85E-06	6,61E-05
Ctsl	3,2726	9,46E-11	5,28E-09
Dram1	3,2713	2,68E-05	0,00046826
Tfe3	3,2694	1,75E-11	1,09E-09
Gm44949	3,2597	0,00726241	0,04776501
Fam46c	3,2567	7,42E-11	4,20E-09
Gm43499	3,2567	0,00585744	0,04084683
Cpq	3,2521	0,00028054	0,00349838
Ftl1	3,2499	2,19E-07	6,69E-06
St3gal5	3,2395	1,84E-05	0,00033888
Slc35f6	3,2364	3,38E-09	1,48E-07
Naaa	3,2286	1,20E-05	0,00023285
Art2a-ps	3,2177	1,16E-06	2,98E-05
Oas3	3,2177	7,43E-12	4,93E-10
Cd40	3,2173	2,62E-07	7,78E-06
Armc6	3,2170	0,00769856	0,04979106
Ophn1	3,2145	0,00085726	0,00883311
Hexa	3,2092	4,00E-11	2,34E-09
Slc16a7	3,2085	0,00054786	0,00616705
B830042I05Rik	3,2070	3,00E-09	1,34E-07
Tacc2	3,2028	0,00106468	0,01053766
Stx3	3,2013	3,32E-09	1,46E-07
Ifit2	3,2006	1,76E-09	8,09E-08
E230029C05Rik	3,2004	4,22E-06	9,26E-05
Pak6	3,2003	0,00156274	0,0143848
Ube2l6	3,1908	2,61E-05	0,0004596
Ccrl2	3,1897	2,67E-06	6,23E-05
Ell2	3,1895	4,73E-14	4,51E-12
Coq3	3,1812	0,00090924	0,00926329
Fam129c	3,1742	0,00208802	0,01833288
Gm15832	3,1730	0,00025989	0,00327596
Rgs12	3,1727	0,00131615	0,01248851
Pkib	3,1702	1,01E-06	2,62E-05
Ms4a4c	3,1672	3,91E-06	8,67E-05
Map7	3,1634	0,00032683	0,00398428
Gpam	3,1599	0,0021392	0,01865911
Zfp516	3,1598	0,00104063	0,01036244
Nol4l	3,1592	3,07E-09	1,36E-07
Mpo	3,1591	0,0068966	0,04598958
Fndc3b	3,1566	2,33E-05	0,00041611
B3gnt3	3,1559	0,00496136	0,03596652
Tfpi	3,1530	3,52E-06	7,90E-05
Arhgap19	3,1529	5,55E-14	5,20E-12
Acp2	3,1496	5,19E-09	2,18E-07
Scel	3,1468	0,00101369	0,01013752
Mfsd11	3,1462	7,20E-06	0,0001485
Gm42962	3,1449	0,00560571	0,03958764
Gcsam	3,1445	0,00362364	0,02828066
P4ha1	3,1405	1,16E-09	5,48E-08
Tns1	3,1348	0,00109747	0,01076417
E230016K23Rik	3,1335	0,00227246	0,01958062
Wdr41	3,1247	1,66E-08	6,31E-07
Mitf	3,1219	5,03E-05	0,0008149
Nrp2	3,1213	8,95E-05	0,00133141

Gene	FC	pval	padj
Fam135a	3,1179	0,00507668	0,0365911
Dnase1l1	3,1170	0,00013502	0,00188552
Cstb	3,1165	1,03E-10	5,71E-09
Rhag	3,1161	0,00518097	0,0371949
Nudt1	3,1077	0,00060467	0,00669572
B4galt6	3,1004	3,99E-06	8,80E-05
Dpp7	3,0977	0,00090707	0,00924697
Rasal2	3,0873	0,00046988	0,00542029
Ldlrad3	3,0839	7,90E-05	0,00119411
Tgfbr1	3,0820	1,23E-12	9,37E-11
Wwc2	3,0774	5,62E-05	0,00089734
Cyp27a1	3,0759	0,0006215	0,00682183
Cul7	3,0680	0,00467711	0,03424069
Rasa4	3,0630	6,85E-05	0,00105187
Bnip3	3,0588	2,56E-05	0,00045223
Sort1	3,0564	0,00212298	0,01855729
Btk	3,0545	0,00361822	0,02826477
Ccdc136	3,0451	0,00750388	0,04895451
Cst3	3,0432	2,67E-06	6,23E-05
Pik3r6	3,0418	9,70E-06	0,00019345
Pdgfa	3,0367	0,00233396	0,02000487
Gm42462	3,0331	0,00301778	0,0244769
Hsd17b7	3,0319	0,00058753	0,00653255
Gm37967	3,0303	0,00769573	0,04979106
Cdh5	3,0284	0,00017548	0,00236163
Gm16094	3,0282	0,00767278	0,0497024
Cd200r1	3,0221	0,00018131	0,00243204
Chst14	3,0200	0,0003389	0,00410372
Kcnj10	3,0175	0,00098855	0,00993839
Gm37354	3,0143	0,00247043	0,02097381
Itgb3	3,0128	5,92E-06	0,00012592
Zeb2os	3,0107	0,00120824	0,01157224
Il1f9	3,0064	0,00049566	0,0056695
Cln6	3,0009	0,00023038	0,00297622
Dnajc25	2,9959	1,08E-09	5,12E-08
Gm16464	2,9929	0,00311602	0,02520262
Rogdi	2,9907	0,00156559	0,01440291
Bcl2a1b	2,9876	8,41E-06	0,00017155
Cd22	2,9835	0,00015699	0,00214283
Alas1	2,9792	0,00024755	0,00315199
Scarb1	2,9792	8,07E-08	2,70E-06
Homer2	2,9766	0,00601192	0,04166065
Dnal1	2,9693	0,00628404	0,04294322
Mgat4b	2,9669	5,69E-05	0,00090647
Dna2	2,9604	1,20E-05	0,00023294
Wrb	2,9589	0,00013097	0,0018353
Cd302	2,9560	0,00066609	0,00720944
AI661453	2,9544	0,00401874	0,03065931
Ccl17	2,9481	0,00693733	0,0461856
Gins2	2,9429	0,0003722	0,00445083
Bpifc	2,9422	0,00260755	0,02184472
Bcar3	2,9414	0,00552057	0,03915042
1700030K09Rik	2,9413	0,0031194	0,02521335
Lonrf3	2,9383	0,00266323	0,02219718
Marcksl1	2,9319	0,00398369	0,03046321
Rnase6	2,9308	0,00223183	0,01931212
Dock4	2,9281	0,00275396	0,02277867
Sh2d1b2	2,9259	9,96E-05	0,00144832
Anxa4	2,9247	1,76E-11	1,09E-09
Tdrkh	2,9227	0,00502267	0,03626596
Cdkn1a	2,9209	3,97E-06	8,77E-05
Sgcb	2,9187	0,00518846	0,03721589
Cd300lf	2,9151	5,44E-09	2,27E-07
Arhgef12	2,9126	8,20E-05	0,00123287
5730409E04Rik	2,8991	0,00238421	0,02034996
2310022B05Rik	2,8986	0,00649174	0,04393642
Ift27	2,8977	0,00487319	0,03545347
Rhbdf2	2,8950	2,64E-06	6,18E-05
Ncf1	2,8858	7,89E-13	6,41E-11
Cenpn	2,8845	0,00280129	0,02306507

Gene	FC	pval	padj
Gm37058	2,8808	0,00109847	0,01076749
Bst2	2,8788	4,99E-08	1,76E-06
Hfe	2,8780	3,96E-05	0,00066019
Irak3	2,8726	0,00083878	0,00868383
B430306N03Rik	2,8702	1,27E-06	3,22E-05
Hdac9	2,8665	3,25E-09	1,43E-07
Atp1a3	2,8623	0,00021759	0,00283477
Lamp1	2,8621	7,13E-11	4,06E-09
Ppargc1b	2,8609	0,00063877	0,00696452
Sox11	2,8600	0,00753773	0,04906141
Gart	2,8583	9,84E-09	3,88E-07
Msra	2,8572	0,00012893	0,00181431
Mpp1	2,8544	7,98E-08	2,67E-06
Cd2ap	2,8390	5,31E-09	2,22E-07
Ccnd1	2,8366	0,00520285	0,03726995
Nek6	2,8270	8,63E-09	3,46E-07
Ifi27l2a	2,8232	0,00034214	0,00413687
Rnf141	2,8132	9,27E-17	1,34E-14
Serpinb6a	2,8128	9,14E-09	3,66E-07
Ptgs1	2,8121	5,78E-05	0,00091989
Senp8	2,8113	0,00594811	0,04135535
Fcgr3	2,8080	1,17E-05	0,00022892
Galk1	2,8069	0,00325191	0,02606907
Soat1	2,8053	1,85E-13	1,66E-11
Uevld	2,8047	5,96E-05	0,0009396
Mx1	2,7912	1,55E-06	3,80E-05
Alpk1	2,7860	0,00159183	0,01459489
4933423P22Rik	2,7799	0,00443952	0,03295997
Stard9	2,7766	0,0005241	0,00594767
Trpm2	2,7749	4,70E-07	1,33E-05
Ptrhd1	2,7661	0,00643329	0,04368788
Pros1	2,7572	0,00110315	0,01080209
Gaa	2,7489	0,00013113	0,00183588
Cpne2	2,7480	0,00047393	0,00546312
Ero1l	2,7471	1,52E-07	4,82E-06
Mfsd13a	2,7407	0,00703115	0,04660102
5031439G07Rik	2,7397	1,24E-05	0,00023887
Wdr11	2,7386	3,44E-06	7,77E-05
Ift57	2,7360	0,0006431	0,00699774
Zfp839	2,7327	2,06E-06	4,94E-05
Oxnad1	2,7276	0,00225759	0,01949364
Gm7160	2,7158	0,00313182	0,02526363
Pik3r2	2,7148	0,00077465	0,00814347
Espl1	2,7102	0,0004235	0,00496246
Gm43844	2,7099	0,00578034	0,04043013
Npc2	2,7040	5,98E-08	2,07E-06
Rbpj	2,7003	2,05E-12	1,46E-10
Pwwp2b	2,6996	0,0073411	0,04805002
Idh1	2,6934	8,03E-06	0,00016413
Matk	2,6930	0,00562071	0,03963659
Csf3r	2,6885	0,00095814	0,00968887
Vegfb	2,6837	0,00589505	0,04103894
Mob3b	2,6805	0,00026167	0,00329077
Swap70	2,6790	1,61E-08	6,13E-07
Fut4	2,6784	0,00602119	0,04166809
Lap3	2,6772	5,44E-05	0,00087063
Mtmr10	2,6722	5,21E-06	0,00011208
Eml6	2,6656	0,00096649	0,00975519
Xylt1	2,6539	4,46E-10	2,29E-08
Zfp992	2,6429	6,66E-05	0,00102855
Itsn1	2,6362	0,00069725	0,00747723
Pygl	2,6323	0,00020849	0,00274233
Trip13	2,6301	0,00224455	0,01941123
Irf5	2,6216	0,00037211	0,00445083
Hgh1	2,6201	0,00136431	0,01288399
Eef1e1	2,6201	3,73E-05	0,00062711
Siglecg	2,6189	0,00339936	0,02691603
Abhd12	2,6163	1,45E-07	4,63E-06
Evi2a	2,6137	6,08E-05	0,00095414
Mcfd2	2,6129	1,81E-05	0,00033528

Gene	FC	pval	padj
Smox	2,6120	1,18E-06	3,02E-05
Zfp111	2,6073	0,00422156	0,03182605
Galc	2,6066	6,43E-05	0,00100269
Lpxn	2,6063	0,00012358	0,00174821
Pqlc1	2,6023	0,00718682	0,04744002
Nme6	2,6020	0,00571436	0,04014078
Mlh3	2,6013	0,00566533	0,0399167
Best1	2,6011	0,00449385	0,03325734
Tmem50b	2,6001	9,43E-05	0,00138939
Bri3bp	2,5992	0,00010176	0,0014767
6820402A03Rik	2,5972	0,00040139	0,00474079
Skap2	2,5922	1,37E-07	4,42E-06
Lrp4	2,5905	0,00751107	0,04895451
Plac8	2,5882	0,00053166	0,00600959
Prdx4	2,5879	0,00545714	0,03873656
Cd81	2,5859	9,91E-05	0,00144146
Creg1	2,5848	0,0001386	0,00192894
Nfxl1	2,5837	9,76E-07	2,55E-05
Lrrtm2	2,5832	0,001882	0,01685739
Epas1	2,5824	1,19E-05	0,00023155
Maf	2,5822	1,06E-16	1,51E-14
Pgpep1	2,5821	0,00399042	0,03050036
Cndp2	2,5816	1,71E-11	1,08E-09
Tpd52	2,5764	9,92E-06	0,00019716
Sphk1	2,5725	0,00727084	0,04778173
Map4k3	2,5724	2,63E-06	6,18E-05
Dhx58	2,5639	9,59E-05	0,00140585
Slc25a13	2,5636	0,00014992	0,00206005
Spon1	2,5610	0,00019629	0,00260729
Ext1	2,5593	9,76E-05	0,00142532
Brca2	2,5569	0,00012929	0,00181635
Coq7	2,5548	0,00405236	0,03084373
Mcm8	2,5523	0,00640303	0,0435347
Nxpe5	2,5500	0,00518383	0,03719906
Slc31a2	2,5482	9,06E-06	0,00018173
Kif20a	2,5461	0,00233851	0,02002278
F7	2,5416	0,00526024	0,03758206
Bhlhe41	2,5414	0,00626703	0,04290531
Papss2	2,5410	6,12E-05	0,00095814
Prg4	2,5371	0,00521822	0,03734723
F630040K05Rik	2,5319	9,15E-05	0,00135463
Cln8	2,5316	0,00037545	0,00447985
Cadm1	2,5313	0,0049522	0,03591609
Slc17a8	2,5290	0,00077645	0,00815494
Ifit1	2,5285	0,00442211	0,0328906
St3gal2	2,5274	0,00104356	0,01037898
Sema6d	2,5267	0,00453739	0,03346899
C130089K02Rik	2,5227	0,00226602	0,01954573
Cyth3	2,5218	0,00017095	0,00231204
Mpv17l2	2,5139	0,00315793	0,02544914
Tmem156	2,5093	0,0027745	0,02291384
Phf11d	2,5078	6,08E-06	0,00012848
Fam129b	2,5073	0,00068346	0,00735835
Cyfip1	2,5062	1,72E-11	1,08E-09
Gm37780	2,5035	0,00461615	0,03395563
Fcgr2b	2,5035	1,46E-06	3,65E-05
Adam9	2,5034	6,60E-05	0,00102295
Ccdc88a	2,5012	2,64E-06	6,18E-05
Fgd6	2,4984	0,00018922	0,00252652
Gm17259	2,4982	0,00426853	0,03208823
Ubac1	2,4935	0,0027061	0,02242848
Cmpk2	2,4895	0,00024615	0,00313864
Nxt2	2,4882	0,00028206	0,00350928
Alcam	2,4834	0,00025344	0,00321196
Zfp821	2,4824	0,00279643	0,02303668
Atg14	2,4814	0,00616239	0,04239735
Gcnt2	2,4798	0,00210948	0,01847388
Erbb3	2,4770	0,00134185	0,01270282
Specc1	2,4763	6,54E-05	0,00101589
Atp6ap2	2,4687	4,19E-06	9,22E-05

Gene	FC	pval	padj
Trpm4	2,4674	0,002052	0,01811158
Gm11870	2,4669	0,00652602	0,04407697
Cep70	2,4626	0,00148766	0,0138579
Fnbp1l	2,4556	0,00023306	0,00300038
Yae1d1	2,4539	7,83E-08	2,64E-06
Aldh6a1	2,4521	0,00474111	0,03464708
Ddx60	2,4402	1,24E-05	0,00023844
Vwa5a	2,4371	2,53E-09	1,14E-07
Ifih1	2,4367	5,72E-06	0,00012212
Pak4	2,4348	8,66E-05	0,00129057
Tln2	2,4332	0,00077814	0,00816246
Pnp	2,4291	3,63E-07	1,05E-05
Dpp4	2,4290	0,00416095	0,03149311
Slc45a4	2,4242	0,00011239	0,00160802
Rnd3	2,4239	0,00566207	0,039911
Lipa	2,4186	7,10E-09	2,89E-07
Gm42989	2,4179	0,00359199	0,02810634
Tmem51	2,4155	0,00464485	0,03405037
Ndrg1	2,4139	0,00014141	0,00196469
Osbpl1a	2,4123	0,00174142	0,01578014
Pomk	2,4086	0,00261007	0,0218546
Coq4	2,4079	0,00376006	0,02906648
Irf7	2,4067	7,30E-05	0,0011126
Ak6	2,4039	0,00148953	0,01386746
Csf2rb2	2,4017	0,0001512	0,00207422
Nagpa	2,3901	6,82E-05	0,00104884
Nmnat3	2,3887	0,00314777	0,02537975
Cep76	2,3877	3,27E-05	0,00055834
Itga1	2,3830	1,22E-05	0,00023613
Hspbap1	2,3823	0,00426899	0,03208823
Gpr157	2,3822	0,00110864	0,01083468
Hilpda	2,3786	0,00012974	0,0018196
Rflnb	2,3774	0,00180186	0,01627358
Ogfrl1	2,3708	3,30E-06	7,47E-05
Trf	2,3691	0,00014317	0,00198404
Ly96	2,3662	0,00558017	0,03948197
Fads1	2,3609	0,00185285	0,01666948
Plin3	2,3608	0,00209844	0,018409
Blvra	2,3602	0,00031399	0,0038479
Gla	2,3582	3,66E-07	1,06E-05
Naglu	2,3543	0,0009359	0,00951122
1500015A07Rik	2,3536	0,00595778	0,04140488
Zfp458	2,3528	0,00567656	0,03996128
Fos	2,3493	0,0008481	0,00876079
Lyrm2	2,3473	0,00258049	0,02167376
Rnh1	2,3471	2,50E-08	9,21E-07
Skp2	2,3417	7,07E-06	0,00014632
Filip1l	2,3417	5,97E-12	4,02E-10
Igfbp4	2,3415	0,00010524	0,0015178
Tmem65	2,3383	2,22E-06	5,31E-05
Nceh1	2,3354	9,57E-06	0,00019096
Slc16a1	2,3340	0,00285724	0,02340755
E330009J07Rik	2,3291	0,00044665	0,00518896
Slamf6	2,3291	0,00375127	0,02904784
Dse	2,3238	2,10E-08	7,83E-07
Synj2	2,3232	0,00277807	0,02293174
Gm15601	2,3225	0,0025318	0,02138587
Ano10	2,3211	0,00154242	0,01427003
Adamtsl4	2,3161	0,00089986	0,00918829
Gusb	2,3151	8,60E-06	0,00017454
Mthfd2	2,3137	0,00259216	0,02174933
Psmg3	2,3134	0,0063855	0,04346989
Ccne1	2,3117	0,00586635	0,04089147
Ets2	2,3114	1,78E-06	4,33E-05
Sgpl1	2,3008	1,03E-05	0,00020406
Hbb-y	2,3002	0,00256799	0,02159096
Cxcr2	2,2984	0,00052684	0,0059676
Dnhd1	2,2977	0,0075562	0,04912283
Heatr5a	2,2890	5,17E-15	5,74E-13
Vps26a	2,2663	3,37E-10	1,76E-08

Gene	FC	pval	padj
Naa40	2,2653	0,00187405	0,01681386
Ocrl	2,2652	3,69E-06	8,24E-05
Dclre1c	2,2572	2,27E-12	1,61E-10
Litaf	2,2569	3,75E-09	1,62E-07
Msrb1	2,2512	0,00039849	0,00472068
Hs1bp3	2,2497	0,00729184	0,04784281
Emilin2	2,2476	4,43E-05	0,00072769
Umps	2,2465	0,00011455	0,00163472
Kmo	2,2391	0,00335349	0,02663034
Dennd2a	2,2268	0,00061998	0,00681435
Slc43a2	2,2261	7,20E-06	0,0001485
Hivep3	2,2226	2,29E-07	6,98E-06
Tmem206	2,2176	1,30E-05	0,00024778
Ttc27	2,2173	0,00626748	0,04290531
Oas1a	2,2164	0,00038977	0,00463045
Sh3pxd2a	2,2084	0,0069692	0,04632219
Sema4b	2,2058	4,74E-09	2,01E-07
Prdx1	2,2031	4,64E-09	1,98E-07
Erlin1	2,2031	0,00016711	0,00227149
Hexb	2,2026	1,53E-06	3,78E-05
Gch1	2,2023	1,30E-05	0,00024808
Ydjc	2,1997	0,00274002	0,02268653
Aacs	2,1985	0,00327906	0,02623086
Mtmr4	2,1985	7,22E-05	0,00110257
Cd274	2,1958	1,83E-06	4,43E-05
Lamp2	2,1926	4,13E-05	0,00068463
Mfsd1	2,1898	3,58E-11	2,12E-09
Gpr146	2,1866	0,00037607	0,004484
Gclm	2,1844	0,00011388	0,00162656
Gfra2	2,1820	0,0072238	0,04764211
Hsd17b11	2,1817	0,00014417	0,00199459
Slc30a1	2,1732	1,79E-06	4,34E-05
Atpif1	2,1704	0,00014718	0,00202928
Abcg1	2,1655	1,85E-06	4,47E-05
Ciita	2,1617	0,00543731	0,03862716
Pigl	2,1533	0,00058487	0,00651176
Stat2	2,1526	1,41E-06	3,53E-05
Dennd1a	2,1460	8,28E-08	2,76E-06
Klhl21	2,1458	0,00382863	0,02947084
Dnajc4	2,1445	0,00435788	0,03250174
Frmd4b	2,1444	2,38E-06	5,64E-05
Clcn5	2,1433	2,81E-06	6,53E-05
Lair1	2,1431	0,00024099	0,00309022
Pgd	2,1427	1,42E-07	4,55E-06
Evi5	2,1423	0,00014526	0,00200447
Frmd4a	2,1410	7,23E-06	0,00014878
Cacna2d4	2,1403	0,0001481	0,00204023
D630030B08Rik	2,1399	0,00662868	0,04458574
Sat1	2,1380	4,06E-05	0,00067435
Atp6v1c1	2,1275	3,53E-09	1,54E-07
Sh3tc1	2,1232	0,00258631	0,02171144
Tep1	2,1212	0,00022249	0,00288937
Slc9a6	2,1149	0,00462274	0,03397967
Selenop	2,1130	8,17E-10	4,01E-08
Mettl6	2,1038	2,48E-07	7,46E-06
Pofut2	2,1036	0,00048129	0,00553621
Akr1a1	2,1032	7,97E-07	2,13E-05
Ndc1	2,0985	0,00032907	0,00400556
Lxn	2,0880	2,55E-05	0,00045016
Capg	2,0863	1,31E-05	0,00024921
Smim3	2,0855	0,00061941	0,00681267
Rnf215	2,0821	0,00451872	0,03339597
Abcc5	2,0807	7,99E-05	0,00120616
Agpat5	2,0788	0,00254606	0,02145084
Fam213a	2,0770	0,0028979	0,0236456
Rell1	2,0768	6,24E-05	0,00097629
Qpct	2,0732	0,00677168	0,0453978
Rgl1	2,0658	1,21E-05	0,00023412
Fam84b	2,0653	0,00177301	0,01604546
Ssx2ip	2,0525	0,00450695	0,03332405

Gene	FC	pval	padj
Tspan3	2,0511	0,00575882	0,0403142
H1f0	2,0468	6,48E-05	0,00100787
Scrn3	2,0464	0,0047799	0,0348569
Itpripl2	2,0460	9,08E-07	2,39E-05
Ssfa2	2,0431	1,02E-05	0,00020189
Jup	2,0404	4,71E-07	1,33E-05
4931406C07Rik	2,0402	0,00711198	0,04707935
Tmem104	2,0374	0,00269305	0,02238856
Wdr46	2,0353	1,96E-05	0,00035889
Mxi1	2,0341	0,00060565	0,00670198
Sgk3	2,0313	0,00108079	0,01063895
Champ1	2,0220	0,00040646	0,00479377
Fam76a	2,0183	0,00156752	0,01441251
Ddhd1	2,0102	9,46E-09	3,75E-07
Ly6e	2,0074	1,58E-05	0,00029576
Tbc1d24	2,0074	0,00137481	0,01296964
Cables1	2,0065	0,00744367	0,04860436
Rdh10	-2,0096	0,00337013	0,02673645
Ubxn11	-2,0110	0,00073136	0,00778156
Bach2	-2,0112	1,10E-05	0,00021682
A130071D04Rik	-2,0176	0,00011791	0,00167675
Zhx2	-2,0232	1,11E-05	0,00021791
Klra3	-2,0243	0,00044288	0,00515617
Abtb2	-2,0266	0,00471772	0,03449155
Scfd2	-2,0305	0,00098857	0,00993839
Gfod1	-2,0310	5,40E-05	0,00086656
Zdhhc15	-2,0315	0,00053367	0,00601979
1700025G04Rik	-2,0329	6,92E-07	1,88E-05
Dxo	-2,0364	0,00132798	0,0125934
Lrrc28	-2,0409	0,00598286	0,04154382
Serpinb9	-2,0421	0,00026128	0,00329077
Cd247	-2,0422	0,00068494	0,00736944
Rab37	-2,0426	0,0011279	0,01098338
Arhgef4	-2,0428	0,0067296	0,04517143
Stk10	-2,0488	2,65E-06	6,19E-05
Spata13	-2,0532	2,29E-06	5,46E-05
Asap2	-2,0665	9,55E-05	0,00140239
Ets1	-2,0697	3,20E-05	0,00054709
Fyn	-2,0726	2,81E-05	0,00048876
Tas1r3	-2,0733	0,00684383	0,04566306
Ndnf	-2,0737	0,00036305	0,00436057
Gigyf1	-2,0748	0,00248731	0,02108654
Tmtc4	-2,0790	8,76E-07	2,31E-05
Rbm12	-2,0814	5,60E-07	1,54E-05
Rarg	-2,0870	0,00730062	0,04788112
Kif21b	-2,0870	5,29E-10	2,68E-08
Gnal	-2,0899	1,21E-05	0,0002343
Rasgrp2	-2,0905	6,46E-05	0,00100713
Hip1r	-2,0916	2,46E-07	7,41E-06
Ipcef1	-2,0959	3,87E-06	8,59E-05
Depdc1b	-2,1003	0,0071982	0,04749587
Slc2a4rg-ps	-2,1006	0,00172037	0,01561549
Deb1	-2,1047	0,0013864	0,01306385
Arhgef3	-2,1068	8,04E-10	3,97E-08
Fbxo32	-2,1070	0,00093052	0,0094707
Klra1	-2,1102	0,00752014	0,04898601
Tulp4	-2,1169	1,68E-06	4,10E-05
Tspan32	-2,1179	6,27E-06	0,00013139
Gimap8	-2,1251	0,00326089	0,02609959
Zfp212	-2,1317	3,56E-05	0,00060229
Atg4d	-2,1346	0,00154606	0,01427957
Fam184a	-2,1347	0,00186657	0,01676521
Atg4b	-2,1388	9,26E-06	0,00018532
Vps37b	-2,1405	0,00122251	0,0116952
Gimap4	-2,1427	0,00042537	0,00497718
Gimap3	-2,1490	0,00012654	0,00178695
S1pr4	-2,1512	3,02E-05	0,00052012
1810034E14Rik	-2,1583	0,00461285	0,03395318
Ccdc88c	-2,1636	1,54E-05	0,00028884
Smad3	-2,1643	5,86E-07	1,61E-05

Gene	FC	pval	padj
Atp2a3	-2,1778	0,00010735	0,00154407
Gm7967	-2,1780	0,00338904	0,02686033
Gm38384	-2,1896	0,00299081	0,02430648
Hsd11b1	-2,1986	0,00177365	0,01604546
Zfp235	-2,1989	0,00598768	0,0415596
Phf1	-2,2070	8,55E-05	0,00127778
Rfx3	-2,2137	2,54E-06	5,99E-05
Plppr3	-2,2168	3,31E-05	0,00056405
Card6	-2,2208	2,46E-07	7,40E-06
Ptpn4	-2,2225	2,62E-05	0,0004596
Dgka	-2,2234	0,00017367	0,00233912
Cwf19l1	-2,2245	0,00382487	0,0294558
Gm37702	-2,2340	0,00484585	0,03527025
Fcho1	-2,2451	1,59E-05	0,00029765
Satb1	-2,2486	0,00117809	0,01136359
Sh2d3c	-2,2498	2,26E-07	6,90E-06
Pde7a	-2,2551	4,97E-09	2,10E-07
Ifng	-2,2564	0,00483601	0,03521432
Prkag1	-2,2582	0,00051553	0,00586792
Tmc8	-2,2716	1,36E-05	0,00025803
Gm11346	-2,2723	0,00753383	0,04905559
Gm19585	-2,2743	0,00095234	0,00964816
Spry2	-2,2744	0,00027185	0,00340307
Raver2	-2,2774	0,00211698	0,01852471
Sec22c	-2,2810	0,00180442	0,01628773
AA465934	-2,2849	0,00116126	0,01122782
Zfp945	-2,2859	3,72E-05	0,00062605
Fam65b	-2,2970	1,47E-06	3,65E-05
Ccnd2	-2,3039	7,66E-09	3,09E-07
Pim2	-2,3050	1,34E-05	0,00025562
Dusp2	-2,3096	4,52E-05	0,00074057
Nxpe3	-2,3130	0,00018235	0,00244398
Plekhg2	-2,3167	3,13E-06	7,12E-05
Itga4	-2,3224	1,55E-07	4,89E-06
Cd27	-2,3259	0,00217045	0,01888894
Tob1	-2,3392	0,00010373	0,00150123
Ncr1	-2,3447	0,00101776	0,01017194
Hrh2	-2,3527	0,00033777	0,00409317
B930095G15Rik	-2,3538	0,00532769	0,03798073
Gm26586	-2,3697	0,00320943	0,02582585
Ccnd3	-2,3755	5,26E-05	0,00084637
Mxd4	-2,3774	1,21E-05	0,00023412
Gm43747	-2,3819	0,00529496	0,03781355
Nkg7	-2,3822	3,70E-05	0,00062338
Skap1	-2,3856	7,80E-05	0,00118395
Poc5	-2,3910	0,00056545	0,0063254
Mmgt2	-2,3917	6,07E-05	0,00095414
Amotl1	-2,3930	0,0061575	0,04239735
D430013B06Rik	-2,3957	0,00306165	0,02482035
Zfhx2	-2,3971	1,13E-12	8,76E-11
Aknaos	-2,4095	0,00010939	0,00157207
Baiap2	-2,4115	8,64E-06	0,00017489
Lpin1	-2,4158	2,99E-09	1,33E-07
Slc26a10	-2,4237	0,00057486	0,00640473
Klrb1c	-2,4339	2,21E-06	5,28E-05
2810039B14Rik	-2,4415	0,00078583	0,00821121
Gm38243	-2,4427	0,00433519	0,03240665
Gpc1	-2,4430	0,00027106	0,00339571
Adamts14	-2,4435	5,59E-06	0,00011961
Klrd1	-2,4496	0,00011847	0,00168323
B3gnt7	-2,4518	0,00050865	0,00579779
Klra9	-2,4620	0,00026804	0,00336055
Syne3	-2,4621	0,00011718	0,00166925
Zscan20	-2,4736	0,00101107	0,01012377
Gm26189	-2,4791	0,00723915	0,04766969
Rap1gap2	-2,4833	3,07E-05	0,00052612
Rab11fip4	-2,4925	9,40E-05	0,00138932
Zfp275	-2,4936	0,00017007	0,002304
Slc25a53	-2,4958	0,00010045	0,00145899
Gm4956	-2,5068	0,00078314	0,00819686

Gene	FC	pval	padj
Ascc1	-2,5088	2,62E-05	0,0004596
Gm43062	-2,5124	0,00248321	0,02106273
Prkca	-2,5156	0,00037019	0,00443655
Camk2n1	-2,5295	6,33E-06	0,00013246
F2rl2	-2,5372	3,84E-08	1,38E-06
Chrne	-2,5385	0,00086633	0,00889839
Zfp473	-2,5385	0,00492728	0,0357831
Klrb1f	-2,5464	2,92E-06	6,75E-05
Rbm38	-2,5549	3,69E-05	0,00062317
Rtm34	-2,5556	0,00028106	0,00350224
Gzma	-2,5852	0,00011078	0,00159061
Dab2ip	-2,5920	1,79E-06	4,34E-05
Galntl6	-2,5972	0,00756349	0,04915061
Fbxl2	-2,5989	0,00360127	0,02814583
Sorcs2	-2,6085	0,00095408	0,00965981
Llgl2	-2,6086	0,0025786	0,02166901
Dnah8	-2,6098	1,55E-05	0,00029022
Amigo1	-2,6130	0,00012669	0,00178754
Sbk1	-2,6141	0,00453461	0,03346785
Gm4759	-2,6149	0,00073097	0,00778156
Ddx43	-2,6229	0,00145071	0,01354467
Gm26762	-2,6266	0,00061303	0,00675828
Cnrip1	-2,6300	0,00075453	0,00798648
Gm36931	-2,6350	0,00067172	0,00725594
Gm38126	-2,6394	0,00178873	0,01616989
Gm10125	-2,6493	0,00103755	0,01033809
Atxn7l2	-2,6496	0,0001026	0,0014862
C230085N15Rik	-2,6509	0,00120053	0,01151198
Dpy19l3	-2,6578	5,45E-07	1,51E-05
Stat4	-2,6624	1,38E-07	4,44E-06
Ankrd13d	-2,6670	0,00519648	0,03724067
Sytl3	-2,6690	7,04E-06	0,00014615
Pias3	-2,6711	0,00030205	0,00371266
Vopp1	-2,6750	1,50E-10	8,15E-09
6030443J06Rik	-2,6759	0,00461735	0,03395563
Rnf157	-2,7002	6,87E-08	2,35E-06
Gm42684	-2,7065	0,00036637	0,00439401
Zfp831	-2,7068	0,00056931	0,00636029
Il12rb2	-2,7221	1,46E-06	3,64E-05
D8Ertd82e	-2,7255	4,19E-10	2,16E-08
A930006L05Rik	-2,7321	0,00452464	0,0334094
Tmtc1	-2,7438	0,00107443	0,01060514
Gm19557	-2,7477	3,82E-05	0,0006403
Itgb7	-2,7589	1,15E-07	3,75E-06
Klra6	-2,7644	1,13E-06	2,91E-05
Spn	-2,7708	2,45E-11	1,50E-09
AI847159	-2,7737	1,49E-06	3,70E-05
Gm16334	-2,7928	0,00186012	0,01672571
Gm37520	-2,7971	0,00739152	0,0483425
Gjb2	-2,8145	0,00125622	0,0119966
Mirt1	-2,8203	8,79E-06	0,00017727
Klra13-ps	-2,8248	4,94E-05	0,00080184
Gm42585	-2,8440	0,00099913	0,01002266
1810024B03Rik	-2,8450	0,00669764	0,04497536
Lrrn4cl	-2,8483	0,00698125	0,04636451
Gm37023	-2,8533	0,00329574	0,02633848
Zfp937	-2,8551	3,94E-08	1,41E-06
Klrk1	-2,8703	1,14E-06	2,93E-05
Zfp420	-2,8770	9,09E-05	0,00134777
Klra14-ps	-2,8910	7,68E-05	0,00116806
Polm	-2,8938	1,18E-05	0,00022964
Lrrc75a	-2,8946	1,79E-05	0,00033142
Hs3st3b1	-2,9002	5,79E-06	0,00012338
Bach2it1	-2,9014	0,00036257	0,00435803
Rbp	-2,9071	0,00346583	0,02730976
Gm12216	-2,9104	2,54E-05	0,00044892
Gm38224	-2,9110	6,26E-05	0,00097839
Gm37979	-2,9116	0,00475156	0,03469233
Borcs7	-2,9148	2,81E-14	2,81E-12
Rfx2	-2,9191	0,00255115	0,02147155

Gene	FC	pval	padj
Phactr3	-2,9419	0,00022371	0,00290283
Tbx21	-2,9437	0,00044274	0,00515617
Arhgef18	-2,9438	8,57E-07	2,27E-05
Bcl9l	-2,9461	2,59E-11	1,57E-09
Adgrl4	-2,9598	0,00571272	0,04014078
Scn3b	-2,9651	0,00449807	0,03327345
Rnf125	-2,9843	0,00046683	0,00539266
Zfp941	-2,9857	0,00560649	0,03958764
Gm37452	-2,9935	0,00587469	0,0409321
Gm37766	-2,9983	0,00715535	0,04727055
Gm16329	-2,9997	0,00263473	0,02199339
B3gnt5	-3,0018	3,36E-06	7,58E-05
Zfp946	-3,0155	0,00243121	0,02070784
Dyrk2	-3,0267	3,64E-13	3,09E-11
Gm37248	-3,0482	0,00077486	0,00814347
Plcb4	-3,0500	4,95E-06	0,00010737
Itgam	-3,0524	0,0037958	0,02928725
A430078G23Rik	-3,0529	3,79E-07	1,09E-05
Gm18853	-3,0566	0,00330421	0,02636741
Itga2	-3,0744	0,00012864	0,00181197
Cdc20b	-3,0899	0,00585286	0,04083232
Cspg5	-3,0927	0,00416278	0,03149311
Mcam	-3,1123	0,00188089	0,01685739
Elovl7	-3,1273	0,000815	0,00847801
Zdhhc12	-3,1381	0,00055676	0,00625432
D130040H23Rik	-3,1409	0,00013266	0,00185422
Pxylp1	-3,1536	0,00041977	0,00493291
Gm27240	-3,1732	4,17E-05	0,00069041
Gm37266	-3,1743	0,00147366	0,01373536
Gm26910	-3,1841	0,00167285	0,01523501
Gm42572	-3,2151	1,06E-05	0,00020943
Prss30	-3,2186	0,00669422	0,04497093
Gm42822	-3,2531	2,63E-05	0,00046028
Gm43214	-3,2592	0,00694337	0,04619703
E430014B02Rik	-3,2596	9,79E-06	0,00019501
4930481A15Rik	-3,2611	0,00381699	0,02940905
Gramd3	-3,2645	0,00010618	0,00152988
Mgst2	-3,2919	2,98E-05	0,00051401
C330011M18Rik	-3,3009	1,09E-05	0,00021501
Pde2a	-3,3107	2,21E-05	0,00039672
Mss51	-3,3193	0,00107422	0,01060514
Gm29157	-3,3217	0,00624323	0,04282308
Il18rap	-3,3274	8,44E-05	0,00126471
Il18r1	-3,3301	0,00268337	0,02231949
Arl4d	-3,3330	6,09E-07	1,67E-05
Katnb1	-3,3364	1,60E-05	0,00029945
A630072L19Rik	-3,3509	0,00192544	0,01715469
Baiap3	-3,3577	9,22E-06	0,00018467
Gm45235	-3,3758	0,00572678	0,04017612
Klf12	-3,3865	0,00013166	0,00184172
Gm16239	-3,3936	0,00298323	0,02426487
Tmed1	-3,4016	0,00407576	0,03097847
Lat	-3,4087	1,90E-05	0,00034852
Tshz3	-3,4182	2,10E-09	9,54E-08
Gm26580	-3,4212	0,00019912	0,00263412
Ccl5	-3,4222	1,85E-07	5,73E-06
H2-Ob	-3,4375	3,03E-06	6,95E-05
Sell	-3,4412	3,06E-08	1,12E-06
Gm43203	-3,4427	0,0033565	0,02664126
Gm24119	-3,4457	0,00246307	0,02093543
Rab6b	-3,4599	2,28E-06	5,43E-05
2010300F17Rik	-3,4685	0,00031129	0,00381765
Flywch1	-3,4918	0,00677838	0,04542407
6720464F23Rik	-3,4943	0,00159873	0,01464997
Dlg3	-3,5002	8,46E-06	0,00017227
Gm16845	-3,5045	0,00015505	0,00211982
Tmem71	-3,5451	2,14E-10	1,14E-08
Btbd11	-3,5482	4,95E-08	1,75E-06
Gm20518	-3,5609	0,00119217	0,01146552
Gm15854	-3,5822	0,00066483	0,00720059

Gene	FC	pval	padj
Gm29155	-3,5940	0,00566897	0,03992514
Klrc3	-3,5947	8,72E-06	0,00017628
Klrc1	-3,5987	1,05E-06	2,72E-05
Cdk5r1	-3,6102	0,00196839	0,01748714
Klri1	-3,6206	2,56E-07	7,63E-06
Gm26792	-3,6212	0,00208027	0,01830162
Klrb1a	-3,6425	1,85E-07	5,73E-06
Slc2a10	-3,6632	0,00075999	0,00803908
Qprt	-3,6887	1,08E-07	3,53E-06
Gm29123	-3,7148	1,25E-05	0,0002396
Gm38026	-3,7761	2,23E-07	6,81E-06
St6galnac2	-3,7794	0,0029083	0,02371699
Gm44746	-3,7910	0,00048523	0,00557365
Kcnc1	-3,7956	4,75E-05	0,00077339
Tgfb3	-3,8285	0,0009778	0,00985547
4930431P19Rik	-3,8391	0,00114196	0,01109383
Gm21909	-3,8436	1,37E-05	0,00025904
Gm22779	-3,8551	0,00513028	0,03692851
Gm37176	-3,8585	0,00076659	0,00807737
Gm10490	-3,8624	0,0062268	0,04272838
Gm38309	-3,8644	0,00043449	0,00507295
Gm38118	-3,8667	2,60E-05	0,00045761
Heatr9	-3,8988	3,15E-06	7,16E-05
Gm11655	-3,9020	0,00560218	0,03958764
Gm14125	-3,9135	0,00267399	0,02227547
Klrc2	-3,9217	1,01E-07	3,34E-06
Gm45107	-3,9409	0,00609441	0,04206765
Cyp17a1	-3,9413	0,00331704	0,02640917
Serpini1	-3,9478	3,88E-07	1,11E-05
Gm16479	-3,9559	0,00041056	0,00483509
Gm13807	-3,9670	3,55E-05	0,00060133
Cldnd2	-4,0546	6,79E-06	0,00014152
5430400D12Rik	-4,0936	0,00385823	0,02967068
Cacna2d2	-4,1292	0,00045298	0,00525501
Gm43172	-4,1322	0,00329762	0,02634058
G0s2	-4,1841	0,0019172	0,01709752
Gm25635	-4,2264	0,00191014	0,01705325
Muc4	-4,2268	0,00051806	0,0058927
Wdr86	-4,2272	0,00163434	0,01490927
Plekhg5	-4,2341	1,63E-15	1,93E-13
Gm10522	-4,2690	9,07E-05	0,00134715
Gm43860	-4,2946	0,00191204	0,01706084
Gm10505	-4,3106	0,00188708	0,01689361
Gm37593	-4,3221	9,87E-05	0,00143695
Gm28277	-4,3612	0,00213293	0,01861435
Gm37785	-4,3975	0,00064283	0,00699774
Gm24724	-4,4004	0,00221467	0,01921464
Klrb1	-4,4021	1,86E-06	4,48E-05
Sspo	-4,4122	0,00114448	0,0111117
Rac3	-4,4690	0,0005658	0,0063254
Cdc42ep1	-4,5971	5,12E-05	0,00082644
2810468N07Rik	-4,6006	0,00014886	0,00204729
Gm13375	-4,6475	0,00020898	0,00274233
Fam132b	-4,7309	0,00026803	0,00336055
Casq1	-4,7581	0,00043618	0,00508905
Bmp10	-4,7882	0,00016816	0,00228197
Gm43913	-4,8036	5,40E-05	0,00086656
A3galt2	-4,8067	0,0003494	0,00421525
Gm6934	-4,8923	2,72E-05	0,00047484
Ablim2	-4,9209	0,0002455	0,00313331
Camsap3	-4,9434	0,00013767	0,00191887
Fam124b	-5,0117	0,00024241	0,00309866
Gm27241	-5,0414	5,94E-05	0,00093755
St6galnac3	-5,0558	7,38E-07	1,99E-05
Gm26744	-5,0955	0,00015497	0,00211982
E230020A03Rik	-5,0981	4,19E-05	0,0006928
Ccdc38	-5,1495	5,99E-05	0,00094458
Fibcd1	-5,2128	0,000286	0,00354748
9130008F23Rik	-5,3625	2,60E-06	6,12E-05
Gm10130	-5,5650	1,75E-05	0,00032602

Gene	FC	pval	padj
Anxa8	-5,7120	1,88E-07	5,80E-06
Tmem74b	-5,8824	2,03E-05	0,00036754
Sync	-6,2754	4,45E-06	9,75E-05
D830036C21Rik	-6,3229	6,65E-06	0,0001388
Ccdc146	-6,3407	1,89E-09	8,61E-08
Cym	-6,7192	7,19E-08	2,44E-06
Nap1l5	-6,8915	1,34E-08	5,20E-07

Table A.5. Comparison V. All differentially expressed genes from the comparison V: uterine Eomes^{-}CD49a^{+} (ILC1) subset vs uterine Eomes^{+}CD49a^{+} (trNK) subset. FC: fold change, padj: adjusted p-value.

Gene	FC	pval	padj
Aplnr	5,0496	6,26E-05	0,00504772
Gm27241	4,4456	0,00041432	0,02159677
Gm15987	3,9392	2,73E-06	0,0004615
Gm10522	3,9053	0,0003522	0,01887779
9130008F23Rik	3,7796	0,00097806	0,03852492
Adgre4	3,6980	4,85E-08	2,55E-05
Ace	3,6852	1,19E-06	0,0002814
Palm	3,6636	0,00061672	0,0280977
Gm37979	3,5102	0,00065058	0,0293859
C920021L13Rik	3,5077	4,06E-05	0,00363311
Ccdc102a	3,4482	1,90E-05	0,00209489
Gm42585	3,2837	0,0001434	0,00951428
Gm16121	3,2798	0,0001842	0,01154865
Treml4	3,2742	5,58E-09	4,49E-06
Hes1	3,2085	0,00085346	0,03525448
Igkc	3,1713	0,0002597	0,01478965
Kmo	3,1188	1,22E-05	0,00151485
Scarna3b	3,1146	0,00103707	0,04006996
Cd300e	3,1016	6,85E-09	4,68E-06
Sirpb1a	3,0948	9,30E-07	0,00022697
Skint3	2,9532	0,00031637	0,01729642
B4galt4	2,8950	0,00014611	0,00964738
Ciita	2,8132	0,00022497	0,01342742
Tmem176b	2,8132	1,33E-07	5,34E-05
Cyp4f16	2,8035	3,43E-06	0,00054469
Clec9a	2,7758	0,00048389	0,02361934
Sirpb1c	2,7674	0,00078001	0,03357541
Dpp4	2,7476	0,00085634	0,03525448
Pilrb2	2,6831	1,45E-05	0,00171952
Rasgrp4	2,6741	0,000415	0,02159677
Nxpe4	2,6699	6,49E-06	0,00093431
Klra2	2,6257	4,22E-06	0,00063342
Gm561	2,5694	0,0013506	0,04819844
Tmem176a	2,5533	0,00010935	0,00764432
Gm8953	2,5299	1,96E-07	7,23E-05
H2-Aa	2,5054	2,62E-05	0,00273628
I830077J02Rik	2,5020	0,0008274	0,03458395
Kynu	2,4816	0,00082457	0,03458395
Mgl2	2,4457	0,00088375	0,03605712
Pilra	2,4219	3,44E-05	0,00319678
H2-Ab1	2,3892	5,44E-05	0,00450649
Ear2	2,3815	4,17E-05	0,00367408
Clec4a1	2,3809	0,00039539	0,02078532
H2-Eb1	2,3790	2,46E-06	0,00043184
Spon1	2,3696	0,00050507	0,02435356
H2-DMb1	2,3345	0,00037695	0,01996954
Lifr	2,3167	2,04E-05	0,00221665
Cd74	2,3111	7,49E-05	0,00568488
Tax1bp3	2,2193	0,0004434	0,02244572
Cd300ld	2,1988	1,02E-05	0,00130177
Lilra5	2,1943	9,77E-05	0,00703106
Fgd2	2,1829	3,88E-05	0,00351213
1600010M07Rik	2,1385	0,00010962	0,00764432
Smad1	2,0967	0,00016498	0,01063651
Tifab	2,0883	0,00042229	0,02176349
Ppfia4	2,0474	0,00022444	0,01342742
Clec4a3	2,0303	0,00046176	0,02285796
Fam49a	2,0290	4,10E-06	0,00062567
Pld4	2,0256	0,00014328	0,00951428
fam49a	2,0140	1,56E-09	1,34E-06
Ikzf3	-2,0041	7,16E-05	0,00559347
Bcl2	-2,0072	5,72E-08	2,79E-05
Gimap4	-2,0169	0,00094281	0,03767917
Pabpc4	-2,0278	1,91E-06	0,00036684
Rmdn3	-2,0574	0,00081031	0,03428888
Ptch1	-2,0574	0,0001524	0,00999904
Kctd9	-2,0788	4,73E-05	0,00403496
Osbpl5	-2,0846	0,00136174	0,04846924
Gm43481	-2,0998	0,00052174	0,02479064
Pole	-2,1047	0,00016233	0,01051495

Gene	FC	pval	padj
Ppp3cc	-2,1115	2,69E-05	0,00278543
Bbs9	-2,1149	0,00092056	0,03700647
Nfatc2ip	-2,1248	0,00037076	0,01971823
Padi2	-2,1397	1,00E-05	0,00129683
Nedd4	-2,1462	2,45E-05	0,00259101
Gem	-2,1464	0,00017611	0,01119578
Xcl1	-2,1708	0,00119996	0,04531157
Acot7	-2,1832	7,91E-05	0,00591007
Camk2n1	-2,1945	0,00027867	0,01548341
Fktn	-2,2090	0,00021168	0,0128017
Brca1	-2,2259	0,000216	0,01300573
Eef2k	-2,2294	0,00050603	0,02435356
Klrb1c	-2,2487	1,45E-05	0,00171952
Arsb	-2,2582	1,23E-07	5,08E-05
Slain1	-2,2698	7,54E-05	0,00569643
Bspry	-2,2733	0,00068256	0,03041489
Rhof	-2,2772	0,00014069	0,0094262
Lef1	-2,2831	0,00043795	0,02233538
Slc14a1	-2,2959	3,66E-05	0,0033598
Gm20743	-2,2987	0,00065144	0,0293859
Gm44226	-2,2997	5,65E-05	0,00464868
Dab2ip	-2,3052	7,39E-05	0,00563961
Ahdc1	-2,3165	0,00020667	0,01261039
Trbc1	-2,3202	0,00052237	0,02479064
Ablim1	-2,3322	2,50E-05	0,00262804
Xrcc5	-2,3340	0,00057651	0,0266207
1300002E11Rik	-2,3415	0,00018109	0,0114307
Pcgf2	-2,3462	0,0007775	0,03357541
Limk2	-2,3569	1,31E-06	0,00030052
Tnfrsf18	-2,3702	0,0005649	0,02638089
Gm38346	-2,3745	0,00047077	0,02314551
Gfod1	-2,3872	6,29E-06	0,00091954
Cd96	-2,3986	0,00117238	0,0445114
Samd3	-2,3993	0,00028948	0,01601882
Chst11	-2,4225	6,80E-08	3,10E-05
Klri2	-2,4256	0,00031078	0,0170591
Tnfrsf26	-2,4287	1,53E-06	0,00031237
Itgb3	-2,4314	0,00025364	0,014566
2900026A02Rik	-2,4517	6,89E-05	0,00544638
Adamts14	-2,4568	6,79E-06	0,00096455
Cd28	-2,4762	0,00020608	0,01261039
Katnal1	-2,4863	6,86E-05	0,00544638
Gimap1os	-2,4926	0,00139434	0,0493725
Capn5	-2,4932	0,00056872	0,02638089
Gimap7	-2,4961	0,00024688	0,01424265
Tanc1	-2,5030	0,00098382	0,0385295
Zdhhc15	-2,5388	5,72E-05	0,00468462
Ets1	-2,5391	4,65E-07	0,00013531
Bzrap1	-2,5623	0,00052552	0,02485418
Pitpnm2	-2,5643	0,00012015	0,00825203
Klra14-ps	-2,5684	0,0010517	0,04049173
Mctp2	-2,5714	2,64E-07	9,26E-05
Klhl8	-2,6086	1,98E-06	0,00036684
Gimap3	-2,6158	3,55E-06	0,00055755
Plod2	-2,6199	4,58E-05	0,00395799
Ubxn11	-2,6405	4,68E-05	0,00402194
Fcrl6	-2,6518	0,00033877	0,01837423
Unkl	-2,6749	1,43E-05	0,00171952
Arhgef5	-2,6791	0,00050068	0,02426705
Icos	-2,6875	6,28E-05	0,00504772
Ctsw	-2,6975	3,62E-05	0,00334533
Slc17a8	-2,7108	0,00044878	0,02246844
Cst7	-2,7236	0,00010759	0,00758002
Sytl2	-2,7288	3,13E-07	0,00010421
E030018B13Rik	-2,7292	0,00134823	0,04819844
Asb1	-2,7304	3,25E-05	0,00308231
Cd247	-2,7357	1,39E-05	0,00169348
Nkg7	-2,7417	2,56E-06	0,00044214
Cbwd1	-2,7531	0,0005683	0,02638089
Gzma	-2,7555	3,85E-05	0,00350989

Gene	FC	pval	padj
Slc7a2	-2,7606	1,75E-05	0,00196409
Ltbp3	-2,7616	3,12E-05	0,00299843
Il2rb	-2,7694	7,43E-07	0,00019532
Gzmc	-2,7755	0,00056939	0,02638089
Itk	-2,7794	2,92E-05	0,0029161
Ppp1r16b	-2,7860	1,36E-06	0,00030052
B230216N24Rik	-2,7864	0,00048491	0,02361934
Gm43660	-2,7889	0,0010938	0,04175985
Dnah8	-2,7956	1,13E-05	0,00142071
Epas1	-2,8122	1,98E-06	0,00036684
F2rl2	-2,8162	4,29E-08	2,35E-05
Gpnmb	-2,8276	7,36E-06	0,00102671
Epcam	-2,8278	0,00075365	0,03270124
C230085N15Rik	-2,8290	0,00097108	0,03847173
Trdc	-2,8291	0,00078711	0,03361957
Fsd1l	-2,8444	0,00079914	0,03392122
Clnk	-2,8595	5,09E-06	0,0007557
F2r	-2,8735	1,69E-06	0,00033957
Prkcq	-2,8741	1,07E-07	4,63E-05
Ly75	-2,8869	1,70E-05	0,00193831
E430021H15Rik	-2,8944	0,00124566	0,0461495
Zap70	-2,9013	0,00023355	0,01369995
Dapk2	-2,9264	3,18E-06	0,00051061
Klra7	-2,9437	7,73E-06	0,00106704
Tmem163	-2,9453	1,82E-05	0,00202566
Phactr3	-2,9677	0,00101354	0,03946724
Chrne	-2,9690	0,0005294	0,02495132
Car2	-2,9793	1,53E-06	0,00031237
Lzts1	-2,9815	0,00082553	0,03458395
Acap1	-2,9969	1,99E-06	0,00036684
Cdkl2	-3,0000	0,00060968	0,02788477
Ctsk	-3,0038	0,00120009	0,04531157
Chpf	-3,0205	0,00067871	0,03041489
Gm14029	-3,0316	2,88E-05	0,00289881
Gimap1	-3,0391	3,46E-07	0,00010951
Gm10804	-3,0421	0,00133763	0,04811252
Gfi1	-3,0512	0,00020392	0,01261039
Akap17b	-3,0562	2,61E-06	0,00044593
Tnfrsf9	-3,0639	6,85E-06	0,00096455
Wdr6	-3,0729	0,0001529	0,00999904
Sh2d2a	-3,0822	9,25E-07	0,00022697
Kcnk5	-3,0824	4,09E-05	0,00363311
Tmem41a	-3,0897	0,00053321	0,02504432
Ptprcap	-3,0904	6,96E-07	0,00018761
Zfp507	-3,0953	0,00083937	0,03497703
Tcf7	-3,1132	3,10E-05	0,00299843
Emid1	-3,1167	6,33E-08	2,98E-05
Scin	-3,1628	9,27E-05	0,00674007
Gm37691	-3,1800	9,43E-06	0,00123867
Rnf43	-3,1894	4,43E-07	0,00013451
Gzmb	-3,2254	4,56E-07	0,00013531
Cd2	-3,2307	2,45E-06	0,00043184
Armcx4	-3,2354	0,0001285	0,0087817
Ifitm10	-3,2356	1,72E-05	0,00193903
Sh2d1b2	-3,2452	1,69E-05	0,00193831
Zfpm1	-3,2865	2,80E-06	0,00046622
Rab37	-3,2874	9,59E-07	0,00022987
Kif14	-3,2876	2,16E-05	0,00232404
Avil	-3,2889	0,00046119	0,02285796
Acsbg1	-3,3033	0,00124592	0,0461495
Myo10	-3,3088	4,08E-05	0,00363311
Txk	-3,3236	6,69E-09	4,68E-06
Itih5	-3,3355	3,39E-07	0,00010951
Klra6	-3,3494	2,25E-06	0,00040417
Itga1	-3,3578	1,08E-09	9,86E-07
Vwf	-3,3783	0,00050995	0,02445599
Plscr4	-3,4160	0,0008655	0,03552216
Tnik	-3,4198	6,79E-09	4,68E-06
Cd55	-3,4335	2,13E-07	7,67E-05
Sla2	-3,4605	2,84E-05	0,0028731

Gene	FC	pval	padj
Dennd3	-3,4762	8,71E-06	0,00116685
Skap1	-3,4789	5,20E-08	2,63E-05
Itm2a	-3,4869	2,43E-05	0,00259101
Gm38340	-3,4969	0,00070253	0,03094855
Gzmg	-3,5051	0,00128208	0,0472213
Nhsl1	-3,5591	3,39E-05	0,00317619
Gzme	-3,5804	2,03E-06	0,00037086
Klrg1	-3,6002	1,69E-08	1,05E-05
4930590J08Rik	-3,6106	0,00095147	0,03791466
Dusp4	-3,6295	0,00086804	0,03552216
Inhba	-3,6515	9,25E-06	0,00122762
Adgrg1	-3,6662	0,00101272	0,03946724
Csf2	-3,6844	0,00041557	0,02159677
Gm44205	-3,6938	0,00137074	0,04866296
Prf1	-3,7493	9,05E-11	1,37E-07
Itgad	-3,7563	8,53E-05	0,00630039
Gm28988	-3,7688	7,77E-05	0,00583198
Ift27	-3,7926	0,00046325	0,02285796
5830454E08Rik	-3,8163	0,00140648	0,0495458
Crtam	-3,8249	2,83E-07	9,68E-05
Gm26584	-3,8503	0,00128867	0,0472213
Cd320	-3,8947	0,00091018	0,03669724
Ptpn13	-3,9082	0,00024696	0,01424265
Frmd5	-3,9288	0,00023791	0,01383706
Gzmf	-3,9652	0,00012953	0,00880773
Gzmd	-3,9793	1,40E-06	0,00030052
Mamdc2	-4,0066	7,29E-05	0,00563961
Slc27a6	-4,0190	8,67E-05	0,00636862
Adgrg3	-4,0200	0,00030537	0,0168296
Gm6637	-4,0246	9,11E-07	0,00022697
Klf12	-4,1351	0,00010568	0,00752272
Adgrb2	-4,1380	0,00038724	0,02043542
Gpr87	-4,1425	0,00090465	0,03658205
Sh2d1a	-4,1806	1,08E-11	2,12E-08
Klhl30	-4,1825	1,16E-12	3,17E-09
Chst2	-4,2061	5,74E-10	5,66E-07
Cep170b	-4,2342	1,51E-15	1,03E-11
Ksr2	-4,2520	0,00013159	0,00890375
Thy1	-4,2606	2,25E-12	5,13E-09
Dixdc1	-4,2673	1,44E-07	5,47E-05
Khdc1b	-4,2715	3,01E-05	0,00297674
Chl1	-4,2943	1,70E-05	0,00193831
Wdr95	-4,3011	0,00041795	0,02163852
Plb1	-4,3450	5,73E-07	0,00016329
Kcnq5	-4,3802	1,09E-08	7,11E-06
Oit3	-4,4719	0,00115536	0,0439874
Eomes	-4,4825	4,39E-16	6,00E-12
Atp1b1	-4,4852	6,87E-15	3,13E-11
Cdon	-4,5783	3,13E-06	0,0005092
Map7	-4,5991	1,77E-06	0,00034886
Eya2	-4,6272	1,51E-10	2,06E-07
Zfp566	-4,6984	8,31E-06	0,00113529
Fhl2	-4,9263	2,93E-11	5,01E-08
Ctla4	-4,9362	1,37E-06	0,00030052
Nefh	-4,9729	1,05E-05	0,00133148
Ppm1j	-5,0447	1,79E-06	0,00034886
Zfp239	-5,0459	1,61E-05	0,00188647
Ptpn3	-5,0781	5,80E-10	5,66E-07
Mrvi1	-5,1902	3,04E-05	0,00297674
Epdr1	-5,3080	3,05E-05	0,00297674
Kcnip3	-5,3250	3,74E-13	1,28E-09
Spry4	-5,3252	2,20E-08	1,25E-05
Reck	-5,4889	2,52E-10	2,86E-07
Slc35f2	-5,5301	7,00E-07	0,00018761
Mid2	-5,7496	1,01E-05	0,00129683
Kif26b	-6,9672	1,96E-08	1,16E-05

nature COMMUNICATIONS

ARTICLE

DOI: 10.1038/s41467-018-06918-3 OPEN

Molecular definition of group 1 innate lymphoid cells in the mouse uterus

Iva Filipovic[1,2,3], Laura Chiossone[4,10], Paola Vacca[5,6,7], Russell S. Hamilton[3], Tiziano Ingegnere[7], Jean-Marc Doisne[1,11], Delia A. Hawkes[1], Maria Cristina Mingari[5,6,8], Andrew M. Sharkey[3,9], Lorenzo Moretta[7] & Francesco Colucci[1,3]

Determining the function of uterine lymphocytes is challenging because of the dynamic changes in response to sex hormones and, during pregnancy, to the invading foetal trophoblast cells. Here we provide a genome-wide transcriptome atlas of mouse uterine group 1 innate lymphoid cells (ILCs) at mid-gestation. Tissue-resident Eomes^{+}CD49a^{+} NK cells (trNK), which resemble human uterine NK cells, are most abundant during early pregnancy, and have gene signatures associated with TGF-β responses and interactions with trophoblast, epithelial, endothelial, smooth muscle cells, leucocytes and extracellular matrix. Conventional NK cells expand late in gestation and may engage in crosstalk with trNK cells involving IL-18 and IFN-γ. Eomes^{-}CD49a^{+} ILC1s dominate before puberty, and specifically expand in second pregnancies when the expression of the memory cell marker CXCR6 is upregulated. These results identify trNK cells as the cellular hub of uterine group 1 ILCs, and mark CXCR6^{+} ILC1s as potential memory cells of pregnancy.

[1] Department of Obstetrics and Gynaecology, University of Cambridge School of Clinical Medicine, NIHR Cambridge Biomedical Research Centre, Cambridge CB2 0SW, UK. [2] Department of Physiology, Development and Neuroscience, University of Cambridge, Cambridge CB2 3EG, UK. [3] Centre for Trophoblast Research, University of Cambridge, Cambridge CB2 3EG, UK. [4] G. Gaslini Institute, Genoa, 16147 Genoa, Italy. [5] Policlinico San Martino IRCCS per l'Oncologia, Genoa, 16132 Genova, Italy. [6] Department of Experimental Medicine (DIMES), University of Genoa, 16132 Genova, Italy. [7] Department of Immunology, IRCCS Bambino Gesù Children's Hospital, 00165 Rome, Italy. [8] Center of Excellence for Biomedical Research (CEBR), University of Genova, 16132 Genova, Italy. [9] Department of Pathology, University of Cambridge, Cambridge CB2 1QP, UK. [10] Present address: Innate Pharma Research Labs, Innate Pharma, 13009 Marseille, France. [11] Present address: Department of Immunology, Pasteur Institute, 75015 Paris, France. These authors contributed equally: Iva Filipovic, Laura Chiossone, Paola Vacca. Correspondence and requests for materials should be addressed to F.C. (email: fc287@medschl.cam.ac.uk)

Most innate lymphoid cells (ILCs) reside in tissues, where they integrate the local environment and its physiology. While group 2 and 3 ILCs are well characterised across tissues in humans and mice[1], the definition of group 1 (g1) ILCs is the most difficult due to their heterogeneity[2], as illustrated by human and murine liver g1 ILCs[3]. G1 ILCs include cytotoxic, conventional NK (cNK) cells and tissue-resident ILCs in liver, uterus, spleen, gut, salivary glands and thymus, which share with cNK cells expression of surface markers, transcription factor T-bet and production of IFN-γ. Little is known, however, about the physiological role of tissue g1 ILCs, whereas tissue ILC2s and ILC3s contribute to barrier integrity in lung and intestinal mucosa, promote tolerance of gut bacteria and regenerate lung epithelium upon viral infection[4]. G1 ILCs participate in early responses to infection through production of IFN-γ[5,6], however conversion of cNK cells into ILC1s under the influence of TGF-β undermines their anti-viral and anti-tumour responses[7,8]. Evidence also suggests g1 ILCs are involved in chronic inflammation in lung or intestine, where environmental cues drive ILC3s to convert into IFN-γ-producing ILC1s, which exacerbate pathology[9,10]. Thus, more information is available about tissue g1 ILCs in pathology than physiology[6].

Uterine ILCs contribute to optimal pregnancy outcome in mice[11–13] and g1 ILCs are the most abundant in both human and mouse uterus[14,15]. Among g1 ILCs, human uterine NK (uNK) cells maintain the integrity of endometrial arteries[16] and, during pregnancy, mediate key developmental processes and actively regulate placentation[17] and reviewed in ref. [18]. For example, they modulate trophoblast invasion, reshape uterine vasculature and promote foetal growth[17,19–21]. Genetic epidemiology studies have shown associations of pregnancy disorders with genetic variants of Killer-cell Immunoglobulin-like Receptors (KIRs) expressed on NK and some T cells and their variable HLA-C ligands[22,23]. Other functions have been suggested for uterine lymphocytes, including immunological tolerance[24], defence against pathogens[25,26], and roles in pregnancy complications such as miscarriage, although the evidence for this is controversial (reviewed in ref. [27]). Uterine ILC3s may also contribute to tissue physiology through production of IL-22, which maintains epithelial integrity[28]. A population of immature NK cells phenotypically overlaps with ILC3s, suggesting potential plasticity between uterine g1 ILCs and ILC3s[29]. Mouse uNK cells regulate uterine vascular adaptions to pregnancy[30] as well as foetal growth[31], but uterine g1 ILCs are heterogeneous[32] and could contribute to both physiology and pathology of reproduction[30,33].

Functional heterogeneity of uterine g1 ILCs may reflect division of labour, or result from the conversion of a subset into another under certain conditions determined by the stage of reproductive life orchestrated by sex hormones. Puberty, blastocyst implantation, placentation, parturition, and lactation are accompanied by remarkable tissue remodelling, which likely impacts on and is influenced by tissue lymphocytes. Additionally, ILC composition and function may be also marked by innate memory of pregnancy, which could contribute to the well-known better outcome of second pregnancies and their less frequent complications[34].

Determining the function of uterine cell types is challenging because of the changing nature of the organ and the limited access to human samples. Moreover, lack of knowledge on gene expression profiles of mouse uterine g1 ILC subsets precludes cell type-specific gene targeting approaches in mice. Modern immunology relies on systems biology to decode cell heterogeneity and ascribe functions to discrete subsets. Here we set out to begin to resolve the heterogeneity of g1 ILCs and provide a whole-genome transcriptome atlas of mouse uterine g1 ILCs.

We have previously characterised three uterine g1 ILCs[14], including Eomes$^+$CD49a$^+$ tissue-resident (tr)NK cells, which resemble human uNK cells, Eomes$^-$CD49a$^+$ ILC1s, which may be analogous to human uterine ILC1s;[13,15] and Eomes$^+$CD49a$^-$ cNK cells, which are presumably circulating cells in both species. Here we determine their whole-genome transcriptional profile. The results show that trNK cells express genes that make them interact with most other cell types in the pregnant uterus and therefore, akin to human uNK cells, emerge as the central g1 ILC subset. cNK cells in the uterus may support the function of trNK cells by producing IFN-γ and responding to IL-18. ILC1s are most abundant before puberty, and CXCR6$^+$ ILC1s specifically expand in the uterus, not in the liver, in second pregnancies, appearing as attractive candidates for memory cells. Determining the molecular identity and function of mouse uterine g1 ILCs may guide further work with human cells and generate opportunities for new treatments of patients with pregnancy complications.

Results

Dynamic distribution of uterine g1 ILCs. We have previously defined three uterine g1 ILC subsets[13,14]. These subsets are all CD45$^+$CD3$^-$CD19$^-$CD11b$^{low/-}$ NK1.1$^+$ NKp46$^+$ and their surface phenotype in comparison with that of liver subsets is shown in Fig. 1a. Here we set out to determine their distribution during key stages of mouse reproductive life. These were: just before puberty (3 weeks of age), during attainment of sexual maturity (5- and 8-week old), early in gestation (gd 5.5), at mid-gestation (gd 9.5), after placentation (gd13.5), late in gestation (gd17.5) and post-partum (days 1, 10 and 18). The relative abundance of different subsets at different stages was striking (Fig. 1b and Supplementary Fig. 1). Before the onset of puberty and exposure to sex hormones, Eomes$^-$CD49a$^+$ ILC1s are the most abundant. During sexual maturation, ILC1s decrease, while Eomes$^+$CD49a$^+$ trNKs increase. Upon mating, trNK cells are the most abundant in early pregnancy, on gd 5.5. Once the placenta has been established, at gd 13.5, trNKs decrease, while Eomes$^+$CD49a$^-$ cNK cells become the most abundant. A similar landscape with cNK cells being the most abundant is observed both at days 1 and 18 post-partum, which mark respectively the beginning and the end stage of breast-feeding. Fertility is lower during lactation but not at the beginning or the end[35]. We observed marked differences in the distribution of g1 ILCs in the uterus of breastfeeding and non-breastfeeding females at 10 days post-partum, with breastfeeding females having increased trNK cells, similar to the distribution observed at mid-gestation (gd 9.5). These results show a dynamic g1 ILC subset distribution during reproductive lifes that likely reflects subset-specific functions.

Genome-wide transcriptomes of uterine g1 ILCs. Genome-wide transcriptional profiles of the three uterine g1 ILC subsets sorted from Eomes-GFP reporter mice at mid-gestation were analysed in multiple comparisons with the two, well-established liver g1 ILCs subsets. RNA was extracted from uterine and hepatic lineage negative CD45$^+$CD11b$^{low/-}$NK1.1$^+$NKp46$^+$ cells sorted based on Eomes and CD49a expression as in Fig. 1a. This two-dimensional discrimination defines uterine and hepatic Eomes$^+$CD49a$^-$ cNK cells, uterine and hepatic Eomes$^-$CD49a$^+$ ILC1s and, unique to the uterus, Eomes$^+$CD49a$^+$ trNK cells. Expression of CD49a therefore marks resident cells in both tissues[36]. Unbiased principal component analysis (PCA) showed shared transcriptional profiles between uterine ILC1s and trNK cells but highlighted unexpected differences between uterine and hepatic ILC1s. The PCA also confirmed similarities between uterine and hepatic cNK

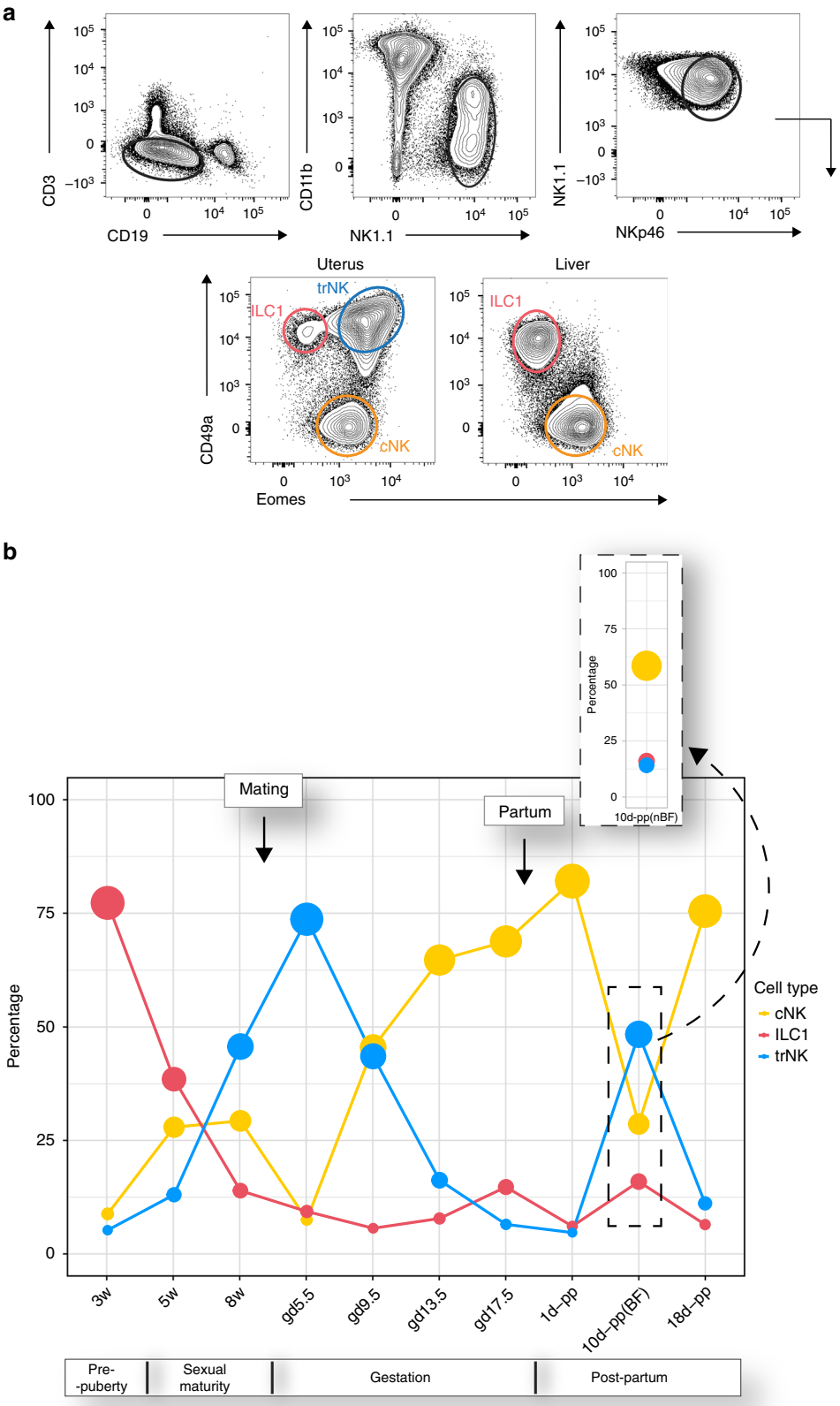

cells (Fig. 2a). Hierarchical clustering using the differentially expressed genes with a log2 fold change cutoff of 7.5 and *p*-value <0.01 confirmed that uterine and hepatic ILC1s cluster apart (Fig. 2b), despite phenotypic similarities (ref. [14] and Fig. 1a). The expression of *Tbx21* (T-bet), *Eomes*, *Ifng*, *Itga1* (CD49a), *Itga2* (CD49b), *Klrb1c* (NK1.1), and *Ncr1* (NKp46) is consistent with the sorting strategy, though expression of *Tbx21*, *Ifng* and *Ncr1* is low in uterine ILC1s (Fig. 2c).

Surprisingly, genes associated with myeloid cells appeared among those defining the principal component 1 (PC1), which

Fig. 1 Dynamic distribution of uterine group 1 innate lymphoid cells (g1 ILCs) during reproductive life. **a** Gating strategy for analysis and sorting by flow cytometry, with all freshly isolated g1 ILCs at mid-gestation (gd 9.5) gated on scatter and then defined as single live CD45$^+$CD3$^-$CD19$^-$CD11b$^{low/-}$NK1.1$^+$NKp46$^+$; ILC1 cells defined as CD49a$^+$Eomes$^-$; tissue-resident NK (trNK) cells defined as CD49a$^+$Eomes$^+$ and conventional NK (cNK) cells defined as CD49a$^-$Eomes$^+$. Each panel is representative of at least a hundred independent samples. **b** Landscape of uterine g1 ILCs during reproductive life; numbers in plot indicate mean percentage of each individual subset of g1 ILCs as gated within live CD45$^+$CD3$^-$CD19$^-$CD11b$^{low/-}$NK1.1$^+$NKp46$^+$ parent population. The size of the mean data points (filled circles) is proportional to the increasing percentage of the indicated subset. Inset shows the same time-point as the dashed rectangle below but in non-breastfeeding females. Data are representative of fifteen independent experiments with three individual animals for each time-point analysed. Mating for experiments (just after animals turn 8-weeks old) and partum (gd 19.5–21.5) time-points are indicated by the arrows on the plot. w week, d day, gd gestation day, pp post-partum, BF breastfeeding, nBF non-breastfeeding

explained 61% of the variance. These included *Clec7a* and *Clec4a3*, encoding Dectin-1 and DCIR3, respectively, *Adgre1* encoding F4/80, and *Mertk* encoding MERTK, a member of the Tyro-3/Axl/Mer (TAM) family of receptor tyrosine kinases (Supplementary Fig. 2A), highly expressed in CD49a$^+$ subsets compared to CD49a$^-$ cNK cells in both uterus and liver, thus defining transcriptomic differences between resident and circulating cells in both tissues. Flow cytometry on uterine subsets showed expression of F4/80 and CD86 on trNK cells, MERTK on both trNK and ILC1s and B220 on ILC1s, with trNK expressing intermediate B220 levels (Fig. 2d). The principal component 2 (PC2) explained 18.8% of the variance, with most genes significantly upregulated in liver ILC1s, with almost no expression in any of the other subsets, explaining in part why hepatic ILC1s do not cluster with uterine ILC1s (Supplementary Fig. 2B). These results mark the uterine resident CD49a$^+$ trNK and ILC1s as unique subsets.

Core gene signatures of uterine g1 ILCs. To compare g1 ILC transcriptomes between and among tissues, we ran 5 comparisons, the results of which are summarised in the UpSet plot, which also selects differentially expressed genes exclusively in the chosen comparison (Fig. 3a). The first comparison was between all liver g1 ILCs (ILC1 + cNK) versus all uterine g1 ILCs (cNK + trNK + ILC1). This comparison identified 265 differentially expressed genes (Fig. 3b). Gene Ontology (GO) analysis of this comparison for classification by biological process showed that the most highly enriched biological pathways in uterine cells relate to vascular endothelial growth factor (VEGF) signalling, including *Kdr*, encoding VEGF receptor 2 and *Pdgfra*, the alpha receptor for the platelet-derived growth factor (PDGF), but also oxygen/gas transport, including haemoglobin chains (*Hbb-Y*, *Hba-X*, *Hbb-BH1*) (Supplementary Fig. 3A and Fig. 3b). Other significantly enriched uterine pathways included response to hypoxia and decreased oxygen levels (*Ang*, *Hif3a*), extracellular matrix organisation (*Flrt2*, *Fbln1*, *Mmp9*, *Tgfbi*), as well as several pathways relating to wound healing and the regulation of blood vessel development. TGF-β signalling genes also distinguished uterine cells, with upregulated *Dab2*, *Tgfb2* and *Inhba* (Supplementary Fig. 3A and Fig. 3b). Supplementary Data 1 includes all differentially expressed genes and pathways highlighted by the 5 comparisons. *Trim2* is one of the genes differentially upregulated only in the uterus and *Itga3* encoding CD49c in the liver (Fig. 3b).

The second comparison was between liver CD49a$^+$ ILC1s and uterine CD49a$^+$ trNK and ILC1s, thus excluding cNK cells, and informing on tissue-specific profiles of CD49a$^+$ resident cells (Fig. 3c). The most highly upregulated genes in uterine CD49a$^+$ cells are *Gzmd*, *Gzme*, *Gzmf*, *Gzmg* encoding non-cytotoxic granzymes, likely involved in tissue remodelling. Indeed, other highly expressed genes regulate extracellular matrix organisation (*Flrt2*), collagen homeostasis (*Ctsb*, *Ctss*), wound healing (*Hmox1*, *Pdgfa*, *Plau*), and proliferation of epithelial cells (*Mmp12*, *Vegfa*) (Fig. 3c and Supplementary Fig. 3B). Upregulated in uterine CD49a$^+$ cells are also genes involved in metabolic regulation of steroids (mainly progesterone metabolism—*Dhrs9* and *Srd5a1*), ketones (*Slc37a2*) and amines (*Paox*). Encoding the orphan monocarboxylate transporter MCT13[37], *Slc16a13* may be specifically upregulated in uterine CD49a$^+$ cells (Fig. 3c). Other upregulated genes in CD49a$^+$ uterine cells are genes regulating migration of both myeloid cells (*Ccl2*, *Ccl12*, *Spp1*) and lymphocytes (*Ccl7*, *Ccl8*, *Ccl17*). Osteopontin-encoding *Spp1* was reported to be upregulated in uterine NK cells[38] and we find that alymphoid *Rag2*$^{-/-}$*Il2rg*$^{-/-}$ dams express less *Spp1* transcripts (Supplementary Fig. 3G). Two other growth-promoting factors, Pleiotropin-encoding *Ptn*, and Osteoglycin-encoded *Ogn* have also been implicated in NK-cell mediated foetal growth[39], however other cells produce these growth-promoting factors[40] and we found no significant difference in expression between wild-type and alymphoid uterus, thus excluding *Ptn* and *Ogn* as NK-cell and lymphocyte-specific factors driving foetal growth (Supplementary Fig. 3G). Expressing *Arg1*, *Arg2*, *Ecm1*, and *Tnfsf4*, uterine CD49a$^+$ cells may regulate type-2 immunity. Unexpected was the discovery of pathways regulating cellular import and phagocytosis, usually associated with antigen-presenting cells. The top enriched pathway in CD49a$^+$ liver cells relative to CD49a$^+$ uterine cells was negative regulation of antigen processing and presentation of peptide via MHC class II (Supplementary Fig. 3B). *H2-Oa* and *H2-Ob* (also identified previously in splenic CD127$^+$ ILC1s[2]) encode H2-O, an inhibitor of MHC class II (H2-DM)-mediated antigen-loading process. Moreover, liver CD49a$^+$ cells may regulate T-cell migration, with upregulated *Cxcr3* and *Ccr6*. Indeed, *Ccr6* may be exclusively expressed in liver ILC1s. Upregulated in liver cells are also *Cd27*, *Cd69* and *Cxcr6*, which encodes a CXCL16 receptor associated with 'memory' liver NK cells[41] (Fig. 3c).

The third comparison between the two CD49a$^+$ uterine subsets versus CD49a$^-$ uterine cNK cells informs on characteristics specific to uterine resident cells (Fig. 3d). Tissue resident cells highly express genes involved in induction of cell death (*Fasl*, *Hvcn1*, *Tnf*), response to both type I interferons and IFN-γ (including *Ccl7* and very highly, *Irf7*) and proteolysis, with nearly all cathepsins significantly upregulated, alongside *C3*, *Plau* and *Cpq* (Supplementary Fig. 3C). This suggests that uterine resident cells are involved in protein processing during tissue remodelling. Enriched pathways are chiefly unsaturated fatty acid biosynthesis (*Mgst1*) and lipid metabolism (*Apoe*, *Psap*) (Fig. 3d and Supplementary Fig. 3C). When analysed by flow cytometry, uterine Eomes$^+$ CD49a$^+$ trNK cells are highly granular[14], like their human counterpart. Consistent with this, the lysosomal transport (*CD68*, *Rab7b*, *Lamp1* and *Lamp2*) is enriched in tissue resident cells. The most upregulated genes in resident CD49a$^+$ cells are *Ccl7*, *Ccl2* and *Tlr1* (Fig. 3d). RT-PCR analysis confirmed higher expression of *Ccl2*, *Ccl7*, and *Ccl12* by uterine trNK (4.9, 9.7 and 25 folds, respectively) and ILC1s (1.4, 3 and 8.3 folds, respectively), compared to cNK cells. Tissue resident cells

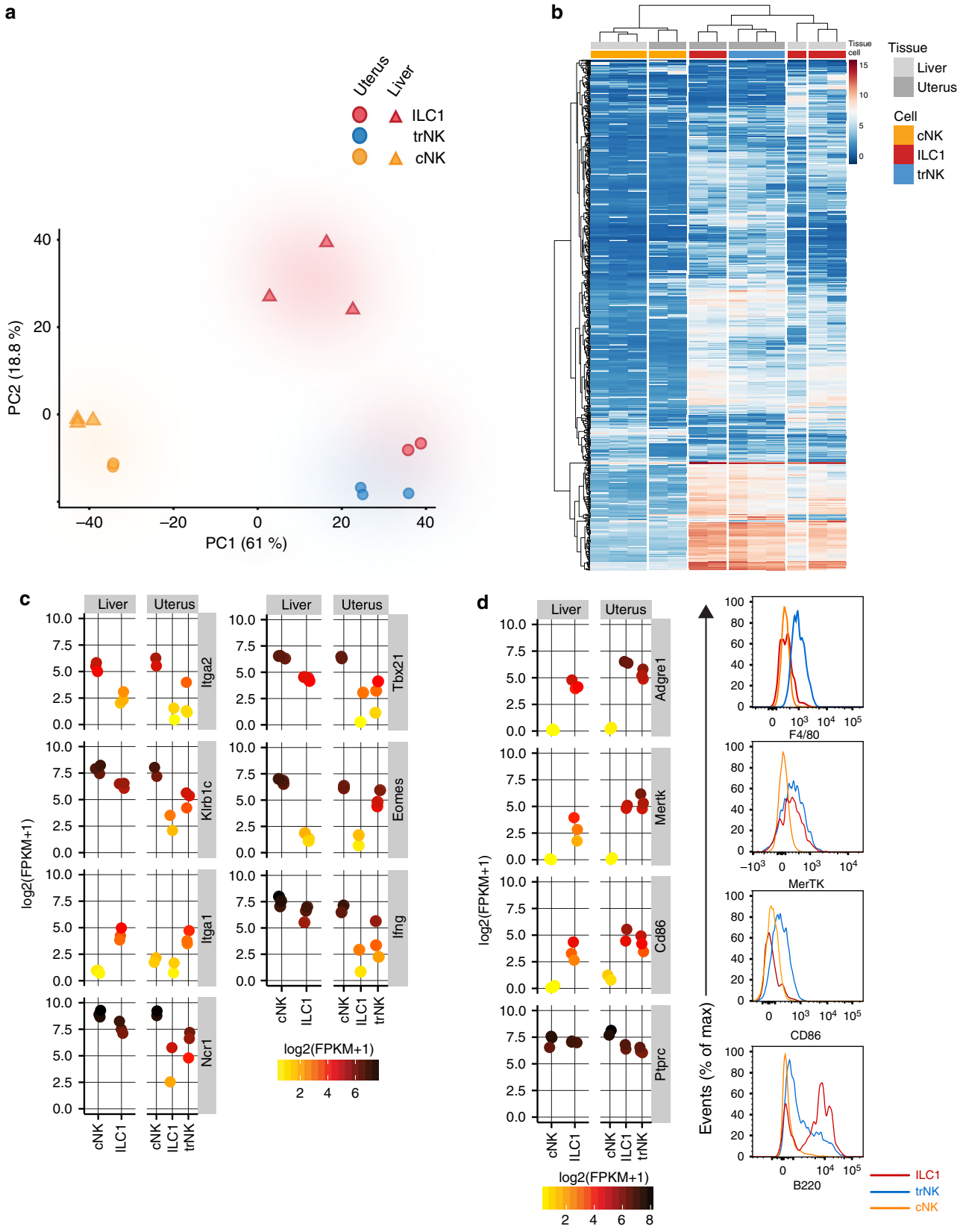

specifically upregulate the transcriptional repressor *Hic2*, as well as *Il6*, *Hint2* and *Clec4b1*. Highly upregulated exclusively in uterine cNK cells, as reported previously for splenic cNK cells[2], is *S1pr5* encoding sphingosine-1-phosphate receptor 5, which regulates NK-cell egress. One of the highest fold-change upregulated genes in uterine cNK cells is *Muc4* encoding Mucin4, involved in epithelial cell integrity and homoeostasis.

The fourth comparison was between uterine trNK cell and cNK cells. The mutually exclusive expression of CD49a (*Itga1*) in trNK cells and CD49b (*Itga2*) in cNK cells reflected the cell-sorting

Fig. 2 Genome-wide transcriptomes of uterine g1 ILCs at mid-gestation. **a** Unbiased principal component analysis (PCA)-based clustering of uterine ILC1s, trNK and cNK cells and of liver ILC1s and cNK cells. The 250 most variable genes and the two principal components were used for clustering and to describe the variance between the subsets. **b** Heat map of all significant differentially expressed genes with a log2fold change >7.5, selected from comparisons described in the text and presented in Fig. 3a. **c** Individual gene expression plots of genes encoding proteins used for sorting g1 ILCs and additional genes used for validation of the ILC and NK-lineages. Scale represents log2(FPKM + 1) transformed normalised reads. **d** Individual gene expression plots of genes encoding F4/80, MERTK, CD86 and B220 in uterine and liver g1 ILCs and flow cytometry validation of their protein products. Histograms show protein expression on three uterine g1 ILCs gated as gated in Fig. 1a (red line-ILC1s, blue line-trNK, orange line-cNK). FPKM fragments per kilobase of exon model per million reads mapped

strategy (Fig. 3e). About 900 pathways were detected in this comparison (Supplementary Fig. 3D), including those involved in responses to IFN-γ and IL-18. Upregulated in trNK cells are *Il18* and *Ifngr2*, while *Ifng*, *Il18r1* and *Il18rap* are upregulated in cNK cells. This suggests that trNK cells respond to IFN-γ and produce IL-18, while cNK cells respond to IL-18 and produce IFN-γ, (Fig. 3e). trNK cells may also respond to and produce IL-1β, through highly expressed *Il1r1*, *Ccl17*, *Ccl8* (cellular response to IL-1) and *Il1b*, *Nlrp1b*, *Nlrp3* (IL-1β production). Among the most highly enriched pathways in trNK cells were those related to cholesterol storage and homoeostasis, with genes such as *Apob*, *Lpl* and *Pparg* upregulated in trNK cells (Fig. 3e and Supplementary Fig. 3D). Interestingly, apoptotic cell clearance was among the enriched pathways, with *Lrp1*, *Axl* and *Mertk* highly upregulated in trNK compared to cNK cells. *Lrp1* encodes CD91, a receptor of many ligands and functions. In addition to roles in apoptosis, and more widely being a haemoglobin scavenger receptor, it also binds growth factors, including TGF-β. Therefore, uterine trNK and ILC1s may be highly responsive to TGF-β, through receptors such as CD91, Tgfbr1 and Tgfbr2. In addition, *Tgfbi*, encoding transforming growth factor-beta induced protein (TGFBIp, BIGH3), is also upregulated in trNK cells. UpSet pointed to *Slc16a1*, encoding the cell exporter of lactate MCT1, to be uniquely upregulated in trNK cells, emphasising the potential importance of anaerobic glycolysis for fuelling uterine CD49a^{+} cells[42]. Biglycan, encoded by *Bgn*, is a CD44 ligand that may be involved in the recruitment of circulating CD16^{-} NK cells into human endometrium[43] and is upregulated in trNK cells (Supplementary Fig. 3F). Regulators of cellular extravasation such as *Adam8*, *Ccl2* and *Ptafr* are upregulated in trNK, while *Itga4* and *Fam65b* are upregulated in cNK, suggesting migratory behaviour in both subsets, albeit through potentially different mechanisms (Supplementary Fig. 3F). *Ly86*, *Ly96*, *CD180*, *Sash1* are all significantly upregulated in trNK and part of highly enriched lipopolysaccharide-mediated signalling pathway. MyD88-dependent toll-like receptor (TLR) signalling is also specific to trNK cells, with *Tlr1*, *Tlr2*, *Tlr8*, and *Tlr9* highly upregulated (Supplementary Fig. 3F). Lysosome organisation pathway is enriched in trNK, just like complement and haemostasis regulation with *C3*, *F7*, *F10* and *Ptrpj*. Also, *C3ar1* and *C5ar1*, involved in complement receptor signalling are upregulated in trNK cells. Some of the most highly upregulated genes in trNK cells include *P2ry1* and *P2rx4*, suggesting that purinergic receptor signalling pathway is highly enriched. *Plau*, *Pdgfa*, *Sema6D*, *Bmpr1a*, *Plxna1*, *Itgb3* are all part of smooth muscle cell migration pathway and upregulated in trNK cells (Supplementary Fig. 3F). Other pathways enriched in trNK cells include hormone and sphingolipid catabolism, prostaglandin synthesis, detection of external biotic stimulus, regulation of nitric oxide biosynthesis, regulation of TGF-β production and tissue remodelling. *Msr1*, encoding macrophage-scavenger receptor 1 and *Clec7a*, encoding Dectin-1 exhibited the highest fold change in trNK compared to cNK (about 300-500-fold, respectively). One of the genes upregulated almost 40-fold in trNKs is *Slc40a1*, encoding ferroportin (FPN1), which is the main exporter of iron from cells, suggesting that iron metabolism may be of importance in uterine trNK cells. Our dataset shows high expression of *Nfe2l2* (NRF2) and significantly upregulated *Nfe2l3* (NRF3) in trNK cells[44]. Both can bind to antioxidant stress response elements and *Nfe2l3* locus has been shown to be associated with endometriosis through genome-wide association studies[45] (Supplementary Fig. 3F).

The fifth comparison between uterine ILC1s and trNK cells highlights transcriptome profiles specific to uterine resident cells (Fig. 3f). The most highly upregulated gene in uterine ILC1s compared to trNK is *Aplnr*, encoding for the adipokine apelin receptor, which is highly expressed in mouse endometrium[46]. Other highly expressed genes in ILC1s include *Adgre4*, encoding the macrophage-specific F4/80 receptor, as well as *Ace*, encoding angiotensin I-converting enzyme of the renin-angiotensin system. The most highly enriched pathway in ILC1s is regulation of protein heterodimerisation activity, including *Hes1*, which interacts with the Notch pathway that is key for ILC development. Among the most highly enriched pathways detected in ILC1s is antigen processing and presentation of peptide via MHC class II, with *H2-Aa*, *H2-DMb1*, *H2-Ab1*, *H2-Eb1* and *CD74* highly expressed, albeit they are also expressed in trNK cells. Enriched in trNK cells and downregulated in ILC1s are *Gzmc*, *Gzmd*, *Gzme*, *Gzmf* and *Gzmg*, assigning tissue-remodelling properties to trNK cells. Most of these granzymes were previously shown to peak in mid- to late gestation[47]. Interestingly, *Xcl1* encoding lymphotactin is highly expressed by trNK cells (Fig. 3f). XCL1 is also produced by human uNK cells and regulates trophoblast invasion[48]. trNK cells highly express *Cd96* encoding for the nectin-binding receptor Tactile, and *Crtam*, encoding a receptor for Nectin-like molecules, *Sh2d1a*, encoding SAP, as well as *Sh2d1b2*, encoding EAT-2B, also a member of SAP-family of adapters. In addition, several T-cell differentiation and activation pathways are enriched in trNK cells, including *CD28*, *Zap70*, and *Itk*. (Fig. 3f). The trNK signature suggests also regulation of myeloid cell differentiation, through *Ets1* and *Itgb3*. Other genes highly expressed in trNK cells regulate protein localisation to plasma membrane, such as *Rab37*, *Sytl2*, *Ptch1*, *Kcnip3*, *Skap1*, *Map7*.

Uterine g1 ILCs express CXCR6, IL22 and some are ex-ILC3s. Although our genome-wide transcriptome analysis showed significant upregulation of *Cxcr6* in liver ILC1s (Fig. 3c), both liver and uterine ILC1s express higher CXCR6 protein levels than trNK cells (Fig. 4a). Because there is some overlapping between immature NK cells, ILC1s and ILC3s in other tissues[2], we investigated the lineage relationship among the uterine g1 ILCs using fate mapping reporter mice in which all cells that have expressed, or actively express the RORγt-encoding *Rorc* gene are marked by YFP. Figure 4b shows presence of YFP^{+} cells among uterine g1 ILCs, which are aligned with 'ex-ILC3s' described in other tissues. The human equivalent cells reported previously as stage 3 precursor NK cells[29] or NKp44^{+} ILC3s[15] produce IL-22. We found that trNK in the mouse uterus at mid-gestation also

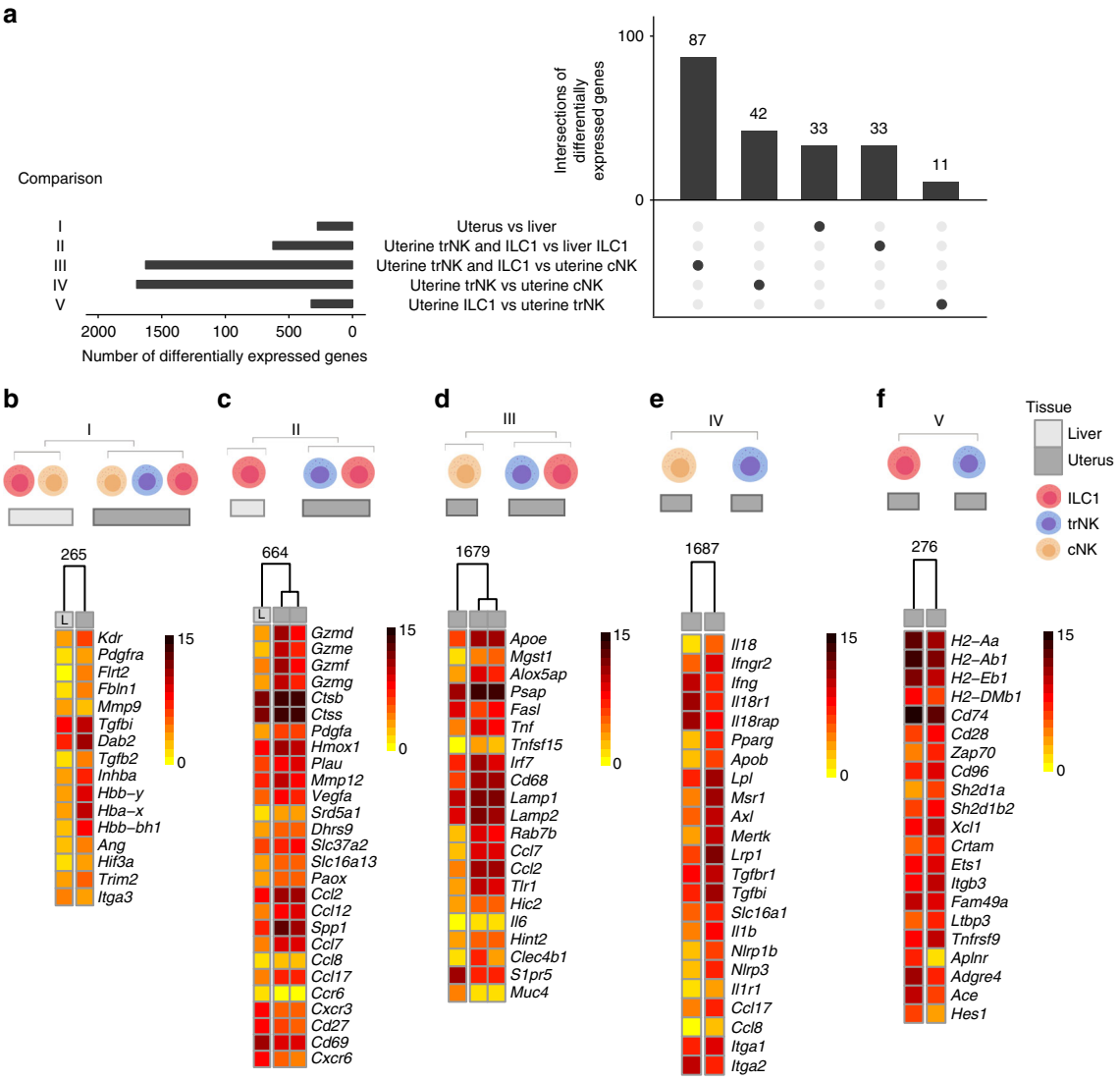

Fig. 3 Core gene signatures of uterine g1 ILCs. **a** UpSetR plot displaying 5 comparisons of g1 ILCs in uterus and liver. **b**–**f** Heat maps showing selected genes for comparisons I–V in **a**. Selected genes were chosen from a total list of differentially expressed genes as some representative genes from enriched pathways shown in Supplementary Figure 3A-E as well as from UpSetR lists of intersections of differentially expressed genes. Numbers above heat maps indicate a total number of genes in a corresponding list of differentially expressed genes in that comparison: **b** comparison I: all uterine g1 ILCs vs all liver g1 ILCs. Selected genes were chosen from enriched pathways in Supplementary Figure 3A; **c** comparison II: uterine ILC1s and trNK vs liver ILC1s. Selected genes were chosen from enriched pathways shown in Supplementary Figure 3B; **d** comparison III: uterine ILC1s and trNK vs uterine cNK cells. Selected genes were chosen from enriched pathways shown in Supplementary Figure 3C; **e** comparison IV: uterine trNK vs cNK cells. Selected genes were chosen from enriched pathways shown in Supplementary Figure 3D; **f** comparison V: uterine ILC1s vs trNK cells. Selected genes were chosen from enriched pathways shown in Supplementary Figure 3E

produce IL-22, regardless of the stimulation and, to a lesser extent so can ILC1s (Fig. 4c–e). Although *Cd27* and *Cd69* are both upregulated in liver CD49a^{+} cells (Fig. 3c), CD27 and CD69 proteins are present at similar levels in both uterine and hepatic cells (Fig. 4f). Both transcripts and Ly49 protein expression levels are slightly higher in trNK cells than in ILC1s and cNK cells within the uterus (Fig. 4f). Despite variable levels of mRNA, all three subsets in the uterus have similar protein levels of NKG2D (Fig. 4f). Bimodal distribution of NKG2A/C/E expression was observed for trNK cells as well. CD62L-encoding *Sell* and CD62L are both upregulated in uterine cNK, similarly to what was reported previously for splenic cNK cells[2]. CD103 is expressed by trNK cells and, to a lower level, by uterine ILC1s, but not by hepatic ILC1s. However, transcripts levels of CD103-encoding *Itgae* are very low in all five subsets, suggesting high mRNA turnover and potential importance of CD103 in maintaining tissue-residency of g1 ILCs (Fig. 4f). trNK cells were also more proliferative at gd 9.5, as measured by the Ki67 stain (Fig. 4f). A prediction model confirmed unique features of uterine g1 ILCs (Supplementary Fig. 4)

CXCR6 marks candidate memory uterine g1 ILCs of pregnancy. Adaptive, or memory NK cells have been described in humans and mice and CXCR6 is associated with memory NK and T cells in mice[49,50]. It is conceivable that subsets of g1 ILCs expand in response to pregnancy-specific cues in second pregnancies and possibly contribute to the lower rate of complications in second pregnancies. We therefore compared the distribution of group 1 ILCs between first and second gestations and found no

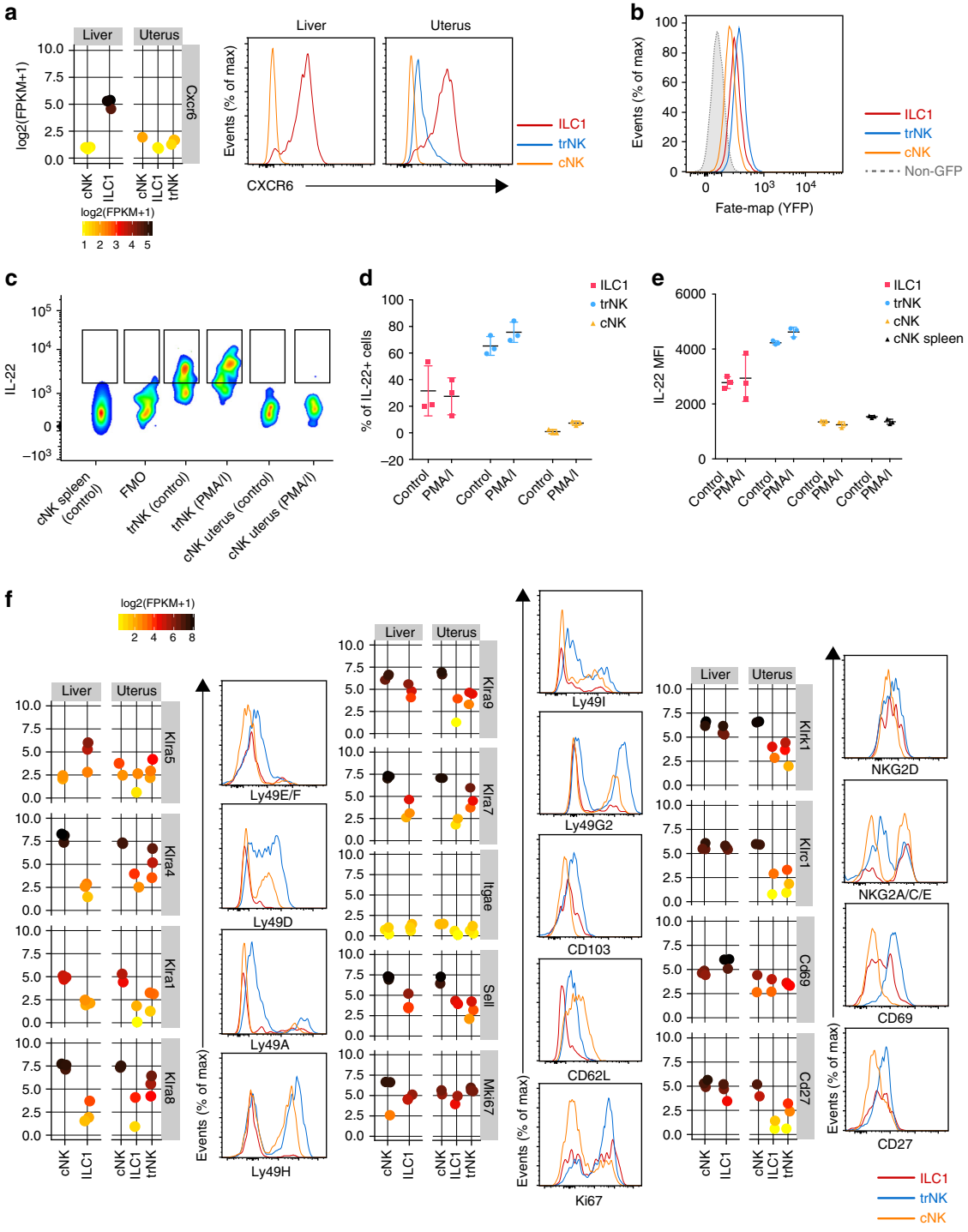

Fig. 4 Uterine g1 ILCs express CXCR6, IL22 and some cells are ex-ILC3s. **a** Individual gene expression plot showing expression of *Cxcr6* in the liver and uterus. Scale represents log2(FPKM + 1) transformed normalised reads. Histograms are showing CXCR6 protein expression on g1 ILCs in both organs at mid-gestation. Red line-ILC1, blue line-trNK, orange line-cNK. G1 ILCs were gated as described in Fig. 1a. **b** Fate-mapping of g1 ILCs in the uterus of *Rorc(γt)-Cre*^{TG}/R26R females. **c** IL-22 production by uterine trNK and cNK at gd 9.5. Control wells were incubated with medium containing protein transport inhibitors only. **d** Quantification of the percentage of IL-22-producing cells in the uterus at gd 9.5. Error bars represent mean ± SD. **e** Quantification of the mean fluorescence intensity of IL-22 on g1 ILCs at gd 9.5. Error bars represent mean ± SD. **f** Flow cytometry validation of various surface receptors on g1 ILCs in the uterus. Data are representative of three independent experiments. FPKM: fragments per kilobase of exon model per million reads mapped

significant differences in trNK or cNK cells composition (Fig. 5a, b). In sharp contrast, both the frequency and absolute numbers of ILC1s at mid-gestation raise 4–5 fold in second pregnancies (Fig. 5a, b and Supplementary Fig. 5) and ILC1s in second pregnancies upregulate CXCR6 (Fig. 5c), suggesting these cells respond to pregnancy-specific cues and expand in second pregnancies. These results mark uterine CXCR6^{+} ILC1s as potential memory cells of pregnancy.

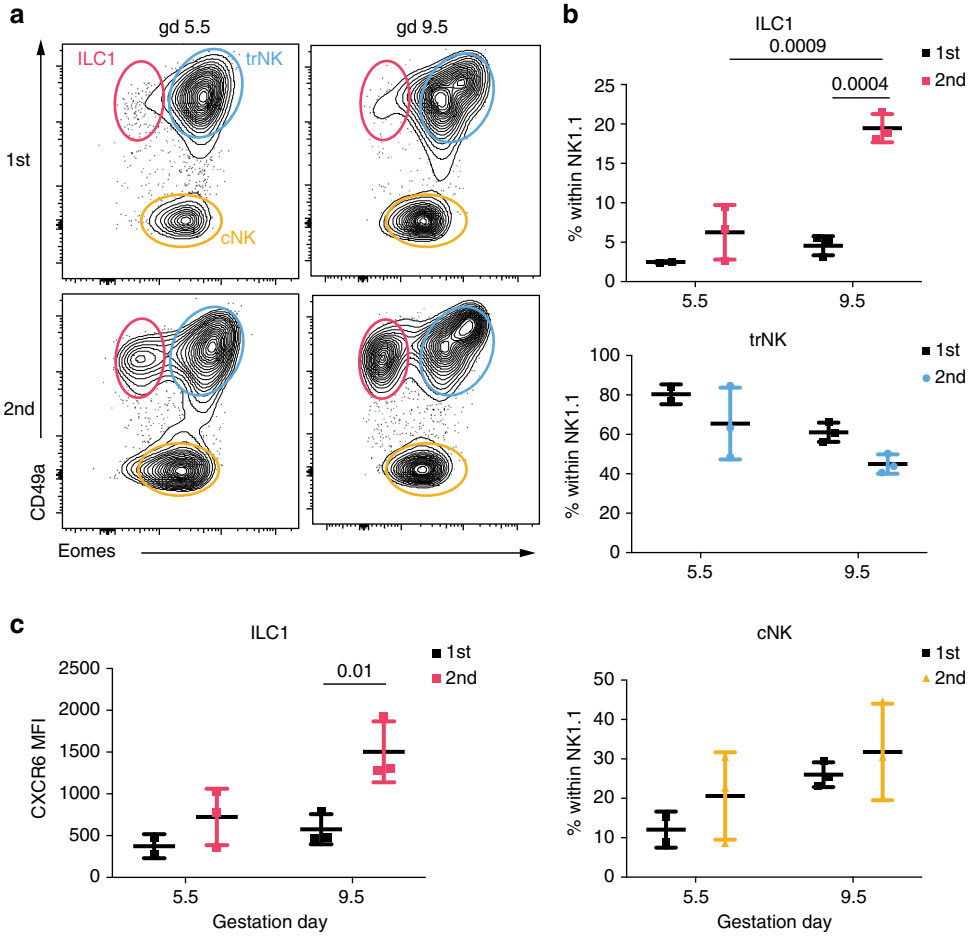

Fig. 5 Eomes^{-}CD49a^{+}CXCR6^{+} g1 ILCs expand specifically in second gestation. **a** Representative plots showing distribution of g1 ILCs (gated as in Fig. 1a) at gd 5.5 and gd 9.5 in first (top row) and second (bottom row) pregnancy. Data representative of two or three independent samples and three independent experiments. **b** Quantification of percentages of ILC1, trNK and cNK presented in **a** in first and second pregnancy at gd 5.5 and gd 9.5. Statistical significance was evaluated by two-way ANOVA with multiple comparisons correction. Error bars represent mean ± SD. **c** Mean fluorescence intensity of CXCR6 on ILC1s in first and second pregnancy at gd 5.5 and gd 9.5 Statistical significance was evaluated by two-way ANOVA with multiple comparisons correction. Error bars represent mean±SD

Disscussion

We show differences in subset composition at different key stages of mouse reproductive life. ILC1s are dominant before puberty, whereas trNKs in early gestation, peaking at gd 5.5 and cNK cells abund in late gestation. The dynamic composition of g1 ILCs, and the whole-genome transcriptome atlas we provide here suggests that g1 ILCs are attuned to uterine remodelling and may have specific functions. The picture emerging is one of trNK cells being the hub of uterine g1 ILCs (Fig. 6), as they interact with the important cell types and factors in the pregnant uterus, including TGF-β, blood vessels, smooth muscle cells, glandular epithelial cells, trophoblast, and leucocytes, including cNK cells. In a cross talk similar to that of macrophages with peripheral NK cells, trNK cells may make IL-18 and stimulate cNK cells in the uterus, which in turn produce IFN-γ and stimulate trNK cells, which unexpectedly also both respond to and produce IL-1. IL-1 and IL-18 are part of the same family of cytokines, which also include the alarmin IL-33, and these are emerging as important factors in reproductive biology and pregnancy complications[12,51]. IFN-γ is the key cytokine required for the reshaping of decidual vasculature in mice that leads to the formation of the placenta. As shown before using histological criteria for subset definitions, cNK cells are the main source of IFN-γ, while other NK-cell subsets produce angiogenic factors[52]. Our data confirm this division of labour among g1 ILCs, with cNK cells supporting trNK cells to engage with vasculature and other components of the pregnant uterus. Because cNK cells expand after the establishment of the placenta, it is tempting to speculate that they specialise in immune function defending the uteroplacental unit against pathogens.

The core signatures of uterine resident trNK cells and ILC1s are marked by genes involved in tissue homoeostasis, metabolism, genes associated with myeloid cells, cell death, interferon signalling, protein processing and fatty acid biosynthesis. The intra-tissue comparison between uterine trNK cells and cNK cells highlighted genes involved in cholesterol storage, apoptotic cell clearance, aerobic glycolysis, TLR signalling, iron transport, TGF-β signalling as well as *Axl* and *Mertk* of the Tyro-3/Axl/Mer (TAM) family of receptor tyrosine kinases. Gas6, a ligand for Mertk is expressed by trophoblast[53]. TGF-β signalling drives the transdifferentiation of cNK cells into ILC1s, through an intermediate state that is the phenocopy of uterine trNK cells[7]. TGF-β may drive a similar plasticity programme in the uterus whereby cNK and trNK cells convert into ILC1s in second pregnancies, thus partly contributing to generation of candidate memory cells. In our fate mapping experiments plasticity between ex-ILC3s and

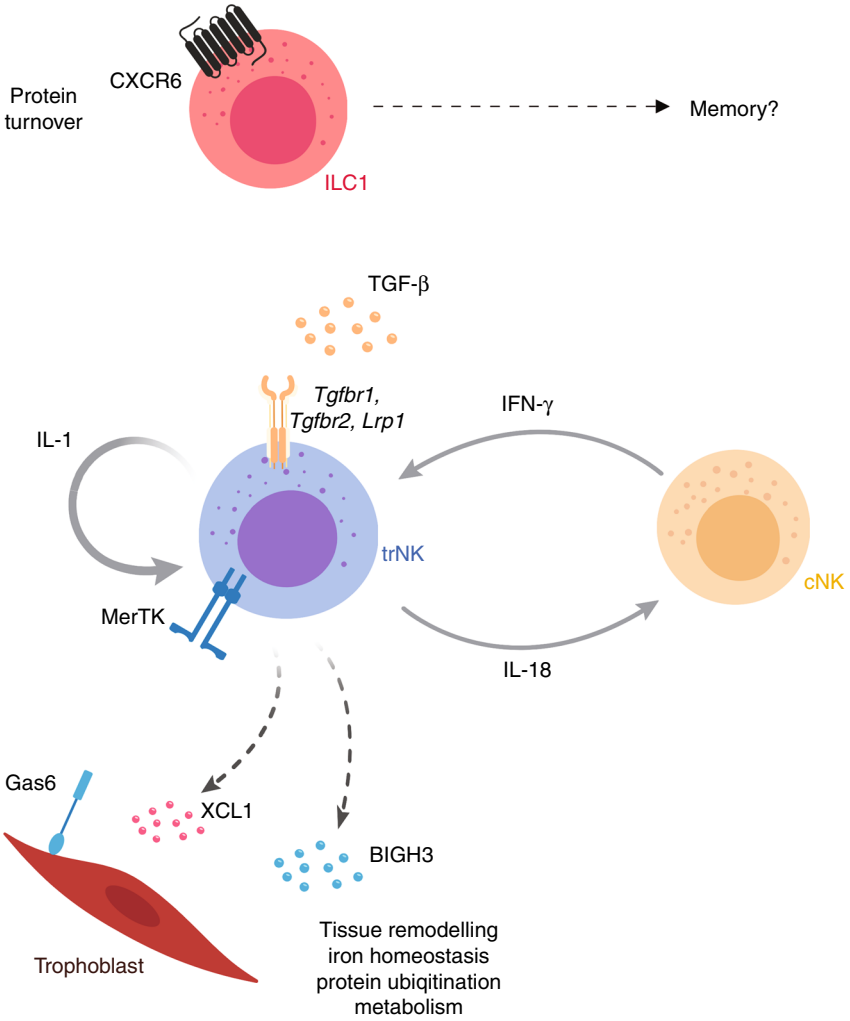

Fig. 6 Suggested g1 ILC functions in the pregnant mouse uterus. Eomes^{-}CD49a^{+} ILC1s are dominant before puberty and specifically expand in second pregnancies, when the expression of CXCR6 is upregulated, marking them as potential memory cells. Eomes^{+}CD49a^{+} NK cells (trNK) are most abundant during early pregnancy and may well be the cellular hub of uterine g1 at mid-gestation. They indeed showcase gene signatures of responsiveness to TGF-β, connections with trophoblast, epithelial, endothelial and smooth muscle cells, leucocytes, as well as extracellular matrix. They also express genes involved in anaerobic glycolysis, lipid metabolism, iron transport and protein ubiquitination. Conventional NK cells expand late in gestation and may engage in crosstalk with trNK cells involving IL-18 and IFN-γ

g1 ILCs was evident. Moreover, IL-22 production by mouse trNK cells aligns them with the previously described human stage 3 uterine NK cells[29], also described as NKp44^{+} ILC3s[15].

The comparison between uterine trNK and ILC1s revealed that trNK cells contribute to tissue remodelling through non-cytotoxic granzymes, cell–cell interactions through nectin receptors CD96 and CRTAM, as well as the chemokine XCL-1 and the transforming growth factor-beta induced protein TGFBIp, also known as BIGH3. XCL-1 is expressed by uNK cells, and its receptors by both uterine myeloid cells and invading trophoblast in humans[48]. Therefore XCL-1 emerges as a key molecule in the interactions between maternal lymphocytes and foetal cells, joining other molecular interactions, which include MHC class I receptors NKG2A, human KIR and LILRB, and murine Ly49 (reviewed in ref. [54]). BIGH3 appears as another good candidate for the molecular interactions between resident uterine g1 ILCs and maternal endothelial, smooth muscle cells, as well as foetal trophoblast cells. With trNK and uILC1s expressing various TGF-β receptors TGF-βr1, -βr2 and CD91, it is tempting to speculate that TGF-β induces the secretion of BIGH3 by these cells, which in turn regulates downstream events essential for successful placentation, such as invasion of trophoblast, vascular remodelling, and angiogenesis. Indeed, previous studies show peak expression of uterine BIGH3 at day 4 of gestation, when trophoblast invasion starts[55].

A number of unexpected genes and pathways were highlighted in trNK cells and ILC1s. Uterine ILC1s may be involved in cross talk to adipocytes through the expression of the receptor for apelin. They also express the angiotensin I-converting enzyme, suggesting a potential role in regulating blood pressure, which is of paramount importance during gestation. Genes involved in complement, IL-1-induced plasminogen activation, as well as haemostasis appear upregulated in trNK cells, which may be involved in inflammation, its accompanying vascular response and the ensuing tissue remodelling. Upregulated in trNK cells are *Fth1* and *Ftl1* encoding ferritin heavy and light chains, with *Fth1* 20-fold upregulated in trNK compared to cNK, and also one of the genes with the highest number of reads. It is therefore possible that trNKs store and export iron or, alternatively, trNK cells respond to oxidative stress induced by iron. Consistently with this possibility, *Hmox1*, which prevents inflammatory tissue injury, is upregulated in trNK cells. Along these lines, genes activated by

oxidative stress and encoding enzymes that detoxify reactive intermediates through glutathione-dependent transferase and peroxidase activities, such as *Mgst1,2* are also upregulated in trNK cells. These pathways are important in the biology of DC and T cells[56,57] and future work will establish if uterine g1 ILCs require these pathways and whether their differentiation is modulated by metabolism. In a recent study, Srebp proteins and genes involved in fatty-acid and cholesterol synthesis appeared essential for the metabolic reprogramming of NK cells in response to cytokine stimulation[58,59]. Interestingly, our analysis reveals that uterine, not liver resident g1 ILCs upregulate *Slc16a13*, which encodes lactate and pyruvate cell exporter MCT13[37]. Warburg-like glycolysis is indeed important for decidual development[60] and trNKs and ILC1s may provide lactate for the development of undifferentiated stromal cells in addition to other sources which function through other MCTs (MCT4). Also, uterine resident g1 ILCs may produce lactate as a signal for arterial remodelling, similar to the tumour microenvironment[61]. The membrane receptor for the high-density lipoprotein cholesterol *Scarb1* is also upregulated in trNK cells, as well as pathways involved in low-density lipoprotein particle remodelling (*Abcg1*, *Pla2g7*, *Mpo*) and lipid storage (*Apoe*, *Soat1*, *Hexb*, *Plin2*, *Gm2a*, *Ehd1*), suggesting that lipid metabolism may be important for trNK cells. Interestingly, human SCARB1 polymorphism associates with the outcome of in vitro fertilisation[62]. Upregulated in g1 ILCs is also Dectin-1, an important glucan receptor for anti-fungal immunity on macrophages. Recently, peripheral NK cells were shown to recognise beta 1,3 glucan through NKp30[63], suggesting macrophage-like recognition patterns in NK cells too. Consistently with this notion, we detected a number of upregulated genes involved in pathways of microbial molecular pattern recognition. Genes associated with B-cells, or for protein turnover, antigen processing and presentation, as well as the macrophage-associated F4/80 marker are upregulated in ILC1s. The role of these B-cell and myeloid markers on uterine ILC1s is unknown, and a recently described subset of NKB cells is controversial[64,65], but might be induced in SIV and HIV infection[66]. The deconvolution model we have applied here confirms that uterine g1 ILCs have expression profiles aligned with those of cell types other than NK cells and including myeloid cells. A clear limitation of the model is that there are no available ILCs defined in the dataset. Therefore, our results provide new data specific to uterine g1 ILCs at mid-gestation as a new resource for building predictive phenotype models.

Both liver and uterine ILC1s express higher levels of 'memory' marker CXCR6, which prompted us to look for potential changes in the subset composition in first and second pregnancies, with the idea that CXCR6$^+$ ILC1s may be more abundant in second pregnancies. This was indeed the case and we suggest these cells may be associated with memory of pregnancy in the mouse and expand specifically in response to local cues. One possibility is that the CXCR6 ligand CXCL16, expressed also by trophoblast cells, drives ILC1 expansion during pregnancy. Interestingly, pregnancy-trained decidual NK cells have recently been described in humans[67], which may contribute to the lower rate of complications that accompany second pregnancies[34].

In conclusion, we provide a transcriptome atlas of uterine g1 ILCs. Many genes in the UpSet lists are annotated genes that do not have a canonical name yet and include pseudogenes, long non-coding RNA and antisense transcripts. These genes may discriminate cell types and prove instrumental in cell-specific gene targeting. Clearly, there may be heterogeneity even within the subsets we have analysed in the uterus and some of the genes may be specific of smaller populations within the parent population. Future work should capture the dynamic transcriptomic changes within cell types and stages to reveal the biology of uterine ILCs.

Methods

Mice. C57BL/6 (B6) WT mice were purchased from Charles River UK and *Rag2*$^{-/-}$*Il2rg*$^{-/-}$ mice maintained in house. Eomes-GFP reporter mice were a gift of Thierry Walzer[68], *Rorc(γt)-Cre*^{TG}/R26R mice from Gérard Eberl[69] and *Rosa26R-EYFP* from Ionel Sandovici. All strains were on B6 background. All animals were used at 8–12 weeks of age and were age-matched for every experiment and all time-matings. The morning of the copulation plug discovery was counted as the gestation day (gd) 0.5 for time-matings. Mice were bred, maintained and mated under pathogen-free conditions at the University of Cambridge Central Biomedical Service in accordance with the University of Cambridge Animal Welfare and Ethical Review Body and United Kingdom Home Office Regulations, as well as at the Animal Facility of the IRCCS-AOU San Martino-IST in accordance with the Italian and European Community guidelines.

Cell isolation and functional assays. Mouse uterus, liver and spleen were processed using a protocol involving both mechanical and enzymatic processing. Finely minced tissues were digested in Accutase (Invitrogen) for 35 min at 37°C with gentle orbital agitation (80 rpm)[70] or in Liberase DH (Roche) as described previously[14] for functional assays. Following digestion, tissues were passed through the cell strainer (100 µm for uterus, 70 µm for liver and 40 µm for spleen) using a plunger to mechanically dissociate remaining tissues. Leucocytes were then isolated using 80%/40% Percoll gradient (GE Healthcare Life Sciences) and red blood cell lysis was performed on the resulting cell pellet using BD Pharm Lyse buffer (BD Biosciences) according to manufacturer's instructions. Single cell suspensions obtained in this way were used for downstream analysis and assays. For in vitro stimulation, cells were incubated in a complete medium containing Cell Stimulation Cocktail (plus protein transport inhibitors) during a 4-hour assay, alongside Protein Transport Inhibitor Cocktail for control (both from Invitrogen).

Flow cytometry. Following biotin- or fluorochrome-conjugated antibodies specific for the following antigens were used, with the dilutions in the brackets, after the clone: CD45 (clone 30-F11, 100), CD3 (17A2, 50), CD19 (1D3, 100), CD11b (M1/70, 100), NK1.1 (PK136, 100), NKp46 (29A1.4, 50), CD49a (Ha31/8, 300), Eomes (Dan11mag, 100), CD86 (GL1, 50), F4/80 (BM8, 100), B220 (RA3-6B2, 100), MerTK (REA477, 200), CXCR6 (SA051D1, 100), IL-22 (1H8PWSR, 100), NKG2D (CX5), NKG2A/C/E (20d5, 100), CD69 (H1.2F3, 50), CD27 (LG.3A10, 50), CD62L (MEL-14, 100), CD103 (2E7, 25), Ly49H (3D10, 100), Ly49G2 (4D11, 100), Ly49I (YLI-90, 100), Ly49A (YE1/48.10.6, 50), Ly49D (4E5, 50), Ly49E/F (CM4, 100), MHC-II (M5/114.15.2, 400), TruStain fcX (anti-mouse CD16/32, 100) for Fc-receptor blocking and Fixable Viability Dye eFluor 506 (dilution: 1000) for live/dead discrimination. All antibodies were purchased from Biolegend, Invitrogen (eBioscience) or BD Biosciences. For intracellular and intranuclear staining, Foxp3/Transcription Factor Staining Buffer Set (Invitrogen) was used according to manufacturer's instructions. Uterine and liver ILC1 were sorted from Eomes-GFP reporter mice and analysed as live CD45$^+$CD3$^-$CD19$^-$CD11b$^{low/-}$NK1.1$^+$NKp46$^+$CD49a$^+$Eomes$^-$, uterine trNK as live CD45$^+$CD3$^-$CD19$^-$CD11b$^{low/-}$NK1.1$^+$NKp46$^+$CD49a$^+$Eomes$^+$ and uterine and liver cNK as live CD45$^+$CD3$^-$CD19$^-$CD11b$^{low/-}$NK1.1$^+$NKp46$^+$CD49a$^-$Eomes$^+$. Samples were acquired on a LSR Fortessa (BD Biosciences), sorted on FACSAria III instrument (BD Biosciences) and analysed using FlowJo vX software (BD Biosciences).

RNA-sequencing and analysis. Group 1 ILCs from uterus and liver were sorted from Eomes-GFP reporter mice into the TRI Reagent (Sigma). RNA extraction was carried out by following TRI Reagent manufacturer's instructions, followed by RNeasy Micro kit (Qiagen). cDNA was amplified using Ovation RNA-seq system V2 (NuGEN) and DNA libraries were produced using Ovation Ultralow System V2 (NuGEN) and following manufacturer's instructions. All mRNA and cDNA quality controls and quantifications were performed using RNA 6000 Pico and High Sensitivity DNA kits (Agilent) on the 2100 Bioanalyzer instrument (Agilent). RNA sequencing was performed on Illumina Hiseq4000 at the Cancer Research UK Cambridge Institute Genomics Core. Data were aligned to GRCm38 mouse genome (Ensembl Release 84) with TopHat2 (v2.1.1, using bowtie2 v2.2.9) with a double map strategy. Alignments and QC were processed using custom ClusterFlow (v0.5dev) pipelines and assessed using MultiQC (0.9.dev0). Gene quantification was determined with HTSeq-Counts (v0.6.1p1). Additional quality control was performed with feature counts (v 1.5.0-p2), qualimap (v2.2) and preseq (v2.0.0). Differential gene expression was performed with DESeq2 package (v1.16.1, R v3.4.2) and with the same package read counts were normalised on the estimated size factors. Proportions of specific immune cell types from bulk RNA-Seq can be estimated using reference data generated from known proportions of the cell types of interest[71]. DeconRNASeq[72] was applied to take these tables of known cell proportions, defined by gene expression profiles, and used to deconvolute bulk dataset generated in this study to estimate cell proportions within each of the sequence's samples. Gene Ontology (biological process) analysis was performed using PANTHER (Protein ANalysis THrough Evolutionary Relationships database http://www.pantherdb.org). Lists of differentially expressed genes (adjusted $p < 0.05$

and log2 fold change two or above) were submitted to PANTHER Over-representation Test (released 2017-12-05), with Fisher's exact testing utilising a false discovery rate multiple test correction and a *Mus Musculus* reference list. Further details on annotation versions and release dates can be found in the Supplementary Data 1.

RT-qPCR. Whole uterus was isolated at time-points of interest, collected in RNA*later* (Invitrogen) to stabilise the RNA and kept at 4 °C overnight. Tissue was homogenised in the Lysing Matrix S homogenisation tubes (MP Biomedicals) on a FastPrep-24 5G Homogenizer (MP Biomedicals) using RNeasy Plus Universal Kit (Qiagen) according to manufacturer's instruction. Isolated RNA quality control and quantification was performed using RNA 6000 Nano kit (Agilent) on the 2100 Bioanalyzer instrument (Agilent). cDNA was amplified using SuperScript VILO cDNA Synthesis kit (Invitrogen) and qPCR was performed using PowerUP SYBR Green Master Mix (Applied Biosystems), on the Quant Studio 6 Flex Real-Time PCR System (Thermo Fisher – Applied Biosystems). *Gapdh* was used as a reference gene. Data were analysed using the ΔΔCt method. Primers were as follows: *Spp1*, 5′-TTCACTCCAATCGTCCCTAC-3′ (forward) and 5′-TTAGACTCACCGCTCT TCAT-3′ (reverse); *Ogn*, 5′-TGCTTTGTGGTCACATGGAT-3′ (forward) and 5′-GAAGCTGCACACAGCACAAT-3′ (reverse); *Ptn*, 5′-TGGAGAATGGCAGTGG AGTGT-3′ (forward) and 5′-GGCGGTATTGAGGTCACATTC-3′ (reverse) and *Gapdh*, 5′-TGCACCACCAACTGCTTAG-3′ (forward) and 5′-GGATGCAGGGA TGATGTTC-3′ (reverse). *Ccl2*, *Ccl7* and *Ccl12* were assayed using Thermo Fisher TaqMan (Assays IDs Mm00441242_m1, Mm00443113_m1, Mm01617100_m1) with *Gapdh* as a reference gene (Assay ID Mm99999915_g1).

Statistical analysis and figure preparation. Statistical parameters and tests applied are reported in the figure legends. All statistical analyses were performed in Prism 7 (GraphPad Software) with a confidence level of 0.95. *p*-values above 0.05 were considered insignificant and are not indicated in the figures. Figures were prepared using BioRender and Illustrator CC 2018 (Adobe).

Data availability

All relevant data are available from the corresponding author upon reasonable request. RNA-sequencing data have been deposited in ArrayExpress database at EMBL-EBI under accession number E-MTAB-6812 (https://www.ebi.ac.uk/arrayexpress/experiments/E-MTAB-6812). An open-source repository (https://github.com/CTR-BFX/2018-Filipovic-Colucci) has been created with access to the code used in this study.

Received: 24 May 2018 Accepted: 26 September 2018
Published online: 29 October 2018

References

1. Nagasawa, M., Spits, H. & Ros, X. R. Innate lymphoid cells (ILCs): cytokine hubs regulating immunity and tissue homeostasis. *Cold Spring Harb. Perspect. Biol.* a030304–16 (2017).
2. Robinette, M. L. et al. Transcriptional programs define molecular characteristics of innate lymphoid cell classes and subsets. *Nat. Immunol.* **16**, 306–317 (2015).
3. Male, V. Liver-resident NK cells: the human factor. *Trends Immunol.* **38**, 1–3 (2017).
4. Klose, C. S. N. & Artis, D. Innate lymphoid cells as regulators of immunity, inflammation and tissue homeostasis. *Nat. Immunol.* **17**, 765–774 (2016).
5. Weizman, O.-E. et al. ILC1 confer early host protection at initial sites of viral infection. *Cell* **171**, 1–27 (2017).
6. Spits, H., Bernink, J. H. & Lanier, L. NK cells and type 1 innate lymphoid cells: partners in host defense. *Nat. Immunol.* **17**, 758–764 (2016).
7. Gao, Y. et al. Tumor immunoevasion by the conversion of effector NK cells into type 1 innate lymphoid cells. *Nat. Immunol.* **146**, 3289–16 (2017).
8. Cortez, V. S. et al. SMAD4 impedes the conversion of NK cells into ILC1-like cells by curtailing non-canonical TGF-β signaling. *Nat. Immunol.* **122**, 1–15 (2017).
9. Bernink, J. H. et al. Human type 1 innate lymphoid cells accumulate in inflamed mucosal tissues. *Nat. Immunol.* **14**, 221–229 (2013).
10. Bal, S. M. et al. IL-1β, IL-4 and IL-12 control the fate of group 2 innate lymphoid cells in human airway inflammation in the lungs. *Nat. Immunol.* **17**, 636–645 (2016).
11. Boulenouar, S. et al. The residual innate lymphoid cells in NFIL3-deficient mice support suboptimal maternal adaptations to pregnancy. *Front. Immunol.* **7**, 1065 (2016).
12. Bartemes, K., Chen, C.-C., Ilijima, K., Drake, L. & Kita, H. IL-33-responsive group 2 innate lymphoid cells are regulated by female sex hormones in the uterus. *J. Immunol.* 200, 229–236 (2018).
13. Montaldo, E. et al. Unique Eomes+NK cell subsets are present in uterus and decidua during early pregnancy. *Front. Immunol.* **6**, 145–11 (2016).
14. Doisne, J. M. et al. Composition, development, and function of uterine innate lymphoid cells. *J. Immunol.* **195**, 3937–3945 (2015).
15. Vacca, P. et al. Identification of diverse innate lymphoid cells in human decidua. *Mucosal Immunol.* **8**, 254–264 (2015).
16. Wilkens, J. et al. Uterine NK cells regulate endometrial bleeding in women and are suppressed by the progesterone receptor modulator asoprisnil. *J. Immunol.* **191**, 2226–2235 (2013).
17. Hanna, J. et al. Decidual NK cells regulate key developmental processes at the human fetal-maternal interface. *Nat. Med* **12**, 1065–1074 (2006).
18. Moffett, A. & Colucci, F. Uterine NK cells: active regulators at the maternal-fetal interface. *J. Clin. Investig.* **124**, 1872–1879 (2014).
19. Xiong, S. et al. Maternal uterine NK cell–activating receptor KIR2DS1 enhances placentation. *J. Clin. Investig.* **123**, 4264–4272 (2013).
20. Hiby, S. E. et al. Maternal KIR in combination with paternal HLA-C2 regulate human birth weight. *J. Immunol.* **192**, 5069–5073 (2014).
21. Colucci, F. & Kieckbusch, J. Maternal uterine natural killer cells nurture fetal growth: in medio stat virtus. *Trends Mol. Med.* **21**, 60–67 (2015).
22. Hiby, S. E. et al. Combinations of maternal KIR and fetal HLA-C genes influence the risk of preeclampsia and reproductive success. *J. Exp. Med.* **200**, 957–965 (2004).
23. Colucci, F. The role of KIR and HLA interactions in pregnancy complications. *Immunogenetics* **69**, 1–9 (2017).
24. Vacca, P. et al. Crosstalk between decidual NK and CD14+ myelomonocytic cells results in induction of Tregs and immunosuppression. *Proc. Natl Acad. Sci. USA* **107**, 11918–11923 (2010).
25. Siewiera, J. et al. Human cytomegalovirus infection elicits new decidual natural killer cell effector functions. *PLoS Pathog.* **9**, e1003257–17 (2013).
26. Crespo, Â. C., Strominger, J. L. & Tilburgs, T. Expression of KIR2DS1 by decidual natural killer cells increases their ability to control placental HCMV infection. *Proc. Natl Acad. Sci. USA* **113**, 15072–15077 (2016).
27. Moffett, A. & Shreeve, N. First do no harm: uterine natural killer (NK) cells in assisted reproduction. *Hum. Reprod.* **30**, 1519–1525 (2015).
28. Croxatto, D. et al. Group 3 innate lymphoid cells regulate neutrophil migration and function in human decidua. *Mucosal Immunol.* **9**, 1372–1383 (2016).
29. Male, V. et al. Immature NK cells, capable of producing IL-22, are present in human uterine mucosa. *J. Immunol.* **185**, 3913–3918 (2010).
30. Ashkar, A. A., Di Santo, J. P. & Croy, B. A. Interferon γ contributes to initiation of uterine vascular modification, decidual integrity, and uterine natural killer cell maturation during normal murine pregnancy. *J. Exp. Med.* **192**, 259–270 (2000).
31. Kieckbusch, J., Gaynor, L. M., Moffett, A. & Colucci, F. MHC-dependent inhibition of uterine NK cells impedes fetal growth and decidual vascular remodelling. *Nat. Commun.* **5**, 1–12 (2014).
32. Yadi, H. et al. Unique receptor repertoire in mouse uterine NK cells. *J. Immunol.* **181**, 6140–6147 (2008).
33. Thaxton, J. E. et al. NKG2D blockade inhibits poly(I:C)-triggered fetal loss in wild type but not in IL-10$^{-/-}$ mice. *J. Immunol.* **190**, 3639–3647 (2013).
34. Hernandez-Diaz, S., Toh, S. & Cnattingius, S. Risk of pre-eclampsia in first and subsequent pregnancies: prospective cohort study. *BMJ* **338**, b2255 (2009).
35. Green, B. *Biology of the Laboratory Mouse* 187–204 (McGraw-Hill Book Company, New York, 1966).
36. Sojka, D. K. et al. Tissue-resident natural killer (NK) cells are cell lineages distinct from thymic and conventional splenic NK cells. *eLife Sci.* **3**, e01659 (2014).
37. Halestrap, A. P. The SLC16 gene family - structure, role and regulation in health and disease. *Mol. Asp. Med.* **34**, 337–349 (2013).
38. Wang, F. et al. Molecular signatures and transcriptional regulatory networks of human immature decidual NK and mature peripheral NK cells. *Eur. J. Immunol.* **44**, 2771–2784 (2014).
39. Fu, B. et al. Natural killer cells promote fetal development through the secretion of growth-promoting factors. *Immunity* **47**, 1100–1113.e6 (2017).
40. Hempstock, J., Cindrova-Davies, T., Jauniaux, E. & Burton, G. J. Endometrial glands as a source of nutrients, growth factors and cytokines during the first trimester of human pregnancy: a morphological and immunohistochemical study. *Reprod. Biol. Endocrinol.* **2**, 58–14 (2004).
41. Peng, H. et al. Liver-resident NK cells confer adaptive immunity in skin-contact inflammation. *J. Clin. Investig.* **123**, 1444–1456 (2013).
42. Velásquez, S. Y. et al. Short term hypoxia synergizes with interleukin 15 priming in driving glycolytic gene transcription and supports human natural killer cell activities. *J. Biol. Chem.* **291**, 12960–12977 (2016).
43. Kitaya, K. & Yasuo, T. Dermatan sulfate proteoglycan biglycan as a potential selectin L/CD44 ligand involved in selective recruitment of peripheral blood CD16(−) natural killer cells into human endometrium. *J. Leukoc. Biol.* **85**, 391–400 (2008).

44. Chevillard, G. & Blank, V. NFE2L3 (NRF3): the Cinderella of the Cap'n'Collar transcription factors. *Cell. Mol. Life Sci.* **68**, 3337–3348 (2011).
45. Painter, J. N. et al. Genome-wide association study identifies a locus at 7p15.2 associated with endometriosis. *Nat. Genet.* **43**, 51–54 (2010).
46. Pope, G. R., Roberts, E. M., Lolait, S. J. & O'Carroll, A.-M. Central and peripheral apelin receptor distribution in the mouse: species differences with rat. *Peptides* **33**, 139–148 (2012).
47. Allen, M. P. & Nilsen-Hamilton, M. Granzymes D, E, F, and G are regulated through pregnancy and by IL-2 and IL-15 in granulated metrial gland cells. *J. Immunol.* **161**, 2772–2779 (1998).
48. Kennedy, P. R. et al. Activating KIR2DS4 is expressed by uterine NK cells and contributes to successful pregnancy. *J. Immunol.* **197**, 4292–4300 (2016).
49. Paust, S. et al. Critical role for the chemokine receptor CXCR6 in NK cell-mediated antigen-specific memory of haptens and viruses. *Nat. Immunol.* **11**, 1127–1135 (2010).
50. Tse, S.-W., Radtke, A. J., Espinosa, D. A., Cockburn, I. A. & Zavala, F. The chemokine receptor CXCR6 is required for the maintenance of liver memory CD8+ T cells specific for infectious pathogens. *J. Infect. Dis.* **210**, 1508–1516 (2014).
51. Huang, B. et al. Interleukin-33-induced expression of PIBF1 by decidual B cells protects against preterm labor. *Nat. Med.* **23**, 128–135 (2017).
52. Chen, Z. et al. DBA-lectin reactivity defines mouse uterine natural killer cell subsets with biased gene expression1. *Biol. Reprod.* **87**, 1–18 (2012).
53. Madeja, Z. et al. Paternal MHC expression on mouse trophoblast affects uterine vascularization and fetal growth. *Proc. Natl Acad. Sci. USA* **108**, 4012–4017 (2011).
54. Moffett, A. & Colucci, F. Co-evolution of NK receptors and HLA ligands in humans is driven by reproduction. *Immunol. Rev.* **267**, 283–297 (2015).
55. Uekita, T., KIM, Y.-J., Yamanouchi, K., Tojo, H. & Tachi, C. Dynamics of BIGH3 mRNA expression during pregnancy in the uterus and the placenta of the mouse: a possible regulatory factor for trophoblastic invasion. *J. Reprod. Dev.* **49**, 243–252 (2003).
56. Rehman, A. et al. Role of fatty-acid synthesis in dendritic cell generation and function. *J. Immunol.* **190**, 4640–4649 (2013).
57. Berod, L. et al. De novo fatty acid synthesis controls the fate between regulatory T and T helper 17 cells. *Nat. Med.* **20**, 1327–1333 (2014).
58. Gardiner, C. M. & Finlay, D. K. What fuels natural killers? Metabolism and NK cell responses. *Front. Immunol.* **8**, 536–538 (2017).
59. Assmann, N. et al. Srebp-controlled glucose metabolism is essential for NK cell functional responses. *Nat. Immunol.* **18**, 1197–1206 (2017).
60. Zuo, R.-J. et al. Warburg-like glycolysis and lactate shuttle in mouse decidua during early pregnancy. *J. Biol. Chem.* 290, 21280–21291 (2015).
61. Romero-Garcia, S., Moreno-Altamirano, M. M. B., Prado-Garcia, H. & Sánchez-García, F. J. Lactate contribution to the tumor microenvironment: mechanisms, effects on immune cells and therapeutic relevance. *Front. Immunol.* **7**, R502–R511 (2016).
62. Yates, M., Kolmakova, A., Zhao, Y. & Rodriguez, A. Clinical impact of scavenger receptor class B type I gene polymorphisms on human female fertility. *Hum. Reprod.* **26**, 1910–1916 (2011).
63. Li, S. S. et al. Identification of the fungal ligand triggering cytotoxic PRR-mediated NK cell killing of Cryptococcus and Candida. *Nat. Commun.* **9**, 1–13 (2018).
64. Wang, S., Xia, P. & Fan, Z. Natural-killer-like B cells function as a separate subset of innate B cells. *Immunity* **47**, 201–202 (2017).
65. Kerdiles, Y. M. et al. Natural-killer-like B cells display the phenotypic and functional characteristics of conventional B cells. *Immunity* **47**, 199–200 (2017).
66. Manickam, C. et al. Progressive lentivirus infection induces natural killer cell receptor-expressing B cells in the gastrointestinal tract. *AIDS* **32**, 1571–1578 (2018).
67. Gamliel, M. et al. Trained memory of human uterine NK cells enhances their function in subsequent pregnancies. *Immunity* **48**, 951–962.e5 (2018).
68. Daussy, C. et al. T-bet and Eomes instruct the development of two distinct natural killer cell lineages in the liver and in the bone marrow. *J. Exp. Med.* **211**, 563–577 (2014).
69. Eberl, G. & Littman, D. R. Thymic origin of intestinal alphabeta T cells revealed by fate mapping of RORgammat+ cells. *Science* **305**, 248–251 (2004).
70. Arenas-Hernandez, M., Sanchez-Rodriguez, E. N., Mial, T. N., Robertson, S. A. & Gomez-Lopez, N. Isolation of leukocytes from the murine tissues at the maternal-fetal interface. *J. Vis. Exp.* **99**, 1–12 (2015).
71. Chen, Z. et al. Inference of immune cell composition on the expression profiles of mouse tissue. *Sci. Rep.* **7**, 1–11 (2017).
72. Gong, T. & Szustakowski, J. D. DeconRNASeq: a statistical framework for deconvolution of heterogeneous tissue samples based on mRNA-Seq data. *Bioinformatics* **29**, 1083–1085 (2013).

Acknowledgements

This work was funded by a Wellcome Trust Investigator Award 200841/Z/16/Z, the Centre for Trophoblast Research (CTR), and the Cambridge NIHR BRC Cell Phenotyping Hub to F.C., the Associazione Italiana Ricerca per la Ricerca sul Cancro (AIRC)-Special Project 5×1000 no. 9962, AIRC IG 2017 Id.19920 and AIRC 2014 Id. 15283 to L. M., and Ministero della Salute RF-2013, GR-2013-02356568 to P.V. I.F. was funded by a CTR PhD fellowship. The Authors are grateful to Thierry Walzer, Gerard Eberl and Ionel Sandovici for sharing resources.

Author contributions

I.F. designed and performed experiments, analysed the data, wrote the manuscript. L.C. and P.V. designed and performed experiments, analysed the data, and revised manuscript. R.S.H. did the computation analysis of the RNAseq data and edited manuscript. J. M.D. designed and performed experiments, analysed the data and edited manuscript. D. A.H. and T.I. performed experiments. A.S. designed experiments, analysed the data and edited manuscript. M.C.M. and L.M. supervised research and revised manuscript. F.C. designed experiments, analysed the data and wrote the manuscript.

Additional information

Supplementary Information accompanies this paper at https://doi.org/10.1038/s41467-018-06918-3.

Competing interests: The authors declare no competing interests.

Reprints and permission information is available online at http://npg.nature.com/reprintsandpermissions/

Publisher's note: Springer Nature remains neutral with regard to jurisdictional claims in published maps and institutional affiliations.